Characterization of Dental Pulp Stem Cells and Their Potential Clinical Applications

Kajohnkiart Janebodin

A dissertation

submitted in partial fulfillment of the

requirements for the degree of

Doctor of Philosophy

University of Washington

2013

Reading Committee:

Morayma Reyes, Chair

Carol B. Ware, Co-Chair

Tracy E. Popowics

Program Authorized to Offer Degree:

Oral Biology

University of Washington

Abstract

Characterization of Dental Pulp Stem Cells and
Their Potential Clinical Applications

Kajohnkiart Janebodin

Chair of the Supervisory Committee:

Assistant Professor Morayma Reyes
Department of Pathology

Professor Carol Ware B. Ware
Department of Comparative Medicine

Dental pulp stem cells (DPSCs) were first isolated and characterized from human teeth and most studies have focused on using human DPSCs for dentin regeneration. However, mouse DPSCs have not been well characterized and their origin(s) have not yet been elucidated. I examined if murine DPSCs are neural crest derived and determined their *in vitro* and *in vivo* capacity. DPSCs from neonatal mice expressed embryonic stem cell and neural crest genes, but lacked expression of mesodermal genes. Cells isolated from the *Wnt1-Cre/R26R-LacZ* mouse, a reporter of neural crest-derived tissues, indicated that DPSCs were *Wnt1*-marked and therefore of neural crest origin. Clonal DPSCs showed multi-differentiation in neural crest lineage for odontoblasts, chondrocytes, adipocytes, neurons, and smooth muscles. *In vivo* subcutaneous transplantation with hydroxyapatite/tricalcium phosphate, based on tissue/cell morphology and specific antibody

staining, revealed that the clones differentiated into odontoblast-like cells and produced dentin/pulp-like structure. Conversely, femur-derived bone marrow stromal cells (BMSCs) gave rise to osteoblast-like cells and generated bone-like structure. Interestingly, the capillary distribution in the DPSC transplants showed close proximity to odontoblasts whereas in the BMSC transplants bone condensations were distant to capillaries resembling dentinogenesis in the former vs. osteogenesis in the latter.

Loss of functional salivary gland causes patients' moribidities from difficulties in swallowing and speech, as well as oral diseases. Stem cell therapy is considered a potential therapeutic alternative. However, combinatory approaches including not only salivary gland stem cells but also supportive cells and appropriate extracellular matrix are necessary to form a functional salivary gland. Like tooth formation, the development of salivary gland requires epithelium interacting with neural crest-derived mesenchyme. I used the human salivary gland (HSG) cell line as a model to study the effects of DPSCs on salivary gland differentiation. *In vitro* differentiation on matrigel showed that HSG alone and HSG co-cultured with *Wnt1-Cre/R26R-LacZ* derived DPSCs (HSG+DPSC) differentiated into acinar-like structures. However, HSG formed more mature (higher expression of LAMP-1 and CD44), larger and increased numbers of acini in HSG+DPSC. Subcutaneous co-transplantation of HSG and DPSCs with hyaluronic acid (HA) hydrogels after 2 weeks was evaluated by Q-RT-PCR, morphology and immunohistology. Compared to HSG transplants which only showed undifferentiated tumor-like cells, HSG+DPSC demonstrated (1) higher expression of murine mesenchymal marker *Fgf-7*, (2) higher expression of mature human salivary gland differentiation marker alpha-amylase-1 *AMY-1*, (3) higher expression of murine endothelial, *vWF*, neuronal, *NF-200*, and angiogenic markers, *Vegfr-3* and *Vegf-c*, (4) mucin-secreting acinar- and duct-like structures with abundant

blood vessels at the interface with DPSCs, and (5) more mature glandular structures double-positive for salivary gland differentiation markers CD44 and LAMP-1. These results indicate that DPSCs supported and enhanced HSG differentiation into functional salivary gland tissue.

In addition, DPSCs have previously demonstrated potential pericyte-like topography and function. However, the mechanisms regulating their pericyte function are still yet to be elucidated. DPSC angiogenic and pericyte function were investigated. *Tie2*-GFP derived dental pulp cells were negative for GFP driven by the endothelial *Tie2* transgene, indicating an absence of endothelial cells. Endothelial cells co-cultured with DPSCs formed more mature *in vitro* tube-like structures as compared to those co-cultured with BMSCs. Many DPSCs were located adjacent to vascular tubes, suggesting a pericyte location and function. *In vivo* DPSCs subcutaneously transplanted in matrigel (MG) (DPSC-MG) induced more vessel formation than BMSC-MG. DPSCs expressed higher *Vegfd*, *Vegfr3*, *EphrinB2* levels. Soluble Flt (sFlt), an angiogenic inhibitor that binds VEGF-A, significantly decreased the amount of blood vessels in DPSC-MG, but not in BMSC-MG. sFlt inhibited VEGFR2 and downstream ERK signaling and down-regulated *Vegfa*, *Vegf receptors* and *EphrinB2* expression in DPSCs. Therefore, DPSC-induced angiogenesis is VEGF-dependent. DPSCs enhance angiogenesis by secreting VEGF-A, -C, -D and forming tight associations with vessels, resembling pericyte-like cells. Taken together, I demonstrate the existence of neural crest-derived DPSCs with differentiation capacity into cranial mesenchymal tissues and other neural crest-derived tissues. I also illustrate the potential of DPSCs as inductive mesenchyme for salivary gland regeneration, repair, and tissue engineering, and provide first insights into the mechanism(s) of DPSC angiogenic capacity and their function as pericytes. DPSCs hold promise as a stem cell source for regenerating neural

crest derived tissues, and the trophic and angiogenic properties of DPSCs also highlight this stem cell source useful for tissue regeneration.

DEDICATION

To His Majesty King Bhumibol Adulyadej of Thailand (King Rama IX)

My beloved father, mother, and sister

In memory of Dr. Asuman Kiyak (my former GSR)

ACKNOWLEDGEMENTS

First, I would like to sincerely express my deep gratitude to the Anandamahidol Foundation for giving me a great opportunity to come to the United States of America for pursuing my doctoral degree, and also providing me both financial and individual support throughout my doctoral study. This dissertation is dedicated to His Majesty King Bhumibol Adulyadej of Thailand, who founded the foundation, and Her Royal Highness Princess Maha Chakri Sirindhorn, the President of the Anandamahidol Foundation. I am perpetually under an obligation to both His Majesty and Her Royal Highness' generosity.

I am deeply indebted to my Ph.D. mentor and chair of my thesis supervisory committee, Dr. Morayma Reyes and Dr. Carol B. Ware for their tremendous help, advice, encouragement, and great care not only for the research but also my well being throughout the Ph.D. program. I would like to extend my sincerest thanks and appreciation to my thesis supervisory committee, Dr. Mark Cooper, Dr. Timothy Cox, Dr. Tracy Popowics, Dr. Linda LeResche, for their support, interest, guidance, valuable suggestions and discussion, which have been fundamental to this thesis project. It is my great opportunity and honor to be able to learn from many marvelous people in a superb environment. Their sense of humor and optimistic views always encourage me to not give up in my research project.

I would like to express my gratitude from the bottom of my heart to my beloved parents, Chaiyan Janebodin and Ornanong Peugtong, as well as, my beloved sister, Anocha Janebodin for their unconditional love, continuing support, unwavering understand, encouragement and inspiration. I gratefully thank the Department of Oral Health Sciences (OHS), Dr. Kenneth Izutsu, Dr. Thomas Morton Jr., Dr. Susan Herring, and Dr. Richard Presland, as well as OHS

staffs, Jennifer Kohn, Rosale Meriales, Eileen Kakida, for their assistance, generous support, and research facilities throughout my entire Ph.D. program. Furthermore, I would like to thank people in Somerman lab especially Dr. Brian Foster who was my first teacher when I did my first lab rotation, Dr. Kevin Tompkins, Dr. Thanaphum Osathanon, people in Institute for Stem Cell and Regenerative Medicine (ISCRM), Tom & Sue Ellison Stem Cell Core, Cunningham lab, Mahoney lab, Kim lab, and all collaborations for their research helps, facilities, and friendships.

Many thanks to current people in Reyes lab, Nicholas Ieronimakis, Aislin Hayes, as well as former members, Gayatri Balasundaram, Dr. Kanit Reesukumal, Dr. Busadee Pratumvinit, Dr. Kiran Srirangam, Dr. Leila Langston, and Dr. Sirisha Bhamidipaty for their friendship, encouragement, support, helpful dialogue, discussion, and suggestions.

On top of that, I am in debt to faculties and staffs in Department of Anatomy, Faculty of Dentistry, Mahidol University for teaching me the immeasurable knowledge and research techniques before entering graduate school. This benefits my life much easier to pass my doctoral study.

Without questions, I deeply thank to my families in Seattle, Shirley and Dean Hobson, Drs. Orapin and Jeremy Horst for their love and support. Many thanks to all of my beloved friends in Oral Biology program for their emotional support and arrangement of such many enjoyable extracurricular activities. Special thanks to my friends both in Thailand and Seattle, who teach me that my life is so beautiful during my Ph.D. study, make me smile and laugh, and always support me.

Words are no measure to describe the endurance and fortitude with which my beloved Noah M. Barnes and Jeffrey Campbell has encouraged and helped me get through the stressful task during the Ph.D. program enabling me to complete this thesis project.

This study was supported by funding from NIH, Department of Pathology and Laboratory Medicine, University of Washington.

TABLE OF CONTENTS

LIST OF FIGURES

LIST OF TABLES

CHAPTER 1

Introduction

Regenerative medicine means the use of biomedical or therapeutic strategies to restore cells, tissues, or organs with a given pathological condition by endogenous cell stimulation or exogenous cell transplantation with the goal of regaining normal function of that particular tissue or organ (Thesleff and Tummers, 2003). Although the regenerative mechanisms are not completely elucidated, the use of progenitor/stem cells or dedifferentiated cells have been proposed as potential cell populations for tissue regeneration (Riazi et al., 2009). In the past two decades, extensive work in regenerative medicine has focused on the use of stem cells (stem cell-based therapy) and their potential for regenerating damaged tissues and organs for clinical application (Egusa et al., 2012).

Stem cell-based therapy holds great potential to treat common health problems from illnesses, injuries, and diseases, including cardiovascular diseases (Mummery et al., 2003), autoimmune diseases (Mahevas et al., 2008), type I diabetes (Rolletschek et al., 2004), neurodegenerative diseases (Feng and Gao, 2012), spinal cord injuries (Mothe and Tator, 2012), bone and cartilage diseases or defects (Tapp et al., 2009), and cancer (Gudjonsson and Magnusson, 2005). In addition to their potential use to treat systemic diseases, stem cell-based therapy also provides a promising strategy to treat oral and dental diseases such as craniofacial defects, dental caries, periodontal disease, oral cancer, salivary gland and temporomandibular joint dysfunction, resulting in poor quality of life in patients (Mao, 2008).

The stem cell applications include: 1) direct differentiation to specific lineage of stem cells (cell therapeutic approach), 2) the induction of regeneration by biologically active exogenous or stem cell-secreted inducers (trophic approach), and 3) transplantation of *in vitro* expanded stem cells combined with a scaffold and growth factors (tissue engineering approach) (Egusa et al., 2012). The identification of a good source of stem cells is an important key for a successful stem cell-based therapy. Stem cells have been isolated from a variety of tissues and organs at different stages: prenatal, neonatal, and postnatal stages, which exhibit different stem cell capacities (Egusa et al., 2012).

In the last decade, stem cells isolated from oral tissues particularly tooth pulp, termed dental pulp stem cells (DPSCs), have extensively been favored among adult stem cell researchers due to their easy accessibility from biological wastes and less invasive procedure. Consequently, the research on DPSCs has been rapidly growing; however, a lot of questions remain to be elucidated. Therefore, a better understanding of the biology and nature of DPSCs will lead to fundamental knowledge in basic and clinical biology that can serve as a foundation for the use of this stem cell population in tissue regeneration.

In this dissertation I describe the isolation and characterization of DPSCs from neonatal mice *in vitro* and *in vivo*. In addition I describe the potential use of DPSCs as neural crest-derived ecto-mesenchyme to enhance salivary gland tissue formation, and pericyte-like cells to induce angiogenesis. As the mesenchyme is important for a functional epithelium and angiogenesis is pivotal for organogenesis and tissue regeneration, the studies herein demonstrating the DPSC capacity to function as supportive mesenchyme and to promote angiogenesis will broaden the clinical application of DPSCs as stem cell-based therapy in the future. In this dissertation, I will take you on a journey that first will briefly and concisely

illustrate the variety of stem cell types and sources, followed by an in depth description of my work on murine DPSCs and their potential use for clinical applications.

1.1 Definition of stem cells

Stem cells are defined as a primitive and undifferentiated cell population which exhibits three important characteristics (Slack, 2008, Hemmat et al., 2010). First, under asymmetrical division, stem cells can give rise to themselves to maintain their unspecialized or stem cell progeny, which is known as "self-renewal" whereas they also give rise to daughter cells which are more committed cells such as progenitor, precursor, or differentiated cells. Secondly, stem cells have the potential to develop into several specific cell types in the body or in specific differentiated cells *in vitro*, which is described as "multi-differentiation" capacity. Lastly, stem cells can reconstitute damaged tissues or regenerate new tissues that can function properly. Stem cells isolated from different tissues and from various developmental stages demonstrate different stem cell capacity. The classification and a brief description of different types of stem cells are discussed below.

1.2 Classification of stem cells

Stem cells can be classified by two criteria, their differentiation potency and origin. Based on the differentiation capacity, stem cells can be categorized into unlimited potency (totipotent and pluripotent), and defined potency (multipotent, bipotent, and unipotent). Based on their origin, two main sources of stem cells are generally described: embryonic stem (ES) cells and adult stem (AS) cells (Fig. 1.1) (Biehl and Russell, 2009, Egusa et al., 2012).

1.2.1 Stem cell classified by differentiation potency

Totipotent stem cells which are cells derived from the zygote (the fusion of an egg and a sperm) or the first few divisions of the fertilized egg (morula cells) can generate a whole new embryo including the extra-embryonic tissues such as placenta (Hemmat et al., 2010). Pluripotent stem cells, the descendents of totipotent stem cells, are derived from the inner cell mass within a blastocyst, a thin-walled hollow sphere with a fluid-filled cavity, which develops after cleavage and before implantation, in approximately 5 days. Pluripotent stem cells can give rise into cells of the three germ layers (ectoderm, mesoderm, and endoderm) excluding the placenta (Thomson et al., 1998). Multipotent stem cells can produce only differentiated cells from a closely related lineage system such as hematopoetic stem cells (differentiating into red blood cells, white blood cells, and platelets), mesenchymal stem cells (differentiating into bone cells, cartilage cells, and fat cells) (Crisan et al., 2009, Calvo et al., 2012). Bipotent and unipotent stem cells are stem cells with more limited differentiation capacities and can produce only two cell types or one cell type, respectively, but still have self renewal capacity which distinguishes them from non-stem cells (Cumano et al., 1992, Rossi et al., 2010)

1.2.2 Stem cell classified by tissue of origin

Stem cells can be isolated from embryonic and postnatal tissues, termed embryonic stem (ES) cells, and adult stem (AS) cells, respectively. In addition, another stem cell type which has recently been generated by genetic manipulation of somatic or adult stem cells is defined as induced pluripotent stem (iPS) cells.

1.3 Embryonic stem (ES) cells

ES cells are stem cells derived from the inner cell mass of developing preimplanted embryos (blastocysts) which have pluripotent differentiation capacity giving rise to cells from three different germ layers; ectoderm, mesoderm, and endoderm (Thomson et al., 1998). In addition to the expression of pluripotent genes and pluripotent differentiation capacity, ES cells exhibit high telomerase activity, resulting in unlimited expansion *in vitro,* and maintain a normal karyotype after multiple cell divisions (Trounson, 2006). Telomerase is an enzyme important for preserving the length of telomere on chromosomal DNA, which prevents the shortening of DNA during replication process (Trounson, 2006). The shortening of telomere due to the absence of telomerase is associated with the aging process (Trounson, 2006). Nevertheless, the presence of this enzyme has also been related to cancer formation (Hemmat et al., 2010). Another property of ES cells is that they can form *in vitro* embryoid bodies and generate *in vivo* teratomas; both of which are structures consisting of cells representing differentiated tissues from the three germ layers (Conley et al., 2004). Although ES cells have a great differentiation capacity into all somatic cell lineages, their embryonic origin is still the major concern as it relates to ethical and moral considerations (Wobus and Boheler, 2005). In addition, the use of ES cells in clinical application is hampered by their allogenicity, leading to immune rejection in allogeneic stem cell therapy. However, ES cells are an instrumental tool to develop *in vitro* model systems and transplantation protocols in animal models to study controlled differentiation of pluripotent stem cells into specific lineages, which is not only useful to better understand developmental biology but can also eventually lead to clinical applications (Egusa et al., 2012).

1.4 Adult stem (AS) cells

AS cells, which are derived from adult or postnatal tissues such as bone marrow, brain, skin, hair follicle, adipose tissue, muscle, dental pulp, and others are found in stem cell niches as self-renewing progenitor cells that are able to give rise into certain specialized cell types needed for maintainance of tissue/organ homeostasis (Biehl and Russell, 2009). AS cells are multipotent but usually give rise into only the cell type derived from their tissue of origin. However, several studies have previously reported that AS cells under certain circumstances exhibit greater differentiation capacity than expected and can differentiate into cells other than their tissues of origin. This phenomenon has being described as stem cell plasticity (Krause et al., 2001, Jiang et al., 2002, Grove et al., 2004, Kogler et al., 2004, Miki et al., 2005, Kadivar et al., 2006, Kerkis et al., 2006, Cho et al., 2008, Junker et al., 2010). Although the concept of stem cell plasticity in AS cells is still controversial, such potential has increased interest in adult stem cells. Unlike ES cells, AS cells are practical to manipulate and differentiate into the desired tissue without the ethical conflict. Therefore, AS cells are attractive stem cell sources for clinical applications. Several AS cells are found in the mesenchymal component of multiple tissues and defined as mesenchymal stem cells (MSCs), which are discussed next.

1.5 Mesenchymal stem cells (MSCs)

MSCs were first isolated and characterized *in vitro* from the bone marrow by their capacity to adhere on tissue culture plates, form colonies and differentiate to various mesenchymal tissues (Friedenstein et al., 1970, Pittenger et al., 1999, Horwitz et al., 2005). Since the populations of adherent cells isolated from the bone marrow are not homogeneous, and definitive markers for distinguishing MSCs have not yet been identified (Ishii et al., 2005),

markers expressed by MSCs are also applied to isolate a more pure cell population including CD44, CD105, CD73 and CD90 and excluding markers not expressed by MSCs such as of CD45, CD34, CD14 or CD11b, CD79α or CD19 and HLA-DR surface molecules (Horwitz et al., 2005). In addition, MSCs must be capable of differentiating to osteoblasts, adipocytes and chondrocytes *in vitro* (Dominici et al., 2006).

1.6 Induced pluripotent stem (iPS) cells

Induced pluripotent stem cells (Fig 1.2), known as iPS cells, were first generated from adult mouse and human dermal fibroblasts (Takahashi and Yamanaka, 2006, Takahashi et al., 2007). Both cell types can be reprogrammed to ES-like cells by retroviral transduction of four pluripotent genes; *Oct3/4, Sox2*, *c-Myc* and *Klf4.* The first iPS cells could create teratomas and form embryoid bodies, but mouse chimeras generated by blastocyst injection with those iPS cells could not survive after E13.5. DNA microarray also showed differential gene expression between iPS cells and ES cells, suggesting that such iPS cells were only partially reprogrammed. Subsequent studies attempted to improve the reprogramming methods by using the *Oct3/4* or *Nanog* selection process, and showed that iPS cells were very close to ES cells, also generated live chimeric mice (Maherali et al., 2007, Wernig et al., 2007).

After somatic stem cells are reprogrammed, the expression of specific proteins associated with pluripotent stem cells is detected such as *alkaline phosphatase* and *stage-specific embryonic antigen 1 (SSEA-1)* including increasing telomerase (Brambrink et al., 2008). iPS cells offer many benefits as the stem cell source for clinical applications, particularly in autologous transplantations (patient-specific cell transplantation therapies) and solving the problem of

ethical issues involved with ES cells. Nevertheless, there are some concerns that still need to be addressed for the clinical use of iPS cells.

The use of the *c-Myc* transgene during iPS cell generation can increase the likelihood of tumorigenesis in the mouse model (Takahashi et al., 2007). To circumvent this concern, iPS cell lines have been generated without *c-Myc* with no tumor formation but lower rate of reprogramming was observed (Nakagawa et al., 2008). *Lin28*, a protective transcription factor applied to induce iPS cells, is another successful approach (Yu et al., 2007). Additionally, small molecules such as RNA interferences (RNAi) or DNA modification enzyme inhibitors, have been recently reported that can increase the success rate of iPS cell generation (Mikkelsen et al., 2008, Anastasia et al., 2010). Adult stem cells isolated from adult mouse and human tissues including DPSCs express some embryonic stem cell markers such as *Oct4, Nanog, Sox2*, suggesting ESC-like potential (Kerkis et al., 2006, Ratajczak et al., 2007). These adult stem cells may be a good source for iPS cell generation as only partial reprogramming may be needed (Egusa et al., 2012).

1.7 Oral and dental stem cells

Oral and dental tissues have recently been shown to be good tissue sources of AS cells. Stem cells can be isolated from several oral tissues such as craniofacial bone, dental pulp, periodontal ligament, dental follicle, tooth germ, apical papilla, oral mucosa, gingival, and periosteum (Fig. 1.3) (Egusa et al., 2012). Nevertheless, stem cells derived from different oral and dental tissues exhibit different stem cell properties. Among oral tissue-derived AS cells, human dental pulp stem cells have been widely studied due to their great clinical potential, easy

accessibility and less invasive harvesting. However, there are still key issues needed to be optimized such as their variable biological capacity.

1.7.1 Craniofacial bone marrow stromal cells (BMSCs)

BMSCs can be isolated from craniofacial bones, maxilla and mandible, during dental surgical treatments such as wisdom tooth extraction, dental implant and orthodontic surgery. Clinical and animal studies have revealed that autologous bone grafts generated from craniofacial bone-derived BMSCs at craniofacial sites showed better results than that from the iliac crest, suggesting BMSC type and location has site-specific regenerative properties (Donovan et al., 1993, Crespi et al., 2007). The maxilla and mandible which are membranous bones derived from cranial neural crest cells while the iliac crest endochondral bone is mesodermal-derived (Chai et al., 2000). Differences in developmental origin of BMSC sources may affect their regenerative potential. A previous study showed that from the same patients craniofacial BMSCs showed higher proliferation and osteogenic differentiation capacity compared with the iliac crest BMSCs both *in vitro* and *in vivo*. The craniofacial BMSCs formed more membranous bone, whereas the iliac crest BMSCs formed more compacted bone with hematopoietic tissue, mimicking the nature of their tissue of origin. In addition, the adipogenic potential of craniofacial BMSCs is less than that of iliac BMSCs, which may decrease randomized fat formation during bone regeneration (Akintoye et al., 2006). Although craniofacial BMSCs may be beneficial for craniofacial bone regeneration, the volume of craniofacial bone marrow is still limited compared with that of iliac crest bone marrow (Han et al., 2009).

1.7.2 Dental tissue-derived stem cells

Epithelial stem cells and MSC-like cells are AS cells that have been characterized in dental tissues. A dental epithelial stem cell niche in teeth is located in the cervical loop of the incisor apex. Dental epithelial stem cells can differentiate into enamel-producing cells, ameloblasts. This niche may be specific to rodents because their incisors continuously erupt throughout their lives, which differs from human in which no information is available regarding the existence of dental epithelial stem cells (Harada et al., 1999).

The existence of dental-derived MSCs is demonstrated by evidence of new attachment of regenerated periodontal ligament and reparative dentine after injury or dental treatments (Schupbach et al., 1993, Kitamura et al., 1999). Nowadays, several MSCs have been isolated and extensively characterized from several sources of dental tissues: dental pulp stem cells (DPSCs), stem cells from exfoliated deciduous teeth (SHED), periodontal ligament stem cells (PDLSCs), dental follicle progenitor cells (DFPCs), tooth germ progenitor cells (TGPCs), and stem cells from apical papilla (SCAP), (Huang et al., 2009, Akiyama et al., 2012, Sedgley and Botero, 2012).

Dental pulp stem cells (DPSCs)

Adult human dental pulp stem cells (DPSCs) were first isolated and characterized in 2000 by Gronthos and Shi (Gronthos et al., 2000). These cells have phenotypic characteristics close to BMSCs and can form colony-forming unit-fibroblasts (CFU-Fs) with various characteristics such as morphology and cell densities, suggesting a different growth rate (Gronthos et al., 2002). Different cell morphologies were also observed within the same colony. DPSCs were able to give rise into osteo-odontogenic, adipogenic, neurogenic, chondrogenic, and myogenic differentiation *in vitro* (Gronthos et al., 2002, Laino et al., 2006, Zhang et al., 2006, d'Aquino et

al., 2007). Following *in vivo* transplantation mixed with hydroxyapatite/tricalcium phosphate (HAP/TCP), DPSCs formed ectopic dentin/pulp-like complex structures surrounded by a layer of odontoblast-like cells expressing dentin sialophosphoprotein (*DSPP*), which produces dentin containing dentinal tubules mimicking natural dentin in immunocompromised mice (Gronthos et al., 2000, Gronthos et al., 2002).

Stem cells from human exfoliated deciduous teeth (SHED)

MSC-like cells have been also isolated from the dental pulp of human deciduous teeth, named stem cells from human exfoliated deciduous teeth or SHED (Miura et al., 2003). Like DPSCs, SHED exhibit stem cell properties, such as self-renewal with higher proliferative rate, multi-differentiation *in vitro* and ability to form the dentin-like structures but without a complex formation *in vivo*. Interestingly, unlike DPSCs, SHED can recruit host cells to form a bone-like matrix with a lamellar structure, which may be explained by the nature of deciduous teeth, whose root resorption occurs by new bone formation surrounding the root (Miura et al., 2003). SHED can also repair critical-sized mouse calvarial defects with substantial bone formation, indicating their osteo-inductive potential (Seo et al., 2008). In addition to their osteo-induction, SHED can differentiate into dopaminergic neuronal-like cells and alleviate symptoms in the rat model of Parkinson's disease (Wang et al., 2010). The injection of human immature dental pulp stem cells (IDPSCs), another term for SHED, into mouse blastocysts showed that IDPSCs survived, proliferated, and differentiated in mouse developing blastocysts and were capable of producing human/mouse chimeras but in very low efficiency, suggesting their potent differentiation plasticity (Siqueira da Fonseca et al., 2009).

Periodontal ligament stem cells (PDLSCs)

Periodontal ligament stem cells (PDLSCs) can be identified from periodontal ligament such as from the root of extracted teeth (Seo et al., 2004). PDLSCs express the MSC-associated markers STRO-1, CDs, and scleraxis, a tendon-specific transcription factor, which is expressed at higher levels in PDLSCs than in DPSCs (Seo et al., 2004). PDLSCs demonstrate multi-potential differentiation *in vitro* by exhibiting osteogenic, adipogenic, and chondrogenic phenotypes under defined differentiation conditions, and the ability to regenerate cementum, periodontal ligament and alveolar bone in animal models (Seo et al., 2004, Seo et al., 2005, Gay et al., 2007, Singhatanadgit et al., 2009, Wang et al., 2011).

Dental follicle stem cells (DFSCs)

MSC-like cells have also been identified in the "developing" dental tissues, such as the dental follicle, tooth germ, and apical papilla. Dental follicle is an ecto-mesenchymal tissue surrounding the enamel organ and the dental papilla of the developing tooth germ prior to eruption. Isolation of DFSCs demonstrates that only a small number of single cells can attach onto the plastic surface and form CFU-F. DFPCs are fibroblast-like and express Nestin and Notch-1, suggesting the presence of undifferentiated cells. DFPCs demonstrate osteogenic differentiation capacity *in vitro* after induction. DFPC dorsal subcutaneous transplantation with HAP/TCP generates a fibrous or rigid tissue structure expressing high level of human-specific for bone sialoprotein (BSP) and osteocalcin (OCN) transcripts, but no expression of dentin, cementum, or bone formation was observed in the transplant, which could be due to the low number of transplanted cells (Morsczeck et al., 2005, Honda et al., 2010).

Tooth germ progenitor cells (TGPCs)

Stem cells in the dental mesenchyme of the discarded third molar tooth germ at the late bell stage, named tooth germ progenitor cells (TGPCs), showed high proliferation and the capability to differentiate *in vitro* into cells of three germ layers including bone cells, neurons and hepatocytes (Ikeda et al., 2008). The transplantation of TGPCs into rats with injured liver showed successful engraftment of the TGPCs in the recipient's rat and the prevention of liver fibrosis progression, contributing to the restoration of liver function (Ikeda et al., 2008).

Stem cells from the apical papilla (SCAP)

Stem cells from the apical papilla (SCAP) were found in the apical part of the roots of developing teeth (Sonoyama et al., 2006). Similar to DPSCs and SHED, SCAP can give rise into osteo-odontogenic and adipogenic lineages *in vitro*. Unlike DPSCs, SCAP significantly express high levels of CD24, and down-regulate its expression in response to osteogenic induction (Sonoyama et al., 2006, Huang et al., 2009). Undifferentiated SCAP show positive staining for several neural markers, suggesting their neurogenic potential (Sonoyama et al., 2008). SCAP were capable to differentiate into functional dentinogenic cells, and generate dentin/pulp-like complexes when transplanted into immuno-compromised mice as described for DPSCs (Sonoyama et al., 2006, Sonoyama et al., 2008). However, SCAP are derived from a developing tissue, suggesting that a population of early stem cells may be a better cell source for regenerative medicine, whereas DPSCs are derived from mature tissues (Huang et al., 2008).

Postnatal MSC-like dental stem cells exhibit self-renewal capacity and multi-differentiation potential into the odontogenic lineage. However, compared with bone marrow-derived MSCs, these stem cell populations can also differentiate to other cell lineages similar to, but different in potency from that of bone marrow-derived MSCs. As a result of their

accessibility, as these tissues are often discarded in the clinic as biological waste, these cells represent an attractive stem cell source for regenerative medicine.

1.7.3 Oral mucosa-derived stem cells

Two different types of human oral mucosa-derived AS cells have been characterized, oral epithelial stem cells and gingiva-derived MSCs (GMSCs). Oral epithelial stem cells are unipotent only developing into epithelial cells, but they exhibited clonogenicity and enable to regenerate a well-organized and highly stratified oral mucosal graft *ex vivo (Izumi et al., 2003)*. Human gingiva-derived MSCs (GMSCs) have been identified in the lamina propria of the gingiva overlying the alveolar ridges and retromolar region which is frequently excised during general dental treatments and considered as a discarded biological sample. GMSCs exhibited clonogenicity, self-renewal, high proliferation and a multi-differentiation capacity (Tomar et al., 2010). In addition, a multipotent neural crest stem cell, a subpopulation of GMSCs known as oral mucosa stem cells (OMSCs), have recently been reproducibly generated from the lamina propria of the adult human gingiva and can differentiate *in vitro* into the three germ layer lineages (Marynka-Kalmani et al., 2010).

1.7.4 Periosteum-derived stem cells

The periosteum is a dense irregular connective tissue covering the outer surface of bone tissue. The histology of periosteum exhibits two distinct layers. The outer layer primarily contains fibroblasts and elastic fibers whereas the inner layer contains MSCs, osteogenic progenitor cells, osteoblasts and fibroblasts, as well as microvessels and nerve innervation (Arnsdorf et al., 2009). Although periosteum-derived stem cells tend to differentiate into osteogenic lineage, these cells are capable of giving rise into osteoblasts, adipocytes and chondrocytes and express the typical MSC markers (Wang et al., 2010). In addition, single-cell-

derived adult human periosteal clones exhibit their multipotency since they differentiate to osteoblast, chondrocyte, adipocyte and skeletal myocyte *in vitro* and *in vivo* (De Bari et al., 2006). Thus, periosteum-derived cells could be beneficial for functional tissue engineering, particularly for bone regeneration.

1.8 Studies in DPSCs

Dental pulp is a loose connective tissue located in the central part of the tooth called pulp cavity. It contains heterogeneous cell populations which are derived from diverse origins and serve different functions; odontoblasts, fibroblasts, immune and inflammatory cells, undifferentiated mesenchymal cells, vascular and perivascular cells (Trowbridge, 2003). A cell population recently defined and proposed to play an important role in dentin regeneration is dental pulp stem cells (DPSCs) which was first discovered by Gronthos and his colleagues (Gronthos et al., 2000). DPSCs were isolated from human adult dental pulp and characterized as highly proliferative cells capable of self renewal, capable of differentiating into adipocytes and neuron-like cells *in vitro*, also forming a dentin/pulp-like complex structure *in vivo* (Gronthos et al., 2000, Gronthos et al., 2002). Several reports have expanded studies in DPSCs describing their capacity to form dental and bone tissues *in vitro* and *in vivo* (Laino et al., 2005, Shi et al., 2005, Laino et al., 2006, Nakashima et al., 2006, Cordeiro et al., 2008, Prescott et al., 2008, Zhang et al., 2008, Huang et al., 2009, Yang et al., 2009).

Initial studies described that DPSCs are heterogenous. Subsequent studies attempted to use clonogenic assays and several stem cell specific markers to isolate more pure cell population (Gronthos et al., 2002, Shi and Gronthos, 2003, Laino et al., 2005, Laino et al., 2006). Nevertheless, the ability to form dentin/pulp-like complexes *in vivo* among different clones of

DPSCs was inconsistent (Gronthos et al., 2002). Additionally, the multi-differentiation capacity of DPSCs *in vitro* and *in vivo* was unpredictable as described in several reports (Gronthos et al., 2000, Gronthos et al., 2002, Zhang et al., 2005, Huang et al., 2006, Laino et al., 2006, d'Aquino et al., 2007, Stevens et al., 2008, Ryu et al., 2009, Spath et al., 2009). Notch signaling, which is an important pathway to determine the fate of stem cells, may specify DPSC niches. Differential Notch expression was shown in different locations within the dental pulp, implying that dental pulp may contain various stem cell subpopulations with different proliferative-differentiation capacity and developmental origins (Lovschall et al., 2005). Alternatively, all DPSCs may derive from the same origin but their niche and location dictate their stem cell behaviors. Variability of the differentiation capacity among DPSCs clones or experiments led to question if there are different stem cell niches and populations in DPSCs. I pursued the study of this question which is fully described in Chapters 2 and 3. Based on the assumption that most cranial mesenchyme is derived from neural crest tissue, I used a neural crest reporter to study to the contribution of neural crest to DPSCs.

1.9 Neural crest contributions

Neural crest is a transient cell population located in between surface ectoderm and the dorsal part of neural tube which is formed during embryogenesis in vertebrate (Bronner-Fraser, 1993). Based on their migration pattern and final destination, neural crest is subdivided into cranial, trunk, vagal, sacral and cardiac neural crests. During development, neural crest cells can give rise to several specific cell types showing their multipotency (Fig. 1.4) (Le Douarin et al., 2004, Trainor, 2005, Wislet-Gendebien et al., 2012). Cranial neural crest (CNC) cells migrate to the first branchial arch and play a role in differentiation of dental mesenchyme in tooth

development (Chai et al., 2000). During oral epithelial-mesenchymal reciprocal interactions, signaling from the oral epithelium induces CNC-derived mesenchyme to develop into dental papilla cells and give rise to odontoblasts which secrete dentin matrix (Thesleff, 2003). In addition to odontoblast differentiation, CNCs can give rise to skeletal and connective tissue components of head and neck areas, as well as, neuron and glial cells in cranial ganglia (Bronner-Fraser, 1995, Abzhanov et al., 2003).

Although cells in the dental pulp are derived from neural crest and non-neural crest tissues during tooth development (Chai et al., 2000), the origin of DPSCs is still unclear. The Eph/ephrin expression and function on DPSCs, which play a crucial role in the neural crest migration, suggests that neural crest contributes to DPSCs (Stokowski et al., 2007). In the past, most of studies involving neural crest contribution were based on vital dye labeling, transplantation and viral transfection of neural crest cells and mostly happened in the avian system (Le Douarin and Teillet, 1973, Kuratani and Kirby, 1991, Murphy et al., 1991, Serbedzija et al., 1992). However, *ex-utero* culturing of embryos, microsurgical manipulation of embryonic tissue, and retaining the dye throughout the long period of embryological development was not potentially practical to obtain a systematic lineage tracing of neural crest derivatives in mammals. Furthermore, all neural crest cells might not be labeled using either dye labeling or viral infection approaches.

The isolation and characterization of DPSCs from specific cell-lineage transgenic mouse models provides comprehensive information to directly study the developmental origin of DPSCs. These lineage tracing studies, for obvious reasons, are not possible to perform in humans. Two transgenic approaches, *P0-Cre/ CAG-CAT-LacZ* (Yamauchi et al., 1999) and *Wnt1-Cre/R26R-LacZ* (Chai et al., 2000), demonstrated the application of the transgenetic

system to mark neural crest derivatives driven by *P0* and *Wnt1* promoters, respectively, during early embryogenesis. Compared to *Wnt1-Cre/R26R-LacZ*, the *P0-Cre/CAG-CAT-LacZ* mouse revealed incomplete expression of *LacZ* in neural-crest derived tissue with significant ectopic expression in notochord derived from non-neural crest origin.

The *Wnt1-Cre/R26R-LacZ* model used to trace neural crest contribution indicates that the majority of dental pulp cells are *Wnt1*-marked, with some contribution from unmarked *Wnt1*-non-neural crest cells (Chai et al., 2000). Stem cell populations in adult human dental pulp have been recently described based on the expression of low-affinity nerve growth factor receptor (LNGFR) and β1-integrin, suggesting that the former population is neural crest-derived (Waddington et al., 2009). Stem cells isolated from rat embryonic mandibular processes, of neural crest origin, showed multi-differentiation to neural and mesenchymal lineages suggesting DPSCs retain the differentiation capacity of embryonic progenitors (Zhang et al., 2006). Collectively, these reports urged me to investigate the origin of DPSCs. Although cells in dental pulp are derived from neural crest and non-neural crest tissues during tooth development, the origin of DPSCs is still unclear. Consequently, that DPSCs are only derived from neural crest is yet to be proven. A full description of the studies that I performed to answer this questions are included in Chapter 3.

1.10 Potential clinical applications of DPSCs

Suitable stem cells for tissue engineering should be able to differentiate into the target tissue/organ and should be easily collected and prepared, and possible immunomodulatory properties can be used to provide a further benefit to ensure the safety of the patient. DPSCs hold great clinical potential due to their differentiation capacity, easy accessibility and

immunomodulative property. I proceeded to study two potential clinical applications of DPSCs: 1) the use of DPSCs to serve as supporting ecto-mesenchyme for salivary gland tissue regeneration, and 2) the angiogenic potential of DPSCs for tissue regeneration.

1.11 Tooth and salivary gland developments

1.11.1 Tooth development

Tooth development begins in the late embryonic period with the formation of the ridge called labiodental lamina. Dental development begins through a thickening of dental lamina on this labiodental lamina that is oriented towards the oral cavity. Deciduous tooth buds develop in the lower and upper jaws on the labial side of the dental lamina, and later (16 weeks since post-ovulation) small permanent tooth buds also form on the oral side through interactions between neural crest and ectoderm (Fig. 1.5) (Ranly, 1998, Sharpe, 2001, Tucker and Sharpe, 2004, Honda et al., 2008).

Each tooth bud has an ectodermal-derived enamel organ that surrounds a neural crest-derived mesenchyme that forms the dental pulp. The edges of the enamel organ grow faster than the middle part, thereby forming a dental bell that arises from the tooth bud in a cap stage. The mesenchyme around the whole tooth bud also condenses and forms the dental follicle, then gives rise into the periodontium (periodontal ligament, cementum of the tooth root, and alveolar bone) (Diekwisch, 2001, McCollum and Sharpe, 2001).

An enamel organ structure contains an outer and an inner enamel epithelium. The enamel pulp is found between two layers of enamel epithelium. The enamel epithelium is nourished by a capillary network from the outside while the enamel pulp always remains vessel-free. The ectodermal-derived ameloblast layer, which forms out of the inner enamel epithelium, produces

the enamel. The neural crest-derived mesenchyme that lies below the inner enamel epithelium organizes itself into the odontoblast layer, which secretes predentin towards the outside. Dentin then arises through calcium deposition in the predentin (Sharpe, 2001, Thesleff, 2003).

After the complete tooth crown formation, the tooth root is formed in the region called Hertwig's epithelial sheath, which is located in the fold between the inner and outer enamel epithelium and no enamel is produced (Diekwisch, 2001, Thesleff, 2003).

1.11.2 Salivary gland development

The human and murine salivary gland systems consist of three pairs of major salivary glands: parotid, submandibular, and sublingual. These glands secrete serous, mucous or mixed saliva via the excretory ducts connecting the openings in the oral cavity. The salivary glands play a major role as exocrine glands to secrete saliva for lubrication, digestion, immunity, and maintenance of homeostasis within the body. However, salivary glands also show an endocrine function by the production of parotin and a variety of cell growth factors (Denny et al., 1997, Amano et al., 2012).

Although murine salivary glands share several similar characteristics with human salivary glands, some differences of these glands between two species are also demonstrated. First, submandibular glands in mice are the largest salivary glands, which differs from humans whom parotid glands are the biggest salivary glands in size. This may be explained by the fact that in mice submandibular salivary glands develop faster than either of the other major salivary glands, in terms of both prenatal morphogenesis and its postnatal accumulation of secretory proteins (Redman and Sreebny, 1971, Lawson, 1972). Second, the histology of murine salivary glands, but not human salivary glands, demonstrates the presence of granular convoluted tubules (GCTs) producing a variety of cell growth factors. The GCT is located between the intercalated

duct and striated duct and well-developed in the murine submandibular gland (Amano et al., 2012). Third, in humans and mice both parotid and sublingual glands are pure serous and sero-mucous glands, respectively. However, the human submandibular gland is a mixed gland composed of both serous and mucous acinar cells whereas the murine one has only the serous type (Amano et al., 2012).

The salivary gland development begins in the later embryonic period. The first sign is a thickening of the oral epithelium on the side of the tongue, outside the dental lamina, followed by branching morphogenesis of the gland (Denny et al., 1997). The interaction of epithelium and mesenchyme is essential for branching morphogenesis of the salivary gland. (Fig. 1.6) (Okumura K, 2012) The salivary gland epithelium of the parotid glands is ectoderm-derived whereas the epithelium of the submandibular and sublingual glands is endoderm-derived. The salivary gland mesenchyme is neural crest-derived (Jaskoll et al., 2002, Yamamoto et al., 2008).

1.11.3 Similarities between tooth and salivary gland development

The development of the tooth shares many similarities with that of the salivary gland. Each tooth demonstrates an independently developing organ system with its own timetable and unique characteristics, as well as many characteristics common to all teeth. Therefore, we speculate that an analogous complex pattern of tooth morphogenesis may share some common characteristics to the early specification of salivary gland formation.

For instance, the epithelial-mesenchymal interactions in tooth and salivary gland formation are similar and molecular cues such as secretion of fibroblast growth factors (FGF-10, FGF-7) by the ecto-mesenchyme and expression of FGF receptors (FGFR-1, FGFR-2) by the epithelium are important for both the development of tooth bud and salivary gland (Hoffman et al., 2002, Jaskoll et al., 2002, Jaskoll et al., 2004, Jaskoll et al., 2005, Madan and Kramer, 2005,

Patel et al., 2006, Yamamoto et al., 2008). Also important morphogens such as Shh, Wnt and FGFs seem to play important roles in tooth bud and saliva gland development (Jaskoll et al., 2004, Dang et al., 2009, Hai et al., 2010).

1.12 Salivary gland regeneration

Salivary hypofunction and xerostomia (dry mouth) can result from local surgery, radiotherapy for head and neck cancer, Sjogren's syndrome, and side effects of certain medications. Hypo-salivation can result in aggressive dental caries and oral ulcers, as well as problems in swallowing and a poor quality of life (Napenas et al., 2009). Recently, stem cell-based therapy has been introduced as a promising therapeutic strategy to restore or regenerate functional salivary gland tissues.

The existence of salivary gland stem cells has been suggested by *in vivo* experimental models (Man et al., 2001). However, a single stem cell that gives rise to all epithelial cell types within the gland has not yet been identified. Salivary gland stem cells were isolated from rat submandibular glands and found that the cells were highly proliferative and expressed acinar, ductal and myoepithelial cell lineage markers (Kishi et al., 2006). An *in vitro* floating sphere culture was used to isolate a specific population of cells expressing stem cell markers from murine submandibular salivary glands. *In vitro* differentiation revealed that these cell populations differentiated into salivary gland duct cells as well as mucin- and amylase-producing acinar cells. In addition, the intra-glandular transplantation of these successfully rescued the function of irradiated salivary glands (Lombaert et al., 2008, Feng et al., 2009, Nanduri et al., 2011). These reports suggest that the salivary gland is a promising stem cell source for future therapies in patients with irradiated head and neck cancer. However, primary cultures of

dissociated cells will always contain a heterogeneous cell population with different origins, such as epithelial parenchymal cells, mesenchymal stromal cells, blood vessel cells, and nerve cells, which makes it difficult to select salivary gland stem cells. Additionally, primitive MSC-like cells were isolated from the human salivary gland, but potentially from salivary gland stroma, which expressed embryonic and adult stem cell markers and could be guided to differentiate into mesenchymal lineage (adipogenic, osteogenic and chondrogenic) *in vitro* (Gorjup et al., 2009).

Tissue engineering for salivary gland restoration is limited by availability of stem cells or cell sources capable of providing all the cellular components necessary to generate a functional salivary gland tissue. Furthermore, vascularization and innervation of engineered salivary gland tissue is a long-lasting challenge. In Chapter 4, based on the reviews in salivary gland development and regeneration as well as tooth development, I will describe the studies I performed to gain insights into the capacity of DPSCs to serve as ecto-mesenchyme for salivary gland tissue regeneration.

1.13 Dental pulp, pericyte, and angiogenesis

Dental pulp is a loose connective tissue, containing heterogeneous cell populations, fibers, ground substance, blood vessels, and nerve innervations. Dental pulp is enclosed within rigid dentin walls and forms with the dentin. The pulp cells are continuously interacting with the extracellular matrix (ECM), which explains the physiologic properties of this tissue. Pulp cell can proliferate and differentiate in response to growth factors, which regulate cell survival and behavior (Trowbridge, 2003).

During primary dentinogenesis, a rich vasculature develops in the odontogenic zone of the dentine–pulp complex, showing increased vessel fenestration for odontoblast nourishment.

After dentine formation is completed, vessel fenestration decreases and withdraws from the odontoblastic layer, so that, the capillary network is found in the sub-odontoblastic layer in close relationship to odontoblasts in the mature tooth (Yoshida and Ohshima, 1996). Angiogenesis is crucial for organogenesis, wound healing and the regenerating process in all tissues, including pulp development, repair or regeneration (Madeddu, 2005). During pulp repair, the sub-odontoblastic capillary plexus appears to reorganize responding to a specific reparative dentin formation (Kitamura et al., 1999, Roberts-Clark and Smith, 2000, Tran-Hung et al., 2006).

Pericytes are a cell population located at the interface between endothelial cells and surrounding tissues, and play an active role in vasculogenesis and angiogenesis, aka neovascularization (Allt and Lawrenson, 2001). Pericytes are defined by their location adjacent to micro-vessels. Some markers, although not completely specific for pericytes, such as alpha-SMA, RGS5, nestin, NG2, and PDGFR-B have been used to identify pericyte cells (Nehls and Drenckhahn, 1993, Cho et al., 2003, Dore-Duffy et al., 2006, Huang et al., 2010, Winkler et al., 2010). Previous studies have shown that pericytes may act to promote new blood vessel formation from pre-existing blood vessels, angiogenesis by responding to physiological/angiogenic stimuli and signaling endothelial cells to form new vessels. In addition to paracrine signaling and induction, pericytes may function via direct cell-cell interaction controlling endothelial cell proliferation, migration and differentiation, thereby extending blood vessel length (Gerhardt and Betsholtz, 2003). In some diseases such as cancer, diabetic microangiopathy, tissue fibrosis, atherosclerosis and Alzheimer's disease, pericytes dysfunction resulting in pathological angiogenesis is manifested (Robison et al., 1991, Xian et al., 2006, Dalkara et al., 2011).

Angiogenesis (neo-vascularization) is the new capillary formation from pre-existing micro-vessels. The formation of blood vessels is a complex and multistep process involving a series of cellular events, extracellular matrix remodeling, proteolytic enzyme secretion, endothelial cell migration and proliferation, capillary formation, and branching. Angiogenesis is essential to many events, such as embryogenesis, wound healing and repair, and pathological processes that involve blood vessel growth such as inflammation and tumor growth (Armulik et al., 2005, Bergers and Song, 2005, Madeddu, 2005).

Angiogenesis is initiated and regulated by abundant cytokines and angiogenic growth factors which can have either a positive or negative regulation (Gerhardt and Betsholtz, 2003, Madeddu, 2005, Ribatti, 2005, Ahmad et al., 2011). Those factors may act either directly to regulate endothelial cell function or indirectly to regulate growth-factor expression by other cell types. Among all the pro-angiogenic stimuli, vascular endothelial growth factor (VEGF) is considered the most important for the differentiation of the vascular system (Ferrara and Henzel, 1989, Ferrara et al., 2003). Pulp cells express VEGF in healthy and pathological situations such as irreversible pulpitis, suggesting a role for pulp cells in angiogenesis (Tran-Hung et al., 2006). However, the nature and origin of the angiogenic stimuli in these reparative states are still unclear. In Chapter 5 I present my studies about the angiogenic capacity of pericyte-like DPSCs both *in vitro* and *in vivo*.

1.14 Vascular endothelial growth factors (VEGF) and its receptors

1.14.1 VEGF ligands

VEGF, a 45-kDa heparin-binding glycoprotein, induces the differentiation, proliferation, invasion, and migration of endothelial cells, as well as vascular permeability and cell survival

(Ferrara and Henzel, 1989, Grando Mattuella et al., 2007). The VEGF family of proteins currently includes 5 structurally related members: VEGF-A, -B, -C, -D, -E, and platelet-derived growth factor (PDGF). VEGF-A and VEGF-B are intimately related to angiogenesis whereas VEGF-C and VEGF-D play an important role in lymphangiogenesis.

Vascular endothelial growth factor-A (**VEGF-A**) specifically functions on endothelial cells and has multiple effects, including increasing vascular permeability, inducing angiogenesis, vasculogenesis and endothelial cell growth, promoting cell migration, and inhibiting apoptosis of endothelial cells (Grando Mattuella et al., 2007). The alternative messenger RNA (mRNA) splicing of a single gene involving eight exons codifies a large number of VEGF isoforms, with polypeptide subunits containing 121, 145, 165, 189, and 206 amino acids (Ribatti, 2005). Among the five presented isoforms, VEGF165 is the most abundantly found and functions to stimulate endothelial cell growth (Grando Mattuella et al., 2007). VEGF-A activity has been studied mostly on endothelial cells; however, it has effects on other cell types such as monocyte/macrophage, neurons, tumor cells, kidney epithelial cells (Ferrara et al., 2003). VEGF-A has been shown to stimulate endothelial cell mitogenesis and cell migration *in vitro* (Ribatti, 2005). VEGF-A is also a vasodilator, vascular permeability factor, and increases microvascular permeability (Ribatti, 2005). VEGF-A gene mutations have been associated with diabetic retinopathy (Watanabe et al., 2005). Expression of VEGF-A is induced by myocardial ischemia and a higher level of expression of VEGF-A has been associated with better collateral circulation development during ischemia, suggesting VEGF-A as a potential therapeutic strategy of ischemic heart disease (Banai et al., 1994, Chalothorn et al., 2007). VEGF-A induces angiogenesis by binding to the cell surface receptors VEGFR-1 and VEGFR-2, two tyrosine kinases located in endothelial cells (Huusko et al., 2010). The binding of VEGF-A to VEGFR-2

results in the dimerization of VEGFR-2. Subsequently, the receptor itself auto-phosphorylates, which allows an activation of signal transduction within the cell through the nucleus such as the mitogen-activated protein kinase (MAPK/ERK) signaling (Dougher-Vermazen et al., 1994, Khokhlatchev et al., 1998). Unlike the tyrosine kinase activity of VEGFR-2, that of VEGFR-1 is less efficient, and its activation alone is not sufficient to mediate the proliferative effects of VEGF-A (Seetharam et al., 1995). However, the primary role of VEGFR-1 is to recruit the cells responsible in blood cell development (Shibuya, 2001).

Vascular endothelial growth factor-B (**VEGF-B**) plays a less important role in the vascular system. VEGF-B seems to function in the maintenance of new blood vessel formation during pathological conditions (Zhang et al., 2009). In addition, VEGF-B plays an important role on several types of neurons (Falk et al., 2009), and control endothelial uptake and transport of fatty acids in cardiac and skeletal muscles (Lahteenvuo et al., 2009, Wafai et al., 2009). VEGF-B exerts its effects via binding with VEGFR-1 (Li et al., 2009).

Vascular endothelial growth factor-C (VEGF-C) is important in angiogenesis, lymphangiogenesis, endothelial cell growth and survival, and can also affect the vascular permeability (Orpana and Salven, 2002). The secreted VEGF-C effectively binds and activates VEGFR-3. However, only the fully processed form of VEGF-C can bind and activate VEGFR-2 (Grando Mattuella et al., 2007). The over-expression of VEGF-C can result in the enlargement of lymphatic vessels and possibly enhance metastasis (Ohno et al., 2003).

Vascular endothelial growth factor-D (**VEGF-D**) functions similarly to VEGF-C in angiogenesis, lymphangiogenesis, and controls the growth of endothelial cells. VEGF-D binds and activates VEGFR-2 and VEGFR-3 (Grando Mattuella et al., 2007). However, the interaction between VEGF-D and VEGFR-3 predominantly expressed in lymphatic vessels plays a crucial

role in restructuring lymphatic system, thereby altering its functions related to fluid and cell transportation. Like VEGF-C, the over-expression of VEGF-D has been shown in several types of tumor tissues in human (Lin et al., 2012).

1.14.2 VEGF receptors

VEGF receptors are expressed on the surface of vascular endothelial cells. They are of the tyrosine-kinase (RTK) type and are present in three forms: the fms-like tyrosine-kinase-1 (Flt-1) or VEGFR-1; the fetal liver kinase-1 (Flk-1 in mouse), kinase domain region (KDR in human) or VEGFR-2; and the fms-like tyrosine-kinase-4 (Flt-4) or VEGFR-3 (Ribatti, 2005, Grando Mattuella et al., 2007). They also interact with a co-receptor family, the neuropilins (NRP) to increase the effectiveness of the signal transduction (Ferrara, 2001). These receptors possess different signal transduction properties and mediate different functions because of their distinct affinity to VEGF ligands (Ferrara, 2005). The receptors show an overlapping but distinct expression pattern. However, there is still a predominant pattern of VEGFR-1 expression in monocytes and macrophages, VEGFR-2 in vascular endothelial cells, and VEGFR-3 in lymphatic endothelial cells (Fig. 1.7) (Grando Mattuella et al., 2007, Hadj-Slimane et al., 2007). In response to VEGF, VEGFR-2 undergoes tyrosine phosphorylation and mediates cell proliferation, migration, and vascular permeability whereas VEGFR-1 has a weak response. The VEGF produced by human pulp cells acts in an autocrine manner and promotes chemotaxis, cell proliferation, and/or differentiation of endothelial cells (Matsushita et al., 2000). This action is mediated by VEGFR-2 although both receptors (VEGFR-1 and VEGFR-2) are present in pulp cells.

VEGFR-1 signaling

VEGFR-1 is expressed by a broad range of cell types, and its kinase activity is weak and not required for endothelial cell function. On the other hand, VEGFR-1 functions mainly as a negative regulator for VEGFR-2 by binding VEGF, thereby regulating monocyte migration during inflammation (Ferrara, 2001, Shibuya, 2001, Ferrara et al., 2003). VEGFR-1 binds VEGF-A, VEGF-B, and PDGF. VEGFR-1 exists as a full-length form and an alternatively spliced, soluble form (sFlt or sFlt-1) (Kendall and Thomas 1993). Full-length and soluble VEGFR-1 both bind VEGF-A with higher affinity than does VEGFR-2. Binding of VEGF-A to VEGFR-1 may therefore prevent activation of VEGFR-2. Consequently, sFlt-1 has been implicated as a negative regulator of angiogenesis (Ambati et al., 2006, Ambati et al., 2007, Ponticelli et al., 2008). VEGFR-1 appears not to be required as a signaling receptor in endothelial cells. Instead, VEGFR-1 may serve to capture VEGF to control VEGFR-2 signaling and angiogenesis (Kappas et al., 2008).

VEGFR-2 signaling

VEGFR-2 is the main VEGF receptor important for endothelial cell functions during development and in the adult, in physiological and pathological conditions. VEGFR-2 binds VEGF-A, but with a lower affinity than VEGFR-1 (Koch et al., 2012). In contrast to VEGFR-1, VEGFR-2 also binds VEGF-C and VEGF-D (Grando Mattuella et al., 2007). VEGFR-2 is alternatively spliced to a soluble VEGFR-2 (sVEGFR-2), which is found in various tissues such as the skin, heart, spleen, and kidney, and binds VEGF-C to prevent binding to VEGFR3, consequently inhibiting lymphatic endothelial cell proliferation (Albuquerque et al., 2009). VEGFR-2 is expressed in endothelial cells and their precursors, with highest expression during vasculogenesis and angiogenesis (Millauer et al., 1993) and during pathological stages such as

tumor angiogenesis (Millauer et al., 1994). VEGFR-2 is the main mediator of VEGF-A effects on endothelial cell differentiation, proliferation, migration, and formation of the vascular tubes. VEGF-A stimulates endothelial proliferation through VEGFR-2 via the RAS/RAF/ERK/MAPK pathway (Zachary, 2001).

VEGFR-3 signaling

VEGF-C/VEGFR-3 are critical regulators of lymphangiogenesis (Orpana and Salven, 2002). Loss-of-function VEGFR-3 mutants in humans cause lymphedema. In addition, VEGFR-3 is expressed in vascular endothelial cells and becomes up-regulated during active angiogenesis. VEGFR-3 forms homodimers as well as heterodimers with VEGFR-2. VEGFR-3 binds VEGF-C and VEGF-D (Koch et al., 2012).

Angiogenesis is a natural phenomenon which is important for tissue repair and regeneration including dentin/pulp repair and regeneration. Although several studies have investigated the role of VEGF in the dental pulp tissue and showed that VEGF signaling is mediated by VEGFR-2, the angiogenic function of VEGF signaling in DPSCs is still undetermined. In Chapter 5 I present my studies involving the angiogenic capacity of DPSCs, and demonstrate that the angiogenic induction by pericyte-like DPSCs is dependent on VEGF signaling.

1.15 Summary

Stem cell-based therapy holds a great promise to solve health problems from both systemic and oral diseases. The identification of a good stem cell source is a major key for a success in tissue regeneration. Although stem cells can be isolated from a variety of tissues at various developmental stages with different stem cell capacities, adult stem (AS) cells are

attractive multipotent stem cell sources for clinical applications without ethical concerns. Human dental pulp stem cells (DPSCs), dental tissue-derived AS cells, have been widely studied due to their great clinical potential as a mesenchymal stem cell source, easy accessibility and less invasive harvesting. Since the first discovery of DPSCs in 2000, studying in DPSCs grows rapidly. Nevertheless, there are still questionable issues needed to be optimized and answered such as the variable biological capacity of DPSCs. Variability of the differentiation capacity among DPSCs clones or experiments urged me to address if there are different stem cell niches and populations from different origins in DPSCs.

Oral tissue engineering such as salivary glands is a potential clinical approach to treat salivary gland dysfunction such as xerostomia or irradiation-induced salivary gland in patients with oral cancers. However, the integration cellular components, vascularization and innervation is necessary to generate a functional salivary gland tissue. Due to similarities between tooth and salivary gland formation, DPSCs are proposed as potential ecto-mesenchyme supportive cells for salivary gland formation.

Angiogenesis is crucial for organogenesis, wound healing and the regenerating process in all tissues, including dentin/pulp regeneration. DPSCs are located in the perivascular niche and play an important role in dentin/pulp regeneration via angiogenesis, suggesting their pericyte-like characteristics. However, no direct study has proven the angiogenic capacity of pericyte-like DPSCs.

In summary, I pursued the characterization of neural crest-derived murine DPSCs and studied two potential clinical applications of DPSCs: the use of DPSCs to serve as supporting ecto-mesenchyme for salivary gland tissue regeneration and the angiogenic potential of DPSCs

for tissue regeneration. Better understanding of DPSC nature and biology will provide more basic knowledge, and broaden the use of DPSCs in clinical applications.

In this dissertation I will introduce my research goal during my graduate training including three specific aims, underlying hypotheses, and research strategies. Then, I will present the experimental studies and results demonstrating the characterization of neural crest-derived DPSCs in murine neonatal mice. Subsequently, two potential biological capacities of DPSCs in clinical applications will be discussed both *in vitro* and *in vivo*. The use of DPSCs to serve as supporting ecto-mesenchyme for salivary gland tissue regeneration will first be determined, followed by the angiogenic potential of DPSCs for tissue regeneration. Lastly I will review my research objectives, results, conclusions, and discussion about direction of future studies and clinical applications.

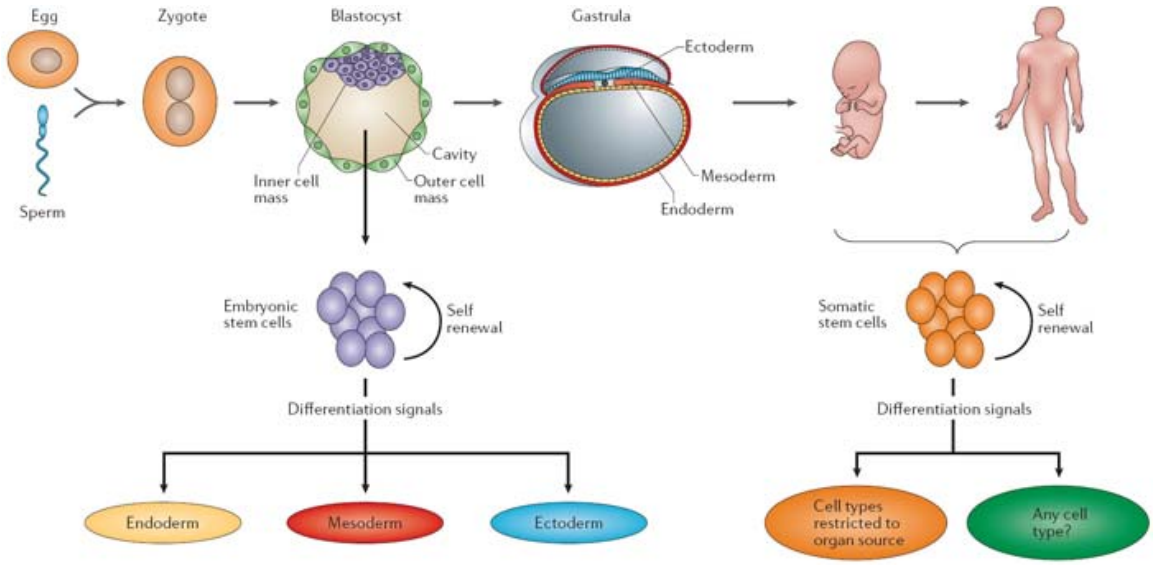

Figure 1.1 Classification of stem cells by tissue of origin: embryonic and adult (somatic) stem cells (O'Connor and Crystal, 2006). See details in sections 1.3 Embryonic stem cells, and 1.4 Adult stem cells.

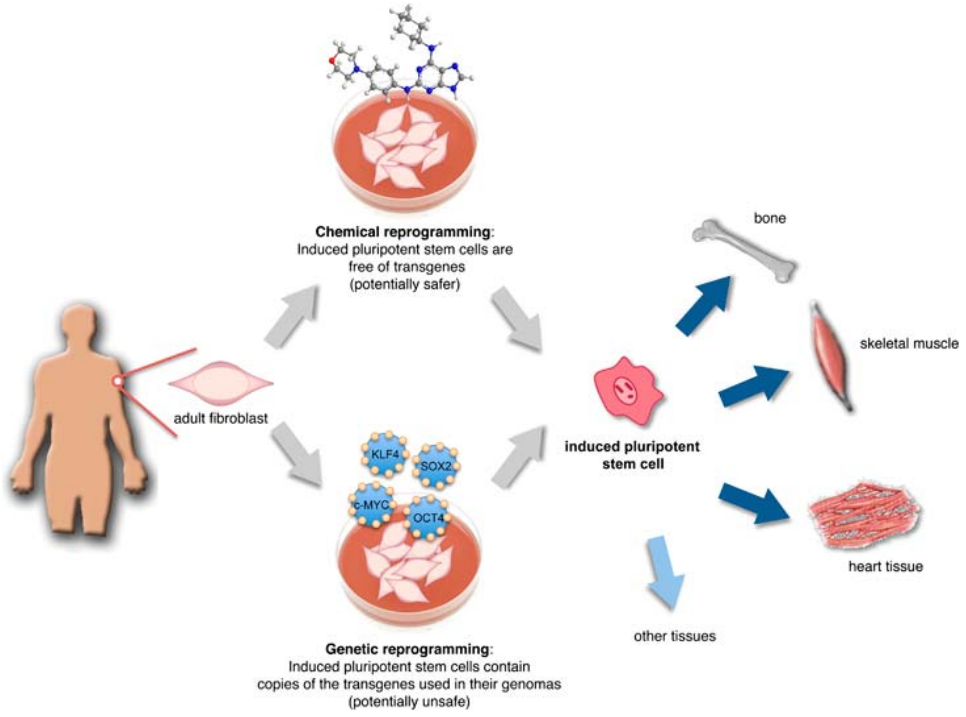

Figure 1.2 Induced pluripotent stem (iPS) cells are considered as a new source of patient-specific pluripotent cells for regenerative medicine (Anastasia et al., 2010). Details are discussed in section 1.6

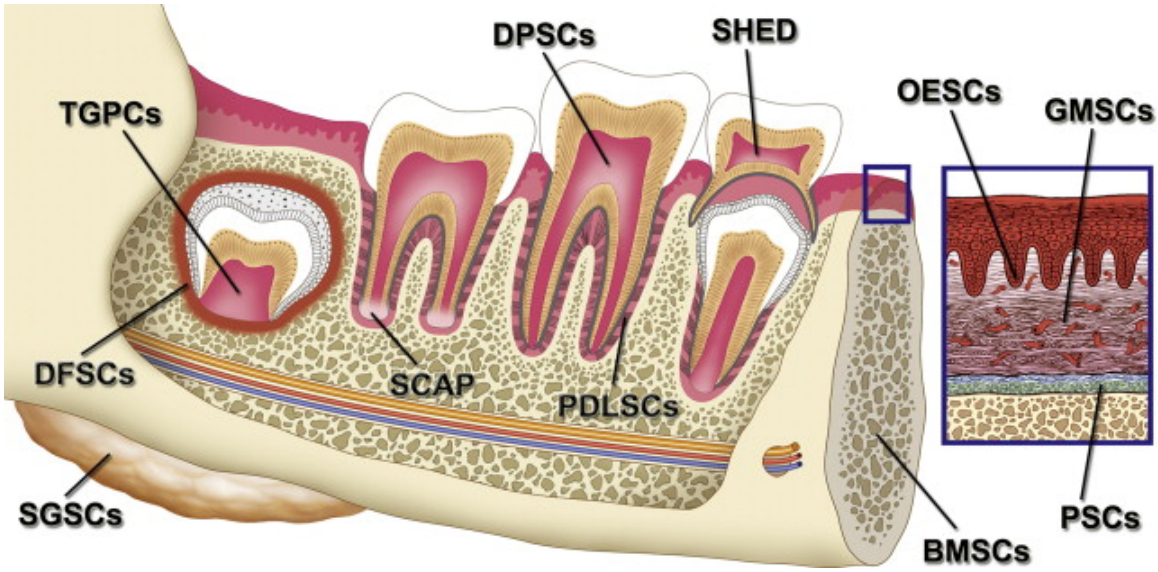

Figure 1.3 Sources of oral and dental tissues-derived adult stem cells. BMSCs: bone marrow-derived MSCs from orofacial bone; DPSCs: dental pulp stem cells; SHED: stem cells from human exfoliated deciduous teeth; PDLSCs: periodontal ligament stem cells; DFSCs: dental follicle stem cells; TGPCs: tooth germ progenitor cells; SCAP: stem cells from the apical papilla; OESCs: oral epithelial progenitor/stem cells; GMSCs: gingiva-derived MSCs; PSCs: periosteum-derived stem cells; SGSCs: salivary gland-derived stem cells (Egusa et al., 2012). See details in section 1.7 Oral and dental stem cells.

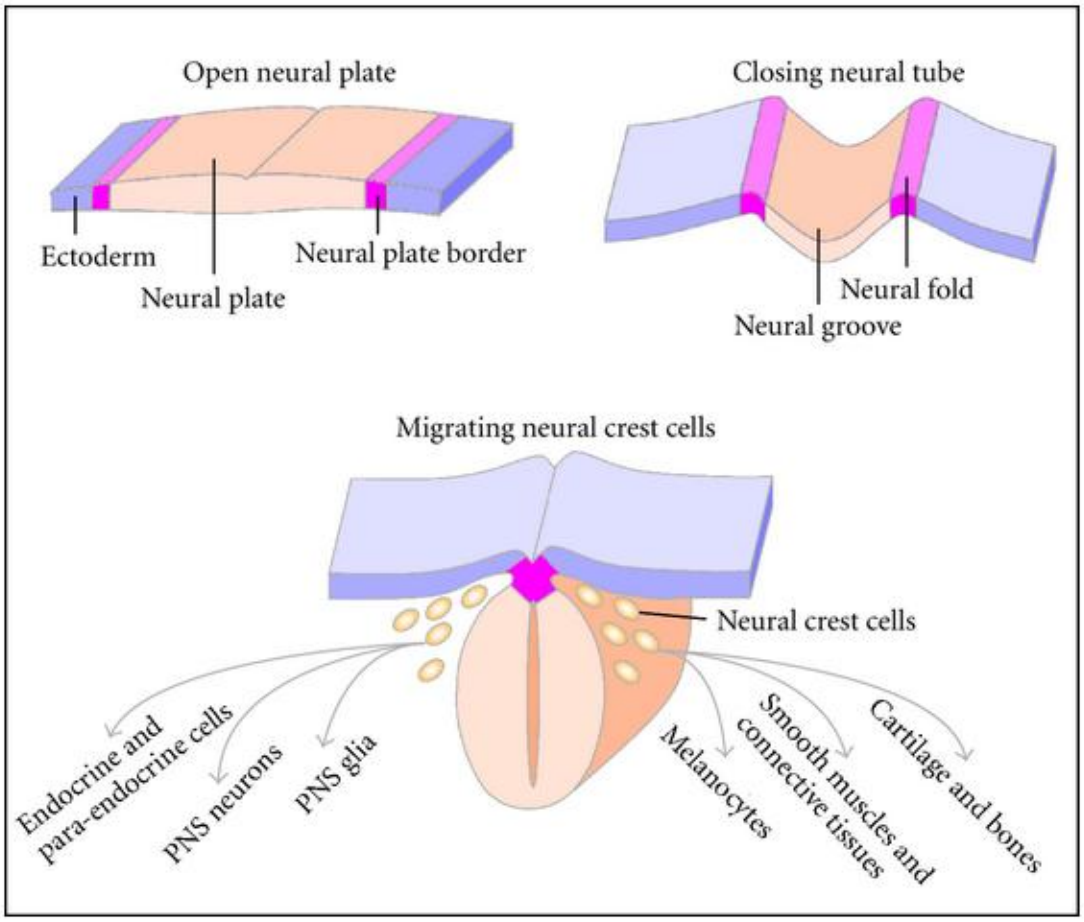

Figure 1.4 Neural crest migration and contribution (Wislet-Gendebien et al., 2012). See details in section 1.9 Neural crest contributions.

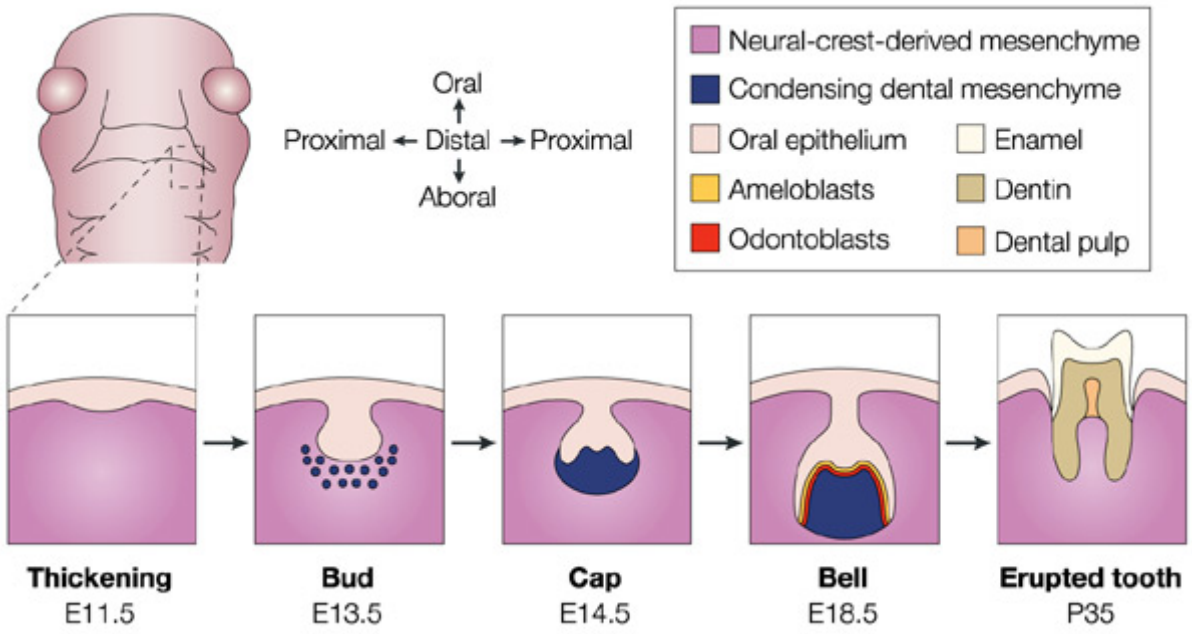

Figure 1.5 Brief overview of tooth development. A schematic frontal view of an embryo head at embryonic day (E) 11.5 is demonstrated with a dashed box to indicate the site where the lower molars will form. Below, the stages of tooth development are shown from the first signs of oral epithelium thickening at E11.5 to eruption of the tooth at around 5 weeks after birth. The tooth germ is formed by the interaction between oral epithelium and neural-crest-derived mesenchyme. At the bell stage of development, the ameloblasts and odontoblasts form in adjacent layers at the site of epithelial-mesenchymal interaction, and produce the enamel and dentin in the tooth, respectively (Tucker and Sharpe, 2004).

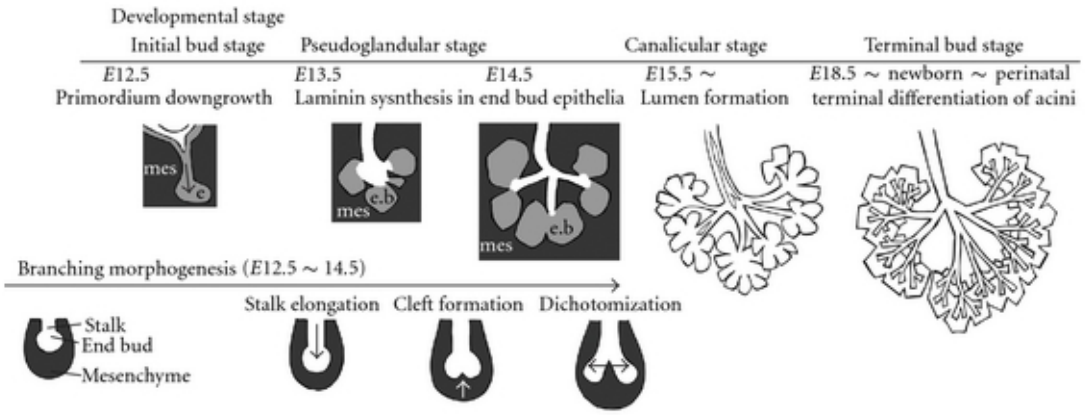

Figure 1.6 Brief overview of salivary gland development in mice. Schematic diagram of the 4 stages of salivary gland development: initial bud, pseudoglandular, canalicular, and terminal bud stages. Laminin-producing epithelia in end buds are indicated in light grey (pseudoglandular stage). Laminin-producing epithelia are only present in end buds but not in the stalk portion and interact with neural crest-derived mesenchyme to form branching structures during branching morphogenesis. A schematic diagram of the 3 steps in branching morphogenesis, stalk elongation, cleft formation, and dichotomization is also shown. Salivary mesenchyme is indicated in dark grey, and epithelia in white. The epithelial-mesenchymal interaction enhances the branching morphogenesis in salivary gland. See text in section 1.11.2. Abbreviations: mes: mesenchyme; e: epithelium; e.b: epithelial bud (Okumura K, 2012).

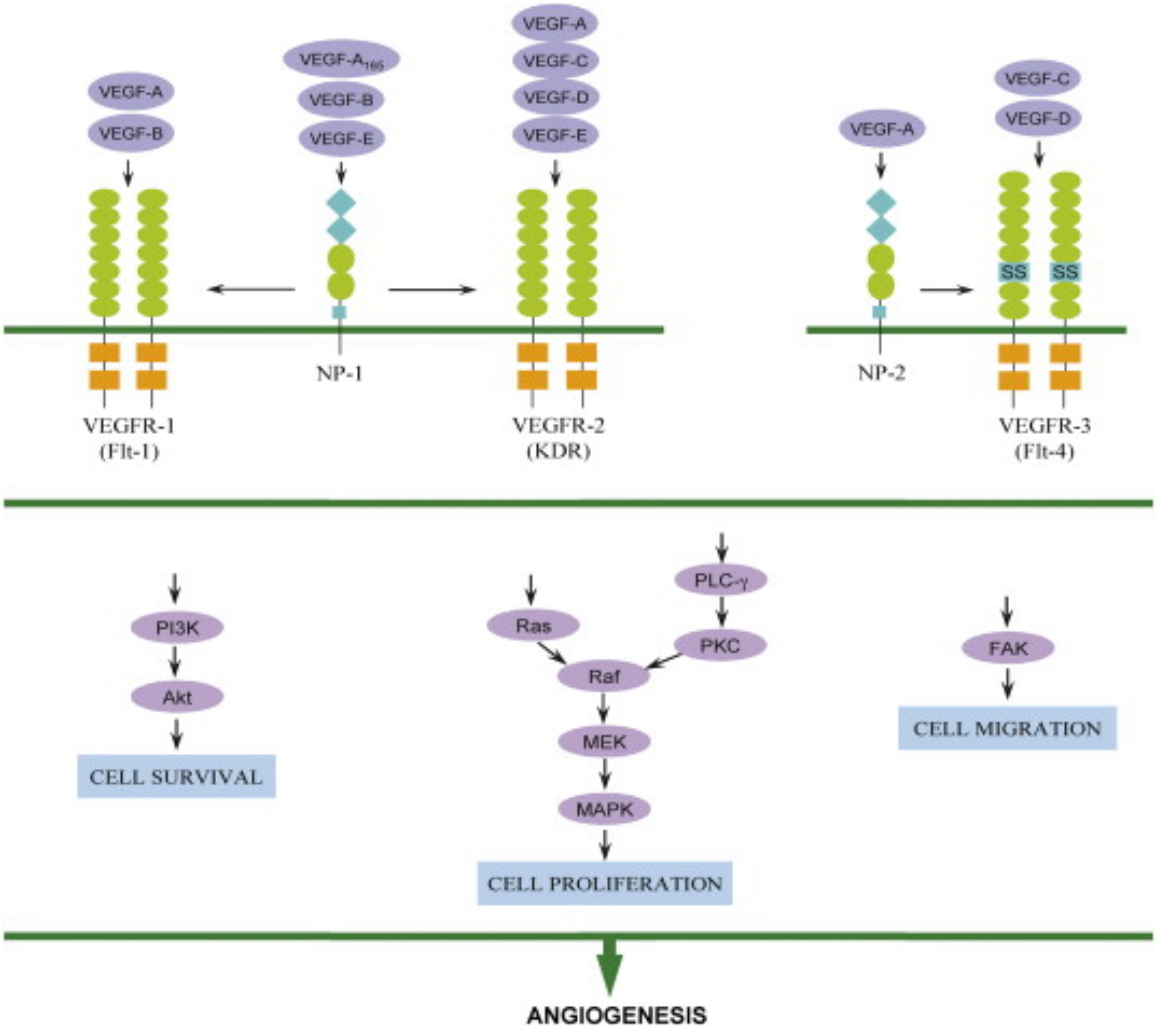

Figure 1.7 VEGF ligands, their receptors (VEGFR), and their signaling. Neuropilin-1/-2) and classical VEGFR1-3 (KDR, Flt-1, Flt-4) can bind members of VEGF family (VEGF-A, -B, -C, -D and -E). All of the classical VEGFRs (KDR, Flt-1, Flt-4) separately mediate VEGF signaling. However, VEGFRs also form receptor duplexes coupling KDR, Flt-1 or Flt-4 to neuropilin (NP) that transduce a newer VEGF signal. This schematic representation of VEGFR bindings and signals clearly shows the complexity of angiogenesis involved receptors. VEGF signaling pathway is subdivided in cell migration, proliferation and survival, resulting in angiogenesis (Hadj-Slimane et al., 2007). See details in section 1.14 for more explanation.

CHAPTER 2

Research goals and specific aims

Dental pulp stem cells (DPSCs) isolated from human tooth pulp have been shown capable of extensive proliferation, multi-differentiation *in vitro*, and generation dentin/pulp-like complex structure *in vivo***.** Furthermore, DPSCs have been reported to contribute to non-dental tissues such as mesenchyme, neuron, and muscle. Nonetheless, DPSC differentiation capacity reported by several scientific groups is highly variable and this inconsistency raises questions about the quality and assurance of DPSCs proposed to be used for clinical applications. Possible causes that may explain these inconsistencies are proposed to study. DPSC heterogeneity may be caused by variable contribution of cells derived from different origin(s). During tooth development, a majority of dental pulp cells originate from neural crest although a significant minority of non neural crest-derived cells resides in the dental pulp. Thus, I aimed to determine the developmental origin of DPSCs, whether they are derived from neural crest and/or non-neural crest.

Irreparable salivary gland tissue dysfunction can be generated by salivary gland diseases such as xerostomia and radiation treatment for head and neck tumor (Dirix et al., 2008). Postnatal stem cells isolated from salivary glands have been characterized and demonstrated capable to give rise into all the epithelial components of the salivary gland tissue such as ductal and acinar cells (Lombaert et al., 2008); nevertheless, their application for salivary gland tissue regeneration is hindered by the need of other supportive cells, vasculature, innervations and matrix necessary for regeneration of the functional salivary gland tissue (Bucheler and Haisch,

2003). The interaction of epithelium and mesenchyme is essential for the branching morphogenesis of the salivary gland. Importantly, the epithelial-mesenchymal interactions in tooth and salivary gland formation are similar and molecular cues such as secretion of fibroblast growth factors (FGF-10, FGF-7) by the ecto-mesenchyme and expression of FGF receptors (FGFR-1, FGFR-2) by the epithelium are important for both the development of tooth bud and salivary gland (Hoffman et al., 2002, Jaskoll et al., 2002, Jaskoll et al., 2004, Jaskoll et al., 2005, Madan and Kramer, 2005, Patel et al., 2006, Yamamoto et al., 2008). Due to similarities in tooth bud and salivary gland development, I aimed to study the capacity of neural crest-derived DPSCs to support and induce salivary epithelium differentiation.

Human and mouse dental pulp stem cells (DPSCs) have been isolated, characterized both *in vitro* and *in vivo*, and proposed for regenerating dental tissue for clinical application (Gronthos et al., 2000, Huang et al., 2006, Janebodin et al., 2011). Anatomically, DPSCs are shown to be located in a perivascular niche (Shi and Gronthos, 2003, Lovschall et al., 2007). In turn, the anatomical position and developmental origin of DPSCs suggest a role as pericytes. However, the capacity of DPSCs to function as pericytes is yet to be elucidated. Angiogenesis is important for successful tissue regeneration, repair, and healing. Without adequate blood supply, tissue regeneration cannot be accomplished and subsequently necrotic or scar tissues are formed (Madeddu, 2005). Therefore, stem/progenitor cells that can function as pericyte-like cells that promote angiogenesis are an attractive stem cell source for tissue regeneration.

To address this hypothesis, the specific aims and approaches are set as follows:

Specific Aim 1: To determine a presence of dental pulp stem cells (DPSCs) in neonatal mice, and their developmental origin. Hypothesis: Dental pulp from neonatal mouse teeth

contains DPSCs with mesenchymal stem cell properties which are neural crest-derived. Strategies: a) Determine the DPSC location in *Tie2*-GFP and *Wnt1-Cre/R26R-LacZ* derived dental pulp; b) Isolate and culture DPSCs from *Tie2*-GFP and *Wnt1-Cre/R26R-LacZ* in stem cell media to obtain DPSC clones; c) Determine the expression of pluripotent stem cell and neural crest-related genes and markers in DPSCs, and d) Determine the multipotency of DPSCs by *in vitro* differentiation and *in vivo* intramuscular and dorsal subcutaneous transplantations.

Specific Aim 2: To determine function of neural crest derived-DPSCs in salivary gland tissue formation. Hypothesis: Neural crest derived-DPSCs are able to function as ecto-mesenchyme and support salivary gland tissue formation. Strategies: a) Determine the formation of salivary gland acini by *in vitro* co-culture between human salivary gland cell line (HSG) and murine DPSCs on matrigel; b) Determine the expression of neural crest-derived salivary gland mesenchymal genes and angiogenic-related genes in DPSCs, and c) Determine the capacity of salivary gland tissue formation by xeno-transplantation of HSG and DPSCs with hyaluronic acid (HA) hydrogel plugs.

Specific Aim 3: To determine a role of DPSCs as pericyte-like cells in angiogenesis. Hypothesis: DPSCs function as pericyte-like cells to enhance angiogenesis via VEGF-dependent pathway. Strategies: a) Determine the angiogenic capacity of DPSCs on endothelial cells using *in vitro* co-culture vascular tube formation, compared with femur-derived bone marrow stromal cells (BMSCs); b) Determine the angiogenic gene expression in DPSCs before and after sFlt-1 treatment *in vitro*, and c) Determine the effect of untreated DPSCs and sFlt-1 treated DPSCs in angiogenesis *in vivo* using matrigel plug transplantation, compared with BMSCs.

All of the research techniques and results obtained are described and discussed in details in the following chapters.

DPSCs are easily accessible from wisdom or supernumerary teeth. These results will broaden the knowledge of DPSC biology which will be instrumental to develop translation protocols for their clinical use for regeneration of dental tissues, and also regeneration of non-dental tissues in the body.

CHAPTER 3

Isolation and characterization of neural crest-derived dental pulp stem cells from *Tie2*-GFP neonatal mice (Janebodin et al. 2011)

3.1 Introduction

Dental pulp stem cells are adult stem cells which were first discovered by Gronthos and Shi et al. (Gronthos et al., 2000). They isolated dental pulp, which is loose connective tissue located in the central part of tooth, from human third molar. Among heterogeneous cell populations and blood vessels as well as innervation in dental pulp, they characterized a cell population with high proliferative capacity, forming calcified nodules *in vitro*, and dentin/pulp-like structures *in vivo*, named dental pulp stem cells (DPSCs). On the other hand, they demonstrated that bone marrow stromal cells (BMSCs) formed mineralized nodules, gave rise to adipocytes *in vitro*, and generated bone-like structure *in vivo* (Gronthos et al., 2000). Another study from the same group showed more evidence that this cell population has stem cell properties such as colony formation, adipogenic and neurogenic *in vitro* differentiation, and also the generation of dentin/pulp-like structures (Gronthos et al., 2002, Batouli et al., 2003). Nevertheless, various DPSC clones exhibited different *in vitro* and *in vivo* capacities. This may be from either the heterogeneity of DPSCs or the cell hierarchy of stem cells and committed progenitor cells in dental pulp (Gronthos et al., 2002). Although diversity was observed among DPSC clones, DPSCs were distinguished from BMSCs, suggesting differences in the developmental nature of both stem cell populations (Shi et al., 2001, Batouli et al., 2003). The following studies attempted to isolate and characterize DPSCs in purer populations by using

several methods such as clonogenic assays (Gronthos et al., 2002), isolating cells with the specific stem cell surface receptors or side population property (Shi and Gronthos, 2003, Laino et al., 2005, Laino et al., 2006). However, the variable multi-differentiation capacity of DPSCs to form dental and bone tissues *in vitro* and *in vivo* was reported (Gronthos et al., 2002, Huang et al., 2006, d'Aquino et al., 2007, Stevens et al., 2008, Ryu et al., 2009, Spath et al., 2009).

Notch expression, which is an important signaling molecule for determination of stem cell fate, may be involved in the specification of DPSC niches (Lovschall et al., 2005). Differential Notch expression was observed in different locations within the dental pulp, implying that dental pulp may harbor several subpopulations of stem cells with different proliferative-differentiation capacity and developmental origins (Lovschall et al., 2005). Alternatively all DPSCs may derive from the same origin but their niche and location dictate their behaviors. These variable results in the differentiation capacity among DPSC clones led me to question if there are different stem cell niches and/or stem cell populations in dental pulp.

In this chapter, I aimed to exploit a *Tie2*-GFP transgenic mouse as a model to isolate and characterize murine dental pulp stem cells (DPSCs) from neonate both *in vitro* and *in vivo* for further experimental analyses.

3.2 Materials and Methods

3.2.1 Dental pulp isolation

Dental pulp tissue were isolated in pools (5 mice per preparation) from 4-8 day old *Tie2*-GFP neonates (Jackson Stock Laboratory, Bar Harbor, ME, USA) (n=3 different preparations) in accordance with approved Institutional Animal Care and Use Committee (IACUC) guidelines. Mandibles were placed in a petri dish with stem cell media described below, separated from

maxillae, and cleaned by removing connective tissues to better expose the first and second lower molars. The molar teeth without root formation were separated from the medial aspect of mandible. Pulp tissue was gently isolated from tooth crowns and kept in stem cell media. The procedure was done by using the gauge needle #26 (Becton-Dickinson, NJ) under stereomicroscope (Stereomaster, Fisher). The tissue was washed with phosphate buffer saline (PBS; HyClone, Logan, UT) and digested with a 1.2 units/ml dispase II, 2 mg/ml collagenase type IV (Worthington, Lakewood, NJ) supplemented with 2 mM $CaCl_2$ in PBS for 60 min at 37°C. An equal volume of stem cell media was subsequently added to the digest for enzyme neutralization prior to filtering through 70 mm nylon cell strainers with a filter area of 3.14 mm^2 (BD Falcon, Franklin Lakes, NJ), and then centrifuging at 300 g for 10 min at room temperature. The cell pellets were then resuspended in stem cell media and single cell suspensions were plated at 1000 cells/cm^2.

3.2.2 DPSC culture

Mononuclear cells (1000 cells/cm^2) were cultured at 37°C under 5% O_2 and 5% CO_2 in stem cell media, containing a final concentration of 60% low-glucose DMEM (Gibco, Invitrogen), 40% MCDB201 (Sigma), 2% heat-inactivated fetal calf serum (HyClone) selected previously for optimal growth of murine mesenchymal stem cells, ITS (Sigma), linoleic acid with bovine serum albumin (LA-BSA) (Sigma), 10^{-9} M dexamethasone (Sigma), 10^{-4} M ascorbic acid 2-phosphate (Sigma), 100 units/ml penicillin with 100 mg/ml streptomycin (HyClone), and $1x10^3$ units/ml leukemia-inhibitory factor (LIF-ESGRO, Millipore), supplemented with 10 ng/mL EGF (Sigma) and 10 ng/mL PDGF-BB (R&D) (Breyer et al., 2006). Once adherent cells were more than 50% confluent, they were detached with 0.25% trypsin-EDTA (Invitrogen) and replated at a 1:4 dilution under the same culture condition with fresh media.

3.2.3 Clonal culture of DPSCs

Cultured DPSCs at passage 4-7 were plated at 50-100 cells/cm^2. Clones were derived from all three non-clonal lines but only clones from line 1 at passage 7 were used in the experiments described here. 24 h after plating, adherent cells were observed and single isolated cells were marked by circling the bottom of the plate with a lab marker. After 10 days, cell colonies were observed and isolated by using 8x8mm cloning rings (Millipore). The clonal populations were expanded every 4 days and transferred to larger size culture dishes beginning with 96-well, 48-well, 24-well, 12-well, 6-well, 60 mm and 100 mm, respectively, until finally being seeding in 150 mm culture plates by day 32. The DPSC clones were cultured at a 1:4 dilution until reaching the appropriate cell number for further experiments.

3.2.4 Reverse transcription-polymerase chain reaction (RT-PCR)

DPSCs were extracted for total RNA by using the RNeasy Mini kit (Qiagen) according to the manufacturer's protocol. Quantity and purity of RNA was determined by 260/280 nm absorbance. First-strand cDNA was synthesized from 500 ng of RNA using the High Capacity cDNA synthesis kit from Applied Biosystems (Foster City, CA) per manufacturer's protocols using a randomized primer. cDNA (20 ng) was diluted in a final volume of 20 µl per reaction using the Immomix PCR Mastermix from Bioline (Randolph, MA). PCR for each specific target gene was performed using the following thermal cycling conditions; 95°C 7 min for initial activation followed by 95°C/30 s; 57°C/30 s; 72°C/45 s, for 40 cycles, with a final 5-min extension at 72°C. Mouse-specific primers are listed in Table 3.1. 10 µl of each RT-PCR product was separated on 2% agarose/ethidium bromide gels and viewed under UV light. Glyceraldehyde-3-phosphate dehydrogenase (*GAPDH*) was utilized as control housekeeping gene. RNA extracted from mouse embryonic stem cells (mESC), salivary gland, brain, liver,

calvarial bone cells (a gift from Dr. Thanaphum Osathanon, Chulalongkorn University, Thailand), and cementoblast cell line (a gift from Dr. Martha Somerman, University of Washington) were used as positive control while negative controls lacked cDNA.

3.2.5 Quantitative reverse transcription-polymerase chain reaction (Q-RT-PCR)

20 ng cDNA for Q-RT-PCR were prepared using the SYBR green PCR master mix from from Applied Biosystems. Reactions were run on the ABI 7900HT PCR system with the following parameters: 50°C/2 min and 95°C/10 min, followed by 40 cycles of 95°C/15 s and 60°C/1 min. Mouse-specific primers are listed in Table 3.1. Results were analyzed using SDS 2.2 software and relative expression calculated using the comparative Ct method. A Ct-value showed how many PCR cycles were necessary to obtain a certain level of fluorescence. Amplification efficiency of different genes was determined relative to *GAPDH* as an endogenous control to normalize RNA expression ($dCt = Ct_{gene}-Ct_{GAPDH}$). Messenger RNA (mRNA) in each sample was calculated using a comparative ddCt ($dCt_{gene}-dCt_{control}$) value method. The fold change in gene expression relative to the control was calculated using 2^{-ddCt}. Each sample was run in triplicate reactions for each gene. cDNA of mESC and mouse aortic smooth muscle cells (a gift from Dr. William Mahoney Jr., University of Washington) were used to calibrate samples.

3.2.6 *In vitro* multi-differentiation

The compositions of each differentiation media and cell densities are listed in Table 3.2. DPSCs were plated at corresponding cell density in 24-well plates (BD) and incubated overnight in stem cell media at 37°C under 5% O_2 and 5% CO_2. After 24 h, media was switched to corresponding differentiation media for 21 days with media change every 3 days. Each differentiation media comprised of serum-free media supplemented with specific growth factors for each respective differentiation lineage. The serum-free media was made using the same

components and concentrations as stem cell media but without fetal calf serum, PDGF-BB, EGF, and LIF.

3.2.7 Immunocytochemistry and immunofluorescence

For immunocytochemistry, cells were fixed with ice cold methanol for 5 min, permeabilized with 0.1% Triton-X 100 (Sigma) in PBS with 1% bovine serum albumin (BSA) for 10 min, inhibited endogenous peroxidase activity with 0.3% hydrogen peroxide in methanol for 30 min, and blocked non-specific binding sites with 10% goat or horse serum (Vector Burlingame, CA) for 1 h. All primary antibodies listed in Table 3.3 were used and incubated overnight at 4°C. Stained cells were incubated with a biotinylated antibody at 1:100 (Vector Burlingame, CA) for 1 h, washed and treated with the Vectastain ABC kit and 3, 3'-diaminobenzidine (DAB) or 3-amino-9-ethylcarbazole (AEC) substrate kit according to manufacturers protocol (Vector Burlingame, CA).

For immunofluorescence, cells were fixed with 4% formaldehyde for 5 min, washed with PBS, and stained with primary antibodies as described in Table 3.3. Donkey-derived Alexa 488 or goat-derived Alexa 594 or goat-derived Alexa 647-conjugated secondary antibodies (Invitrogen) were diluted at 1:800 and incubated for 1 h. Cells were stained with 4', 6-diamine-2-phenylindol (DAPI) at 1:1000 to visualize the nuclei. All antibodies were diluted in 0.1% Triton-X 100 in PBS with 1% BSA. Controls omitting the primary antibody and/or that stained with IgG isotype were used as negative control included for all staining.

3.2.8 Histochemical staining

Toluidine blue was performed to determine proteoglycan producing cells in chondrogenic culture (Kiernan, 2009). Briefly, 1% toluidine blue (Fisher Biotech) in 70% ethanol was diluted in 1% sodium chloride to 0.1% working solution. Cells were fixed with cold methanol (-20°C) 5

min, stained with fresh toluidine blue working solution 1-2 min, rinsed 3 times with distilled water.

Oil Red O was used for characterizing lipid-containing cells in adipogenic culture (Kiernan, 2009). Briefly, 0.5% Oil Red O (Alfa Aesar) in isopropanol diluted in distilled water to 0.25% working solution was incubated 60 min at room temperature and filtered. Cells were fixed with cold methanol 5 min, incubated in fresh Oil Red O working solution 3-5 min, rinsed 3 times with distilled water.

3.2.9 *In vivo* transplantation

In accordance with approved IACUC protocols, $1x10^6$ of murine non-clonal DPSCs, clonal DPSCs, and femur-derived BMSCs were separately transplanted into 1-month-old male *Rag1* null mice (Jackson Laboratory, Bar Harbor, ME, USA) by two methods (n=3 mice/ cell line); 1) intramuscular (IM) injection in the tibialis anterior, and 2) subcutaneous (SC) transplantation with hydroxyapatite tricalciumphosphate (HAp/TCP) (Zimmer) in the dorsum. BMSCs were isolated and cultured as previously described (Reyes et al., 2005). Prior to transplantation, cells were labeled with the fluorescent membrane dye PKH-26 (Sigma) according to manufacturer's instructions. Grafts were harvested after 2-wk and 12-wk IM, 5-wk and 12-wk SC transplantations. For SC-transplanted tissues, samples were fixed with Bouin's fixative solution (Sigma) overnight in 4ºC, then washed with 70% ethanol several times, and demineralized for 7-14 days in demineralizing AFS solution containing acetic acid, 10% neutral buffered formalin, and sodium chloride at 4^oC. Transplanted tissues were embedded in optimal complete tissue (OCT) medium, frozen with liquid nitrogen cooled isopentane and cut to 10-13 μm thick sections. Some SC-transplants were embedded in paraffin and cut to 5 μm thick

sections. Sections were analyzed by Hematoxylin & Eosin (H&E) staining, Masson trichrome, immunohistochemistry, and immunofluorescence (Kiernan, 2009).

Masson trichrome staining was performed for characterization of collagen matrix which was formed by transplanted cells. Briefly, samples were stained in Hematoxylin solution which stained nuclei in blue-black for 5 min, then washed in running tap water for 5 min and rinsed in deionized water. Next, the samples were stained in Biebrich Scarlet-Acid Fuschin (Sigma) which stained cytoplasm in red for 5 min, then rinsed in distilled water. The samples were subsequently placed in Phosphomolybdic (Sigma): Phosphotungstic Acid Solution (Sigma): distilled water (1: 1: 2) for 10 min to allow for the uptake of the Fast Green stain. Then, the samples were stained in 2% Fast Green which stained collagen in blue for 5 min before rinsing briefly in distilled water. Afterwards, the slides were placed in 1% acetic acid for 5 min. The slides were dehydrated by 95% ethanol, absolute ethanol, and xylene, respectively, before mounting with Permount.

3.3 Results

3.3.1 DPSCs in culture demonstrated high proliferative capacity.

Dental pulp was isolated from lower molar teeth of 4-8 day old neonatal *Tie2*-GFP mice because these developing teeth have not formed roots yet (Figs. 3.1A, B), which makes pulp dissection feasible. Since the dental pulp is a highly vascularized tissue, I used the *Tie2*-GFP model to determine the contribution of endothelial cells and hematopoietic cells in my dental pulp cultures. *Tie2*-GFP is a transgenic mouse model in which the vascular endothelial cells express green fluorescent protein (GFP) under the driven of the endothelial-specific receptor tyrosine kinase (*Tie2*) promoter (Motoike et al., 2000). Following constant monitoring for the presence of GFP, all dental pulp cultures derived from *Tie2*-GFP were completely negative for

GFP, indicating my cultures did not contain endothelial and/or hematopoietic cells (data not shown). In addition, cells harvested from early cultures were negative for endothelial expressed genes *vWF (von Willebrand Factor)*, *CD31 (PECAM)*, angiopoietin receptors *Tie1* and *Tie2* and *Ve-Cadherin* by RT-PCR (data not shown).

To identify highly proliferative populations, freshly isolated dental pulp mononuclear cells were cultured at low density, 1000 cells/cm^2, in stem cell media with 2% serum as a selective condition to enrich for stem cell outgrowth, and 5% CO_2/O_2 to more accurately replicate physiological conditions (Ma et al., 2009). Within two days in culture, cells began to proliferate and form individual colonies (Fig. 3.1C). By day 10 in culture, cells formed larger, confluent colonies (Fig. 3.1D), that were split and subsequently sub-cultured approximately every 4 days. In each passage, I used a 1:4 dilution as the standard ratio for cell expansion. Although cells were cultured until passage 14 (day 90), they grew at a consistent and steady proliferation rate without signs of senescence, suggesting that DPSCs are highly proliferative. DPSCs from three independent isolations were characterized; each of which demonstrated similar growth pattern and proliferation rate. The morphology of cultured cells was heterogeneous in early culture but most appeared spindle-shaped (Fig. 3.1E).

3.3.2 DPSCs expressed stem cell and neural crest-related genes.

In addition to highly proliferative capacity, to gain insights into the stem cell properties and possible origin of DPSCs, the expression of stem cell genes as well as neural crest and mesodermal genes were surveyed in freshly isolated dental pulp tissue and three DPSC cell lines generated from early to late cultures. RT-PCR (Fig. 3.2A) demonstrated negative *Oct4* in both fresh tissue and cells in early culture while *Sox2* was generally expressed. However, *Oct4* was expressed in the late culture (passage 7) of two DPSC lines (lines 1 and 2). Surprisingly, there

was consistently high *Klf4* expression even in late passages in all three isolations. *Klf4* and *Sox2* are two of four pluripotency genes required to generate inducible pluripotent stem (iPS) cells (Takahashi et al., 2007). Moreover, *Nanog*, which is important for the maintenance of pluripotency in embryonic stem cells, was up-regulated in culture (Boyer et al., 2005). The expression of some pluripotent genes suggests the existence of a primitive stem cell population in our cultures and indicates that these culture conditions support self-renewing cells. DPSCs also expressed variable levels of *c-Kit. C-Kit*, encoding a tyrosine kinase receptor for the cytokine stem cell factor, plays an important role in cell survival, proliferation, and differentiation in multiple tissues and stem cell types (Li et al., 2006). Moreover, *c-Kit* is expressed in a subpopulation of neural crest stem cells destined to form melanocytes (Randall et al., 2008). Therefore, expression of *c-Kit* on DPSCs, although variable, may indicate the presence of stem cells from neural crest cell origin in our cultures.

To characterize the potential origin of DPSCs, the early developmental markers were determined in DPSCs (Fig. 3.2B). As expected, a complete absence of genes expressed by mesodermal cells during development; *Brachyury* (Martin and Kimelman, 2008) and *Mesp2* (Saga et al., 1997), was observed in all DPSC cultures. In contrast, *Goosecoids (Gsc)* (Sawada et al., 2000) and *Gata6* (Kamnasaran and Guha, 2005), which are genes associated with neural crest development, were expressed by DPSCs. In addition, DPSCs expressed embryonic neural crest and neuronal stem/precursor cell associated genes (Fig. 3.2C); *tyrosine kinase C* (*TrkC*) , *platelet-derived growth factor receptor-alpha* (*Pdgfra*), *low-affinity nerve growth factor receptor* (*LNGFR)*, *Twist*, *Snail*, *Slug, Sox10, neural cell adhesion molecule* (*Ncam),* and *musashi1* (*Msi1*).

TrkC is expressed in many neural crest derivatives including tooth forming mesenchyme. In the tooth, *TrkC* is observed in the core of the dermal papilla (Tessarollo et al., 1993) which develops into dental pulp. *Pdgfra* is a marker for skeleto-odontogenic neural crest cells, and has been strongly detected on the bone-forming cranial neural crest cells of mice, as well as in teeth and other first branchial arch derivatives (Takakura et al., 1997). *LNGFR* is one of the two receptor types for the neurotrophins that stimulate neuronal cells to survive and differentiate, and *LNGFR* is a specific cell phenotype that has been used to isolate mammalian neural crest stem cells from fetal sciatic nerve (Morrison et al., 1999). *Twist, Snail, Slug,* and *Sox10* are four neural crest specifiers activated in migrating neural crest cells and function by turning on the expression of effector genes, which results in certain properties of neural crest such as migration and multipotency (Meulemans and Bronner-Fraser, 2005). *Ncam* is a binding glycoprotein expressed on the surface of neural progenitor cells (Tibbitts et al., 2006), and also found in DPSCs (d'Aquino et al., 2009). *Msi1* is a marker expressed in neural precursor cells and cardiac neural crest stem cells (Tomita et al., 2005).

The presence of neural crest associated proteins in DPSCs was further examined by immunocytochemistry to confirm the transcriptional results. Undifferentiated cells showed positive staining for the pluripotent transcription factor KLF4, and neural crest-related markers; MSI1, and SOX10 (Fig. 3.3). Although I cannot rule out the existence of non-neural crest cells in these cultures, these results suggest that a neural crest derived population existed in my DPSC cultures. To determine if the presence of such pluripotent genes indicates the existence of stem cell populations in the dental pulp, I further examined the stem cell capacity of DPSCs by their multi-differentiation.

3.3.3 DPSCs differentiated into neural crest-lineage cells *in vitro.*

During head and neck development, neural crest cells migrate to the cephalic region and give rise to bone, cartilage, fat, neurons, glia, and connective tissues, including dentin-forming cells, odontoblasts (Bronner-Fraser, 1995, Chai et al., 2000, Abzhanov et al., 2003). *In vitro* differentiation of DPSCs into neural crest lineages supports the hypothesis that DPSCs maintain embryonic neural crest potential. Thus, I studied the capacity of DPSCs to differentiate into neural crest-lineage, specifically cranial neural crest derived tissues.

3.3.3.1 DPSCs differentiated into osteoblast-like, adipocyte, and chondrocyte-like cells.

DPSCs exposed to osteogenic, chondrogenic, and adipogenic media for 21 days stained positive for specific differentiation markers (Figs. 3.4A-K) and expressed transcripts (Fig. 3.4L) specific to each respective differentiation lineage.

Osteogenic differentiation

Immunoperoxidase staining of DPSCs cultured in osteogenic media, containing serum, β-glycerophosphate, ascorbic acid, and dexamethasone, showed cytoplasmic pattern of bone sialoprotein (BSP) and osteopontin (OPN) in differentiated cells, but not in undifferentiated cells (Figs. 3.4A-D) (Gronthos et al., 1994). RT-PCR showed that differentiated cells expressed osteogenic markers (Fig. 3.4L, Osteogenic differentiation); *runt related transcription factor 2* (*Runx2)*, *osterix* (*Osx*), *Opn, Bsp* and *dentin matrix protein1* (*Dmp1*). *Runx2* is a transcription factor important for osteo-odontoblast differentiation in mesenchymal cells and regulates many bone- and tooth-related gene expressions (Ducy et al., 1997, Lian et al., 2006). *Osx* is another osteoblast-specific transcription factor and is expressed in tooth germ mesenchymal cells (Nakashima et al., 2002). OPN, BSP and DMP1 proteins are present in mineralized tissues such

as bone, dentin, and cementum (Sommer et al., 1996, Feng et al., 2003). These results suggest that DPSCs cultured in osteogenic media differentiate into osteoblast/odontoblast-like cells.

Adipogenic differentiation

Small clusters of lipid-containing cells were first observed on day 7 in cells exposed to adipogenic media (data not shown) (Gregoire, 2001). Treated cells showed expression of *peroxisome proliferator-activated receptor gamma* (*Pparg2)* and *CCAAT/enhancer binding protein alpha (CEBPa)*, which are transcription factors for adipocyte differentiation, as well as, *leptin* and *adipsin*, which are specific markers of adipocytes (Fig. 3.4L, Adipogenic differentiation) (Gregoire, 2001). Despite *Pparg2* and *leptin* expression in undifferentiated cells, Oil Red O-positive lipid-containing adipocytes were observed only in differentiated cells but not in undifferentiated cells (Figs. 3.4E-F). Small clusters of lipid-containing cells were first observed on day 7 in cells exposed to adipogenic media (data not shown) (Gregoire, 2001). Treated cells showed expression of *peroxisome proliferator-activated receptor gamma* (*Pparg2)* and *CCAAT/enhancer binding protein alpha (CEBPa)*, which are transcription factors for adipocyte differentiation, as well as, *leptin* and *adipsin*, which are specific markers of adipocytes (Fig. 3.4L, Adipogenic differentiation) (Gregoire, 2001). Despite *Pparg2* and *leptin* expression in undifferentiated cells, Oil Red O-positive lipid-containing adipocytes were observed only in differentiated cells but not in undifferentiated cells (Figs. 3.4E-F).

Chondrogenic differentiation

DPSCs cultured in chondrogenic media were first observed to display changes from spindle-shaped cells to clusters of round and cuboidal cells representing chondrocyte-like morphology on day 10 (Pavlov et al., 2003, Tscheudschilsuren et al., 2006). After 21 days, these cells secreted matrix with high proteoglycan content which stained positive for toluidine blue

(Fig. 3.4H) and collagen type II (COL II) (Fig. 3.4J) and formed calcified nodules (Fig. 3.4K), indicating that these cells form cartilage matrix (Oesser and Seifert, 2003). RT-PCR demonstrated that treated cells in chondrogenic media expressed *Sox9* and increased expression of pro-collagen type II (*Col2a1*) genes which are specific markers for chondrocyte differentiation (Lefebvre et al., 1997). I did not observe these chondrogenic hallmarks in undifferentiated cells despite chondrogenic gene expression in such cells (Fig. 3.4L, Chondrogenic differentiation).

RT-PCR showed chondrogenic and adipogenic markers in cells treated with osteogenic media; however, COL II- and/or Oil Red O-positive cells were not observed in this culture (data not shown). Interestingly, I found BSP- and OPN-positive cells, as well as Oil Red O positive-adipocytes in the chondrogenic media (data not shown). This is consistent with previous studies that showed BMP2 is an inducer of not only chondrogenic differentiation but also osteoblastic and adipogenic differentiations (Ji et al., 2000). *Osx, Bsp, Dmp1, Pparg2, leptin, Sox9,* and *Col2a1*, expressed in confluent undifferentiated cells in stem cell media at day 21 (Fig. 3.4L), suggesting these are default differentiation pathways of DPSCs in confluent cultures. Alternatively, it has been previously demonstrated that bone marrow stromal cells display an osteogenic imprinting program and express messengers of these proteins in undifferentiated cells (Satomura et al., 2000).

Intriguingly, Q-RT-PCR showed that *Nanog* and *Klf4* were down-regulated during differentiation of DPSCs (Fig. 3.5), suggesting that like embryonic stem cells, these pluripotent genes play a role in maintaining DPSC stemness and thus are down-regulated during differentiation (Zhang et al., 2010).

2.3.3.2 DPSCs differentiate into neuronal-like and smooth muscle-like cells. After exposing DPSCs to neurogenic media, differentiated cells stained positive for N-CAM, a

neuronal adhesion molecule, and γ-aminobutyric acid (GABA), an inhibitory neurotransmitter produced by GABAergic neurons (Figs. 3.6A-D) (Jiang et al., 2003, Amoh et al., 2005). I also treated DPSCs with PDGF-BB to induce smooth muscle differentiation (Ross et al., 2006). Following day 21 of PDGF-BB, DPSCs showed smooth muscle-like morphology, and stained positive for α-smooth muscle actin (SMA) (Figs. 3.6E, F). However, I could not observe any positive cells of either neurogenic or smooth muscle differentiations in the undifferentiated cells (Figs. 3.6A, C, E).

3.3.4 DPSCs generate single cell colonies

Colony-forming capacity is a characteristic growth pattern of many adult stem cells including bone marrow mesenchymal stem cells, and has been used as an indicator of self-renewal (Friedenstein et al., 1976). Indeed, a single stem cell should create a colony of progeny cells with all or some daughter cells identical to the original cell. Initially, I attempted to demonstrate colony formation from single DPSC by Fluorescent Activated Cell Sorting (FACS) mediated single cell deposition. Unfortunately, this approach was unsuccessful possible due to sensitivity of DPSCs to cell sorting. Thus, I utilized clonal rings commonly used to generate single cell colonies from mesenchymal stem cells (Guilak et al., 2006). I first seeded cells at several dilutions and determined that the limiting dilution to obtain single colonies was 50-100 cells/cm^2. After 24 hrs adherent single cells were marked and monitored everyday for the formation of colonies. At day 10, I observed 12 colonies in 600 cm^2 (four 150 cm^2 petri dishes) (Figs. 3.7A-D). After clonal isolation, I cultured these clones in several passages and 5 of 12 (approximately 42%) survived and proliferated for further characterization.

Like the non-clonal populations, RT-PCR of clones expressed the pluripotent genes, *Klf4* and *Nanog*, and neural crest developmental genes, but not mesodermal developmental genes

(Fig. 3.7E). Compared to non-clonal populations, clones definitively expressed higher and consistent levels of *Pax3,* a cardiac neural crest developmental gene (Conway et al., 1997). All clones demonstrated strong expression of neural crest and neural precursor genes; *Msi1*, *Twist*, *Snail*, *Slug, Pdgfra,* and also *Vimentin* (Fig. 3.7F)**.** *Vimentin* is expressed in mesenchymal cells irrespective of their origin or in cells undergoing epithelial-mesenchymal transition such as migratory neural crest cells (Rao and Anderson, 1997). Additionally, the clones showed variable *Dmp1* but not *Dspp*, indicating an undifferentiated state of dental pulp cells (Yu et al., 2007).

3.3.5 DPSC clones show *in vitro* multi-differentiation in neural crest lineage, but not adipocyte.

To determine if DPSC clones show multi-differentiation in neural crest lineages, we performed *in vitro* differentiation by exposing 5 clones (C5-C9) to the same differentiating media used to differentiate the non-clonal populations (Gronthos et al., 1994, Gregoire, 2001, Jiang et al., 2003, Ross et al., 2006, Tscheudschilsuren et al., 2006, Noth et al., 2007)**.** Prior to differentiation, I analyzed gene expression levels for *Klf4* and *Nanog* compared to non-clonal populations and dental pulp tissue (Fig. 3.8). In turn, *Nanog* and *Klf4* expression were variable among the clones but comparable to the non-clonal populations. Thus, I assumed that clonal populations should exhibit same differentiation capacity and fate as compared to non-clonal populations (Figs. 3.9A-J, L, M).

Unlike differentiation of non-clonal cultures (Figs. 3.9A, C), I did not observe any differentiated clonal cells positive for BSP and OPN in osteogenic media (Figs. 3.9B, D), corresponding to low expression of *Bsp* in differentiated clones (Fig. 3.9K). BSP is the osteoblast-specific protein found in bone matrix and highly secreted by osteoblasts (Lee et al., 2009). In contrast, consistent with *Dmp1* expression (Fig. 3.9K), non-clonal and all clones in

osteogenic media stained positive for DMP1 (Figs. 3.9E, F), dentin sialoprotein (DSP) (Figs. 3.9G, H) and osteocalcin (OCN) (Figs. 3.9I, J); all of which are non-collagenous proteins secreted by odontoblasts and found in dentin matrix (Papagerakis et al., 2002, Braut et al., 2003, Feng et al., 2003). DSP is particularly considered a dentin-specific protein which is highly expressed by odontoblasts (Lee et al., 2009).These results suggest the presence of odontoblast-like cells more abundant in clonal differentiations. This osteogenic media has been used to differentiate odontoblast-like cells from dental pulp cells in previous studies, thus it is not surprising that DPSCs can differentiate into odontoblast-like cells when induced with such media (Zhang et al., 2005)**.** However, the clonal populations showed a more odontogenic than osteogenic phenotype under this condition. Furthermore, all non-clonal DPSCs and 4 out of 5 DPSC clones stained positively for COL II (Figs. 3.9L, M) after treatment with chondrogenic media, which was confirmed by the *Sox9* and *Col2a1* expression (Fig. 3.9N).

In contrast, all non-clonal and clonal DPSC cultures acquired a smooth muscle-like morphology and stained positive for α-smooth muscle actin (SMA) after treatment with PDGF-BB media (Figs. 3.6F, 3.10B). In addition, Q-RT-PCR of smooth muscle genes showed higher expression of smooth muscle- and pericyte-related genes (*Sm22-alpha*, *Sma*, *SMHC*, and *calponin*) in the undifferentiated clonal populations as compared to non- clonal (Fig. 3.11). In turn, the differentiated progeny derived from the clonal populations showed a pattern of smooth muscle maturation with significantly increased levels of *myocardin, Sm22-alpha, Sma*, *SMHC*, and *calponin* (>10 folds higher than non-clonal differentiated cells and >100 folds higher compared to smooth muscle cells) whereas in the non-clonal populations this trend of maturation is not apparent (Fig. 3.11) (Wang et al., 2003, Grabski et al., 2009). Three out of five clones stained positive for neurofilament (NF-160/200) (Fig. 3.10D), S100 (Fig. 3.10F), and NG2 (Fig.

3.10H) which are neuronal cytoskeletal, glial, and oligodendrocyte markers, respectively, after induction with neurogenic media (Nishiyama et al., 2005). The NF staining was confirmed with RT-PCR of neurofilament-light (NFL) and -heavy (NFH) (Fig. 3.10I). In conclusion, 3 out 5 clones could differentiate into odontoblast-like, chondrocyte-like, smooth muscle-like and neuronal-like cells, demonstrating their neural crest stem cell capacity (comparison summarized in Table 4.4). Nevertheless, each clone showed some variability in lineage differentiation capacity and efficiency, which reflects heterogeneity and/or a complex hierarchy of progenitor/stem cells in our cultures.

3.3.6 DPSCs show plasticity depending on the *in vivo* niche.

To determine *in vivo* differentiation of DPSCs, I transplanted DPSCs labeled with a red fluorescence dye (PKH-26) intramuscularly and subcutaneously in immune compromised *Rag1* null mice to avoid immune rejection (Horan and Slezak, 1989). We used murine femur-derived bone marrow stromal cells (BMSCs) cultured and transplanted under the same conditions in order to compare DPSCs *in vivo* differentiation capacity with another mesenchymal line derived from a different origin (mesodermal).

Two-weeks after intramuscular (IM) transplantation, non-clonal DPSCs identified as PKH-26+ (Fig. 3.12A), created compacted collagen bundles as indicated by Masson's trichrome (Fig. 3.12B). The presence of collagen fibers was confirmed with polarized light microscopy (Fig. 3.12C). Staining for dentin or bone proteins was only slightly positive (data not shown), suggesting that the compacted collagen bundles did not resemble dentin- or bone-like structure. I then hypothesized that longer *in vivo* transplantation will result in more mature phenotype of the transplanted cells. Nonetheless, 12-week IM transplantations of non-clonal, clonal DPSCs, and BMSCs, only generated abundant immature collagen fibers that stained blue in Masson's

trichrome (Figs. 3.12D-F), and polarized light (Figs. 3.12G-I) but were negative for dentin or bone proteins (data not shown). This indicates that the skeletal muscle is not an inductive environment for formation of mature mineralized matrix.

To explore if DPSCs can form more mature matrix structures *in vivo*, I used a more permissive model of matrix formation, subcutaneous (SC) transplantation with hydroxyapatite/tricalcium phosphate scaffolds (HAp/TCP) (Gronthos et al., 2000). Here I transplanted three clones separately, which expressed high levels of *Nanog* and *Klf4* by Q-RT-PCR (Fig. 3.8), and showed multi-lineage neural crest differentiation capacity (Table 4.4). In these transplants we also used femur-derived BMSCs as control cell line.

Five weeks after SC transplantation with HAp/TCP, PKH26-labeled DPSC clones (Fig. 3.13A) generated collagen forming-tissue demonstrated by Masson trichrome (Fig. 3.13C) and polarized light (Fig. 3.13D, white arrowheads). In addition, PKH-26+ clonal cells produced extracellular matrices which showed strong staining for DMP1 (Figs. 3.14A, D), and slightly positive staining for DSP (Figs. 3.14B, E) and BSP (Figs. 3.14C, F). However, strong positive staining of DSP (Fig. 3.14E, black arrowheads) and BSP (Fig. 3.14F, black arrowheads) was observed in the cytoplasm of transplanted cells. DPSC clones were negative for dentin and bone proteins prior to transplantation. All antibodies for dentin and bone matrices showed appropriate staining pattern in tooth sections used as positive control to confirm the antibody specificity (Fig. 3.15). I observed that these mineralized tissues formed by DPSCs contained abundant microvessels that stained positive for CD31, an endothelial marker (Fig. 3.16A). I consistently observed some PKH-26+ (donor DPSCs) cells adjacent to these microvessels. These PKH-26+ cells seem scattered around vessels. Staining for α-smooth muscle actin revealed that these microvessels did not contain a thick muscle layer but were wrapped by pericyte-like cells that

were SMA positive and some were also PKH-26+ (Figs. 3.16C, D, F). Many of these microvessels seemed fenestrated and stained positive for VEGF receptor 3 (Figs. 3.16E, F) (Partanen et al., 2000).

Interestingly, the 12-week SC transplantation showed different composition of mineralized matrices depending on the donor cells, DPSCs and BMSCs. The H&E and Masson's trichrome showed bone-like structure created by BMSCs (Figs. 3.13G, J), but not in non-clonal and clonal DPSC transplantations (Figs. 3.13E, F, H, and I). The structures produced by both DPSC populations demonstrated collagen-forming matrices in many areas that were arranged perpendicularly to the surface, which was confirmed using polarized light (Figs. 3.13K, L). Corresponding to previous studies, the DPSC transplantation showed that elongated cells created collagen fibers which run perpendicularly to HAp/TCP surfaces, resembling the morphology and arrangement of odontoblasts (Figs. 3.13K, L, white arrowheads) (Gronthos et al., 2000, Gronthos et al., 2002, Braut et al., 2003). In contrast, in the BMSC transplantation I observed osteocyte-like cells trapped in matrix of collagen fibers which did not run perpendicularly to the mineralized matrix (Figs. 3.13J, M) (Gronthos et al., 2000, Gronthos et al., 2002).

As negative control, the SC transplantation with only HAp/TCP, did not show any positive staining of DMP1, DSP, and BSP, respectively (Figs. 3.14G-I). Conversely, immunohistochemistry in DPSC transplants showed positive DMP1, DSP, and BSP staining in both cytoplasmic area and extracellular matrices (Figs. 3.14J-O). We observed elongated and polarized cells that were positive for DMP1 and DSP in the DPSC transplantations (Figs. 3.14K, M, N insets). On the other hand, the bone-like structures created by BMSCs were negative for DSP, but positively for BSP (Figs. 3.14Q and R inset). I also observed positive DMP1 staining in both DPSC-derived odontoblast-like cells and BMSC-derived osteoblast-/osteocyte-like cells

(Figs. 3.14M inset, P osteoblast-like cells indicated by arrowheads, osteocyte-like cells indicated by arrows). These results, based on tissue morphology and antibody staining, indicate that *in vivo* DPSCs differentiated into odontoblast-like cells and generated dentin-like matrix whereas BMSCs differentiated into osteoblast-like cells and formed bone condensations.

Upon closer examination of the odontoblastic niche in the 12-week DPSC transplants, similar to 5-week transplants, I observed abundant microvessels in close proximity to odontoblast-like cells with fenestrated morphology surrounded by PKH-26+ cells, in both non clonal and clonal DPSC transplants (Figs. 3.13E, F black arrowheads, 3.16G, 3.17A, B). In contrast, matrices that were generated by BMSC transplants surrounded areas rich in HAp/TCP (Figs. 3.13G black arrowheads, and J). Although microvessels were observed in the BMSC transplants, the BMSC mineralized areas did not show close proximity to vessels (Fig. 3.17C black arrowheads). Interestingly, in the BMSC transplants microvessels were predominantly found in areas rich in adipocytes (Figs. 3.13G and 3.16H). In both transplants, microvessels were mature as circulating red blood cells can be seen throughout (Fig. 3.17D). Therefore, I performed a quantification of the average distance of donor nuclei in condensed matrices to nearest capillaries. Surprisingly, the distance from odontoblast nuclei to nearest capillary was very close (9 μm +/- 4.49) and very consistent across all DPSC transplants whereas the distance of osteocyte nuclei to capillaries in bone condensations were significantly farther (187 μm+/- 76.88) (Fig. 3.17E). This capillary arrangement resembles dentinogenesis and contrasts early osteogenesis. In dentinogenesis, capillaries are in close proximity to odontoblasts and many of these capillaries are fenestrated whereas in osteogenesis the initial bone condensations occur in avascular areas (Thompson et al., 1989, Yoshida and Ohshima, 1996, Carlile et al., 2000).

3.4 Discussion

Differences in DPSC proliferation and differentiation capacities *in vitro* and *in vivo* as described in previous reports indicate heterogeneity within DPSC populations (Gronthos et al., 2002, Huang et al., 2006, d'Aquino et al., 2007). In turn, such heterogeneity may be attributed to distinct developmental origins. The hypothesis that DPSCs are of neural crest origin has been suggested and indirectly related by previous reports (Chai et al., 2000, Zhang et al., 2006, Stokowski et al., 2007, Waddington et al., 2009). Accordingly, human dental pulp contains self-renewing DPSCs capable of giving rise to mesenchymal-lineages and non-mesenchymal cells such as neuron-like, smooth muscle-like, and melanocyte-like cells, indicating that these cells might be derived from neural crest (Alliot-Licht et al., 2001, Gronthos et al., 2002, Stevens et al., 2008). In this study, I explored several criteria to determine if stem cells in dental pulp originate from neural crest. I first investigated the proliferative capacity of murine DPSCs cultured in stem cell selective media, as well as, the expression of stem cell and neural crest genes. Subsequently, I determined *in vitro* and *in vivo* multi-differentiation of DPSCs into neural crest-lineage.

Unlike human, mouse DPSCs have not been well described possibly due to the difficult nature of isolating dental pulp from murine teeth (Gronthos et al., 2000). A recent study characterized progenitors and stem cells in dental pulps of mouse molars in uneruption and eruption states *in vitro* and revealed a small population of mesenchymal multipotent cells in erupted molars but not in the dental pulp of the unerupted molars. Instead, a majority of dental pulp cells of the unerupted molar were osteo-dentogenic progenitor cells (Balic et al., 2010). In my studies, I determined the existence of stem cells in mouse dental pulp from unerupted molars which exhibit high proliferation and multi-differentiation into mesenchymal and non-mesenchymal lineages. DPSCs sufficiently self-perpetuated more than 14 passages (~3 months)

without the alteration in morphology and proliferation rate. DPSCs chosen for all differentiation experiments were harvested near passage 7, the time which *Nanog* and *Klf4* expression was highest (Fig. 3.8). In this study I used the optimal conditions for long-term cultivation of stem cells without any signs of degeneration or spontaneous differentiation; near physiological oxygen concentration, and a low concentration of serum supplemented with platelet derived growth factor-BB (PDGF-BB), epidermal growth factor (EGF), insulin transferrin selenium (ITS), dexamethasone, and leukemia inhibitory factor (LIF) (Breyer et al., 2006, Ma et al., 2009). This combination differs from previously described culture condition used to grow human and mouse DPSCs (Gronthos et al., 2000, Balic et al., 2010). Therefore, a direct comparison of culture conditions must be undertaken to determine if DPSCs described here are equivalent to previously described populations.

Interestingly the expression of embryonic pluripotent genes suggests the existence of primitive stem cells within the DPSC population that share a similar genetic program to embryonic and inducible pluripotent stem cells (Takahashi et al., 2007). Q-RT-PCR showed down-regulation of *Klf4* and *Nanog* after differentiation of DPSCs, suggesting that both transcription factors play a similar role and function for maintenance of DPSC multi-potentiality and undifferentiated state. Consistent with my hypothesis of a neural crest origin, DPSCs expressed multiple neural crest markers whereas they did not show mesodermal developmental markers. To determine that DPSCs fulfill the stem cell criteria, in addition to self-renewal, I also explored their multi-differentiation capacity with emphasis on neural crest lineages.

Explants of cranial and trunk neural crest cells give rise to chondrocytes, glia, neuronal cells, smooth muscle cells, and melanin-forming cells, which are all neural crest-lineage derived during embryogenesis (Abzhanov et al., 2003). In my differentiation conditions, treated DPSCs

expressed markers for osteoblast, chondrocyte, neuron, smooth muscle and adipocyte differentiation, indicating that non-clonal DPSCs contains multipotent stem cells with capacity to differentiate into mesenchymal and non-mesenchymal lineages of neural crest cells. Consistently human DPSCs can *in vitro* differentiate into non-mesenchymal lineages (Alliot-Licht et al., 2001, Gronthos et al., 2002).

DPSC clones, initiated from early passages of non-clonal cultures, were sub-cultured for 1 month without changing cell morphology. Like non-clonal DPSCs, all clones expressed *Klf4*, *Nanog*, and neural crest-related genes, suggesting that clones maintain neural-crest multipotential. My observations showed DPSC clones gave rise to odontoblast-like, chondrocyte-like, smooth muscle-like, and neuronal-like cells, but not adipocyte.

To further assess DPSC plasticity, I transplanted cultured DPSCs to examine their response *in vivo* in two different models: subcutaneous (SC) and intramuscular (IM) transplantations. Interestingly, each transplantation method resulted in different cell fates indicating that DPSCs are not under a fixed program as environmental factors influence their response. Short subcutaneous transplantation with HAp/TCP resulted in the production of a disorganized dentin-like structure, mimicking a structure generated in reparative dentin formation after tooth injury (Sloan and Smith, 2007). Reparative dentin exhibits disorganized arrangement due to lack of signaling from inner enamel epithelium and basement membrane which results in multiple inducing molecules secreted from dentin matrix (Sloan and Waddington, 2009). Lack of epithelium induction may explain why DPSC clones generated a disorganized structure. Like the renal capsule or subcutaneous regions, I used the intramuscular model to transplant DPSCs since we hypothesized that a high vascularized system in muscle may enhance the function of DPSCs (Gronthos et al., 2000, Gronthos et al., 2002, Yu et al., 2007). In

turn, IM transplantation of DPSCs generated well-organized but immature collagen-forming matrix. These results may be explained by several possibilities. First, each transplant environment has a distinct influence on differentiation of DPSCs. Secondly, the IM transplanted structure was more organized possibly because muscle fibers function as scaffold to stabilize and directly instruct transplanted cells toward the proper arrangement and orientation. Thirdly, the length of transplantation in the IM injections was only 2 weeks, 3 weeks shorter than SC transplantation, and thus, longer IM transplantation may result in more mature matrix formation.

To determine if longer transplantations are required for formation of more mature matrices, I performed IM and SC transplantations for 12 weeks. Surprisingly, longer *in vivo* exposure did not result in more mature matrix formation in the IM transplants. However, longer SC transplantations with HAp/TCP resulted in more mature matrix formation in both DPSC and BMSC transplants but the morphology and matrix compositions differed.

First, I observed many abundant small blood vessels in close proximity to odontoblast-like cells in DPSC transplants. Many of these microvessels were fenestrated and stained positive for VEGFR-3. I observed pericyte-like cells adjacent to these microvessels; some of which were donor DPSC-derived. This observation illustrates the perivascular nature of DPSCs and their potential to function as pericytes (Shi and Gronthos, 2003, Marchionni et al., 2009). Although BMSC transplants also contained abundant microvessels, bone condensations were significantly distant to vessels. Interestingly, in BMSC transplantations I observed a large number of microvessels in areas rich in adipocytes. These cells may be from BMSC-derived or derived from host cells which were signaled by BMSCs to differentiate into adipocytes.

Secondly, long-term DPSC transplantation resulted in a more organized mineralized matrix formed by elongated and polarized cells resembling odontoblast-like morphology which

were in close proximity to microvessels. These matrices represent dentin-like structure with strong positive staining for dentin matrix proteins, DMP1, DSP, and BSP. In contrast, BMSC transplantation showed mineralized matrices with osteocyte-like cells in lacunae. Consistently, the matrices produced by BMSCs were positive for the bone protein, BSP, but not positive for the dentin protein, DSP. However, some studies reported that certain states of bone or tooth development can express low levels of dentin or bone proteins, respectively; therefore, I cannot distinguish bone or dentin structures by only protein expression (Papagerakis et al., 2002, Feng et al., 2003). As mentioned above, the combination of cell / tissue morphology and matrix protein expression is important to characterize the structure created by DPSCs and BMSCs (Gronthos et al., 2000, Braut et al., 2003, Yu et al., 2007).

Thirdly, as described previously in human DPSC *in vivo* transplantation, murine DPSCs can create collagen fibers arranging perpendicularly to the scaffold/matrix surface whereas BMSCs created collagen fibers running parallel to the scaffold/matrix surface (Gronthos et al., 2000, Gronthos et al., 2002). Lastly, the distribution and association of odontoblasts with microvessels resembles dentinogenesis whereas the formation of bone condensation in avascular areas resembles early osteogenesis (Thompson et al., 1989, Yoshida and Ohshima, 1996, Carlile et al., 2000).

3.5 Conclusion

In this study, I first showed dental pulp stem cells isolated from mouse neonates with neural crest-related stem cell properties *in vitro* and *in vivo*. However, to confirm their neural crest origin, I proposed to use another transgenic mouse model which is more specific of neural

crest lineage, *Wnt1-Cre/R26R-LacZ* , to demonstrate their neural crest origin of murine dental pulp stem cells. The results from these studies will be discussed in the next chapter.

Table 3.1 The mouse-specific primer sequences

RT-PCR primers			
Gene	**Forward primer (5'→3')**	**Reverse primer (5'→3')**	**GenBank Accession number**
Adipsin	GTGCTGCACACTGCATGGAT	CCGGGTTCCACTTCTTTGTC	NM_013459
Brachyury	CCCCTATGCTCATCGGAACA	GTAGGTGGGCTGGCGTTATG	NM_009309
Bsp	AGAACAATCCGTGCCACTCACT	CCCTGGACTGGAAACCGTTT	NM_008318
CD105	CTTCGTACAGGTGAGCGTGTCT	GCTAGGGCGCAGAGCTAAGTT	NM_007932
CEBPa	GCCAAGAAGTCGGTGGACAA	AGTTGCCCATGGCCTTGAC	NM_007678
c-Kit	AGCCTGGCGTTTCCTACG T	GCCCGAAATCGCAAATCT TT	NM_001122733
Col2a1	AGGATGGCTGCACGAAACA	TCAGTGCAGATCCTGGAGTGACT	NM_031163
Dmp1	TTGGGAGCCAGAGAGGGTAGA	AGTCCACCAGCCGGTCTGTA	NM_016779
Dspp	CCCCTCGGAGGCTTTGA	ACTCGGAGCCATTCCCATCT	NM_010080
GAPDH	CTCGTCCCGTAGACAAAATGG	CGCTCCTGGAAGATGGTG	NM_008084
Gata6	AGCAGGACCCTTCGAAACG	GCGCTTCTGTGGCTTGATG	NM_010258
Gsc	ACGCTGTCGCGCACTGA	CTCCGGCGAGGCTTTTG	NM_010351
Klf4	GGTTTTGGTTTGAGGTTTTGTTTCT	CCTCACGCCAACGGTTAG TC	NM_010637
Leptin	ACCTGCTCCGGGTACATGTTC	TGGGCAGACCCATCAATAGG	NM_008493
LNGFR	GAGGCACCGCTGACAACCT	CAGGCCTCGTGGGTAAAGG	NM_033217
Lpl	GGATGGACGGTAACGGGAAT	CATGGGCTCCAAGGCTGTAC	NM_008509
Mesp2	CCCCAAATACAGTCACCCTTACAC	GGCTGTAGTCTCTGGCATGATG	NM_008589
Msi1	GACCCCTGCAAGATGTTCATC	CTCTGTGCCTGTTGGTGGTTT	NM_008629
Nanog	TCTCAAGTCCTGAGGCTGACAAG	GTGCTGAGCCCTTCTGAATCA	NM_028016
Ncam	TGCTCGTGTGTCCTCCTTGA	GCTTGGCAGCAACTGACCAT	NM_001081445
NFH	CGTAAAACACGCGTCTAAAAACTG	GAGTACACCCTGGCGTGG TT	NM_010904
NFL	GCCTTGGACATCGAGATTGC	CAGCTTTCGTAGCCTCAATGG	NM_010910
Ocn	TTGGTGCACACCTAGCAGACA	TCGTCACAAGCAGGGTTAAGC	NM_001032298
Oct4	CTGGGCGTTCTCTTTGGAAA	TCGGGCACTTCAGAAACATG	NM_013633
Opn	CAGTGATTTGCTTTTGCCTGTT	TCGTCGTCCATGTGGTCATG	NM_009263

RT-PCR primers			
Gene	**Forward primer (5'→3')**	**Reverse primer (5'→3')**	**GenBank Accession number**
Osx	AGAGATCTGAGCTGGGTAGAGGAA	AAGTTGAGGAGGTCGGAGCAT	NM_130458
Pax3	CGCTGTCTGTGATCGGAACA	TCTGCTCCTGCGCTGCTT	NM_001159520
Pdgfra	TTTGTGCCTCTCGGGATGA	TGACGGGCAGCACATTCA	NM_011058
Pparg2	CAAGAATACCAAAGTGCGATCAAA	GGATCCGGCAGTTAAGATCACA	NM_011146
Runx2	AATGCCTCCGCTGTTATGAAA	GAATGCGCCCTAAATCACTGA	NM_001146038
Slug	CACTGTGATGCCCAGTCTAGGA	GCAGATGTGCCCTCAGGTTT	NM_011415
Snail	TGACCTCGCTGTCCGATGA	GTGCTTGTGGAGCAAGGACAT	NM_011427
Sox10	CAGCCACGAGGTAATGTCCAA	GTGTAGGCGATCTGGGAAGTG	NM_011437
Sox2	CCGGACCGCGTCAAGAG	TCATGAGCGTCTTGGTTTTCC	NM_011443
Sox9	ACCCACCACTCCCAAAACC	GATGCCGTAACTGCCAGTGTAG	NM_011448
TrkC	GGGTCCTGTGGCTGTTATCAG	GGCTCCCTCACCCAATTCTC	NM_008746
Twist	GACGAGCTGGACTCCAAGATG	GCCCCTCTGGGAATCTCTGT	NM_011658
Vimentin	CCAGAGAGAGGAAGCCGAAA	TTCATACTGCTGGCGCACAT	NM_011701
Q-RT-PCR primers			
Gene	**Forward primer (5'→3')**	**Reverse primer (5'→3')**	**GenBank Accession number**
Calponin	ATGCCCAGACCTGGCTCAAA	ACTGCAGATGGGCACCAACA	NM_009922
GAPDH	GGGAAGCCCATCACCATCT	GCCTCACCCCATTTGATGTT	NM_008084
Klf4	AGACATCGCCGGTTTATATTGAA	AACCAAAACCCCCAGATTGC	NM_010637
Myocardin	ACACTCCTGGGGTCTGAACA	GCGGTATTAAGCCTTGGTTAGC	NM_145136
Nanog	AAGCGGTGGCAGAAAAACC	GTGCTGAGCCCTTCTGAATCA	NM_028016
Sm22-alpha	CAACAAGGGTCCATCCTACGG	ATCTGGGCGGCCTACATCA	NM_178598
Sma	TACATGGCGGGGACATTGAA	CCGATAGAACACGGCATCATCA	NM_007392
SMHC	AAGCTGCGGCTAGAGGTCA	CCCTCCCTTTGATGGCTGAG	NM_013607
SRF	GGCCCCACAGCAAGCGTCTC	GTGGCGGGCAACGTCACTGT	NM_020493

Table 3.2 Lists of differentiation media

Differentiation	Cell density (cells/cm^2)	Media composition	Reference
Osteogenic (Osteo-odontogenic)	2x10^{4}cells plated on plastic surface	Serum-free media supplemented with 10% FBS, 10 mM β-glycerophosphate (CalBiochem), 0.2 mM L-ascorbic acid, and 100 nM dexamethasone	(Gronthos et al., 1994)
Chondrogenic	2x10^{4}cells plated on plastic surface	Serum-free media supplemented with 10% FBS, 100 ng/ml BMP-2 (Shenandoah Biotech), 0.2 mM L-ascorbic acid, and 100 nM dexamethasone	(Tscheudschilsuren et al., 2006)
Adipogenic	2x10^{4}cells plated on plastic surface	Serum-free media supplemented with 10% horse serum, 100 µM indomethacin (Alfa Aesar), 0.5 mM 3-isobutyl-1-methyl-xanthine (ACROS), and 1 µM dexamethasone	(Gregoire, 2001)
Neurogenic	1x10^4 cells plated on glass surface coated with 5 ng/ml fibronectin	Serum-free media with three series of growth factors; 1) media with 100ng/ml bFGF for the first week; 2) media with 10 ng/ml FGF-8b and 100 ng/ml Shh for the second week; and 3) media with 10 ng/ml BDNF (all from R&D) and 10 ng/ml EGF (Sigma) for the last week of culture	(Jiang et al., 2003)
Smooth muscle	1.5x10^4 cells plated on plastic surface coated with 5ng/ml fibronectin	Serum-free media supplemented with 100 ng/ml PDGF-BB (R&D)	(Ross et al., 2006)

Table 3.3 Lists of antibody for staining

Marker	Antibody	Species	Dilution	Company
BSP (cells)	Monoclonal	Mouse	1:100	Developmental Hybridoma Bank
BSP (tissues)	Polyclonal	Rabbit	1:200	Renny Franceschi, School of Dentistry, University of Michigan
Calponin	Monoclonal	Mouse	1:100	Sigma
Caldesmon	Monoclonal	Mouse	1:100	Sigma
CD31-FITC	Monoclonal	Rat	1:100	eBioscience
COLII	Monoclonal	Mouse	Whole supernatant	Developmental Hybridoma Bank
DMP1	Polyclonal	Rabbit	1:400	Takara
DSP	Polyclonal	Rabbit	1:200	Larry Fisher, NIDCR/NIH
GABA	Monoclonal	Rabbit	1:500	Sigma
KLF4	Polyclonal	Rabbit	1:250	Abcam
MSI1	Polyclonal	Rabbit	1:250-1:500	Abcam
N-CAM	Monoclonal	Rat	1:100	BD PharMingen
NF-160/200	Monoclonal	Mouse	1:500	Abcam
NG2	Polyclonal	Rabbit	1:400	Abcam
OCN	Polyclonal	Rabbit	1:1000	Takara
OPN	Monoclonal	Mouse	1:400	Developmental Hybridoma Bank
S100	Polyclonal	Rabbit	1:400	Dako
SMA-Cy3	Monoclonal	Mouse	1:400	Sigma
SMA-FITC	Monoclonal	Mouse	1:400	Sigma
Smooth muscle myosin heavy chain	Monoclonal	Mouse	1:100	Sigma
SOX10	Polyclonal	Rabbit	1:400	Abcam
VEGFR-3	Monoclonal	Rat	1:100	eBioscience

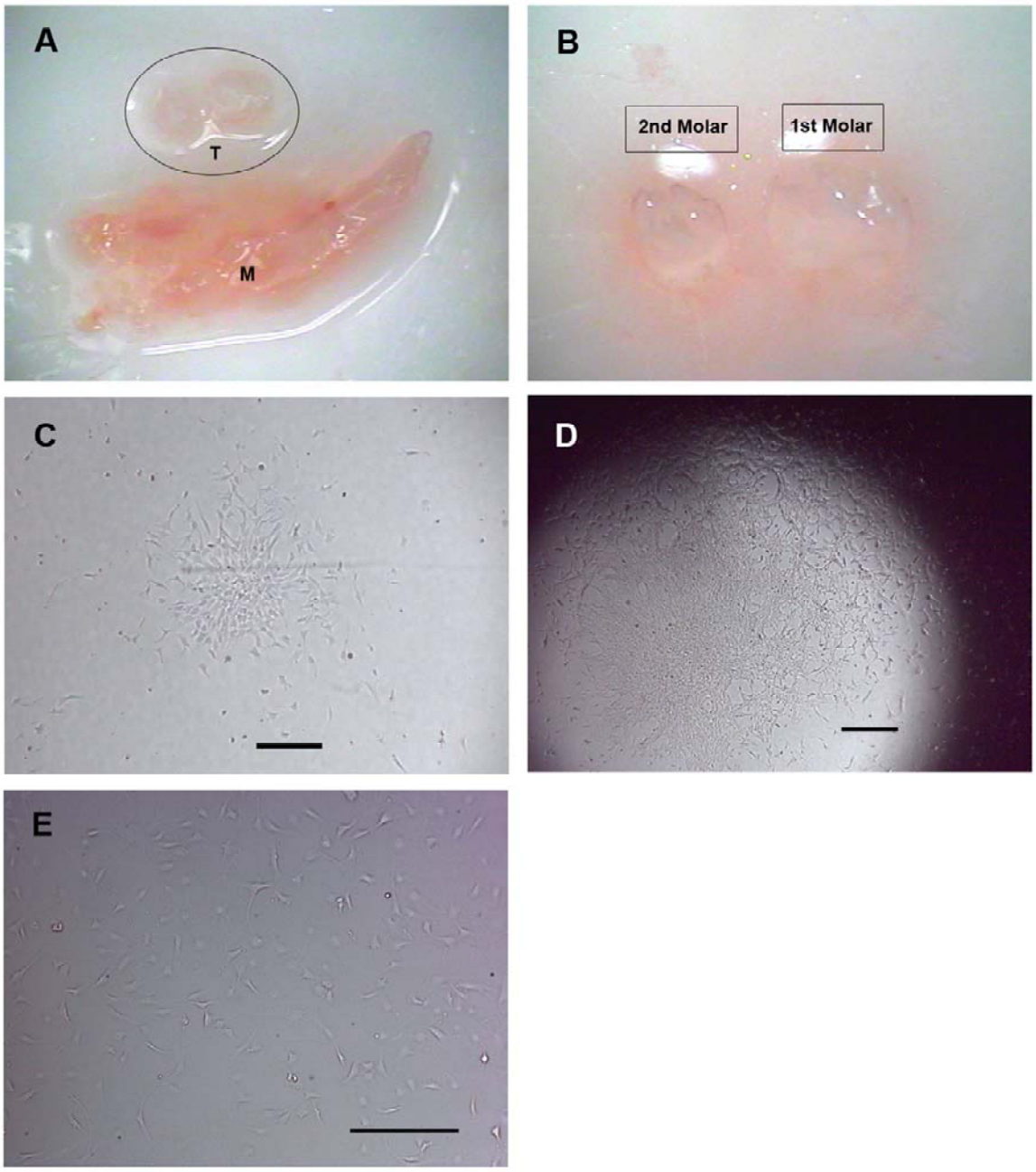

Figure 3.1 DPSC isolation and culture. (A, B) First and second developing molar teeth of 4-8 day-old neonatal mice were isolated from mandible. (C) DPSCs started to proliferate and form a small colony after 2 days in stem cell media under 5% O_2 incubation. (D) DPSCs at day 10 formed larger colonies and were confluent. (E) The cell morphology of DPSCs in early cultures was heterogenous; most of which were spindle-shaped cells. T = teeth, and M = mandible. Scale bars indicate 200 μm.

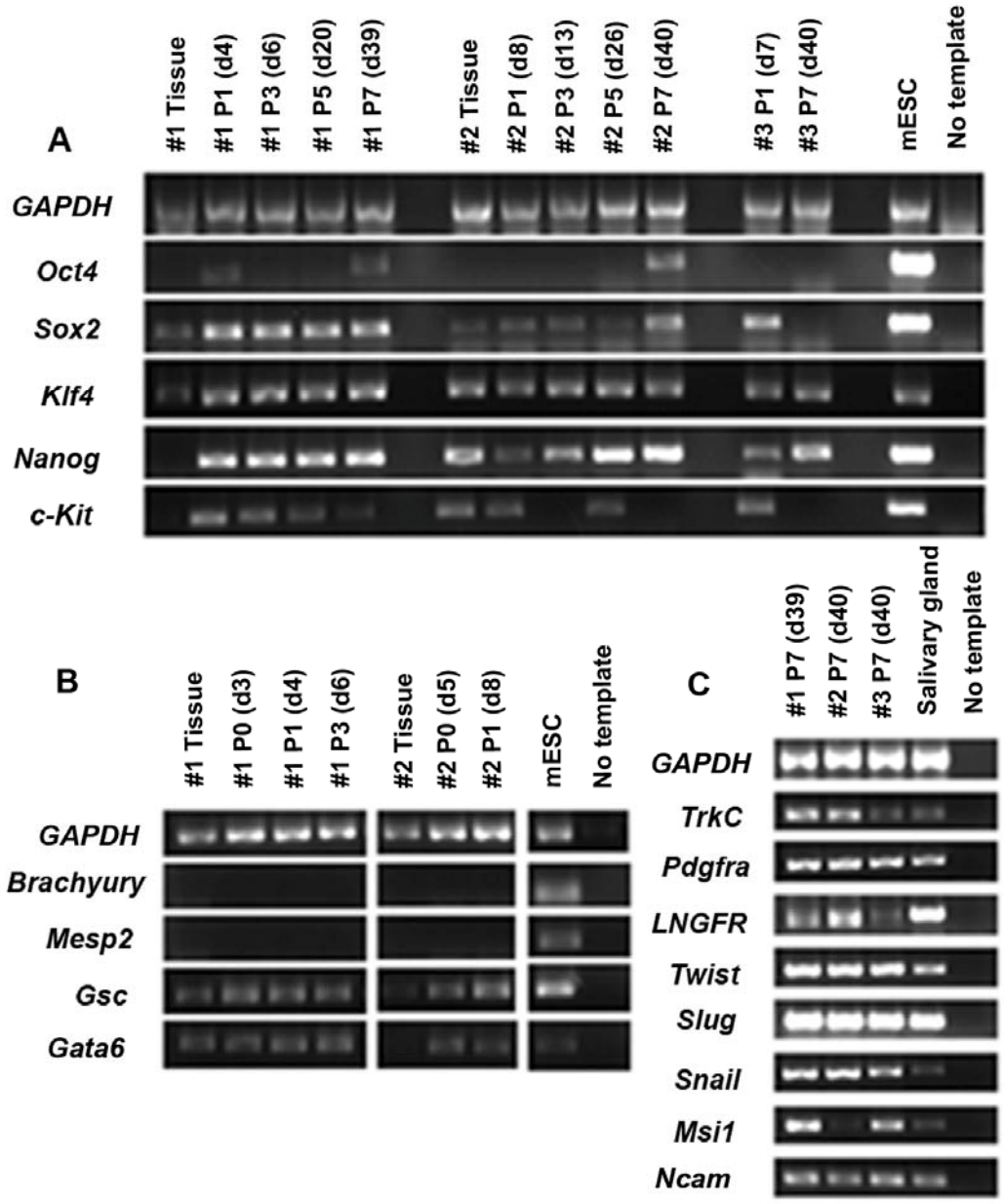

Figure 3.2 Gene profile of DPSC cultures. Gene expression of fresh dental pulp and DPSCs cultured several passages from three isolations (#1, #2 and #3) are shown. (A) Stem cell genes, *Oct4*, *Sox2*, *Klf4*, *Nanog* and *c-Kit,* were observed; however, *Oct4* was inconsistent and transient from early to late passages. (B) In contrast to neural crest developmental genes *Gsc* and G*ata6,* early mesodermal developmental genes *Brachyury* and *Mesp2* were not expressed. (C) Neural crest-related genes *TrkC, Pdgfra, LNGFR, Twist, Slug, Snail, Msi1*, and *Ncam*, were continuously expressed in all three non-clonal DPSCs. RNA isolated from mouse embryonic stem cells (mESC) and salivary gland were used as positive control for the expression of stem cell/early developmental genes and neural crest genes, respectively. The PCR reaction without template was used as negative control.

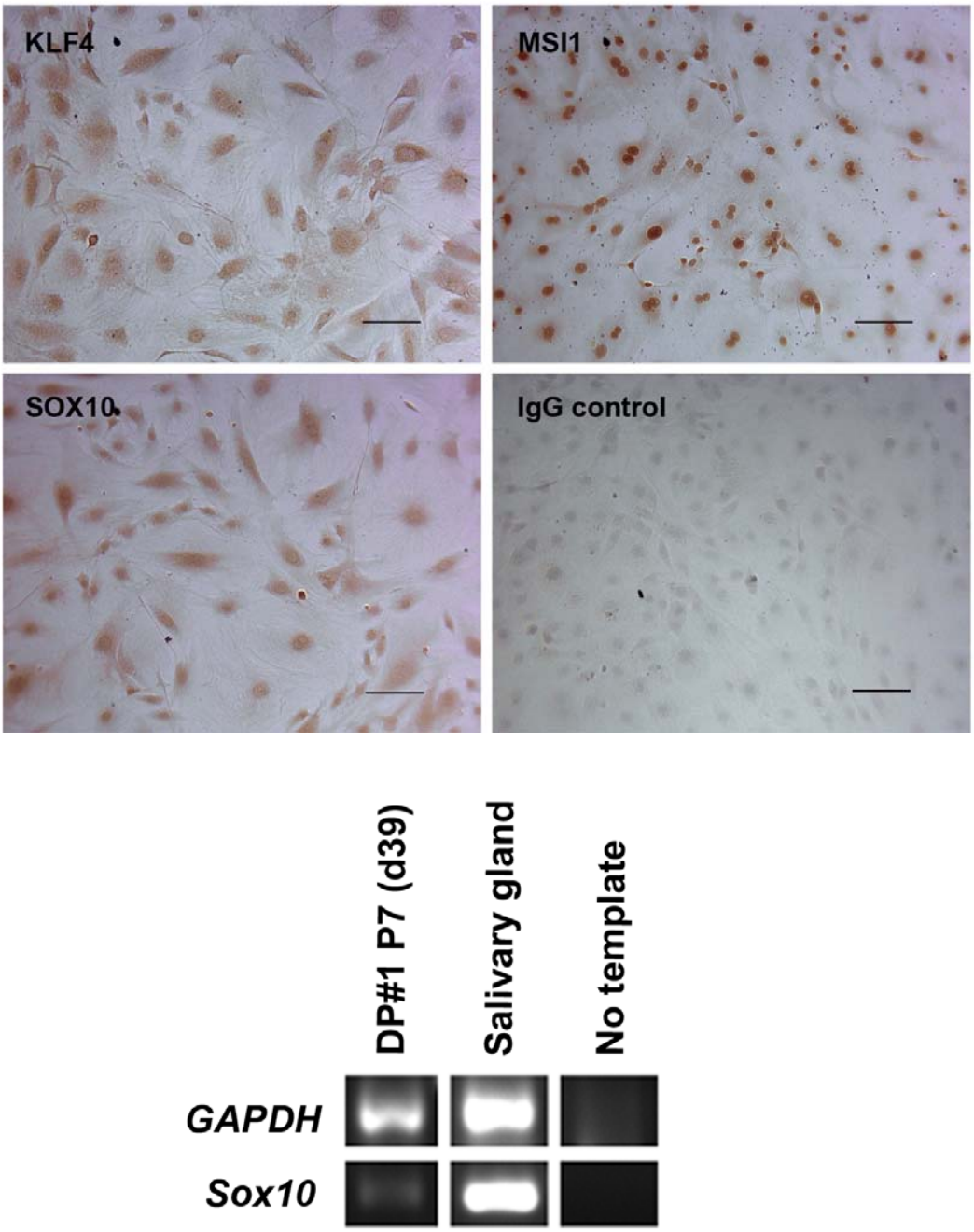

Figure 3.3 Gene and protein expression of undifferentiated DPSCs. Immunocytochemistry showed positive staining of KLF4 to confirm the pluripotency gene *Klf4* expression, and of neural crest-related proteins, MSI1 and SOX10. KLF4 and SOX10 showed nuclear and perinuclear staining. Perinuclear localization of KLF4 and SOX10 has been described in previous reports (Cheung et al., 2005, Chen et al., 2009). Staining with IgG isotype was used as negative control. RT-PCR also showed the expression of *Sox10* in undifferentiated cells. RNA of salivary gland was used as positive control while the reaction without cDNA was used as negative control. Scale bars indicate 100 μm.

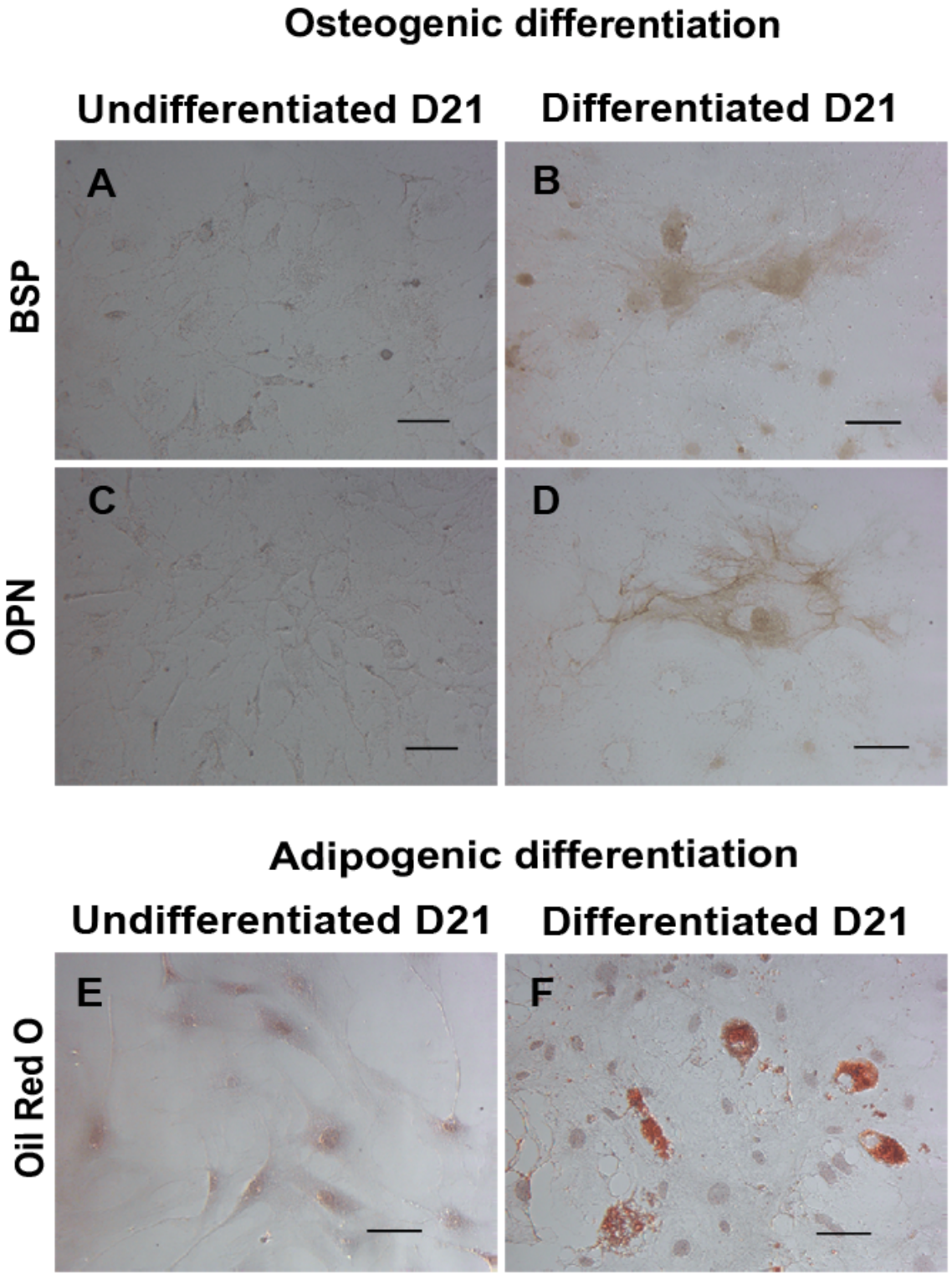
Osteogenic differentiation
Undifferentiated D21
Differentiated D21
BSP
OPN
A
B
C
D
Adipogenic differentiation
Undifferentiated D21
Differentiated D21
Oil Red O
E
F

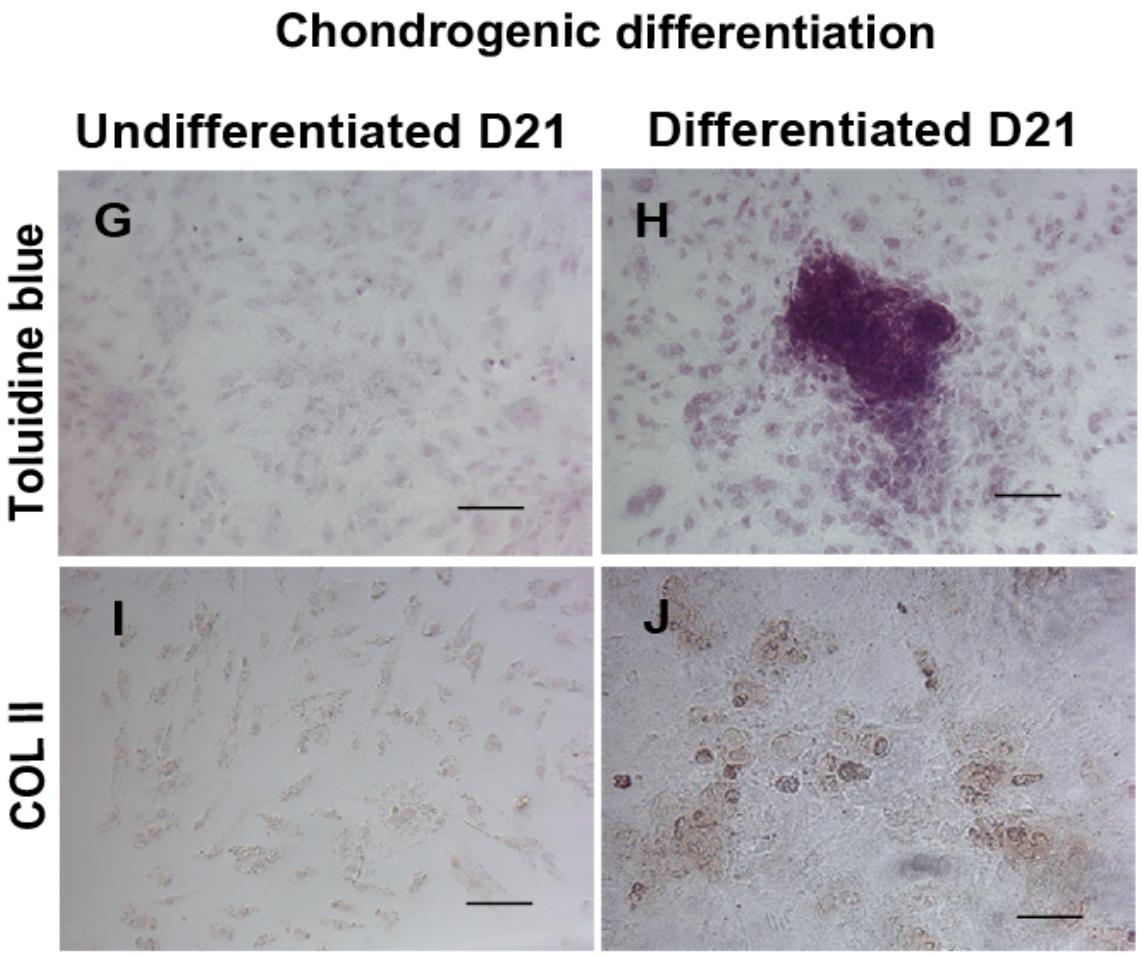
Chondrogenic differentiation
Undifferentiated D21
Differentiated D21
Toluidine blue
COL II
G
H
I
J

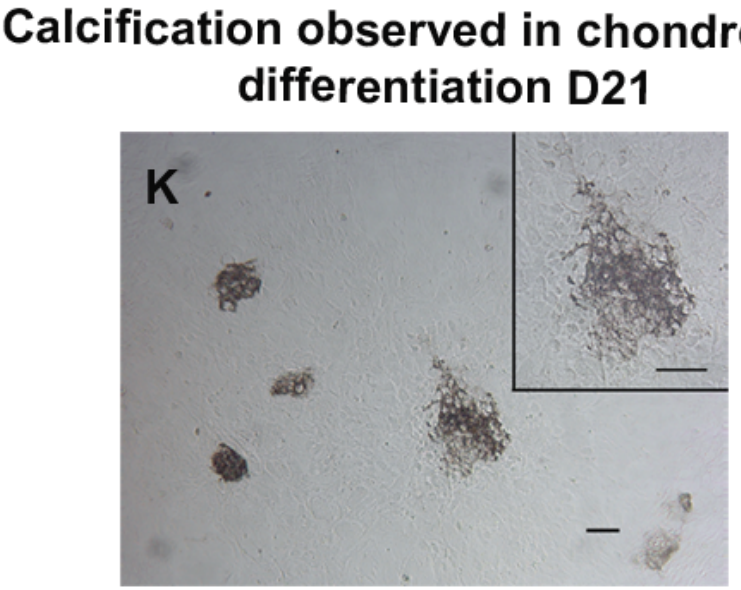
Calcification observed in chondrogenic differentiation D21
K

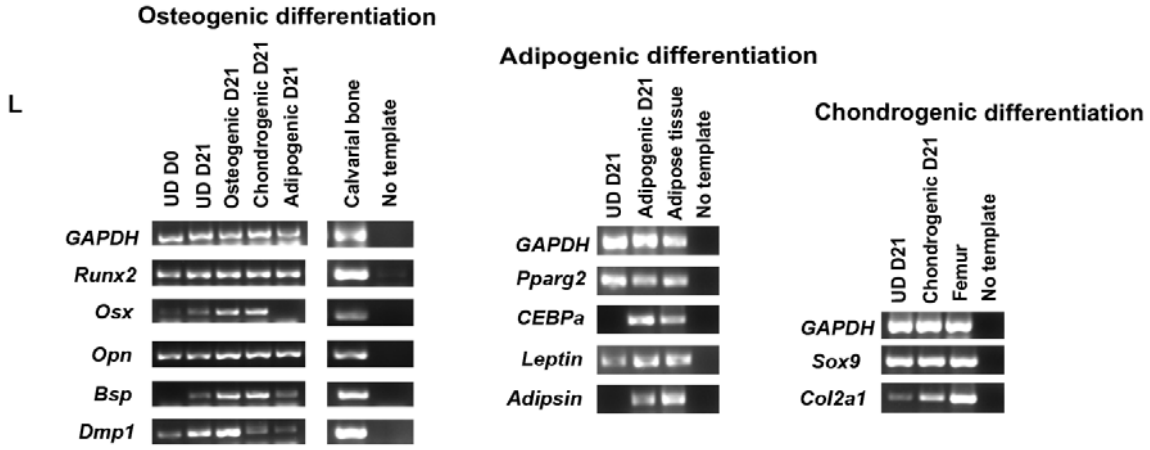

Figure 3.4 DPSC cultures differentiate into neural crest-derived mesenchymal lineages. (A-D) After 21 days in osteogenic media, differentiated DPSCs (Differentiated D21) were positive for BSP and OPN in a membranous location but this pattern was not seen in undifferentiated cells (Undifferentiated D21). (E, F) Cultures in adipogenic media (Differentiated D21), but not in stem cell media (Undifferentiated D21), showed lipid droplets-containing cells positive for Oil Red O. (G-J) Cultures in chondrogenic media (Differentiated D21), but not in stem cell media (Undifferentiated D21), showed cells in clusters positive for toluidine blue and COL II. (K) Mineralized nodules were observed in cells treated with the chondrogenic media after 21 days. The inset depicts a mineralized nodule in high magnification. (L) RT-PCR confirmed the staining results. For osteogenic differentiation (Osteogenic D21), RT-PCR showed expression of osteoblast-associated genes; *Runx2*, *Osx*, *Opn*, *Bsp,* and *Dmp1*. For adipogenic differentiation, induced cells (Adipogenic D21) expressed *Pparg2* and *CEBPa*, adipogenic transcription factors, as well as *Leptin* and *Adipsin,* markers of adipocytes. For chondrogenic differentiation, treated cells (Chondrogenic D21) expressed chondrocyte-associated genes; *Sox9* and *Col2a1*. (A, C, E, G, and I) Confluent undifferentiated cells cultured in stem cell media at day 21 (UD D21) expressed some of differentiation genes, but were negative by staining for all differentiation markers and Oil Red O. Cells were counterstained with hematoxylin. RNA isolated from mouse calvarial bone, adipose tissue, and femur was used as positive control while the reaction without cDNA was used as negative control for gene expression. Scale bars indicate 100 μm.

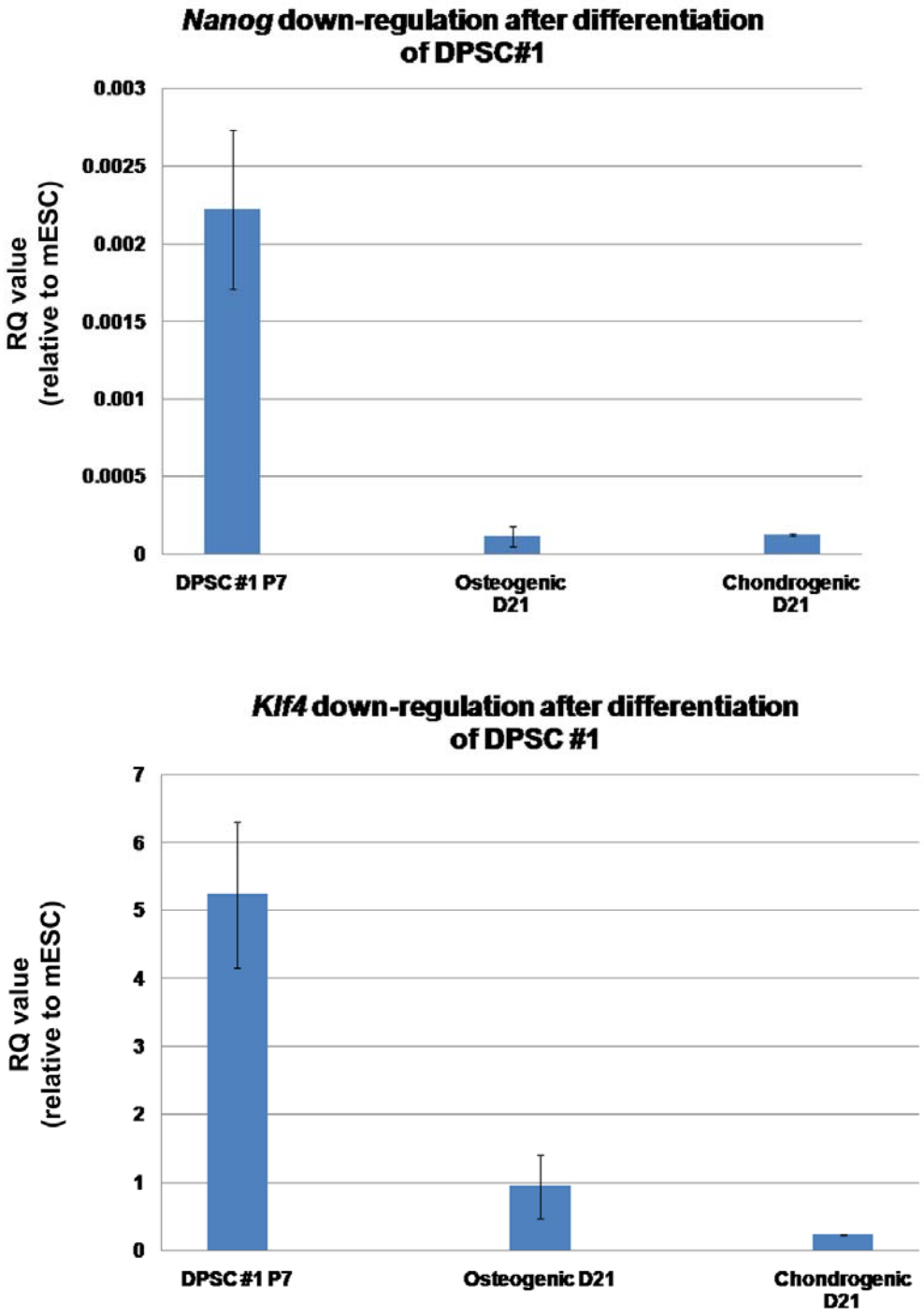

Figure 3.5 Down-regulation of *Nanog* and *Klf4* after differentiation of DPSCs. Q-RT-PCR analyses showed that *Nanog* and *Klf4* were down-regulated after osteogenic and chondrogenic differentiation of DPSC line 1. RQ (Relative Quantification or Relative Expression) values were relative to the gene expression of mouse embryonic stem cells (mESC). Similar results were observed for DPSC line 2. *GAPDH* was used as the internal control for normalization. Error bars represent ± Standard Error of the Mean (SEM).

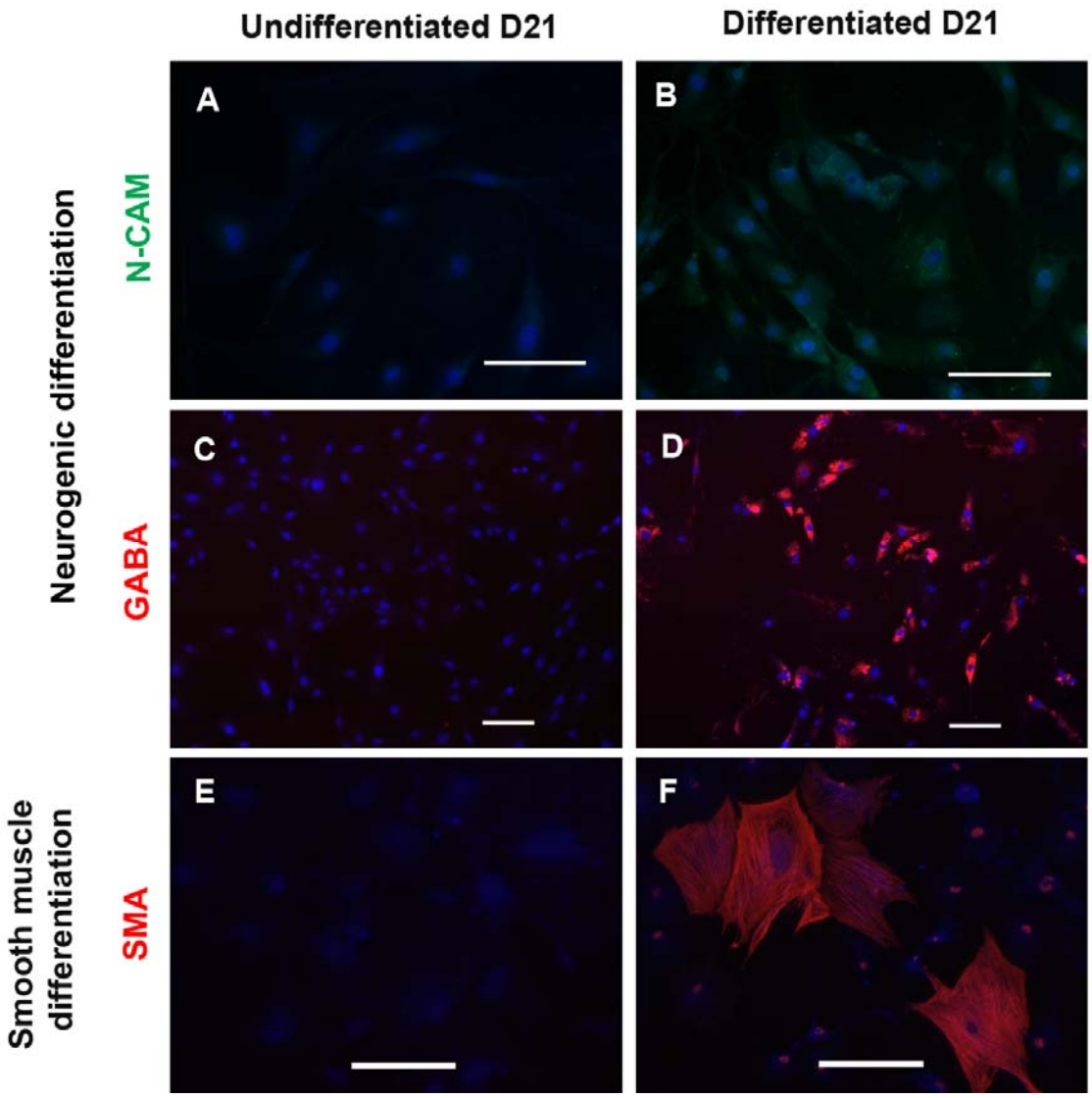

Figure 3.6 DPSC cultures differentiate into neural crest non-mesenchymal lineages.
(B, D) Neuronal-induced cells stained positively for neuronal markers; N-CAM (in green), and GABA (in red). (F) DPSCs in smooth muscle differentiation media showed smooth muscle-like phenotype that stained positively for smooth muscle actin (SMA) (in red). (A, C, and E) Undifferentiated cells in stem cell media at day 21 did not stain positively for any of the three differentiation markers. DAPI used for nuclei staining is depicted in blue. Scale bars indicate 100 µm.

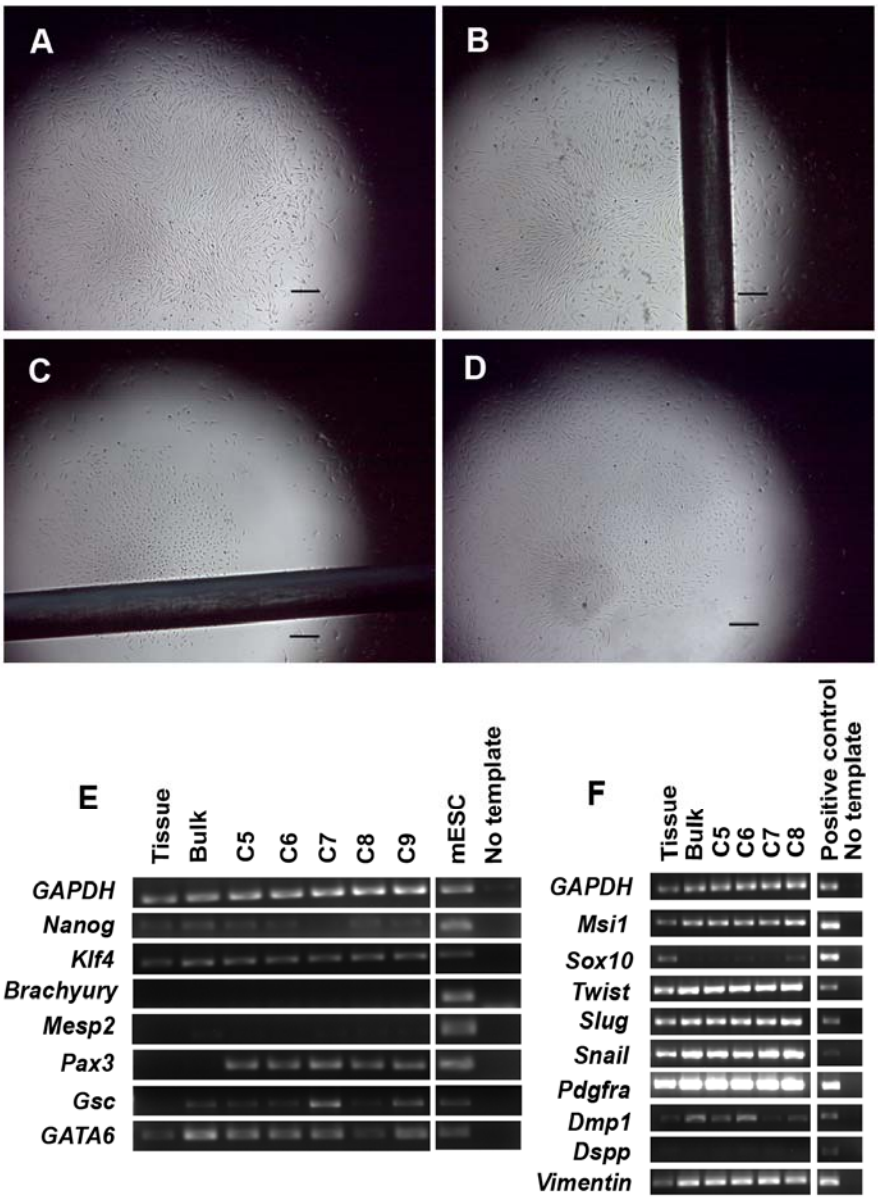

Figure 3.7 DPSC clonal isolation and gene profile. (A-D) At day 10, colonies derived from single cells can be visualized. (E and F) Gene expression of cells from fresh dental pulp (Tissue), cultured non-clonal DPSC line 1 (Non-clonal), and different DPSC clones (C5-C9). (E) RT-PCR showed variable *Nanog* and stable *Klf4* expression among different clones. All clones showed the absence of early mesodermal genes *Brachyury* and *Mesp2*, but showed expression of neural crest developmental genes *Pax3, Gsc,* and *Gata6*. (F) Several neural crest-related genes *Msi1, Twist, Slug, Snail,* and *Pdgfra*, and mesenchymal-related gene *Vimentin*, were strongly expressed in clones. *Dmp1*, but not *Dspp*, was also observed in the clones. RNA of mouse embryonic stem cells (mESCs), salivary gland, clavarial bone and cementoblast cell line were used as positive control while the reaction without cDNA was used as negative control. Scale bars indicate 300 μm.

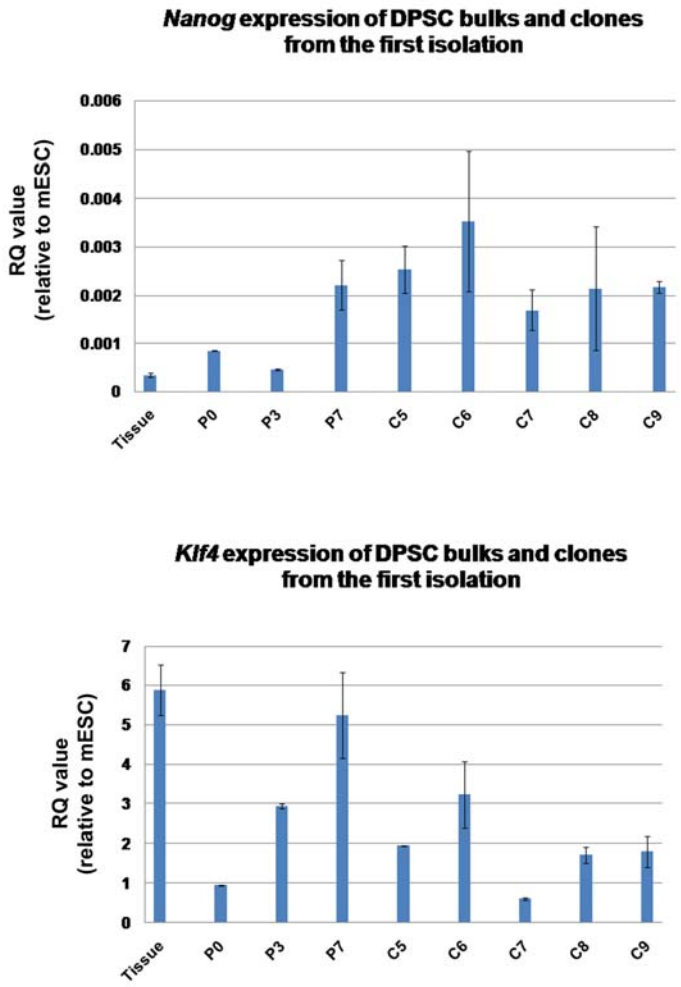

Figure 3.8 *Nanog* and *Klf4* expression of undifferentiated non-clonal and clonal DPSCs. Q-RT-PCR showed RQ (Relative Quantification or Relative Expression) values demonstrating differential *Nanog* and *Klf4* expression in fresh dental pulp (Tissue), non-clonal (bulk) DPSCs in several passages (P0, P3, and P7), as well as, DPSC clones derived from the non-clonal populations (C5-C9). The non-clonal DPSC passage 7 showed the highest expression of *Nanog* and *Klf4* among different passages of cultured non-clonal DPSCs, which we chose for differentiation assays. Nevertheless, dental pulp tissue expressed higher level of *Klf4* than that of cultured cells, possibly due to contamination of odontoblasts expressing *Klf4* during pulp isolation but thereafter the stem cell-like population probably outgrew primary mature odontoblasts under stem cell culture conditions (Chen et al., 2009). DPSC clones 6, 7, and 8 showed higher expression of *Nanog* as compared to non-clonal populations. These clones showed neural crest multi-lineage differentiation capacity (Table 4.1). C5 and C9 showed higher levels of *Nanog* and *Klf4* than that of C7 and C8 but were not able to differentiate into most neural crest-lineages (Table 4.1). Consequently, DPSC clones 6, 7 and 8 were chosen for *in vivo* transplantation. RQ values were relative to the expression of mouse embryonic stem cells (mESC). *GAPDH* was used as the internal control for normalization. Error bars represent ± Standard Error of the Mean (SEM).

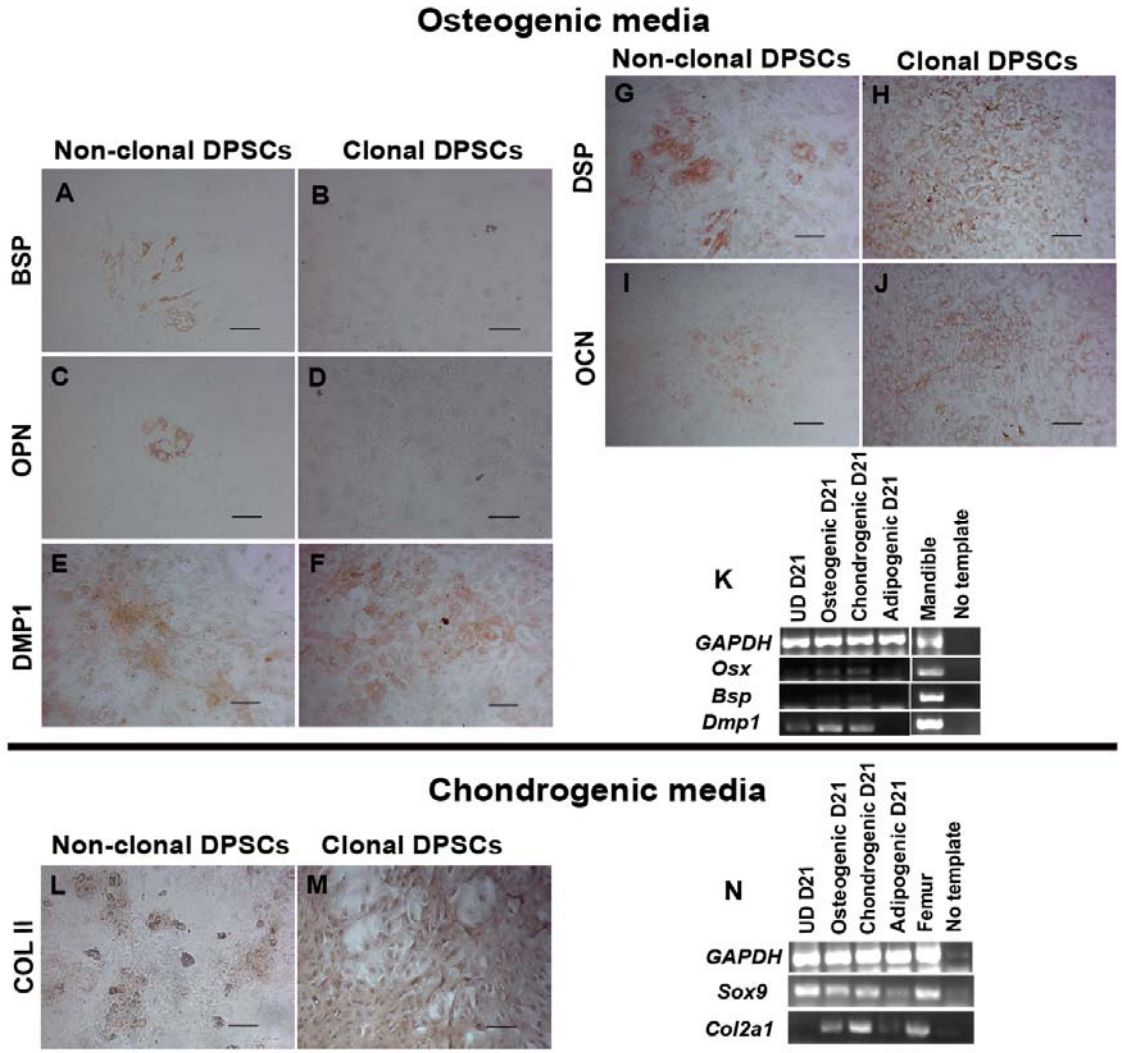

Figure 3.9 Non-clonal and clonal DPSC cultures differentiate into mesenchymal lineages. Treatment of DPSC clones with osteogenic media resulted in different outcomes compared to the differentiation of non-clonal DPSCs. (A-D) Clones did not produce positive cells for BSP and OPN while non-clonal populations showed clusters of positive cells for these markers. (E-J) Non-clonal and all clonal DPSC cultures in osteogenic media stained positively for DMP1, DSP, and OCN. (K) Corresponding to staining results, RT-PCR shows the expression of differentiation genes following treatment of clones with osteogenic media, lack of *Bsp*, but strong expression of *Dmp1* was observed in the differentiation of DPSC clones (Osteogenic D21). (L and M) Non-clonal and 4 out of 5 clones (C5-C8) stained positively for COL II after treatment with chondrogenic media. (N) RT-PCR shows strong expression of chondrogenic markers, *Sox9* and *Col2a1*, in DPSCs cultured in chondrogenic media (Chondrogenic D21). Staining and RT-PCR are all derived from a representative clone (C6). RNA isolated from mouse mandible and femur was used as positive control for gene expression. Scale bars indicate 100 μm.

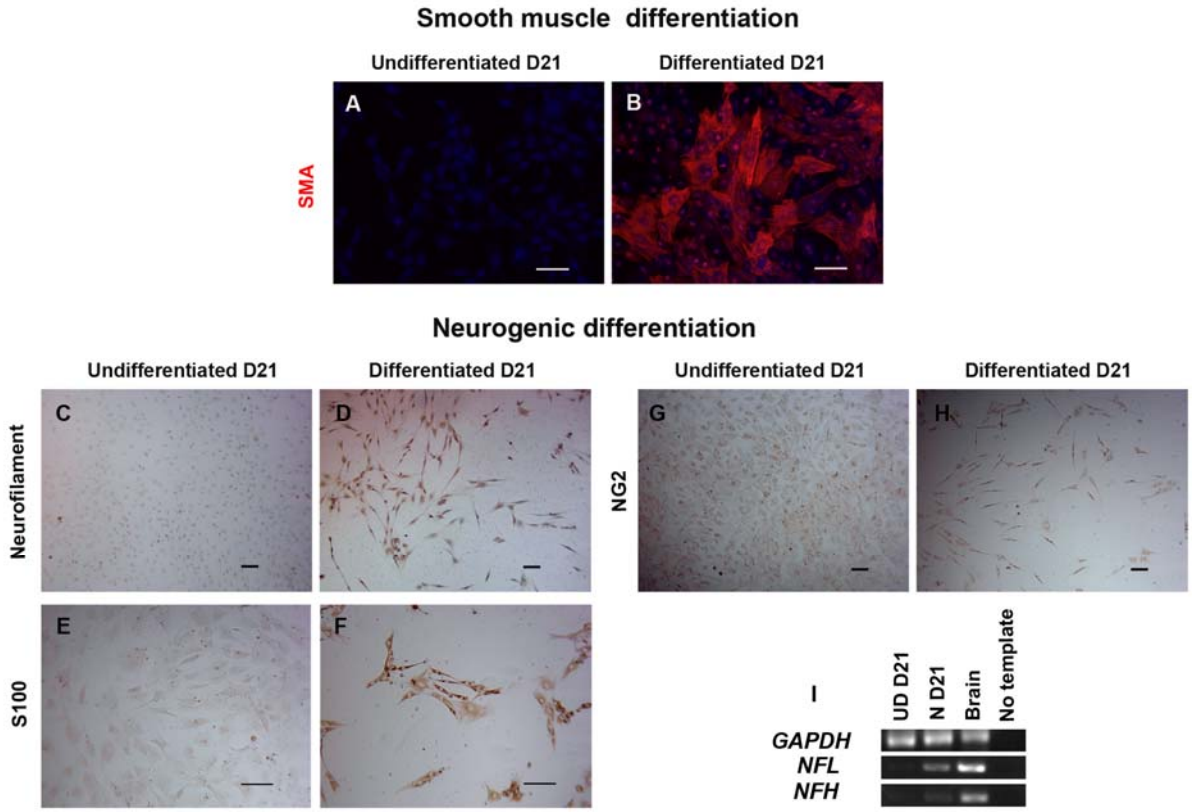

Figure 3.10 DPSC clones differentiate into neural crest non-mesenchymal lineages. (B) All clones showed smooth muscle-like cells positive for smooth muscle actin (SMA) (in red). (D, F, and H) Three clones (C6-C8) showed positive cells for neurofilament (NF-160/200), S100, and NG2. (I) The NF staining was confirmed by RT-PCR of neurofilament-light (NFL) and -heavy (NFH). (A, C, E, and G) Undifferentiated clones were negative for smooth muscle and neuronal markers. DAPI used for nuclei staining is depicted in blue. Scale bars indicate 100 μm.

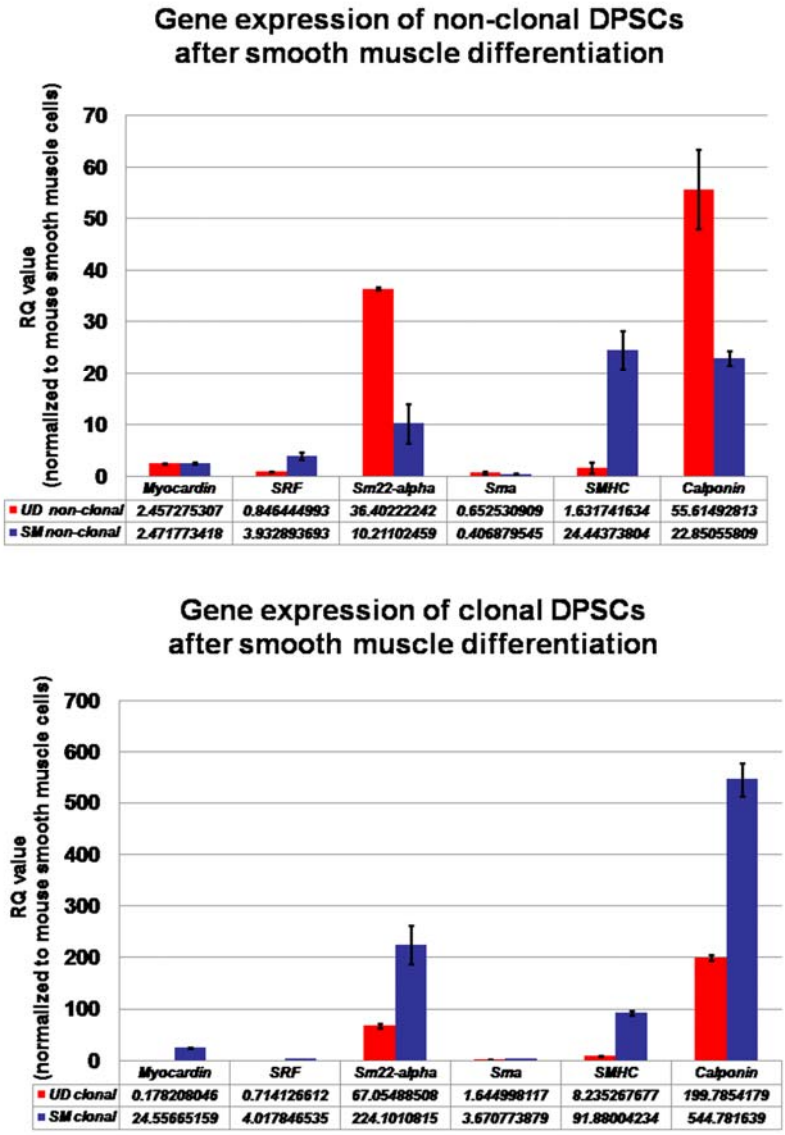

Figure 3.11 Gene expression of non-clonal and clonal DPSCs after smooth muscle differentiation. Q-RT-PCR showed RQ (Relative Quantification or Relative Expression) values demonstrating smooth muscle genes of non-clonal and clonal DPSCs after 21-day culture in smooth muscle differentiation media. As compared to non-clonal DPSCs, higher expression of *Sm22-alpha*, *Sma*, *SMHC*, and *Calponin,* which are smooth muscle- and pericyte-related genes, were observed in the undifferentiated clonal DPSCs. The differentiated cells derived from the clonal populations showed a pattern of smooth muscle maturation with significantly increased levels of *Myocardin, Sm22a, Sma*, *SMHC*, and *Calponin* (about 10 folds higher than non-clonal differentiated cells and >100 folds compared to aortic smooth muscle cells) while in the non-clonal populations this trend of maturation is not apparent. RQ values were relative to the expression of mouse aortic smooth muscle cells. *GAPDH* was used as the internal control for normalization. Error bars represent ± Standard Error of the Mean (SEM).

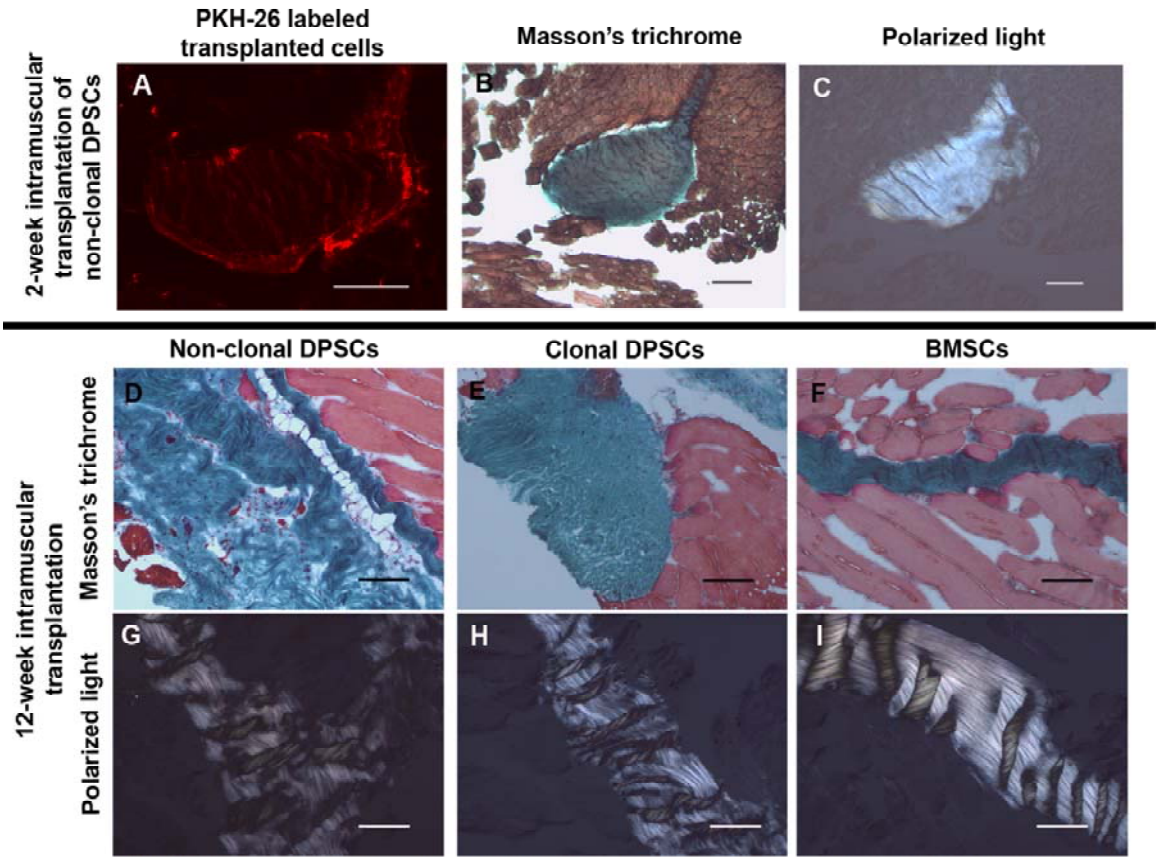

Figure 3.12 Intramuscular transplantation of DPSCs and BMSCs. (A) Non-clonal DPSCs were identified as PKH-26 positive cells. (B, D-F) 2- or 12-week intramuscular non-clonal DPSC, clonal DPSC, and BMSC transplants showed donor cells formed compacted collagen bundles which were strongly positive for Masson's trichrome in blue, but slight positive for DMP1, DSP, and OCN (data not shown). Skeletal muscles were shown in red. (C, G-I) Polarized light confirmed the formation of collagen fibers from all transplanted cells. Scale bars indicate 100 μm.

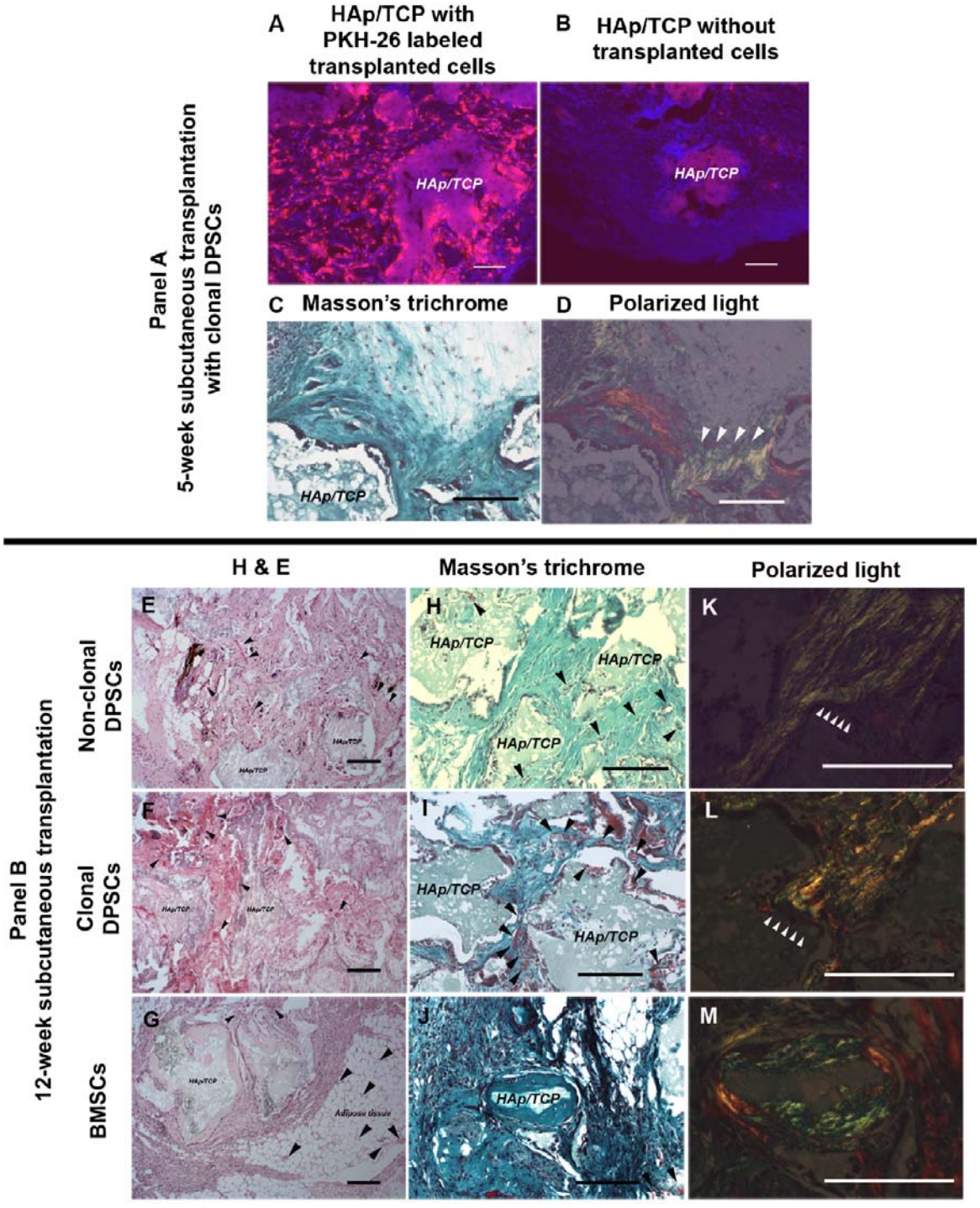
Panel A
5-week subcutaneous transplantation with clonal DPSCs
A HAp/TCP with PKH-26 labeled transplanted cells
B HAp/TCP without transplanted cells
HAp/TCP
HAp/TCP
C Masson's trichrome
D Polarized light
HAp/TCP
Panel B
12-week subcutaneous transplantation
H & E
Masson's trichrome
Polarized light
Non-clonal DPSCs
Clonal DPSCs
BMSCs
E
F
G
H
I
J
K
L
M
HAp/TCP
HAp/TCP
HAp/TCP
HAp/TCP
HAp/TCP
HAp/TCP
Adipose tissue

Figure 3.13 Subcutaneous transplantation of DPSCs and BMSCs. Non-clonal and clonal DPSCs (C6-C8) were labeled with PKH-26 before transplantation to track cells *in vivo*. Panel A shows 5-week subcutaneous (SC) transplantation of DPSC clones with HAp/TCP. (A and B) PKH-26+ cells SC transplanted with HAp/TCP were identified in bright red fluorescent color whereas the HAp/TCP scaffold without cells was devoid of red fluorescent cells despite some autofluoresence derived from HAp/TCP. The HAp/TCP scaffold without cells did not show mineralized tissues (data not shown). Most of transplanted cells surrounded HAp/TCP. (C) These clonal cells generated collagen-forming matrix shown in blue of Masson's trichrome. (D, white arrowheads) Polarized light was used to confirm collagen formation. Panel B shows 12-week SC transplantation of non-clonal DPSCs, clonal DPSCs, and BMSCs with HAp/TCP. (E-G) H&E staining showed the morphology of tissues created by non-clonal, clonal DPSCs and BMSCs. Capillaries and small blood vessels near mineralized matrices were found in DPSC transplants. In contrast, BMSCs formed bone condensations near HAp/TCP devoid of vessels. In BMSC transplants capillaries were found mainly in the adipose tissue. The black arrowheads indicate the location of capillaries and small blood vessels. (H-J) Masson's trichrome showed the intensive staining of collagenous extracellular matrices generated by both DPSCs and BMSCs. (K-M) polarized light images with high magnification of transplanted tissues showed different collagen arrangement produced by DPSCs and BMSCs. (K and L, white arrowheads, and M) The white arrowheads indicate the direction of polarized collagen fibers created by DPSCs run perpendicularly to HAp/TCP while that created by BMSCs do not run perpendicularly to scaffold surface. DAPI used for nuclei staining is depicted in blue. *HAp/TCP* = Hydroxyapatite/tricalcium phosphate. Scale bars indicate 200 μm.

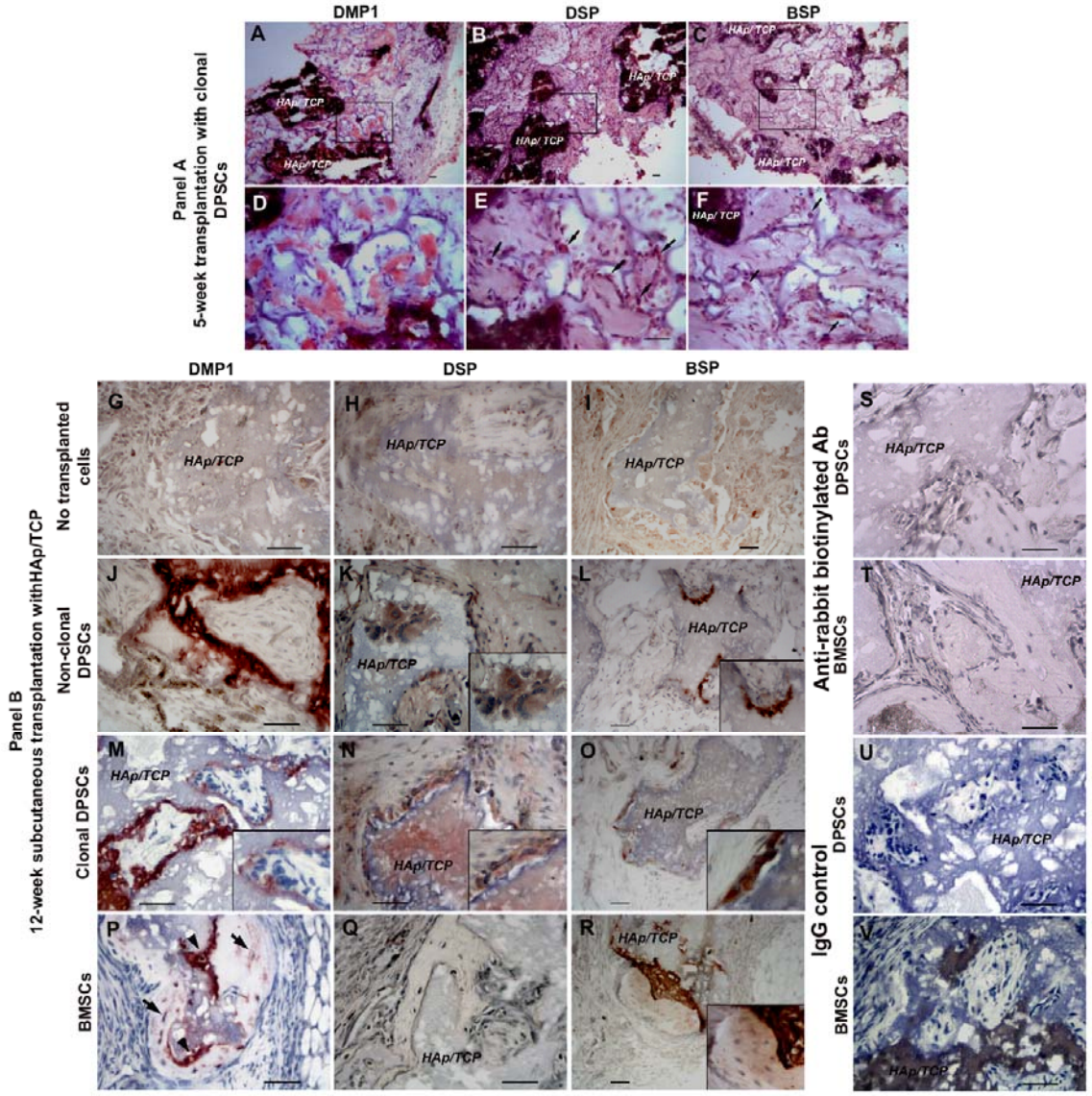

Figure 3.14 Immunohistochemistry of subcutaneous DPSC and BMSC transplanted tissues. Panel A shows the staining of 5-week subcutaneous (SC) clonal DPSC transplanted tissues. (A-C) Three DPSC clones (C6-C8) secreted extracellular matrices which were positive for DMP1, slightly positive for DSP and BSP by immunoperoxidase staining. (D-F) High magnification images correspond to the rectangular areas of A-C. (D) Strong DMP1 staining was seen in the matrices. (E and F, arrows) Strong positive staining for DSP and BSP were observed in the transplanted cells. Panel B shows the staining of 12-week SC transplantations of non-clonal DPSCs, clonal DPSCs, and BMSCs with HAp/TCP. (G-I) Only HAp/TCP transplantation without donor cells did not show any extracellular matrices positive for dentin and bone proteins. (J-O) Both non-clonal and clonal DPSCs secreted extracellular matrices which were strongly positive, but different intensity, to DMP1, DSP, and BSP. All insets in each figure show high magnification images of the transplanted tissues to illustrate the morphology and positive intracellular staining of transplanted cells. (K, M, and N insets) transplanted cells were elongated, polarized, and showed very close relation to scaffold surface, resembling odontoblast-like cell morphology. (K, L, M, N, and O insets) Positive staining of DMP1, DSP, and BSP was

seen in transplanted DPSCs. Some cells showed elongation and polarization. (P, arrowheads and arrows) BMSC transplanted cells showed osteoblast-like cells (arrowheads) lining bone surface, and osteocyte-like cells (arrows) in lacunae which stained positively for DMP1. (Q) Negative staining for DSP was observed in bone matrix and transplanted BMSC cells. (R, inset) Positive staining for BSP was observed in bone matrix secreted by transplanted BMSCs. (S-V) Transplanted sections stained with only anti-rabbit biotinylated antibody or IgG isotype were used as negative control. *HAp/TCP* = Hydroxyapatite/tricalcium phosphate. Scale bars indicate 200 μm.

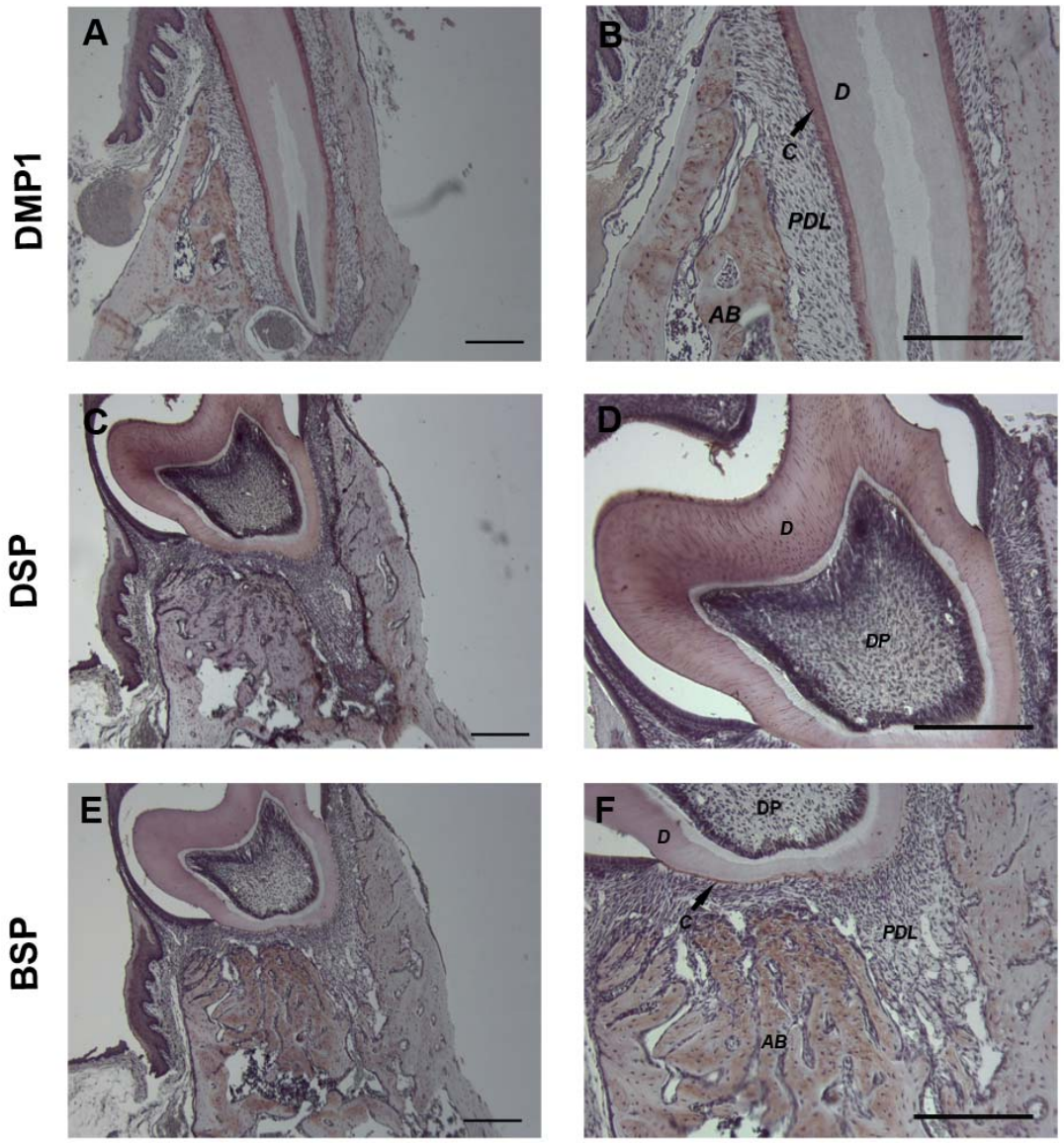
DMP1
DSP
BSP
A
B
C
D
E
F
D
C
PDL
AB
D
DP
DP
D
C
PDL
AB

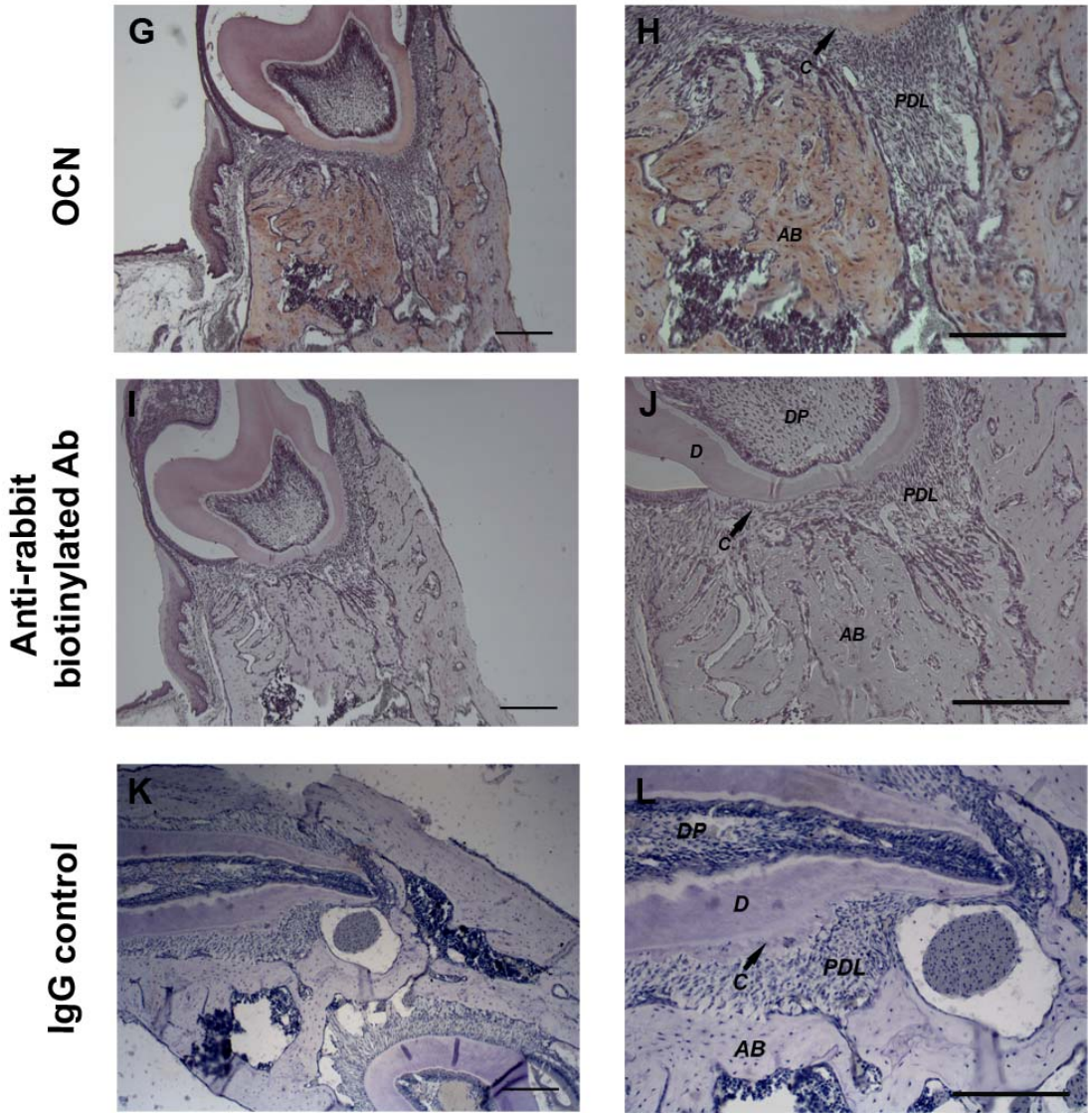

Figure 3.15 Staining of tooth sections for dentin and bone proteins. The specificity of all antibodies for dentin and bone matrix proteins used in this report was confirmed by immunoperoxidase staining with AEC in murine tooth sections as positive control. All tooth sections are a gift from Dr. Martha Somermen, University of Washington. (A and B) The tooth section of 19-day-old Ankylosis (ANK) knockout mice stained by DMP1 antibody showed positive staining in cementum and alveolar bone (Fong et al., 2009). (C-L) Staining of the 26-day-old wild-type (WT) murine tooth section showed positive staining of DSP, BSP, and OCN, as well as, negative controls. (C and D) DSP staining was present in dentin and odontoblast cells lining at the periphery of dental pulp. (E-H) BSP staining was positive in alveolar bone and cementum, but slightly positive in odontoblastic cell layer, as well as, OCN positively stained alveolar bone and odontoblastic cell layer. (I-L) Sections stained with anti-rabbit biotinylated antibody or IgG isotype were used as negative control. Sections were counterstained with hematoxylin. AB = Alveolar bone, DT = Dentin, DP = Dental pulp, C = Cementum, PDL = Periodontal ligament. Scale bars indicate 200 μm.

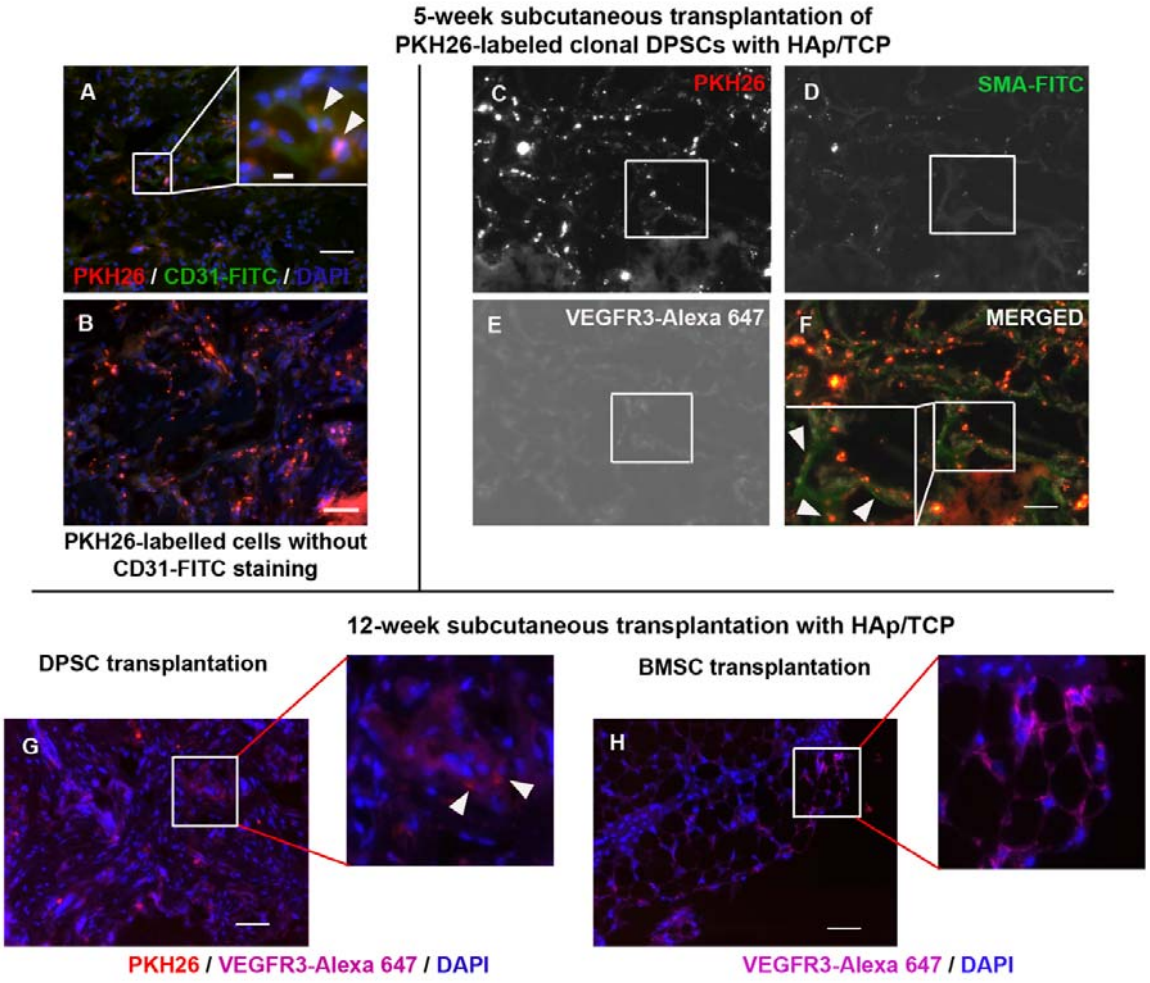

Figure 3.16 Abundant microvessels were observed in DPSC transplantation. (A, inset, indicated by an arrowhead) Abundant microvessels that stained positive for CD31-FITC indicating endothelial cells (green) were observed in mineralized tissues formed by 5-week subcutaneous transplanted DPSCs labeled with PKH-26 (red). Some PKH-26+ (donor DPSCs) cells were adjacent to these microvessels and seem scattered around vessels. (B) Autoflurescence or non-specific green fluorescence was not detected in PKH26-labeled DPSC transplants without CD31-FITC staining. (C-F, inset) Staining for smooth muscle actin (SMA-FITC) in green showed that these microvessels did not contain a thick muscle layer but were wrapped by pericyte-like cells that were SMA+ and some were also PKH-26+ in red (arrowheads). Many of these microvessels seem fenestrated and stained positive for VEGF receptor 3 (VEGFR-3) in pseudo-color white. (G, inset) Similar to 5-week transplants, in the 12-week DPSC transplants abundant microvessels (positive for VEGFR-3 in pseudo-color magenta) in close proximity to odontoblast-like cells with fenestrated morphology surrounded by PKH-26+ cells (indicated by arrows) were observed in DPSC transplants. (H, inset) In the BMSC transplants, microvessels were predominantly found in areas rich in adipocytes, but not close to the bone forming areas. DAPI used for nuclei staining is depicted in blue. Scale bars indicate 100 μm.

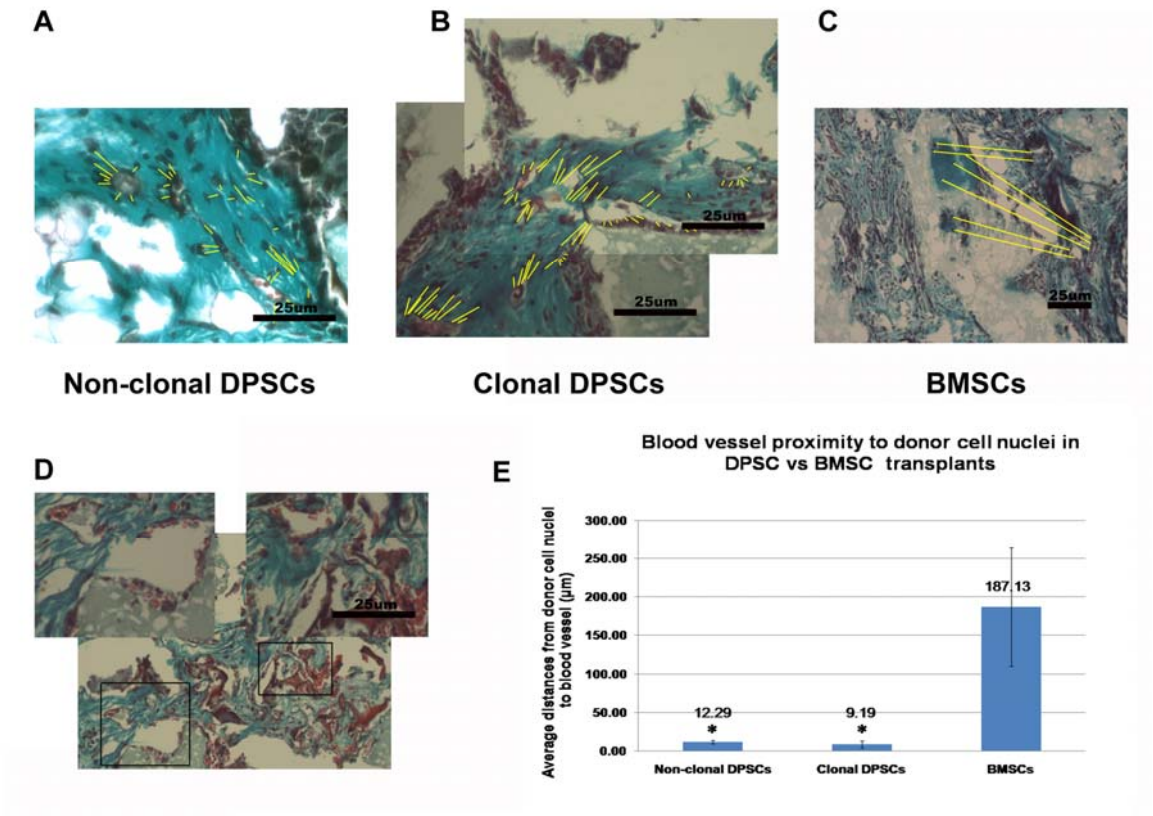

Figure 3.17 Proximity of donor cell nuclei to blood vessels in DPSC and BMSC transplantation. The average distance of donor nuclei in condensed matrices to nearest capillaries was measured using ImageJ v1.43u (Wayne Rasband, NIH; http://rsb.info.nih.gov/ij). The distances between donor nuclei to blood vessels were represented by yellow lines. (A and B) In the 12-week DPSC transplants, abundant microvessels with fenestrated morphology were seen in close proximity to odontoblast-like cells in both non clonal and clonal DPSC transplants. (C) In BMSC transplants microvessels were predominantly found in areas rich in adipocytes whereas mineralized areas formed by BMSCs were distant to microvessels. Microvessels were mature as circulating red blood cells can be seen throughout in both DPSC and BMSC transplants. (D) Abundant microvessels with fenestrated morphology containing circulating red blood cells (insets) are seen in close proximity to mineralized matrix formed by DPSCs. (E) The bar graph shows that the average distance from odontoblast nuclei to nearest capillary was significantly close (9µm ± 4.49) and consistent across all DPSC transplants whereas the average distance of osteocyte nuclei in bone condensations to nearest microvessels were significantly farther (187µm ± 76.88). The average distances from donor cell nuclei to blood vessels in non-clonal DPSCs (n=5, n; numbers of measured area) or clonal DPSCs (n=7) and BMSCs (n=5) are statistically significant. Student's t-test calculated * $p \leq 0.05$. Error bars represent ± Standard Error of the Mean (SEM). Scale bars indicate 25 µm.

CHAPTER 4

Wnt1-Cre/R26R-LacZ mouse used as a model to determine the developmental origin of dental pulp stem cells (Janebodin et al. 2011)

4.1 Introduction

Neural crest is a pluripotent cell population formed in the developing vertebrate embryo and located at the junction between epidermal ectoderm and presumptive neural ectoderm at the dorsal lip of the developing neuroectoderm. During early embryological development, neural crest cells extensively migrate from the lateral margins of the neural tube from four different segments of the neuraxis: cranial, cardiac, vagal, and trunk, and contribute to different specific cell types in several organs of the vertebrate body (Bronner-Fraser, 1995).

Cranial neural crest cells migrate to the first branchial arch and participate in differentiation of dental mesenchyme to develop dental pulp and giving rise to dentin-forming cells, odontoblasts (Thesleff, 2003). In addition, cranial neural crests show multipotent differentiation capacity by giving rise to the majority of the bone and cartilage of the head and face, as well as to neuron and glial cells in cranial ganglia, smooth muscle, connective tissue and pigment cells (Abzhanov et al., 2003). During tooth development, dental pulp which is loose connective tissue containing several cell types with diverse developmental origins is derived from neural crest and non-neural crest tissues (Chai et al., 2000). Although neural crest contributes to a majority of cells in dental pulp, the origin of dental pulp stem cells (DPSCs), a subset of stem cell population found in dental pulp, is still unclear.

Previously, DPSCs have been indirectly suggested to be of neural crest origin. The expression and function of the Eph/ephrin molecules on DPSCs, which play an essential role in the neural crest migration, suggests that neural crest contributes to DPSCs (Stokowski et al., 2007). Stem cell populations in adult human dental pulp have been described based on low-affinity nerve growth factor receptor (LNGFR) and β1-integrin expressions, suggesting that the former population is neural crest-derived (Waddington et al., 2009). In a separate study stem cells isolated from rat embryonic mandibular processes, of neural crest origin, showed multi-differentiation to neural and mesenchymal lineages suggesting DPSCs retain the differentiation capacity of embryonic progenitors (Zhang et al., 2006). Collectively, these reports urged us to investigate the origin of DPSCs.

In the past, most reports studying in the neural crest contribution were based on vital dye labeling, transplantation and viral transfection of neural crest cells and mostly happened in the avian system (Le Douarin and Teillet, 1973, Kuratani and Kirby, 1991, Murphy et al., 1991, Serbedzija et al., 1992). However, *ex-utero* culturing embryos, microsurgical manipulation of embryonic tissue, and retaining the dye throughout the long period of embryological development was potentially difficult to obtain a systematic lineage tracing of neural crest derivatives in mammals. Furthermore, all neural crest cells might not be labeled using either dye labeling or viral infection approaches.

The isolation and characterization of DPSCs from specific cell-lineage transgenic mouse models will provide comprehensive information to directly study the developmental origin of DPSCs, which has been a limitation in human DPSC studies. Two transgenic approaches, *P0-Cre/ CAG-CAT-LacZ* (Yamauchi et al., 1999) and *Wnt1-Cre/R26R-LacZ* (Chai et al., 2000), demonstrated the application of the transgenic system to mark neural crest derivatives driven by

P0 and *Wnt1* promoters, respectively, during early embryogenesis. The expression of the Cre enzyme in neural crest cells will remove a STOP codon flanked by two *loxP* sequences, thereby inducing the *LacZ* expression. Using these transgenic mice, a subset of migrating neural crest cells and a wide variety of cells in the neural crest cell lineage could be marked by *LacZ* expression, facilitating lineage analysis, isolation, and study of the mammalian neural crest cells. Compared to *Wnt1-Cre/R26R-LacZ*, *P0-Cre/CAG-CAT-LacZ* revealed incomplete expression of *LacZ* in neural-crest derived tissue with significant ectopic expression in notochord derived from non-neural crest origin.

I previously demonstrated the successful isolation and characterization of murine DPSCs *in vitro* and *in vivo*. Nevertheless, the developmental origin of DPSCs, which is presumably derived from neural crest, is undetermined. In this chapter, I utilized *Wnt1-Cre/R26R-LacZ* neonatal mice to isolate DPSCs and demonstrate their highly proliferative capacity and multi-differentiation in neural crest-lineage *in vitro* and *in vivo*. Furthermore, the comparison of the niches and mineralized matrix generated by bone marrow stromal cells (BMSCs) and DPSCs when transplanted *in vivo* illustrated main differences in dentinogenesis and osteogenesis and underlying the role of pericytes and microvessels during these processes.

4.2 Materials and Methods

4.2.1 Dental pulp isolation

Dental pulp tissue were isolated in pools (5 mice per preparation) from 4-8 day old *Wnt1-Cre/R26R-LacZ* mouse (n=1 preparation) (a gift from Dr. Michael Cunningham, University of Washington) in accordance with approved Institutional Animal Care and Use Committee (IACUC) guidelines. The molar teeth were separated from the mandible. Pulp tissue was gently

isolated and kept in stem cell media described below. The tissue was washed with PBS (HyClone) and digested with a 1.2 units/ml Dispase II, 2 mg/ml Collagenase type IV (Worthington) supplemented with 2 mM $CaCl_2$ in PBS for 60 min at 37°C. Subsequently an equal volume of stem cell media was added to the digest prior to filtering through 70 mm nylon cell strainers (BD Falcon), and then centrifuging at 300 g for 10 min at room temperature. Cells were then resuspended in stem cell media and single cell suspensions were plated at 1000 cells/cm^2.

4.2.2 DPSC culture

Cells (1000 cells/cm^2) were cultured at 37°C under 5% O_2 and 5% CO_2 in stem cell media, containing a final concentration of 60% low-glucose DMEM (Gibco, Invitrogen), 40% MCDB201 (Sigma), 2% fetal calf serum (HyClone) selected previously for optimal growth of murine mesenchymal stem cells, ITS (Sigma), linoleic acid with bovine serum albumin (LA-BSA) (Sigma), 10^{-9} M dexamethasone (Sigma), 10^{-4} M ascorbic acid 2-phosphate (Sigma), 100 units/ml penicillin with 100 mg/ml streptomycin (HyClone), and $1x10^3$ units/ml leukemia-inhibitory factor (LIF-ESGRO, Millipore), supplemented with 10 ng/mL EGF (Sigma) and 10 ng/mL PDGF-BB (R&D) (Breyer et al., 2006). Once adherent cells were more than 50% confluent, they were detached with 0.25% trypsin-EDTA (Invitrogen) and replated at a 1:4 dilution under the same culture condition with fresh media.

4.2.3 Clonal culture of DPSCs

Cultured DPSCs at passage 4-7 were plated at 50-100 cells/cm^2. Clones were derived from all three non-clonal lines but only clones from line 1 at passage 7 were used in the experiments described here. 24 h after plating, adherent cells were observed and single isolated cells were marked by circling the bottom of the plate with a lab marker. After 10 days, cell

colonies were observed and isolated by using 8x8mm cloning rings (Millipore). The clonal populations were expanded every 4-day and transferred to larger size culture dishes beginning with 96-well, 48-well, 24-well, 12-well, 6-well, 60 mm and 100 mm respectively, until finally being seeding in 150mm culture plates by day 32. The DPSC clones were cultured at a 1:4 dilution until reaching the appropriate cell number for further experiments.

4.2.4 Reverse transcription-polymerase chain reaction (RT-PCR)

DPSCs were extracted for total RNA by using the RNeasy Mini kit (Qiagen) according to the manufacturer's protocol. Quantity and purity of RNA was determined by 260/280 nm absorbance. First-strand cDNA was synthesized from 500 ng of RNA using the High Capacity cDNA synthesis kit from Applied Biosystems (Foster City, CA) per manufacturer's protocols using a randomized primer. cDNA (20 ng) was diluted in a final volume of 20 µl per reaction using the Immomix PCR Mastermix from Bioline (Randolph, MA). PCR for each specific target gene was performed using the following thermal cycling conditions; 95°C 7 min for initial activation followed by 95°C/30 s; 57°C/30 s; 72°C/45 s, for 40 cycles, with a final 5-min extension at 72°C. Mouse-specific primers are listed in Table 4.1. 10 µl of each RT-PCR product was separated on 2% agarose/ethidium bromide gels and viewed under UV light. Glyceraldehyde-3-phosphate dehydrogenase (*GAPDH*) was utilized as control housekeeping gene. RNA extracted from mouse embryonic stem cells (mESC), salivary gland, brain, liver, calvarial bone cells (a gift from Dr. Thanaphum Osathanon, Chulalongkorn University, Thailand), and cementoblast cell line (a gift from Dr. Martha Somerman, University of Washington) were used as positive control while negative controls lacked cDNA.

4.2.5 Quantitative reverse transcription-polymerase chain reaction (Q-RT-PCR)

20 ng cDNA for Q-RT-PCR were prepared using the SYBR green PCR master mix from from Applied Biosystems. Reactions were run on the ABI 7900HT PCR system with the following parameters: 50°C/2 min and 95°C/10 min, followed by 40 cycles of 95°C/15 s and 60°C/1 min. Mouse-specific primers are listed in Table 4.1. Results were analyzed using SDS 2.2 software and relative expression calculated using the comparative Ct method. A Ct-value showed how many PCR cycles were necessary to obtain a certain level of fluorescence. Amplification efficiency of different genes was determined relative to *GAPDH* as an endogenous control to normalize RNA expression ($dCt = Ct_{gene}-Ct_{GAPDH}$). Messenger RNA (mRNA) in each sample was calculated using a comparative ddCt ($dCt_{gene}-dCt_{control}$) value method. The fold change in gene expression relative to the control was calculated using 2^{-ddCt}. Each sample was run in triplicate reactions for each gene. cDNA of mESC and mouse aortic smooth muscle cells (a gift from Dr. William Mahoney Jr., University of Washington) were used to calibrate samples.

4.2.6 *In vitro* multi-differentiation

The compositions of each differentiation media and cell densities are listed in Table 4.2. DPSCs were plated at corresponding cell density in 24-well plates (BD) and incubated overnight in stem cell media at 37°C under 5% O_2 and 5% CO_2. After 24 h, media was switched to corresponding differentiation media for 21 days with media change every 3 days. In addition to monolayer differentiation, for chondrogenic differentiation *Wnt1-Cre/R26R-LacZ* derived DPSCs were cultured in chondrogenic media by 3D-pellet culture technique. The 3D-pellet culture is one of widely used technique for chondrogenic differentiation (Johnstone et al., 1998). Briefly, $2x10^5$ cells were transferred in a 15-ml polypropylene conical tube and centrifuged at 450g for 10 min. The pellets were cultured at 37°C under 5% O_2 condition in 1 ml of chondrogenic media for 21 days with media change every 3 days. After 21 days, the pellets were

fixed 4% formaldehyde/PBS for 30 min and wash with PBS. Then, fixed pellets were embedded in optimal cutting temperature compound (OCT) (Tissue-Tek; Sakura Finetek), frozen with liquid nitrogen cooled isobutane and cut to 8-10 μm thick sections.

4.2.7 Immunocytochemistry and immunofluorescence

For immunocytochemistry, cells were fixed with ice cold methanol for 5 min, permeabilized with 0.1% Triton-X 100 (Sigma) in PBS with 1% bovine serum albumin (BSA) for 10 min, inhibited endogenous peroxidase activity with 0.3% hydrogen peroxide in methanol for 30 min, and blocked non-specific binding sites with 10% goat or horse serum (Vector Burlingame, CA) for 1 h. All primary antibodies listed in Table 4.3 were used and incubated overnight at 4°C. Stained cells were incubated with a biotinylated antibody at 1:100 (Vector Burlingame, CA) for 1 h, washed and treated with the Vectastain ABC kit and 3, 3'-diaminobenzidine (DAB) or 3-amino-9-ethylcarbazole (AEC) substrate kit according to manufacturers protocol (Vector Burlingame, CA).

For immunofluorescence, cells were fixed with 4% formaldehyde for 5 min, washed with PBS, and stained with primary antibodies as described below. Donkey-derived Alexa 488 or goat-derived Alexa 594 or goat-derived Alexa 647-conjugated secondary antibodies (Invitrogen) were diluted at 1:800 and incubated for 1 h. Cells were stained with 4', 6-diamine-2-phenylindol (DAPI) at 1:1000 to visualize the nuclei. All antibodies were diluted in 0.1% Triton-X 100 in PBS with 1% BSA. Controls omitting the primary antibody and/or that stained with IgG isotype were used as negative control included for all staining.

4.2.8 Histochemical staining

Toluidine blue was performed to determine proteoglycan producing cells in chondrogenic culture (Kiernan, 2009). Briefly, 1% toluidine blue (Fisher Biotech) in 70% ethanol was diluted

in 1% sodium chloride to 0.1% working solution. Cells were fixed with cold methanol (-20°C) 5 min, stained with fresh toluidine blue working solution 1-2 min, rinsed 3 times with distilled water.

Oil Red O was used for characterizing lipid-containing cells in adipogenic culture (Kiernan, 2009). Briefly, 0.5% Oil Red O (Alfa Aesar) in isopropanol diluted in distilled water to 0.25% working solution was incubated 60 min at room temperature and filtered. Cells were fixed with cold methanol 5 min, incubated in fresh Oil Red O working solution 3-5 min, rinsed 3 times with distilled water. X-gal was stained for determining the expression of *LacZ* gene in *Wnt1*-marked DPSCs (Kiernan, 2009).

4.2.9 Tooth histology and staining

Mandibles were isolated from 4-8 day-old *Tie2-GFP* or *Wnt1-Cre/R26R-LacZ* mice and cut in halves after removing surrounding connective tissues. To preserve GFP, *Tie2-GFP* derived mandibles were fixed with 0.5% formaldehyde/PBS for 2h at RT, and washed. The first wash was 30 min followed by 20-min and 10-min washes, respectively (Sacco et al., 2005). For *Wnt1-Cre/R26R-LacZ* derived mandibles, they were fixed with 4% formaldehyde/PBS for 2h at 4°C, and wash. After washing, mandibles from both transgenic mice were immersed in 20% sucrose in PBS at 4°C overnight to preserve tissue morphology before embedding in OCT and frozen with liquid nitrogen cooled isobutane. Since those mandibles were incompletely calcified, we did not process decalcification. Therefore, we cut the tissues into 15-20 μm thickness to get a good morphology of tissue section.

For immunofluorescence of tooth section, we did double staining between β-galactosidase or MSI1 and CD44. Briefly, tooth sections were fixed with 4% formaldehyde/PBS for 10 min at RT. Fixed sections were washed and permeabilized with 1% BSA in 0.1% Triton

X-100/PBS. Then sections were blocked with 10% normal goat serum for 1 h at RT, and incubated with rabbit-anti-mouse-β-galactosidase or -MSI1 for 1 h at RT following three times of washing. Stained sections were subsequently incubated with goat-derived Alexa 488 or goat-derived Alexa 647-conjugated secondary antibody (Invitrogen) at 1:800 dilution for 1 h at RT, following three times of washing. Then sections were incubated by the second set of primary antibody which is rat-anti-mouse-CD44 for 1 h at RT, washed, and incubated with goat-derived Alexa 594-conjugated secondary antibody (Invitrogen) at 1:800 dilution for 1 h at RT before washing three times. All immunofluorescence images described in this manuscript was detected using a Zeiss Axiovert 200 fluorescent microscope (Thornwood, NY). Photographs were taken with an onboard monochrome AxioCam MRm camera and colored using Adobe Photoshop (San Jose, CA). Background was reduced using brightness and contrast adjustments, and color balance was performed to enhance colors. All the modifications were applied to the whole image using Adobe Photoshop.

4.2.10 *In vivo* transplantation

In accordance with approved IACUC protocols, $1x10^6$ of murine non-clonal DPSCs, clonal DPSCs, and BMSCs were separately subcutaneously (SC) transplanted into 1-month-old male *Rag1* null mice (Jackson Laboratory, Bar Harbor, ME, USA) (n=3 mice/ cell line) with hydroxyapatite tricalciumphosphate (HAp/TCP) (Zimmer) in the dorsum. BMSCs were isolated and cultured as previously described (Reyes et al., 2005). Prior to transplantation, cells were labeled with the fluorescent membrane dye PKH-26 (Sigma) according to manufacturer's instructions. Grafts were harvested after 5-wk and 12-wk SC transplantations. For SC-transplanted tissues, samples were fixed with Bouin's fixative solution (Sigma) overnight in 4ºC, then washed with 70% ethanol several times, and demineralized for 7-14 days in demineralizing

AFS solution containing acetic acid, 10% neutral buffered formalin, and sodium chloride at 4°C. Transplanted tissues were embedded in paraffin and cut to 5 μm thick sections. Sections were analyzed by Hematoxylin & Eosin (H&E) and Masson trichrome staining, immunohistochemistry, and immunofluorescence (Kiernan, 2009).

4.3 Results

4.3.1 *Wnt1-Cre/R26R-LacZ* derived DPSCs, but not femur-derived BMSCs, demonstrate positive X-gal staining

To conclusively determine the neural crest origin of DPSCs generated in our cultures, we used a genetic lineage tracing model of neural crest derivatives, the *Wnt1-Cre/R26R-LacZ* transgenic mouse. In the *Wnt1-Cre/R26R-LacZ* double-transgenic mice all neural crest derivatives express *Wnt1* reporter driven β-galactosidase, thereby stained positive for X-gal.

DPSCs isolated from the *Wnt1-Cre/R26R-LacZ* neonatal mice showed a majority of *Wnt1*-marked cells in culture stained positive for β-galactosidase with X-gal. Nonetheless, early in culture a minority of cells (approximately 10%) stained negative for X-gal (Fig. 4.1A, arrowheads). Although we could not confirm the origin of this minority, the percentage of β-galactosidase negative cells is consistent with the highest *Cre/lox* efficiencies reported for other transgenic models (Hara-Kaonga et al., 2006, Long and Rossi, 2009). To confirm the neural crest origin of DPSCs, I also isolated femur-derived bone marrow stromal cells (BMSCs) from the same *Wnt1-Cre/R26R-LacZ* mice and cultured in the same condition. Unlike DPSCs, primary culture of BMSCs at day 8 negatively stained for X-gal, indicating their non-neural crest origin (Fig. 4.1B). A previous study using the same transgenic mouse model, *Wnt1-Cre/R26R-LacZ,* reported that BMSCs did not derive from neural crest (Hunt et al., 2009). DPSCs were

successfully cloned on day 7-10 before the first passage. All DPSC clones (n=10) stained 100% positive with X-gal (Figs. 4.1C, D) and were grown for four passages. Since the majority of cells early in culture stained positive with X-gal, it is unlikely that the homogeneous expression of β-galactosidase in clones derived prior to the first passage resulted from epigenetic changes induced by long-term culture. X-gal staining of C57BL6-derived DPSCs in a late passage was negative (Fig. 4.1E) demonstrating specificity of X-gal staining and ruling out non-specific or mammalian endogenous β-galactosidase activity in the X-gal staining.

4.3.2 *Wnt1-Cre/R26R-LacZ* derived DPSC clones expressed pluripotent stem cell and neural crest-related genes

Like my previous DPSCs, RT-PCR showed that *Wnt1-Cre/R26R-LacZ* derived DPSC clones expressed pluripotent stem cell genes, *Nanog, Klf4, Sox2*, and *c-Myc,* but not *Oct4*. As expected, DPSCs expressed neural crest-related genes, *Msi1, Sox10, TrkC, LNGFR, Twist,* and *Snail,* whereas BMSCs did not express these genes. *Twist*, *Snail*, and *Slug* are expressed by cells undergoing epithelial-mesenchymal transition (EMT) process during embryological development such as migratory neural crest cells (Duband et al., 1995). Previous studies have shown that those EMT-related genes can be expressed by mesenchymal stem cells from bone marrow (Battula et al., 2010, Torreggiani et al., 2011).

4.3.3 *Wnt1-Cre/R26R-LacZ* derived DPSC clones stained positive for mesenchymal stem cell markers

Both DPSCs and BMSCs also expressed CD105, also known as endoglin, which is a well-known mesenchymal stem cell (MSC) marker (Fig. 4.1F) (Chamberlain et al., 2007). In addition, immunofluorescence showed that DPSC clones in my culture condition stained positively for CD44, CD73, CD105, three MSC markers previously reported in human DPSCs,

and stained positively for MSI1, a neural crest-related marker (Figs. 4.1G-K) (Shi et al., 2005, Huang et al., 2006, Sloan and Smith, 2007) .

4.3.4 Localization of neural crest-derived dental pulp mesenchymal stem cells

I corroborated the presence of neural crest-derived MSCs in dental pulp of neonatal mice, *Wnt1-Cre/R26R-LacZ* and *Tie2-GFP* that co-expressed MSC and neural crest-related markers. Since neural crest-derived cells of the *Wnt1-Cre/R26R-LacZ* express β-galactosidase under *Wnt1* promoter driven, I studied the expression of MSC markers in *Wnt1* marked cells in dental pulp. From all three of MSC markers expressed by cultured DPSCs (CD44, CD73, and CD105), only CD44 is strongly expressed in dental pulp tissue. Staining of tooth sections with anti-β-galactosidase showed that many dental pulp cells and all odontoblast cells in the *Wnt1-Cre/R26R-LacZ* mouse were positive for β-galactosidase, confirming their neural crest origin (Fig. 4.2A). Cells co-expressing β-galactosidase and CD44 were found in the *Wnt1-Cre/R26R-LacZ* dental pulp particularly in the sub-odontoblastic and perivascular regions, indicating DPSCs are of neural crest origin (Fig. 4.2A, arrowheads and arrows, respectively). *Tie2-GFP* derived dental pulp showed CD44-positive cells in the same areas found in the *Wnt1-Cre/R26R-LacZ* (Fig. 4.2B, arrowheads and arrows). The CD44 staining of both transgenic mice's teeth indicates DPSCs are preferentially localized in perivascular niches as suggested in previous studies (Shi and Gronthos, 2003, Lovschall et al., 2005, Sloan and Waddington, 2009).

Additionally, I used another double staining of MSI1 and CD44 to confirm co-expression of CD44, a mesenchymal stem cell marker, and MS1, a neural crest-related marker, by DPSCs. Like the co-staining of β-galactosidase and CD44, DPSCs stained positively for MSI1 and CD44 preferentially located in the same areas; underneath odontoblast cell layer and surrounding blood vessels (Figs. 4.2C, D arrowheads and arrows, respectively). As expected, I did not observe any

positive cells for β-galactosidase in the *Tie2-GFP* derived dental pulp and IgG isotype control staining (Figs 4.2E, F). Accordingly, I observed blood vessels in the *Tie2-GFP* dental pulp expressing GFP (Figs 4.2B, F, arrowheads). The co-expression of β-galactosidase or neural crest-related and MSC markers indicates the existence of neural crest-derived DPSCs in murine neonatal teeth.

4.3.5 *Wnt1-Cre/R26R-LacZ* derived DPSC clone gave rise into neural crest-derived mesenchymal lineage *in vitro*

I determined *in vitro* multi-differentiation capacity in neural crest lineages of the *Wnt1-Cre/R26R-LacZ* derived clonal DPSCs using the differentiation protocols described in Table 4.2. Cells treated with adipogenic media generated lipid-containing cells positive for Oil Red O (Fig. 4.3A). I performed chondrocyte differentiation in both monolayer and cell pellet methods cultured in chondrogenic media (Johnstone et al., 1998, Wang et al., 2003). After 21 days differentiated cells in the monolayer secreted extracellular matrix stained positively for COLII (Fig. 4.3B). In addition, the chondrogenic pellet culture conditions induced DPSCs to form aggregations in differentiated medium, but not in stem cell media. These aggregates stained positively for toluidine blue and alcian blue, which stain cartilage extracellular matrices (Figs. 4.3C, D) (Johnstone et al., 1998, Tscheudschilsuren et al., 2006). For osteo-odontogenic differentiation, in contrast to undifferentiated cells, treated cells with differentiation media showed clusters of cells stained positively for DMP1 and DSP (Figs. 4.3E-G). The staining results were confirmed by RT-PCR (Figs. 4.3H-J). The gene expression after each differentiation revealed that induced cells expressed higher levels of specific adipogenic, chondrogenic, and osteo-odontogenic markers, respectively.

4.3.6 *Wnt1-Cre/R26R-LacZ* derived DPSC clone gave rise into neural crest-derived non-mesenchymal lineage *in vitro*

In addition to mesenchymal lineages, clonal DPSCs gave rise into neuronal-like cells positive for neurofilament and S100, confirming by NFL and NFH gene expression (Figs. 4.4A-E). DPSCs cultured in smooth muscle media showed smooth muscle-like cells positive for smooth muscle actin; some of which stained positive for smooth muscle myosin heavy chain, calponin, and caldesmon, which are mature markers of smooth muscle cells (Figs. 4.4F-I) (Grabski et al., 2009). Q-RT-PCR showed treating DPSCs in smooth muscle media revealed up-regulation of specific gene expression for smooth muscle differentiation, *serum response factor (SRF), Sm22-alpha, Sma, SMHC*, and *calponin* (Fig. 4.4J). Thus, *Wnt1*-marked DPSCs can successfully differentiate into neural crest lineages. Altogether these results confirm that clonal DPSCs generated in our culture conditions are all derived from neural crest origin.

4.3.7 *In vivo* transplantation of *Wnt1-Cre/R26R-LacZ* derived DPSC clone

To determine the differentiation potential of cultured *Wnt1*-marked DPSCs *in vivo*, *Wnt1*-marked DPSCs were subcutaneously transplanted following the protocol described in Materials and Methods. Transplanted *Wnt1*-marked DPSCs were identified by anti-β-galactosidase staining in transplants (Fig. 4.5A) whereas HAp/TCP only and transplanted tissue stained with IgG isotype control were negative for anti β-galactosidase staining (Figs. 4.5B, C). Transplanted *Wnt1*-marked DPSCs were also positive for CD44 and MSI1, two markers expressed by DPSCs in dental pulp tissue and *in vitro* (Figs. 4.5D, E).

Wnt1-marked DPSC concentrated near HAp/TCP areas, and secreted dense extracellular matrices. Some transplanted *Wnt1*-marked DPSCs were elongated, polarized, and arranged perpendicularly to HAp/TCP, resembling odontoblast-like cells (Figs. 4.5F-H, arrows). In

addition, transplanted *Wnt1*-marked DPSCs also formed clusters of loose connective tissue containing blood vessels, resembling dental pulp-like tissue (Figs. 4.5F-H, arrowheads). As expected, transplanted HAp/TCP without DPSCs tissues were devoid of dense extracellular matrices (Fig. 4.5I). Masson's trichrome confirmed dense collagen matrix formation in DPSC transplants, but not in HAp/TCP transplants only (Figs. 4.5J-M). In addition, DPSCs secreted extracellular matrices which were positive for dentin matrix proteins, DMP1 and DSP (Figs. 4.5N, O). The staining of dentin matrices was completely negative in the transplantation of HAp/TCP only (Figs. 4.5P, Q). Corresponding to my previous results of DPSC transplantation, these observations confirmed that *Wnt1*-marked DPSCs generate odontoblast-like cells, dentin-like matrix and dental pulp-like tissue *in vivo*.

In addition to odontoblast-like cell differentiation, I found that some of DPSCs were strongly positive for smooth muscle actin, and those were located adjacent to blood vessels close to HAp/TCP, suggesting pericyte-like phenotype (Figs. 4.6A-F, arrowheads). DPSC-derived pericyte-like cells were also found surrounding blood vessels distant to HAp/TCP (Figs. 4.5G-I, arrowheads). Nevertheless, some pericytes found in DPSC transplants were not derived from transplanted DPSCs as they did not stain positive for anti β-galactosidase. This transplantation model demonstrated that *Wnt1*-marked DPSCs were able to give rise not only odontoblast-like cells, but also pericyte-like cells.

4.4 Discussion

In the previous chapter, I have shown that non-clonal and clonal DPSCs derived from *Tie2-GFP* express neural crest genes and differentiate into neural crest-lineages *in vitro* and form dentin like structures *in vivo*; however, the developmental origin of my cultured cells collectively

called DPSCs could not completely be distinguished. Therefore, I used a transgenic mouse model, the *Wnt1-Cre/R26R-LacZ* mouse, to demonstrate the genetic lineage tracing of neural crest contribution to stem cells in dental pulp (Chai et al., 2000). Although the *Wnt1-Cre/R26R-LacZ* mouse has been widely used to study neural crest development, to date the origin of DPSCs has not been examined. Staining results of *Wnt1-Cre/R26R-LacZ* tooth sections showed the existence of neural crest-derived DPSCs in sub-odontoblastic and perivascular regions. Those two areas have been reported as stem cell niches in dental pulp tissue (Shi and Gronthos, 2003, Lovschall et al., 2005, Sloan and Waddington, 2009). Under my culture conditions, early dental pulp cells isolated from the *Wnt1-Cre/R26R-LacZ* revealed the majority of cells were of neural crest origin. This is consistent with the study by Chai et al (2000) showing that dental pulp consists of cells from neural crest and non-neural crest origins (Chai et al., 2000). In addition, *Wnt1-Cre/R26R-LacZ*-derived BMSCs, previously known as non-neural crest-derived used as a control showed negative X-gal staining (Hunt et al., 2009).

The X-gal staining of both DPSCs and BMSCs indicates that the *Wnt1-Cre/R26R-LacZ* is a good strategy to study the developmental origin of DPSCs. This model definitely confirms the neural crest origin of DPSCs. In spite of a mixed cell population of DPSC in early culture, after 6-week-*in vitro* expansion, all cells were positive by X-gal staining indicating only neural crest-derived cells remained and were present in late cultures. The *Wnt1-Cre/R26R-LacZ*-derived DPSC clones also expressed strongly pluripotent stem cell and neural crest-related genes, and gave rise to neural crest lineages. In addition to the expression of neural crest genes and differentiation capacity into neural crest-lineage, this lineage tracing data undeniably proves that in my culture condition DPSCs are neural crest-derived stem cells.

Although some studies showed that both neural crest and non-neural crest cells can be found in dental pulp during tooth development, my stem cell conditions select for only the outgrowth of neural crest-derived stem cells (Fig. 4.7A). Thus, future studies should aim at comparing the differentiation capacity, contribution and cross-talk of neural crest- and non-neural crest-derived cells from dental pulp. Upon transplantation, DPSCs formed dentin-like matrix composed of odontoblast-like cells and pericytes associated with microvessels in dental pulp-like tissue recapitulating dentinogenesis (Fig. 4.7B).

The mechanisms that control the differentiation fate of dental pulp stem cells are not completely elucidated but interactions with their niche are important for maintenance of stemness and induction/guidance for differentiation. In my transplantation model, interactions with microvessels seem pivotal for the differentiation of DPSCs into pericytes and odontoblasts. Since the dental pulp tissue is highly vascularized, it is probable that dental pulp stem cells reside in a vascular niche. To date multiple reports have revealed the presence of various adult stem cells residing within the vascular niches (Shi and Gronthos, 2003, Kiel and Morrison, 2006, Crisan et al., 2008, Tavazoie et al., 2008).

In addition, several recent studies have shown the existence of neural crest-derived stem cels in various postnatal tissues (Kruger et al., 2002, Tomita et al., 2005, Sieber-Blum and Hu, 2008). Thus, future studies should also aim at understanding the interactions of neural crest-derived stem cells with their respective niches from multiple adult tissues. Understanding the mechanisms that control organogenesis and adult tissue homeostasis will be instrumental for tissue engineering and tissue regeneration. Thus, studying how neural crest-derived stem cells from multiple organs such as DPSCs interact within each niche to remain either stem cells or

differentiate may help elucidate the mechanisms for maintenance of tissue-specific stem cells and tissue-specific differentiation, in tissue regeneration or homeostasis.

4.5 Conclusion

Using the *Wnt1-Cre/R26R-LacZ* transgenic mouse model to isolate DPSCs in my culture condition indicates that DPSCs are highly proliferative, express stem cell and neural crest-related genes, as well as are capable of differentiating into neural crest-lineage *in vitro* and *in vivo*, confirming the neural crest origin of DPSCs. This will broaden the potential clinical applications of DPSCs as a readily accessible source of neural crest-derived cells for tissue regeneration/homeostasis not only of pulp regeneration but possibly other neural crest derivatives. Moreover, my *in vivo* transplantation of DPSCs demonstrated abundant of blood vessel formation, suggesting the role of pericyte-like DPSCs in angiogenesis which is considered an important key for successful tissue regeneration. This observation provides DPSCs as promising stem cell sources for regenerative therapeutic medicine.

Table 4.1 The mouse-specific primer sequences

RT-PCR primers			
Gene	**Forward primer (5'→3')**	**Reverse primer (5'→3')**	**GenBank Accession number**
Adipsin	GTGCTGCACACTGCATGGAT	CCGGGTTCCACTTCTTTGTC	NM_013459
Bsp	AGAACAATCCGTGCCACTCACT	CCCTGGACTGGAAACCGTTT	NM_008318
CD105	CTTCGTACAGGTGAGCGTGTCT	GCTAGGGCGCAGAGCTAAGTT	NM_007932
Bsp	AGAACAATCCGTGCCACTCACT	CCCTGGACTGGAAACCGTTT	NM_008318
CEBPa	GCCAAGAAGTCGGTGGACAA	AGTTGCCCATGGCCTTGAC	NM_007678
c-Myc	CCTCTGCCCGCGATCA	AGGAAATCCAGCCTTCAAACAG	NM_010849
Col2a1	AGGATGGCTGCACGAAACA	TCAGTGCAGATCCTGGAGTGACT	NM_031163
Dmp1	TTGGGAGCCAGAGAGGGTAGA	AGTCCACCAGCCGGTCTGTA	NM_016779
Dspp	CCCCTCGGAGGCTTTGA	ACTCGGAGCCATTCCCATCT	NM_010080
GAPDH	CTCGTCCCGTAGACAAAATGG	CGCTCCTGGAAGATGGTG	NM_008084
Klf4	GGTTTTGGTTTGAGGTTTTGTTTCT	CCTCACGCCAACGGTTAG TC	NM_010637
Leptin	ACCTGCTCCGGGTACATGTTC	TGGGCAGACCCATCAATAGG	NM_008493
LNGFR	GAGGCACCGCTGACAACCT	CAGGCCTCGTGGGTAAAGG	NM_033217
Lpl	GGATGGACGGTAACGGGAAT	CATGGGCTCCAAGGCTGTAC	NM_008509
Msi1	GACCCCTGCAAGATGTTCATC	CTCTGTGCCTGTTGGTGGTTT	NM_008629
Nanog	TCTCAAGTCCTGAGGCTGACAAG	GTGCTGAGCCCTTCTGAATCA	NM_028016
NFH	CGTAAAACACGCGTCTAAAAACTG	GAGTACACCCTGGCGTGG TT	NM_010904
NFL	GCCTTGGACATCGAGATTGC	CAGCTTTCGTAGCCTCAATGG	NM_010910
Ocn	TTGGTGCACACCTAGCAGACA	TCGTCACAAGCAGGGTTAAGC	NM_001032298
Oct4	CTGGGCGTTCTCTTTGGAAA	TCGGGCACTTCAGAAACATG	NM_013633
Opn	CAGTGATTTGCTTTTGCCTGTT	TCGTCGTCCATGTGGTCATG	NM_009263

RT-PCR primers			
Gene	**Forward primer (5'→3')**	**Reverse primer (5'→3')**	**GenBank Accession number**
Osx	AGAGATCTGAGCTGGGTAGAGGAA	AAGTTGAGGAGGTCGGAGCAT	NM_130458
Pparg2	CAAGAATACCAAAGTGCGATCAAA	GGATCCGGCAGTTAAGATCACA	NM_011146
Runx2	AATGCCTCCGCTGTTATGAAA	GAATGCGCCCTAAATCACTGA	NM_001146038
Slug	CACTGTGATGCCCAGTCTAGGA	GCAGATGTGCCCTCAGGTTT	NM_011415
Snail	TGACCTCGCTGTCCGATGA	GTGCTTGTGGAGCAAGGACAT	NM_011427
Sox10	CAGCCACGAGGTAATGTCCAA	GTGTAGGCGATCTGGGAAGTG	NM_011437
Sox2	CCGGACCGCGTCAAGAG	TCATGAGCGTCTTGGTTTTCC	NM_011443
Sox9	ACCCACCACTCCCAAAACC	GATGCCGTAACTGCCAGTGTAG	NM_011448
TrkC	GGGTCCTGTGGCTGTTATCAG	GGCTCCCTCACCCAATTCTC	NM_008746
Twist	GACGAGCTGGACTCCAAGATG	GCCCCTCTGGGAATCTCTGT	NM_011658
Q-RT-PCR primers			
Gene	**Forward primer (5'→3')**	**Reverse primer (5'→3')**	**GenBank Accession number**
Calponin	ATGCCCAGACCTGGCTCAAA	ACTGCAGATGGGCACCAACA	NM_009922
GAPDH	GGGAAGCCCATCACCATCT	GCCTCACCCCATTTGATGTT	NM_008084
Sm22-alpha	CAACAAGGGTCCATCCTACGG	ATCTGGGCGGCCTACATCA	NM_178598
Sma	TACATGGCGGGGACATTGAA	CCGATAGAACACGGCATCATCA	NM_007392
SMHC	AAGCTGCGGCTAGAGGTCA	CCCTCCCTTTGATGGCTGAG	NM_013607
SRF	GGCCCCACAGCAAGCGTCTC	GTGGCGGGCAACGTCACTGT	NM_020493

Table 4.2 Lists of differentiation media

Differentiation	Cell density (cells/cm^2)	Media composition	Reference
Osteogenic (Osteo-odontogenic)	2x10^{4}cells plated on plastic surface	Serum-free media supplemented with 10% FBS, 10mM β-glycerophosphate (CalBiochem), 0.2mM L-ascorbic acid, and 100nM dexamethasone	(Gronthos et al., 1994)
Chondrogenic	2x10^{4}cells plated on plastic surface or 2x10^5 cells cultured as micromass in a conical tube	Serum-free media supplemented with 10% FBS, 100ng/ml BMP-2 (Shenandoah Biotech), 0.2mM L-ascorbic acid, and 100nM dexamethasone	(Tscheudschilsuren et al., 2006)
Adipogenic	2x10^{4}cells plated on plastic surface	Serum-free media supplemented with 10% horse serum, 100μM indomethacin (Alfa Aesar), 0.5mM 3-isobutyl-1-methyl-xanthine (ACROS), and 1μM dexamethasone	(Gregoire, 2001)
Neurogenic	1x10^4 cells plated on glass surface coated with 5ng/ml fibronectin	Serum-free media with three series of growth factors; 1) media with 100ng/ml bFGF for the first week; 2) media with 10ng/ml FGF-8b and 100ng/ml Shh for the second week; and 3) media with 10ng/ml BDNF (all from R&D) and 10ng/ml EGF (Sigma) for the last week of culture	(Jiang et al., 2003)
Smooth muscle	1.5x10^4 cells plated on plastic surface coated with 5ng/ml fibronectin	Serum-free media supplemented with 100ng/ml PDGF-BB (R&D)	(Ross et al., 2006)

Table 4.3 Lists of antibody for staining

Marker	Antibody	Species	Dilution	Company
β-galactosidase	Polyclonal	Rabbit	1:200	Invitrogen / Abcam
Calponin	Monoclonal	Mouse	1:100	Sigma
Caldesmon	Monoclonal	Mouse	1:100	Sigma
CD105-PE	Monoclonal	Rat	1:50-1:100	eBioscience
CD44-PE	Monoclonal	Rat	1:50-1:100	eBioscience
CD73-PE	Monoclonal	Rat	1:50-1:100	eBioscience
COLII	Monoclonal	Mouse	Whole supernatant	Developmental Hybridoma Bank
DMP1	Polyclonal	Rabbit	1:400	Takara
DSP	Polyclonal	Rabbit	1:200	Larry Fisher, NIDCR/NIH
MSI1	Polyclonal	Rabbit	1:250-1:500	Abcam
NF-160/200	Monoclonal	Mouse	1:500	Abcam
S100	Polyclonal	Rabbit	1:400	Dako
SMA-Cy3	Monoclonal	Mouse	1:400	Sigma
Smooth muscle myosin heavy chain	Monoclonal	Mouse	1:100	Sigma

Table 4.4 Variable differentiation capacity of non-clonal and clonal DPSCs

Differentiation / Clone	Non-clonal #1	Non-clonal #2	C5	C6	C7	C8	C9	*Wnt1*-marked DPSC clone
Osteogenic	POS	POS	NEG	NEG	NEG	NEG	NEG	POS
Odontogenic	POS	POS	POS	POS	POS	POS	POS	POS
Adipogenic	POS	POS	NEG	NEG	NEG	NEG	NEG	POS
Chondrogenic	POS	POS	POS	POS	POS	POS	NEG	POS
Smooth muscle	POS	POS	POS	POS	POS	POS	POS	POS
Neurogenic	POS	POS	NEG	POS	POS	POS	NEG	POS

Table 4.4 shows the summary and comparison of the capacity of non-clonal DPSCs and clones to differentiate into neural crest-derived mesenchymal (osteogenic, odontogenic, adipogenic, and chondrogenic) and non-mesenchymal (smooth muscle and neuronal) lineages. These data indicate that non-clonal DPSCs were able to give rise to all neural crest-lineages. In contrast, DPSC clones differentiated at passage 7 showed differentiation capacity into certain lineages, but lack osteogenic and adipogenic capacity. Nonetheless, the clones still showed multi-differentiation capacity into mesenchymal and non-mesenchymal lineages. Interestingly, DPSC clones isolated from the *Wnt1-Cre/R26R-LacZ* differentiated at passage 4 show the capacity to differentiate into osteoblasts and adipocytes, which differs from that of our previous clones. This may indicate DPSCs lose differentiation capacity to certain lineages during long-term cultures. In addition, differences in the differentiation capacity among the clones indicate heterogeneity or hierarchical relationship of stem cells and progenitors. Note that POS (positive) means that cells can give rise to that lineage whereas NEG (negative) means that cells did not differentiate into that lineage.

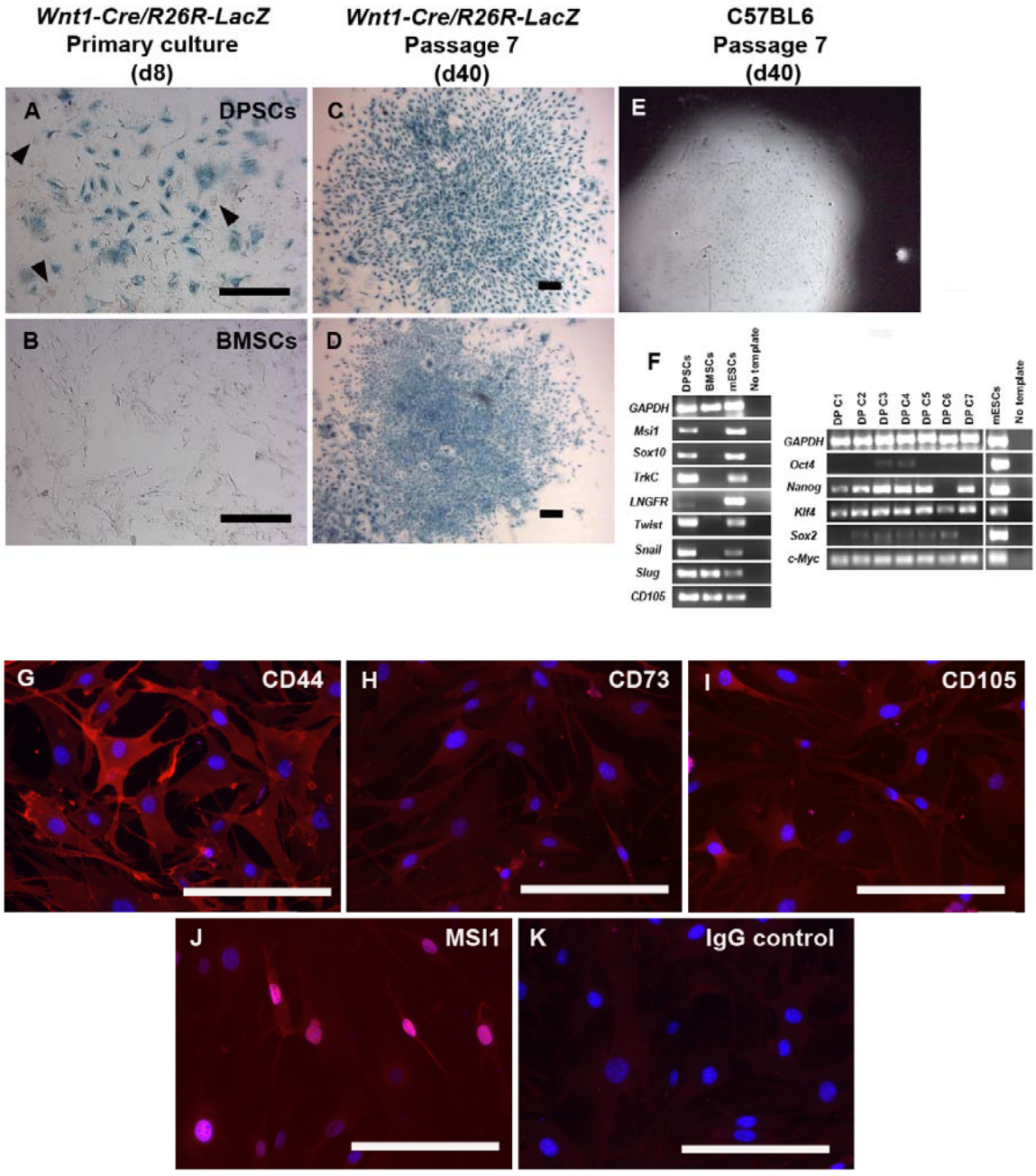

Figure 4.1 DPSC clones from *Wnt1-Cre/R26R-LacZ* mice. (A) DPSCs first isolated from 4-10 day-old *Wnt1-Cre/R26R-LacZ* showed a majority of *Wnt1*-marked cells in primary culture on day 8 (d8) which stained positively for β-galactosidase with X-gal. A significant minority (10%) of negative cells was also observed in early cultures (arrowheads). (B) Femur-derived bone marrow stromal cells (BMSCs) isolated from the same *Wnt1-Cre/R26R-LacZ* cultured in the same condition for 8 days showed negative staining for X-gal. DPSCs were successfully cloned on day 7-10. Following several passages until day 40 (d40), all clones generated in this experiment (n=10) were 100% positive for X-gal. (C and D) Two different *Wnt1* marked clones were shown. (E) A representative DPSC clone from C57BL6 was negative for X-gal. (F) RT-

PCR demonstrated that DPSC clones strongly expressed most of neural crest-related genes, *Msi1, Sox10, TrkC, Twist, Snail,* and slightly expressed *LNGFR*, but not in BMSCs. Both DPSCs and BMSCs expressed *CD105*, a known mesenchymal stem cell marker. DPSC clones also expressed pluripotent stem cell genes, *Nanog, Klf4, Sox2* and *c-Myc.* (G-J) Immunofluorescence showed positive staining of mesenchymal stem cell markers, CD44, CD73, CD105, and neural crest-related marker, MSI1 in DPSC clones (in red). (K) Staining with IgG isotype was used as negative control. DAPI used for nuclei staining is depicted in blue. Scale bars indicate 50 μm.

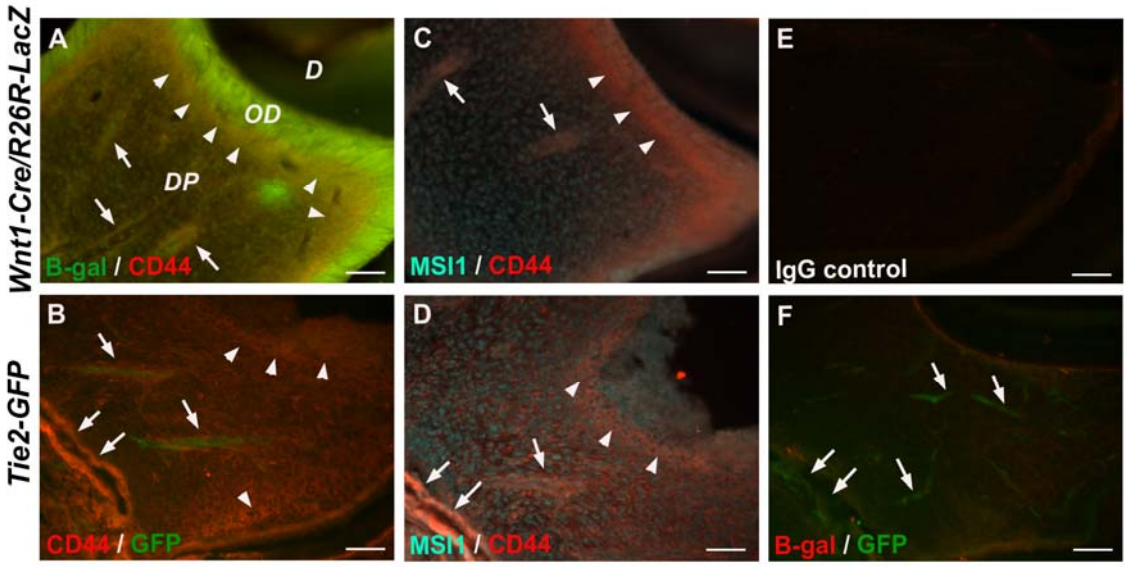

Figure 4.2 Localization of neural crest-derived stem cells in dental pulp of neonatal mice. (A) Immunofluorescence showed *Wnt1-Cre/R26R-LacZ* derived dental pulp cells and odontoblasts expressing β-galactosidase (B-gal, in green). The co-expression of β-galactosidase and mesenchymal stem cell marker, CD44, in plasma membrane (in red) was observed in DPSCs located in sub-odontoblastic (arrowheads) and perivascular regions (arrows). (B) In *Tie2*-GFP dental pulp only vessels express green fluorescent protein (GFP), CD44 positive cells were particularly located in sub-odontoblastic (arrowheads) and perivascular areas (arrows). (C and D) The co-localization of CD44 (in red) and MSI1 (in pseudo-color cyan), a neural crest-related marker, was observed in cells located in sub-odontoblastic (arrowheads) and perivascular areas (arrows) of both *Wnt1-Cre/R26R-LacZ* and *Tie2*-GFP, respectively. (E) Staining with IgG isotypes are shown as negative control. (F) *Tie2*-GFP derived dental pulp cells did not express β-galactosidase, but blood vessels in this transgenic mouse were labeled by GFP (arrows). *D* = Dentin, *DP* = Dental pulp, *OD* = Odontoblasts. Scale bars indicate 100 μm.

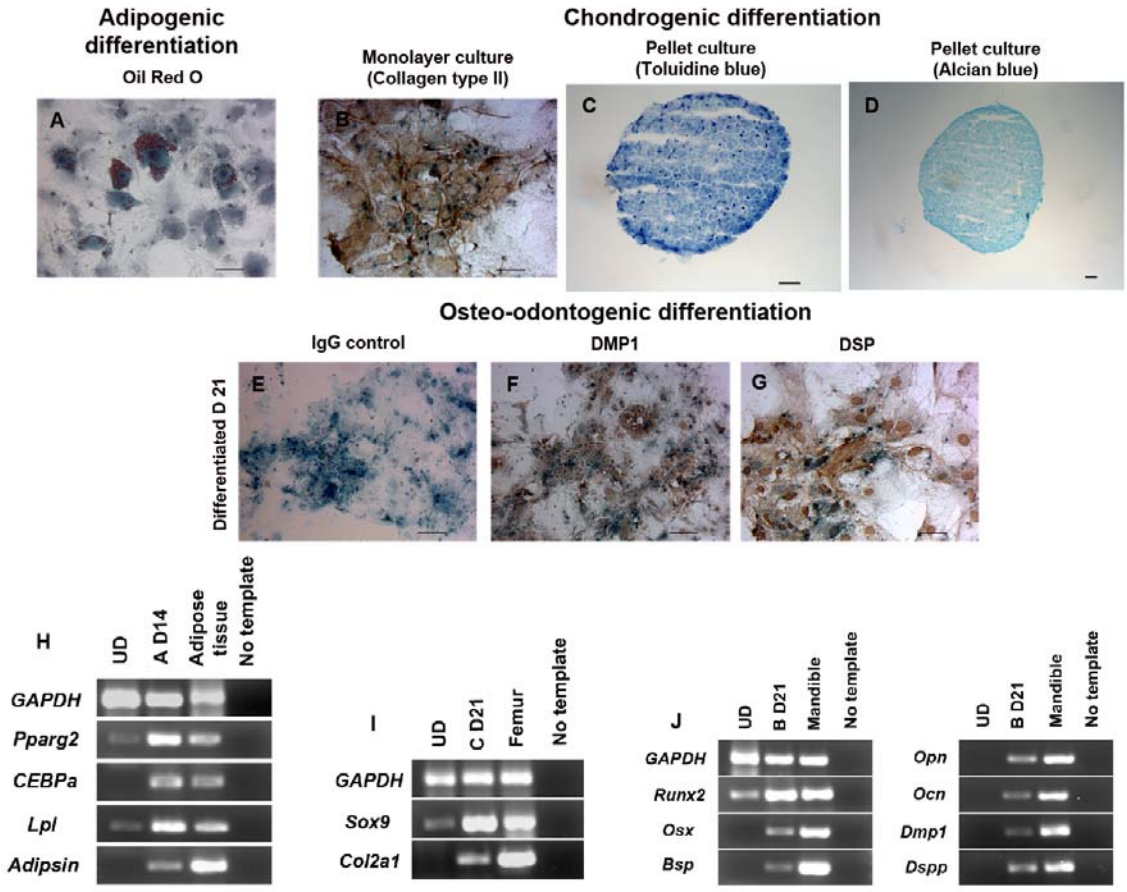

Figure 4.3 Multi-differentiation capacity in neural crest-derived mesenchymal lineages of *Wnt1*-marked DPSCs. (A) Double staining showed that X-gal+ treated cells in adipogenic media demonstrated lipid droplets-containing cells positive for Oil Red O. (B) Chondrogenic differentiation by monolayer method showed that a cluster of chondrocyte-like cells derived from DPSCs secreted extracellular matrices positive for COLII. (C and D) DPSCs cultured in chondrogenic media by pellet method formed aggregates containing highly proteoglycan which stained positively for toluidine blue and alcian blue, respectively. (E) Differentiated DPSCs in osteo-odontogenic media stained with IgG isotype as negative control showed X-gal positive staining. (F and G) DPSCs treated in osteo-odontogenic media for 21 days secreted dentin matrices stained positively for DMP1 and DSP; those extracellular matrices were not found in cells cultured in stem cell media. (H-J) RT-PCR from each differentiation confirmed the staining results. DPSCs treated in each differentiation media up-regulated specific adipogenic (A D14), chondrogenic (C D21), and osteo-odontogenic (B D21) genes after 14 to 21-day culture. RNA of mouse adipose tissue, femur, and mandible was used as positive control while the reaction without cDNA was used as negative control. Scale bars indicate 100 μm.

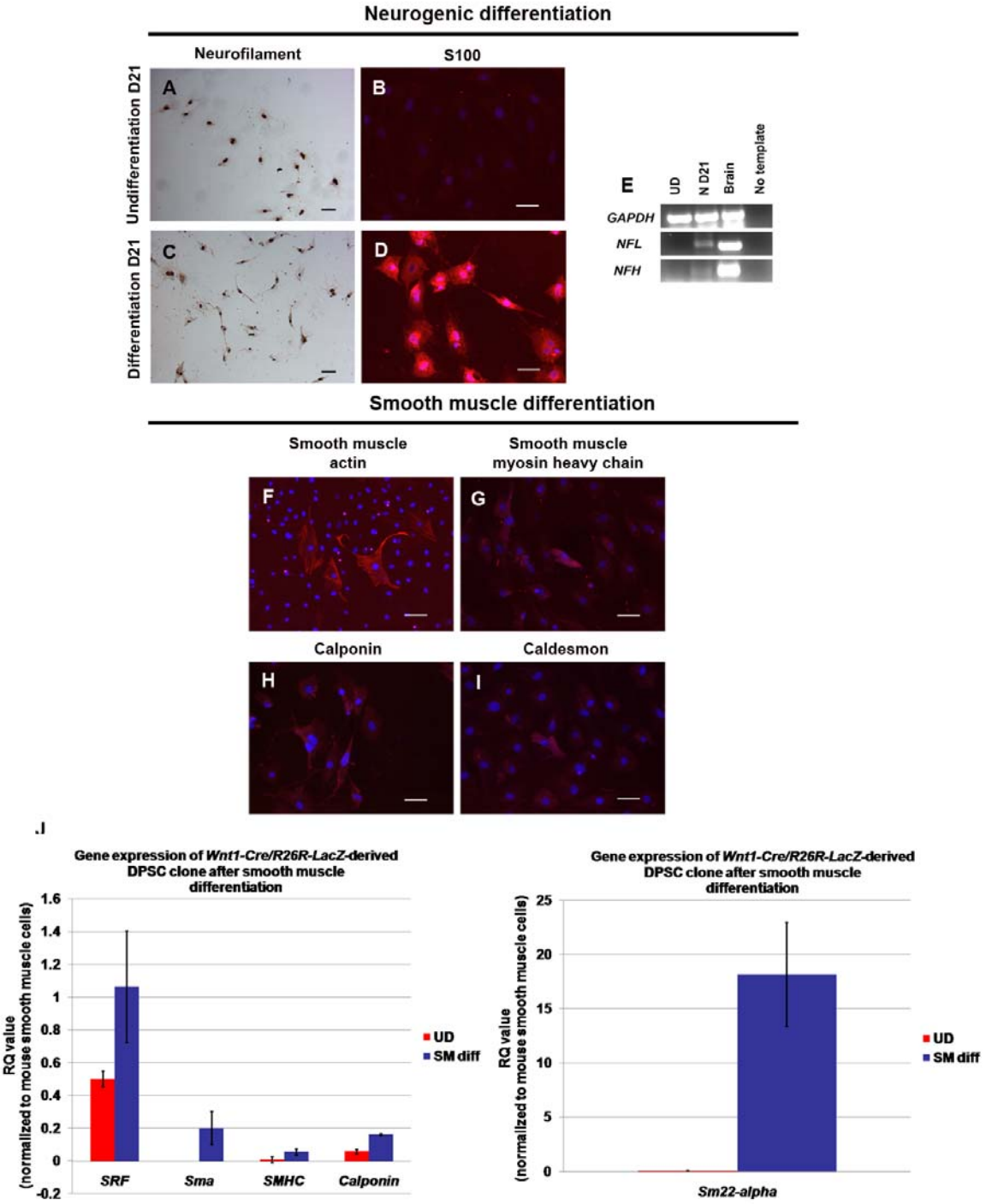

Figure 4.4 *Wnt1*-marked DPSCs gave rise into neural crest-derived non-mesenchymal lineages. (A-D) Neuronal-induced cells stained positively for neuronal markers; neurofilament and S100 (in red). (E) The neurofilament staining was confirmed by the expression of neurofilament-light (NFL) and -heavy (NFH) of treated cells in neurogenic media after 21 days (N D21) (F-I) DPSCs in smooth muscle differentiation media showed smooth muscle-like

phenotype that stained positively in red fluorescence for smooth muscle actin, smooth muscle myosin heavy chain, calponin, caldesmon. DAPI used for nuclei staining is depicted in blue. (J) Corresponding to immunofluorescence, Q-RT-PCR revealed the up-regulation of smooth muscle-specific genes, *SRF, Sm22-alpha, Sma, SMHC,* and *calponin* in DPSCs after cultured in smooth muscle media. Scale bars indicate 100 μm. RQ values were relative to the expression of mouse smooth muscle cells. *GAPDH* was used for the internal control. Error bars represent ± Standard Error of the Mean (SEM).

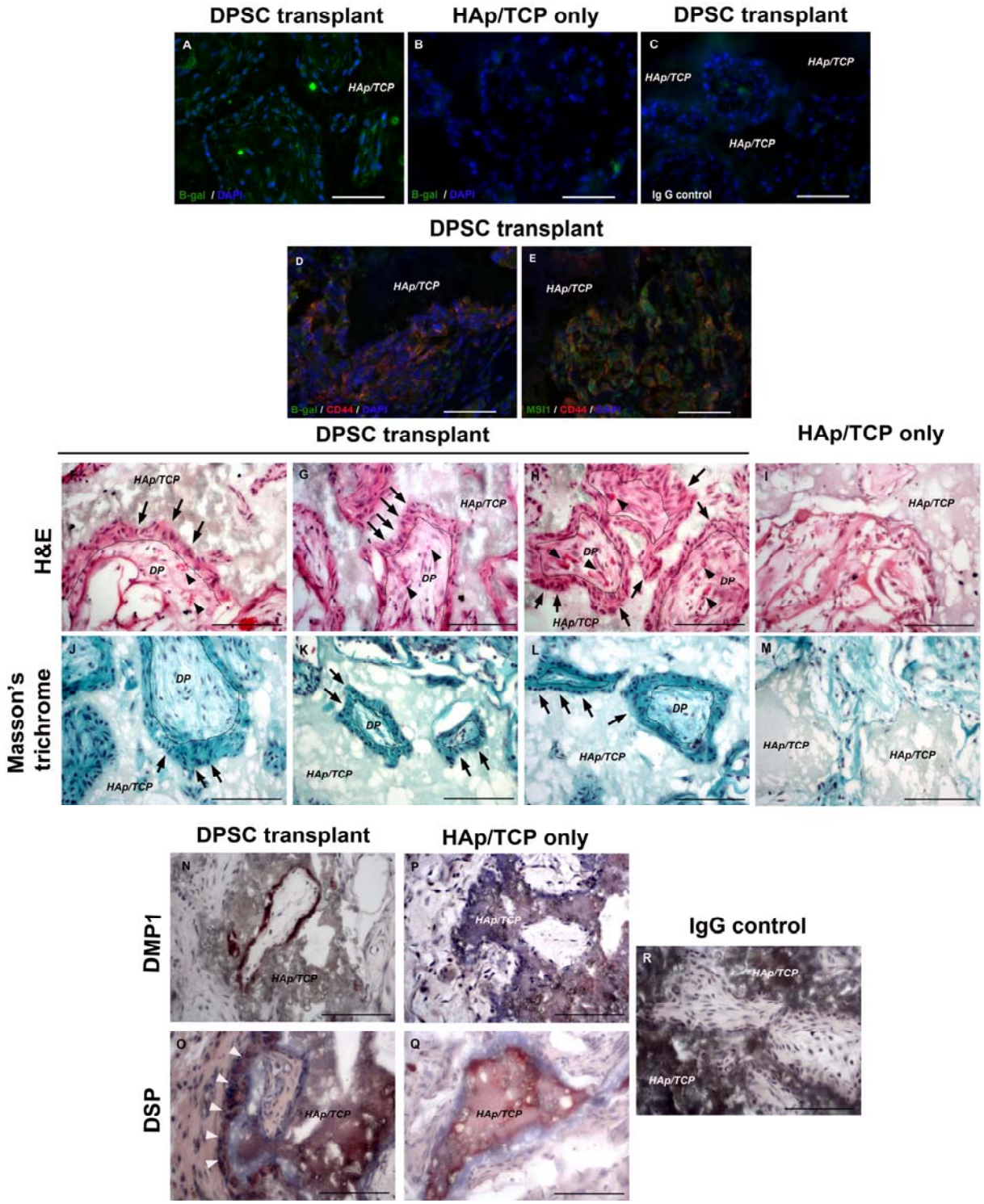

Figure 4.5 *Wnt1*-marked DPSCs gave rise to odontoblast-like cells and generated dentin-like structure *in vivo*. The *Wnt1*-marked DPSCs were subcutaneously transplanted in HAp/TCP scaffolds and analyzed 5 weeks post- transplantation. (A) anti β-galactosidase staining (in green) indicated the location of transplanted cells in DPSC transplantation. (B and C) Negative staining

of anti-β-galactosidase was observed in both transplantation of HAp/TCP only and IgG isotype control, respectively. (D and E) Co-localization of cells positive for β-galactosidase (in green) and CD44 (in red), as well as, MSI1 (in green) and CD44 (in red) were shown in odontoblast-like cells surrounding HAp/TCP scaffold surfaces in DPSC transplants. (F-H) H&E staining demonstrated the morphology of transplanted tissues in DPSC transplants. The transplanted DPSCs concentrated near HAp/TCP surfaces, and secreted extracellular matrices. Some of transplanted cells were elongated, polarized, and located perpendicularly to HAp/TCP surfaces, resembling odontoblast-like cells (indicated by arrows). Many loose connective tissue areas containing small blood vessels (indicated by arrowheads) surrounded by transplanted cells were found in DPSC transplants, resembling dental pulp-like tissues. (I) transplantations of HAp/TCP without cells were devoid of dense extracellular matrix. (J-M) Masson's trichrome staining confirmed the formation of collagen matrices found in DPSC transplants, but not in the transplantation of HAp/TCP only, respectively. (J-L) DPSC transplants showed elongated and polarized transplanted cells (indicated by arrows). (N-Q) DMP1 and DSP staining was strongly positive in DPSC transplants, but negative in the transplantation of HAp/TCP only, respectively. (O) White arrowheads illustrate polarized transplanted cells positive for DSP. (R) Staining with IgG isotype was used as negative control. DAPI used for nuclei staining is depicted in blue. The dot lines represent a boundary between extracellular matrices secreted by DPSCs and dental pulp-like structure. *DP* = Dental pulp-like structure, *HAp/TCP* = Hydroxyapatite/tricalcium phosphate. Scale bars indicate 100 μm.

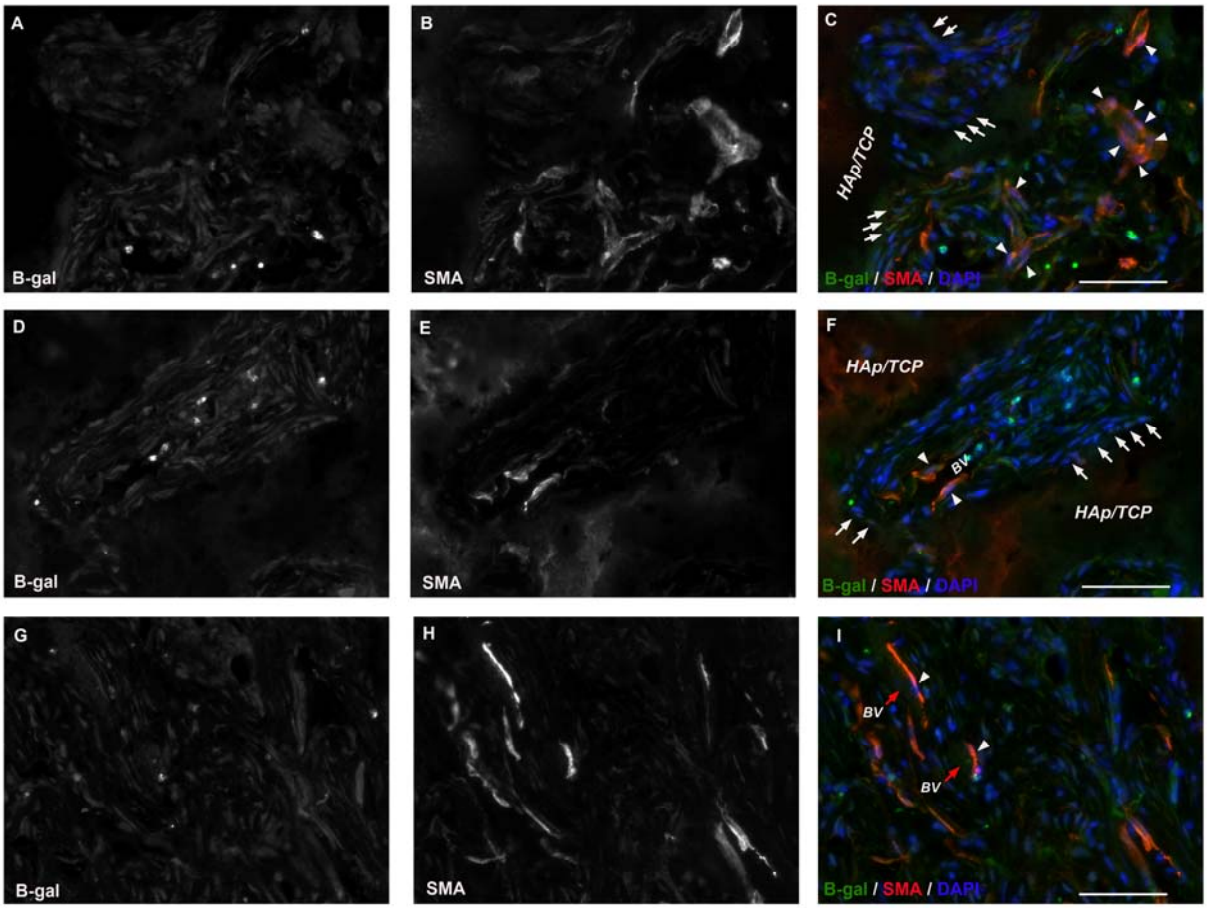

Figure 4.6 *Wnt1*-marked DPSCs gave rise to pericyte-like cells *in vivo*. (A-I) Double staining of anti β-galactosidase (B-gal, in green) and smooth muscle actin (SMA, in red) showed that some transplanted DPSCs labeled by anti B-gal were positive for SMA (indicated by white arrowheads) and located adjacent to blood vessels (indicated by red arrows), indicating pericyte-like phenotype. Some SMA-negative cells were elongated and polarized lining the HAp/TCP surface, representing odontoblast-like cells (indicated by white arrows). (A, D, and G, as well as B, E, and H) Monochromatic figures represented anti β-galactosidase and smooth muscle actin staining, respectively. (C, F, and I) Fluorescence staining was merged to illustrate pericyte-like cells that co-stained positive for anti β-galactosidase and smooth muscle actin (white arrowheads) although some non-specific green and red fluorescence was detected in red blood cells and HAp/TCP, respectively. DAPI used for nuclei staining is depicted in blue. *BV* = Blood vessel, *HAp/TCP* = Hydroxyapatite/tricalcium phosphate. Scale bars indicate 100 μm.

A

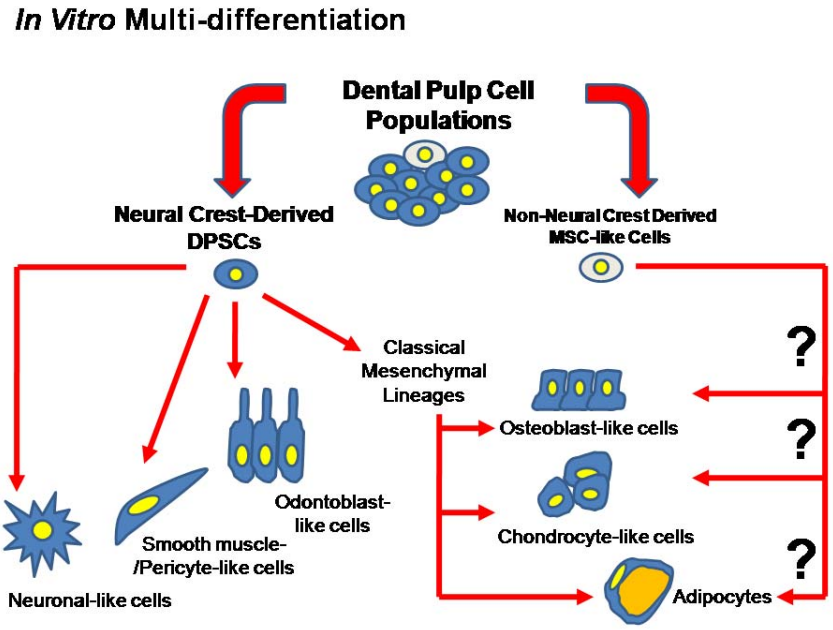
In Vitro Multi-differentiation
Dental Pulp Cell Populations
Neural Crest-Derived DPSCs
Non-Neural Crest Derived MSC-like Cells
Classical Mesenchymal Lineages
Osteoblast-like cells
Chondrocyte-like cells
Adipocytes
Odontoblast-like cells
Smooth muscle-/Pericyte-like cells
Neuronal-like cells
?
?
?

B

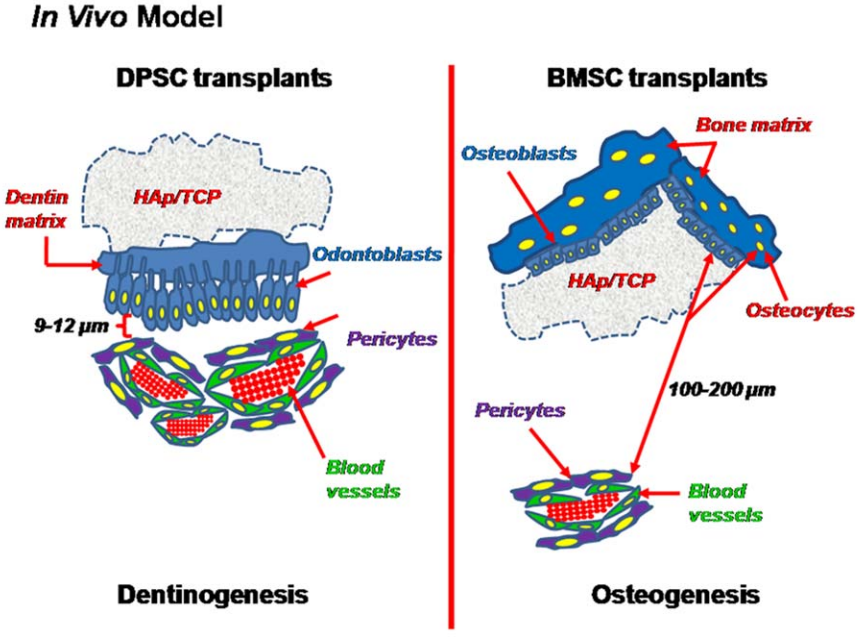
In Vivo Model
DPSC transplants
BMSC transplants
Dentin matrix
HAp/TCP
Odontoblasts
9-12 µm
Pericytes
Blood vessels
Bone matrix
Osteoblasts
HAp/TCP
Osteocytes
100-200 µm
Pericytes
Blood vessels
Dentinogenesis
Osteogenesis

Figure 4.7 Summary of results and working models of neural crest-derived stem cells isolated from murine dental pulp tissue. (A) Base on the *Wnt1-Cre/R26R-LacZ* mouse model, neural crest gene expression, and differentiation capacity, dental pulp stem cell (DPSC) populations contain a majority of neural crest-derived cells (approximately 90%) (shown in blue) while the remaining cell populations were derived from non-neural crest origin (shown in white). In our condition, only neural crest-derived cells can survive and proliferate. After *in vitro* differentiation, these cells can give rise to neural crest-lineages, neuronal-like, smooth muscle/pericyte-like, odontoblast-like cells, including classical mesenchymal cell lineages, osteoblast-like, chondrocyte-like, and adipocytes. Nonetheless, in this study the differentiation capacity of non-neural crest-derived mesenchymal stem cell (MSC)-like cells was not characterized. (B) *In vivo* models show the different capacity between DPSCs and bone marrow stromal cells (BMSCs). Based on the cell/tissue morphology and antibody staining, DPSCs formed dentin-like matrix composed of odontoblast-like cells and pericytes associated with microvessels (close distance about 9-12 μm) recapitulating dentinogenesis. On the other hand, the formation of bone condensation from BMSCs occurred in avascular areas (far distant, about 100-200 μm), resembling early osteogenesis. This model illustrates how two different types of mesenchymal stem cells derived from different origins form different niches and matrices when transplanted under the same conditions. Interestingly, these tissue-specific stem cells recapitulate formation of their own tissue (organogenesis). Understanding the mechanisms of this "memory" of their tissues of origin may be pivotal information for tissue regeneration and cell therapy.

CHAPTER 5

Neural crest derived-dental pulp stem cells function as ecto-mesenchyme to support salivary gland tissue formation (Janebodin and Reyes, 2012)

5.1 Introduction

Irreparable salivary gland tissue dysfunction can be generated by salivary gland diseases such as xerostomia and radiation treatment for head and neck tumor (Dirix et al., 2008). Postnatal stem cells isolated from salivary glands have been characterized and demonstrated capable to give rise into all the epithelial components of the salivary gland tissue such as ductal and acinar cells (Lombaert et al., 2008); nevertheless, their application for salivary gland tissue regeneration is struggled by the need of other supportive cells, vasculature, innervations and matrix necessary for regeneration of the functional salivary gland tissue (Bucheler and Haisch, 2003). Although the salivary gland epithelium of the parotid glands is ectoderm-derived whereas the epithelium of the submandibular and sublingual glands is endoderm-derived, the salivary gland mesenchyme is neural crest-derived (Jaskoll et al., 2002, Yamamoto et al., 2008). The interaction of epithelium and mesenchyme is essential for the branching morphogenesis of the salivary gland. Importantly, the epithelial-mesenchymal interactions in tooth and salivary gland formation are similar and molecular cues such as secretion of fibroblast growth factors (FGF-10, FGF-7) by the ecto-mesenchyme and expression of FGF receptors (FGFR-1, FGFR-2) by the epithelium are important for both the development of tooth bud and salivary gland (Hoffman et al., 2002, Jaskoll et al., 2002, Jaskoll et al., 2004, Jaskoll et al., 2005, Madan and Kramer, 2005, Patel et al., 2006, Yamamoto et al., 2008). Also important morphogens such as Shh, Wnt,

fibroblast growth factors seem to play important roles in tooth bud and saliva gland development (Jaskoll et al., 2004, Dang et al., 2009, Hai et al., 2010). We have recently characterized neural crest-derived dental pulp stem cells (DPSCs) from neonatal mice that can differentiate into neural crest lineages including mesenchyme, Schwann cells, odontoblasts and pericyte-like cells (Janebodin et al., 2011). Due to similarities in tooth bud and salivary gland development, we aimed to study the capacity of neural crest-derived DPSCs to support and induce salivary epithelium differentiation. Both salivary gland mesenchyme and DPSCs are originated from neural crest. Thus, I hypothesized that DPSCs enhanced salivary gland tissue differentiation and formation.

The human salivary gland cell line, HSG, is a neoplastic cell line originally developed from an intercalated duct cell of an irradiated human submandibular salivary gland. The HSG cell line forms primary adenocarcinoma tumors with malignant characteristics when transplanted into nude mice (Hayashi et al., 1985, Sato et al., 1985). Nonetheless, when cultured on matrigel the HSG cell line rapidly differentiates into mature salivary epithelium (Maria et al., 2011). Thus, the HSG cell is a good cell line to study salivary gland tissue differentiation as it is capable of rapid expansion, and differentiation into multiple salivary gland epithelial cell phenotypes including myoepithelial-like, acinar like, keratinocyte-like, chondrocyte-like and mucinous-like cells (Shirasuna et al., 1981, Vag et al., 2007).

In order to study the inductive effects of mouse DPSCs on HSG differentiation I performed *in vitro* xeno-cultures of mouse DPSCs and HSG on matrigel and I observed larger and increased number of acini in the co-cultures as compared to HSG cultures alone. Although matrigel is widely used for *in vitro* culture (Maria et al., 2011, Maria et al., 2011) its immunogenicity limits its *in vivo* application (Cheng and Lambert, 2011).

Thus, I sought extracellular matrix components important for salivary gland tissue development. Hyaluronic acid (HA) is one of the major extracellular matrix components of the developing and adult salivary gland (Cohn et al., 1977, Cutler et al., 1987). HA accounts for 50% of all the glycosaminoglycans (GAGs) in the basal lamina of the developing submandibular salivary gland (Cohn et al., 1977). In adult salivary gland tissue, HA accounts for 25% of all the GAGs synthesized by the secretory units (acini and intercalated ducts) (Cutler et al., 1987). Furthermore, HA is the ligand for CD44 which is highly expressed by DPSCs (Janebodin et al., 2011). Acinar cells also express CD44 (Fonseca et al., 2000). I hypothesized that HA hydrogels will provide a HA rich basement membrane for close epithelial-mesenchymal interaction and will result in induction of differentiated salivary gland three-dimensional (3-D) structures.

Tissue engineering for salivary gland restoration is limited by availability of stem cells or cell sources capable of providing all the cellular components necessary to generate a functional salivary gland tissue. Furthermore, vascularization and innervation of engineered salivary gland tissue is a long-lasting challenge. In this chapter, I performed both *in vitro* and *in vivo* studies by combination of HSG and DPSCs in co-culture and xeno-transplantation to examine the effect of murine DPSCs on the enhancement of human salivary gland differentiation. I report that neural crest-derived DPSCs co-transplanted with HSG in HA hydrogels, secrete fibroblast growth factors, namely FGF-7, angiogenic factors such as VEGF-C and support HSG differentiation into mature salivary gland tissue *in vivo*.

5.2 Materials and Methods

5.2.1 HSG and DPSC culture

HSG cells, derived from a human submandibular salivary gland, were a gift from Dr. Kenneth Izutsu (Department of Oral Health Sciences, University of Washington). The cells were plated in 10,000 cells/cm^2 on plastic tissue culture dishes (BD Biosciences, Franklin Lakes, NJ) and cultured at 37°C under 5% CO_2 in growth media containing Dulbecco's modification of eagle's medium (DMEM) with 4.5g/L glucose, L-glutamine and sodium pyruvate (Cellgro, Manassas, VA) supplemented with 10% heat-inactivated fetal calf serum (FCS) (HyClone, Logan, UT), 100 units/ml penicillin with 100 μg/ml streptomycin (Cellgro).

Murine DPSCs derived from 4-day to 8-day *Wnt1-Cre*/*R26R-LacZ* mice was isolated and cultured as previously described (Janebodin et al., 2011). Briefly, the pulp tissue from molar teeth was gently isolated from tooth crowns and digested with a combination of 1.2 units/ml dispase II, 2 mg/ml collagenase type IV (Worthington, Lakewood, NJ) and 2 mM $CaCl_2$ in phosphate buffer saline (PBS) for 60 minutes at 37°C. The single cell suspension was plated in 1000 cells/cm^2 on plastic tissue culture dishes (BD Biosciences) and cultured at 37°C under 5% O_2 and 5% CO_2 in stem cell media containing 60% low-glucose DMEM (Gibco BRL), 40% MCDB-201 (Sigma), 2% FCS, 1X insulin transferrin selenium (ITS) (Cellgro), 1X linoleic acid bovine serum albumin (LA-BSA) (Sigma), 10^{-9} M dexamethasone (Sigma), 10^{-4} M ascorbic acid 2-phosphate (Sigma), 100 units/ml penicillin with 100 μg/ml streptomycin, and $1x10^3$ units/ml leukemia-inhibitory factor (LIF; ESGRO) (Millipore, Temecula, CA), supplemented with 10 ng/mL EGF and 10 ng/mL PDGF-BB (Sigma). The media were changed every three days and passaged when adherent cells were more than 50% confluent. Both cells were passaged using 0.25% trypsin-EDTA (Cellgro) and replated at a 1:4 dilution under the same culture condition for each cell type.

5.2.2 *In vitro* differentiation of HSG, DPSCs alone, or HSG co-cultured with DPSCs on matrigel

Cells were cultured on either plastic or matrigel-coated surfaces. Growth factor-reduced matrigel (BD Biosciences) was thawed on ice and diluted in DMEM at a final concentration of 2 mg/ml. To form three-dimensional matrix in culture dishes, 100 μl of matrigel was added to 48-well tissue culture plate (0.75 cm^2 per well) and incubated at 37ºC for 1 hour before cell seeding. HSG cells, DPSCs alone, or a combination of HSG with DPSCs (2.5 x 10^4 cells per each cell type/cm^2) were seeded in either non-coated or matrigel-coated plastic surfaces with 100 μl of additional growth media. Culture medium was changed every two days. After 4 days, X-gal was stained to distinguish *Wnt1*-marked DPSCs which express *LacZ* gene from HSG cells. The cells were fixed with 0.2% gluteraldehyde / 2% formaldehyde in PBS for 10 min, and washed with three times of PBS. The fixed cells were subsequently incubated in X-gal solution at 37°C overnight with light protection before washing with three times of PBS. The stained cells were photographed and analyzed.

5.2.3 *In vivo* subcutaneous transplantation of HSG alone or HSG co-transplanted with DPSCs with HA hydrogels

In accordance with approved Institutional Animal Care and Use Committee (IACUC) protocols, HSG alone or HSG combined with murine DPSCs (1x10^6 cells/cell type) were separately transplanted into 2-month-old male *Rag1* null mice (Jackson Laboratory, Bar Harbor, ME, USA) by subcutaneous transplantation with hyaluronic acid (HA) hydrogel (HyStem, Glycosan) (n=3 mice/group) according to the manufacturer's protocol. 100 μl of cell suspension was injected ventrally to the submandibular salivary gland without penetrating the gland. After 2 weeks of transplantation, HA plugs were dissected without involving mouse recipients' salivary

gland tissues and fixed with 10% neutral buffered formalin (NBF) (Sigma) for 30 min at 4^{o}C with agitation, then washed with three times of PBS at RT with agitation. The fixed transplanted tissues were embedded in paraffin and cut to 8-µm thick sections. Sections were analyzed by Hematoxylin and Eosin (H&E), Periodic Acid Schiff (PAS), and immunofluorescence staining.

5.2.4 Quantitative reverse transcriptase -polymerase chain reaction (Q-RT-PCR)

Undifferentiated cultured DPSCs and transplanted tissues (HSG alone or HSG co-transplanted with DPSCs) were extracted for total RNA by using the RNeasy Mini kit (Qiagen) and TRIzol reagent (Invitrogen) according to the manufacturer's protocol, respectively. Quantity and purity of RNA was determined by 260/280 nm absorbance. First-strand cDNA was synthesized from 1000 ng of RNA using the High Capacity cDNA synthesis kit from Applied Biosystems per manufacturer's protocols using a randomized primer. Q-RT-PCR primers are included in Table 5.

cDNA (20ng) was prepared using the SYBR green PCR master mix from Applied Biosystems. Reactions were processed by the ABI 7900HT PCR system with the following parameters: 50°C/2 min and 95°C/10 min, followed by 40 cycles of 95°C/15 s and 60°C/1 min. Results were analyzed using SDS 2.2 software and relative expression calculated using the comparative Ct method. Each sample was run in triplicate reactions for each gene. cDNA of undifferentiated HSG cells and mouse salivary gland tissue were used to calibrate samples.

5.2.5 Immunofluorescence

Cultured cells were fixed with 4% formaldehyde/PBS for 5 min, washed with 1% BSA in 0.1% Triton-X 100/PBS, stained with rat-anti-mouse/human LAMP-1 monoclonal antibody (whole supernatant, Developmental Hybridoma Bank) overnight at 4°C following three times of washing. Goat-derived Alexa 488-conjugated secondary antibody (1:800, Invitrogen) was

incubated for 1 h and washed three times. The cells were double-stained with anti-human CD44 monoclonal antibody directly conjugated with PE (CD44-PE, 1:100, eBioscience) for 1 h at RT, and then washed three times.

Transplanted tissue sections were deparaffinized, rehydrated, and permeabilized with 1% bovine serum albumin (BSA) in 0.1% Triton X-100/PBS. Then sections were blocked with 10% normal goat serum for 1 h at RT, and incubated with primary antibody which is rat-anti-mouse/human LAMP-1 or rabbit-anti-mouse vWF polyclonal antibody (1:400, Dako) overnight at 4°C following three times of washing. The stained sections were subsequently incubated with goat-derived Alexa 488-conjugated secondary antibody (1:800) for 1 h at RT, and washed three times. Then the sections were incubated by the second set of primary antibody which is anti-human-CD44-PE or anti-mouse-SMA monoclonal antibody directly conjugated with Cy3 (1:400, Sigma) for 1 h at RT before washing three times. Cells were stained with 4', 6-diamine-2-phenylindol (DAPI, 1:1000) to visualize the nuclei. All antibodies were diluted in 1% BSA in 0.1% Triton-X 100/PBS.

All immunofluorescence images described in this manuscript was detected using a Zeiss Axiovert 200 fluorescent microscope (Thornwood, NY). Photographs were taken with an onboard monochrome AxioCam MRm camera and colored using Adobe Photoshop (San Jose, CA). Background was reduced using brightness and contrast adjustments, and color balance was performed to enhance colors. All the modifications were applied to the whole image using Adobe Photoshop.

5.2.6 Periodic Acid Schiff (PAS) staining

Transplanted tissue sections were dewaxed and rehydrated. The sections were stained in 1% Periodic Acid solution (Sigma) for 10 min at RT with agitation before rinsing with deionized

water. Then the tissues were incubated in Schiff reagent (Sigma) for 5 min at RT with agitation before washing three times with deionized water. The stained tissues were dehydrated in a series of alcohol solutions, and cleared with xylene before mounting.

5.2.7 Statistical analysis

The number of acini formed in the *in vitro* experiment and the number of blood vessels in the transplanted tissues was quantified using an image analysis program, ImageJ v1.43u (Wayne Rasband, NIH; http://rsb.info.nih.gov/ij). The number of acinar-like structure was counted from 6 wells in each experimental group. The percentage of blood vessel per area was determined upon examination of 10 areas in each experimental group. Data were represented as Means ± the Standard Error of the Mean (SEM) of results from three separate experiments. The data were analyzed by Student's t-test where p-value ≤ 0.05 represented significant differences between HSG alone and HSG co-cultured or co-transplanted with DPSCs.

5.3 Results

5.3.1 HSG co-cultured with DPSCs formed more mature and increased number of acinar-like structures

HSG and DPSCs cultured separately on plastic surfaces showed their different cell morphology; the former were polyhedral-shaped epithelial cells whereas the latter were spindle-shaped fibroblasts (Figs. 5.1A, B). As expected, HSG, DPSCs alone, and HSG co-cultured with DPSCs (HSG+DPSC) grown on non-coated surfaces proliferated, but only formed a confluent monolayer (Figs. 5.1C-E).

After cultured separately on matrigel-coated plastic surfaces for 4 days, HSG underwent dramatically morphological changes in both HSG alone and HSG+DPSC. As previously reported

(Maria et al., 2011), the salivary gland cells initiated to form acinar-like structures after day 1 in matrigel culture; however, the acinar-like structures found in HSG+DPSC were larger and more numerous than those in HSG alone (Figs. 5.1F, H). The acinar-like structures in HSG alone and HSG+DPSC gradually increased in size (Figs. 5.1I, J). DPSCs which were cultured alone on matrigel did not change their cell morphology (Fig. 5.1G). HSG cultured alone on matrigel for 4 days showed small acinar-like phenotypes, represented by spherical structures with polarized nuclei and lumen formation (Fig. 5.1K) (Patel et al., 2006, Tucker, 2007). In contrast, HSG in the co-culture group formed large multi-cellular structures that resembled intact salivary glands with acinar- and duct-like structures (Fig. 5.1L, arrowheads). Noticeably, co-culturing DPSCs shown by positive X-gal staining (in blue) were clustered near HSG-derived acinar-like structure (Fig. 5.1J, arrows).

The HSG-derived acinar structures in both HSG alone and HSG+DPSC were positive for CD44 (in red) and lysosome associated membrane protein-1 (LAMP-1) (in green), confirming the differentiation of HSG to acinar cells (Figs. 5.1K, L). CD44 and LAMP-1 are expressed by HSG and acinar salivary gland (Heffernan et al., 1989, Fonseca et al., 2000, Maria et al., 2011). The acinar structures in the HSG+DPSC group were strongly positive for LAMP-1 when compared to those in HSG alone, suggesting higher maturity of acinar salivary gland structures. Additionally, the number of acinar-like structures quantified in the HSG+DPSC group was significantly larger than those in HSG alone ($*p = 0.002$) (Fig. 5.1M). Taken these results together, this suggests that DPSCs enhance the ability of HSG to differentiate to acinar- and duct-like phenotypes.

5.3.2 DPSCs expressed high level of *Fgf-7* and *Fgf-10*, neural crest-derived mesenchymal genes essential for salivary gland formation

To complement our *in vitro* study and to gain insight into DPSC supportive role to induce HSG differentiation into functional salivary gland units *in vivo*, I transplanted HSG alone or the combination between HSG and DPSCs subcutaneously by direct injection of cell suspension ventrally to the submandibular salivary gland without penetrating in the gland with hyaluronic acid (HA) hydrogel in *Rag1* null mice to avoid immune rejection against the human cells (HSG) (Fig. 5.2A).

Undifferentiated DPSCs in my culture condition showed the expression of ectodysplasin, *Eda*, and fibroblast growth factors, *Fgf-7* and *Fgf-10*. *Eda, Fgf*-7, and *Fgf-10* are proteins secreted by neural crest-derived mesenchymal cells to induce branching morphogenesis during salivary gland development and formation (Morita and Nogawa, 1999, Jaskoll et al., 2005, Tucker, 2007). DPSCs expressed significantly high levels of *Fgf-7* and *Fgf*-10, which is approximately >10 folds greater than endogenous *Fgf-7* and *Fgf-10* expression in mouse submandibular salivary gland (*p = 0.0014 and 0.00005, respectively) (Fig. 5.2B). The high expression of both growth factors combined with my previous study showing that DPSCs are neural crest-derived led me to hypothesize that DPSCs may be a good source of ecto-mesenchymal supportive of salivary gland formation and regeneration (Janebodin et al., 2011). In addition, DPSCs expressed high level of vascular endothelial growth factor receptor 3, *Vegfr-3* (>5 folds greater than endogenous *Vegfr-3, *p = 0.0026), and similar level of its ligand, *Vegf-C* but not *Vegf-A*, when compared with that of mouse salivary gland (Fig. 5.2B). A previous study demonstrated that stimulation of blood vessel formation improved regeneration of submandibular salivary gland (Lombaert et al., 2008). Therefore, the expression of angiogenic genes by DPSCs suggests that their angiogenic potential may be beneficial for salivary gland formation.

5.3.3 Co-transplantation of HSG and DPSCs demonstrated high expression of murine neural crest-derived mesenchymal and human salivary gland differentiation genes

After two-week post-transplantation, HA hydrogel plugs were processed for histological and Q-RT-PCR analyses using primers specific for human salivary gland differentiation genes and mouse specific mesenchymal genes.

DPSCs up-regulated the expression of *Eda*, *Fgf-7*, and *Fgf-10* in the HA hydrogel plugs *in vivo*. The level of all three mesenchymal genes expressed in HSG+DPSC was also greater than that expressed in HSG alone. In particular, the levels of *Fgf-7* showed >10 folds greater than endogenous *Fgf-7* expression in untransplanted mouse submandibular gland (*p = 0.009) (Fig. 5.3A). To confirm the formation of functional salivary gland, I used human specific primers to determine the expression of salivary gland differentiation genes. The HSG alone and co-transplanted with DPSCs expressed higher level of human ectodysplasin receptor (*EDAR*), mucin (*MUC-5B* and *MUC-7*), alpha-amylase-1 (*AMY-1*), and aquaporin-5 (*AQP-5*) (approximately >10-150 folds greater than the expression in undifferentiated human submandibular salivary gland cells) (Fig. 5.3B). Importantly, alpha-amylase-1 which is an enzyme that is secreted by a functional salivary gland, was expressed significantly higher in the co-transplanted tissues (*p = 0.046), suggesting that HSG co-transplanted with DPSCs formed more mature and functional salivary gland.

Next, I studied if DPSCs enhance human salivary gland cells to differentiate and form functional salivary gland by induction of blood vessel and nerve innervating formation. To answer this question, I examined endothelial-specific, neuronal, and angiogenic gene expression by Q-RT-PCR. Accordingly, HSG+DPSC group showed higher level of the endothelial markers, von Willebrand Factor (*vWF*) (*p = 0.018) as well as the neuronal marker, heavy neurofilament

(*NF-200*) ($p = 0.058$), when comparing with HSG group (Fig. 5.3C). Likewise, the HSG+DPSC co-transplanted tissues expressed higher levels of *Vegfr-3* and *Vegf-C* (*p = 0.023 and 0.027, respectively) (approximately >30-35 folds and >2 folds greater than expression in mouse submandibular salivary gland and in HSG transplants, respectively) (Fig. 5.3D). The expression of these transcripts suggests that DPSCs enhance the salivary gland cells to differentiate and form salivary gland tissue by induction of blood vessel and nerve innervating formation.

5.3.4 Glandular structures were observed in the co-transplantation of HSG and DPSCs

In addition to gene expression, I determined the morphology of transplants in HSG alone and HSG+DPSC. H&E staining revealed that HSG hydrogel plugs showed only immature cancer-like cells with large nuclei (Figs. 5.4A-C). Conversely, duct- and acinar-like structures represented by their polarized nuclei were seen in the hydrogel plugs containing HSG and DPSC, particularly at the periphery close to mesenchymal cells (Figs. 5.4D-F) and vessels (Fig. 5.4E, inset).

PAS staining distinguished acinar- from duct-like structures by revealing the formation of mucin/mucopolysaccharide containing cells. PAS-positive cells (in pink) were randomly found in the HSG transplants alone (Figs. 5.4G-I). In contrast, several clusters of PAS-positive acinar-like with some PAS-negative duct-like structures were present in the HSG+DPSC transplants (Fig. 5.4J, inset).

Immunofluorescence showed more mature glandular structures which were double-positive for CD44 and LAMP-1 in the HSG+DPSC co-transplantation group, but not in the HSG alone (Figs. 5.5A, B, arrows). The cells in HSG transplants were immature which stained positive for CD44, but negative for LAMP-1 (Fig. 5.5A). Interestingly, differentiated HSG cells

were observed at the interface with mesenchymal cells (DPSCs) which encapsulated the HSG tumor (Fig. 5.5B, arrowheads). In addition, encapsulating DPSC which stained positive for smooth muscle actin (SMA) integrated deeper into the core of the transplanted tissue and also recruited blood vessels (Figs. 5.4E, K insets, L, 5.5C, D arrowheads, E, F). The blood vessels were recognized by SMA and vWF staining (Figs. 5.5C-F). The quantification of blood vessels in both transplanted tissues showed significantly increased number of blood vessels in HSG+DPSC than that in HSG alone (*p = 0.004) (Fig. 5.5G).

5.4 Discussion

In general stem cell therapy focuses on delivering only the desired stem cell population. This approach works if the stem cell can regenerate the whole organ. For salivary gland regeneration, although a putative salivary gland stem cell can potentially regenerate all the epithelial components it cannot give rise to the supportive tissue including mesenchyme, vasculature and nerves. Since dental pulp stem cells (DPSCs) are neural crest-derived and epithelial-mesenchymal interactions of tooth bud and salivary glands are similar, I hypothesized that DPSCs is a good source of mesenchyme to induce and support salivary gland tissue differentiation.

I first studied the effects of co-culture with DPSCs on HSG differentiation *in vitro*. DPSCs and HSG were co-cultured on matrigel. After 4 days, HSG had formed acini but the number of acini and the size of the acini were significantly increased in the co-cultures with HSG as compared to HSG only cultures.

The unknown composition and immunogenicity of matrigel are some of the disadvantages for its *in vivo* use (Norrby, 2006, Kilarski and Bikfalvi, 2007). Thus, I sought a

more natural matrix for salivary gland formation. Hyaluronic acid (HA) is the most abundant glycosaminoglycan in the developing salivary gland (Cohn et al., 1977). Also, adult salivary gland secretory units produce high amount of HA, which is deposited in the basal lamina (Cutler et al., 1987). Furthermore, acinar epithelial cells express CD44 the receptor for HA (Terpe et al., 1994, Xing et al., 1998). Thus I hypothesized that HA hydrogels will provide a good a natural scaffold for salivary gland formation and epithelial-mesechymal interaction. Therefore, I conducted xeno-transplantation of HSG alone or HSG and DPSCs in HA hydrogels subcutaneously ventrally to the endogenous submandibular gland. Although HA hydrogels have been previously used to induced 3-D formation of salivary secretory units *in vitro* (Pradhan et al.), to my knowledge this is the first report that demonstrate the potential use of HA hydrogels for *in vivo* formation of salivary gland tissue.

I performed transplantation of DPSCs and HSG in *Rag1* null mice. Using this hetero-xeno-transplantation approach, I can clearly monitor and distinguish the contribution of murine DPSCs using murine specific mesenchymal primers compared to untransplanted murine salivary gland tissue as well as the contribution and differentiation stage of HSG using human specific primers of salivary gland epithelial markers. Before transplantation, I observed that DPSCs expressed approximately 10 folds higher levels of *Fgf-7* and *Fgf-10*. These fibroblast growth factors are essential for proper salivary gland formation as their respective knockout and their receptor *Fgfr-1* knockout mouse models result in salivary gland development defects or aplasia (Jaskoll et al., 2005, Makarenkova et al., 2009). Furthermore, upon transplantation, DPSCs expressed significantly higher levels of *Fgf-7* as compared to untransplanted murine salivary gland and HGS only transplants. This is therapeutically significant as FGF-7 (aka Keratinocyte

Growth Factor, KGF) administration has been shown beneficial for salivary gland restoration (Lombaert et al., 2008, Zheng et al., 2011).

Given the tumorigenic nature of HSG, I only performed short term transplantation. Nonetheless, in 2 weeks post-transplantation I showed significant increase in the levels of human salivary gland differentiation markers in both HSG only and HSG with DPSC co-transplantations. Moreover, gene expression of human alpha-amylase-1 (*AMY-1*) was significantly increased in the HSG co-transplanted with DPSC indicating that DPSC induced functional differentiation of HSG *in vivo*. Upon histological examination it became obvious that differentiated glandular structures were observed at the interface with mesenchyme and near vessels. This underlies the importance of epithelial-mesenchymal interaction for proper glandular differentiation and demonstrates that DPSCs is a good source of ecto-mesenchyme. Consistent with my previous observations, DPSCs exhibit great angiogenic capacity *in vivo* (Janebodin et al., 2011). DPSCs express high levels of *Vegfr-3* and *Vegf-C* and significant higher levels of these angiogenic factors were found in the co-transplanted tissue containing DPSCs and HSG as compared to HSG alone. This may explain the increased number of vessels in the co-transplanted tissue. This suggests that angiogenesis may be an important aspect of salivary gland tissue development and regeneration. Furthermore, I observed near significant higher levels of *NF-200* that reached the levels seen in normal submandibular gland. Recently it has been demonstrated that innervation is crucial for normal development of the salivary gland (Knox et al., 2010). Future studies are warranted to understand the mechanisms of DPSC induction of angiogenesis and neurogenesis.

5.5 Conclusion

I provide an evidence of the potential clinical use of neural crest-derived DPSCs as ecto-mesenchyme for induction and support of salivary gland development and formation. DPSCs are considered biological and easily accessible sources of postnatal stem cells isolated from adult and deciduous teeth with less invasive procedure. Their multi-lineage stem cell differentiation capacity combined with their trophic epithelial-morphogenic, angiogenic and neurogenic capacity makes DPSCs ideal inductive and supportive cell source for salivary gland tissue engineering approaches. Further studies should be performed in order to understand better in molecular biological mechanisms or signaling pathways of DPSCs or neural crest-derived mesenchyme to enhance the salivary gland differentiation. Also, studying the effect of DPSCs or neural crest-derived mesenchyme on salivary gland regeneration or formation emphasizing salivary gland functional analyses in mouse models with damaged or diseased salivary gland will provide very useful information to translate into human clinical models.

Table 5. The human- and mouse-specific primer sequences

Q-RT-PCR primers (Human)			
Gene	**Forward primer (5'→3')**	**Reverse primer (5'→3')**	**GenBank Accession number**
GAPDH	GCTCCTCCTGTTCGACAGTCA	TGACGGTGCCATGGAATTT	NM_002046
EDAR	TCTCCCTTCCAGCACGCCCA	TCAGGGCAGTGGCCAGGTGT	NM_022336
MUC-5B	GCTGGGAGAATGCAGGGCACA	GCTGGGGAAGACAGTGACGGG	NM_002458
MUC-7	TGGCTACCAAAATGCCTAGACACAG	GGAATCCTTCCTCCAAGTCTGGTCA	NM_001145006
AMY-1	TCCGTCTTGTCGGTCTGTCAGGG	ACAGCCCACGGTGCTCTGGTA	NM_001008219
AQP-5	TGTGGCACCGCTCAATGCCC	GCCTGGCCCTGCGTTGTGTT	NM_001651

Q-RT-PCR primers (Mouse)			
Gene	**Forward primer (5'→3')**	**Reverse primer (5'→3')**	**GenBank Accession number**
Gapdh	GGGAAGCCCATCACCATCT	GCCTCACCCCATTTGATGTT	NM_008084
Eda	TGGAGGTACTGGTGGACGGCA	ACCACCACCTCGTAGCTGGCA	NM_010099
Fgf-7	GTCCGGAGCAAACGGCTACGA	TGTGTCGCTCGGGGCTGGAA	NM_008008
Fgf-10	TGGTGTCACAGGAGGCCACCAA	CGCACATGCCTTCCCGCACT	NM_008002
vWF	GATGTCCAGCTCCCCTTCCT	AGGCGTTTCCGAAGTCTACCA	NM_011708
NF-200	CATTGAGATTGCCGCTTACAGA	GAGAAGGGACTCGGACCAAAG	NM_011708
Vegfr-3	ATCGGCAACCATCTCAACGT	GCTTTGGCGCCTTCTACCA	NM_008029
Vegf-C	GATTCTCTGCCCCGCTTTG	GGAGGATGCTGTGTTGCTACAA	NM_009506
Vegf-A	GAGCAGAAGTCCCATGAAGTGAT	CAATCGGACGGCAGTAGCTT	NM_001025250

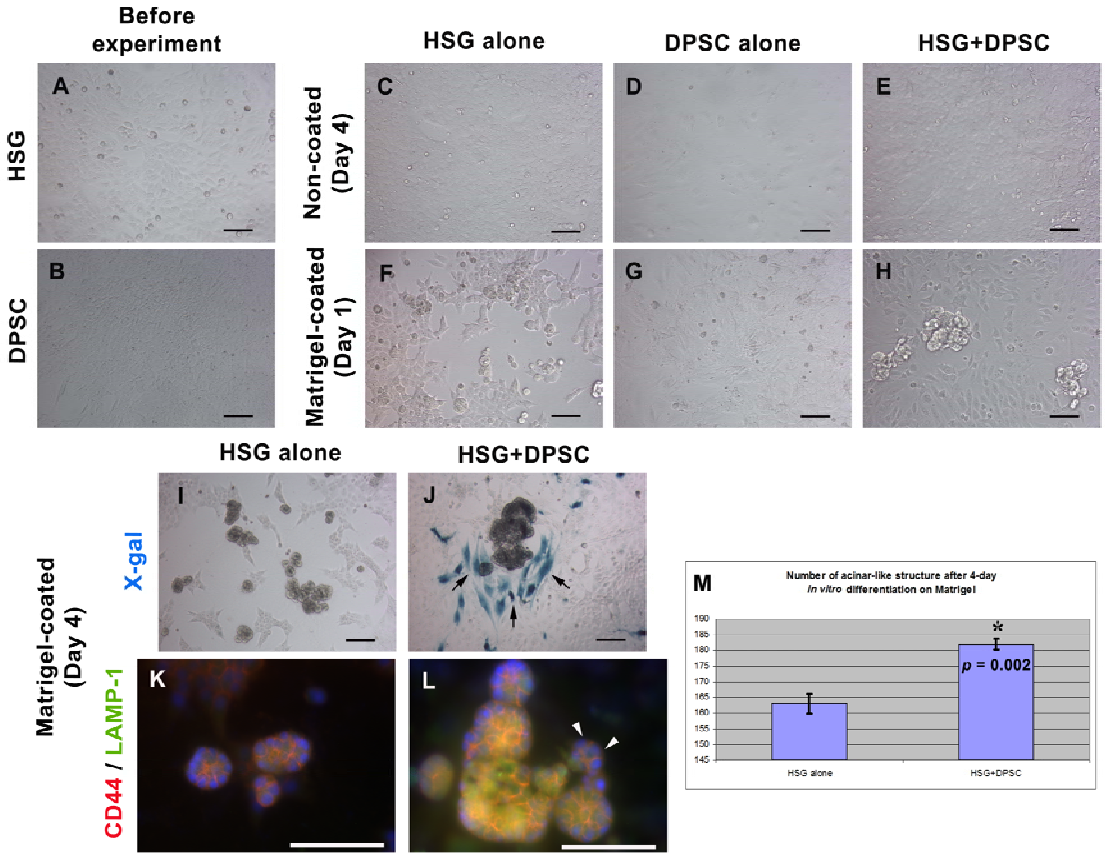

Figure 5.1 Human Salivary Gland (HSG) Cells formed more mature and increased number of acinar-like structures in the presence of Dental Pulp Stem Cells (DPSCs). (A and B) Undifferentiated HSG cells and DPSCs cultured on plastic surfaces before starting experiment showed polyhedral- and spindle- shaped, respectively. (C-E) HSG, DPSCs alone, and HSG co-cultured with DPSCs (HSG+DPSC) cultured on non-coated plastic surfaces proliferated and formed a confluent monolayer. (F-H) HSG, DPSCs alone, and HSG+DPSC cultured on Matrigel-coated surface for 1 day. (F) HSG started to form small acinar-like structures. (G) DPSCs survived, proliferated, and formed a monolayer, but not gave rise to any acinar-like structures. (H) Large HSG-derived acinar-like structures were found in HSG+DPSC group. (I and J) X-gal showed the positive staining of *Wnt1-Cre/R26R-LacZ* derived DPSCs due to the expression of β-galactosidase (β-gal), but not HSG. (I) HSG-derived acinar-like structures increased in size after 4 days cultured on Matrigel. (J) HSG co-cultured with *Wnt-1*/β-gal+ DPSCs (X-gal+ cells shown in blue) formed larger acinar-like structures which closely contacted to DPSCs (arrows). (K and L) The acinar-like structures in both HSG and HSG+DPSC were positively stained for CD44 and LAMP-1. (L) HSG co-cultured with DPSCs formed more mature due to higher expression of LAMP-1 and CD44. The duct-like structure was also seen in this group (arrowheads). (M) The bar graph shows that the number of acinar structures increased in HSG+DPSC (182 ± 0.68 acini) when compared with HSG alone (163 ± 1.32 acini). The number of acini in both groups were counted from 6 wells (n = 6) are statistically significant. Student's t-test calculated * $p \leq 0.05$. Error bars represent ± SEM. Scale bars indicate 100 µm.

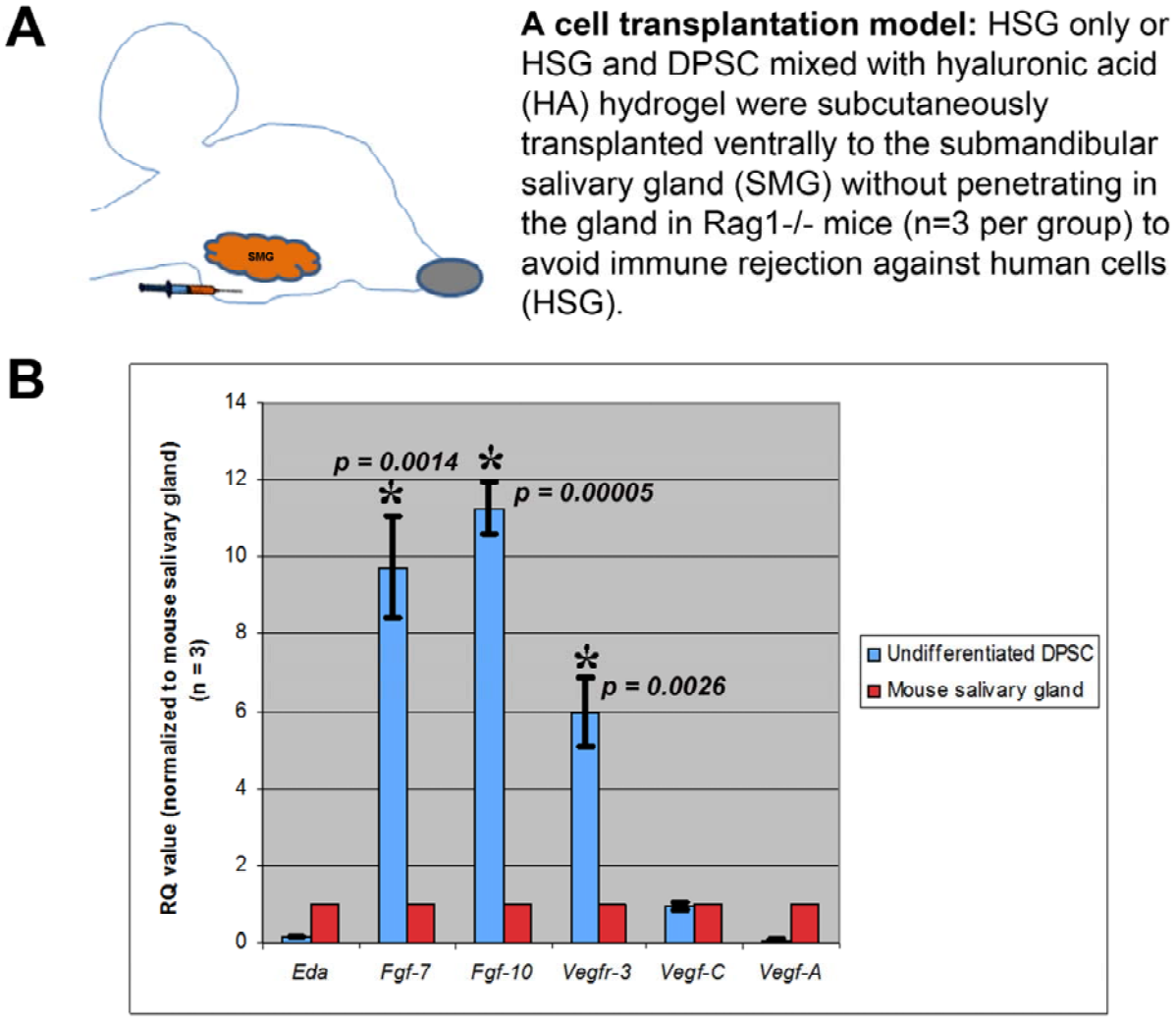

Figure 5.2 Cultured undifferentiated DPSCs expressed high level of *Fgf-7* and *Fgf-10,* neural crest-derived mesenchymal genes involving salivary gland formation. (A) A diagram illustrates the *in vivo* cell transplantation model. HSG alone or the combination between HSG and DPSCs (1 million per cell type) were prepared as cell suspension in hyaluronic acid (HA) hydrogel scaffold and subcutaneously injected ventrally to the submandibular salivary gland (SMG) without penetrating in the gland in 2-month-old *Rag1-/-* null mice (n = 3 mice/group) to avoid immune rejection against the human cells (HSG). (B) Q-RT-PCR showed RQ (Relative Quantification) values demonstrating differential gene expression of *Eda*, *Fgf-7*, *Fgf-10*, *Vegfr-3*, *Vegf-C*, and *Vegf-A* in undifferentiated DPSCs and mouse salivary gland. DPSCs cultured in stem cell media under 5% O_2 incubation, as previously described in Materials and Methods, expressed high level of *Fgf-7*, *Fgf-10*, and *Vegfr-3*, as well as the same level of *Vegf-C*, compared to mouse salivary gland (approximately >10 folds greater than endogenous *Fgf-7* and *Fgf-10* , and >5 folds greater than endogenous *Vegfr-3* expression in mouse submandibular salivary gland. RQ values (n = 3) were normalized by the expression of mouse salivary gland. *Gapdh* was used for the internal control. Student's t-test calculated * $p \leq 0.05$. Error bars represent ± SEM.

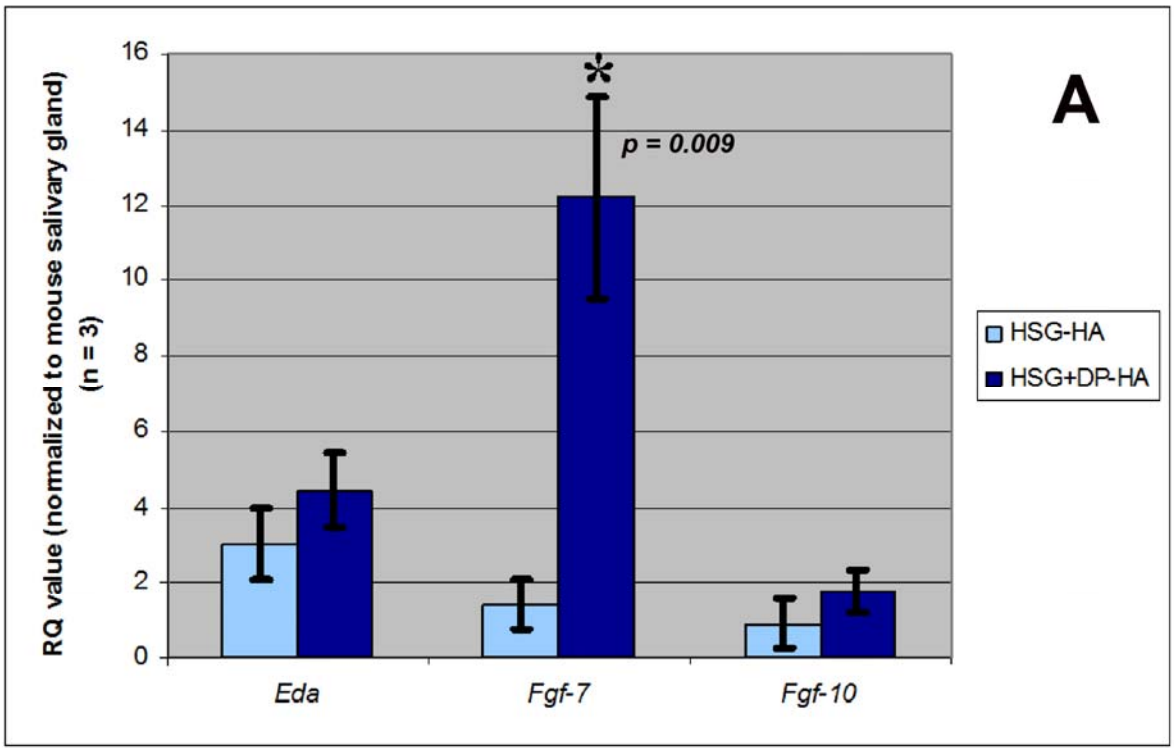
A
RQ value (normalized to mouse salivary gland) (n = 3)
16
14
12
10
8
6
4
2
0
*
p = 0.009
HSG-HA
HSG+DP-HA
Eda
Fgf-7
Fgf-10

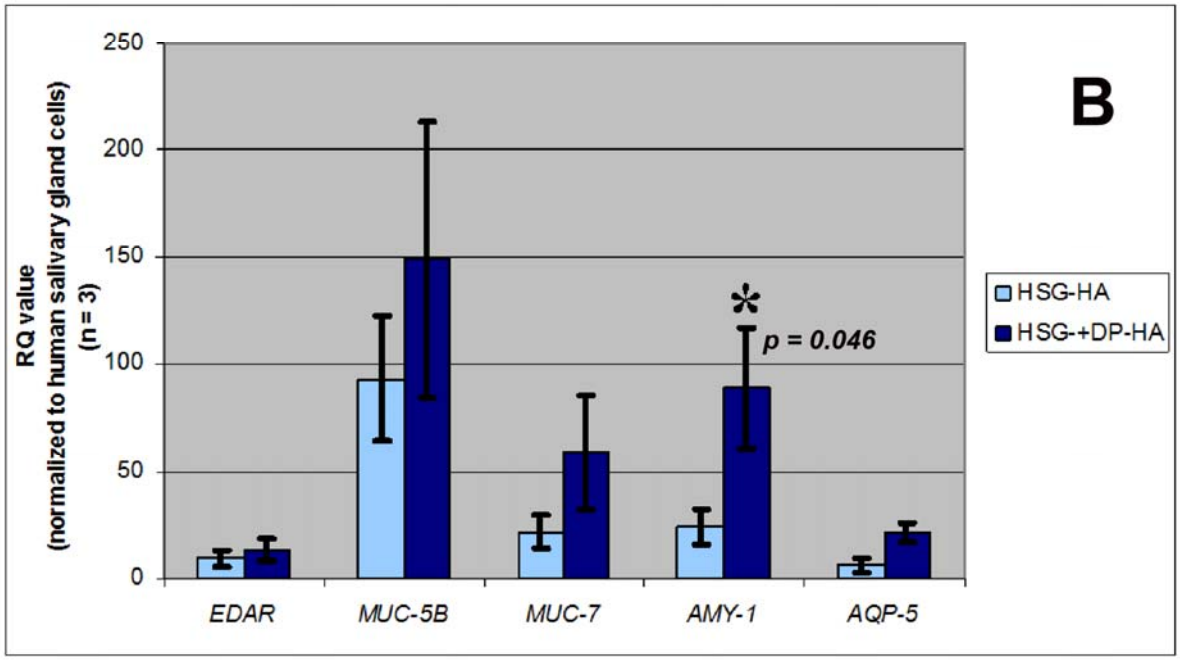
B
RQ value (normalized to human salivary gland cells) (n = 3)
250
200
150
100
50
0
*
p = 0.046
HSG-HA
HSG-+DP-HA
EDAR
MUC-5B
MUC-7
AMY-1
AQP-5

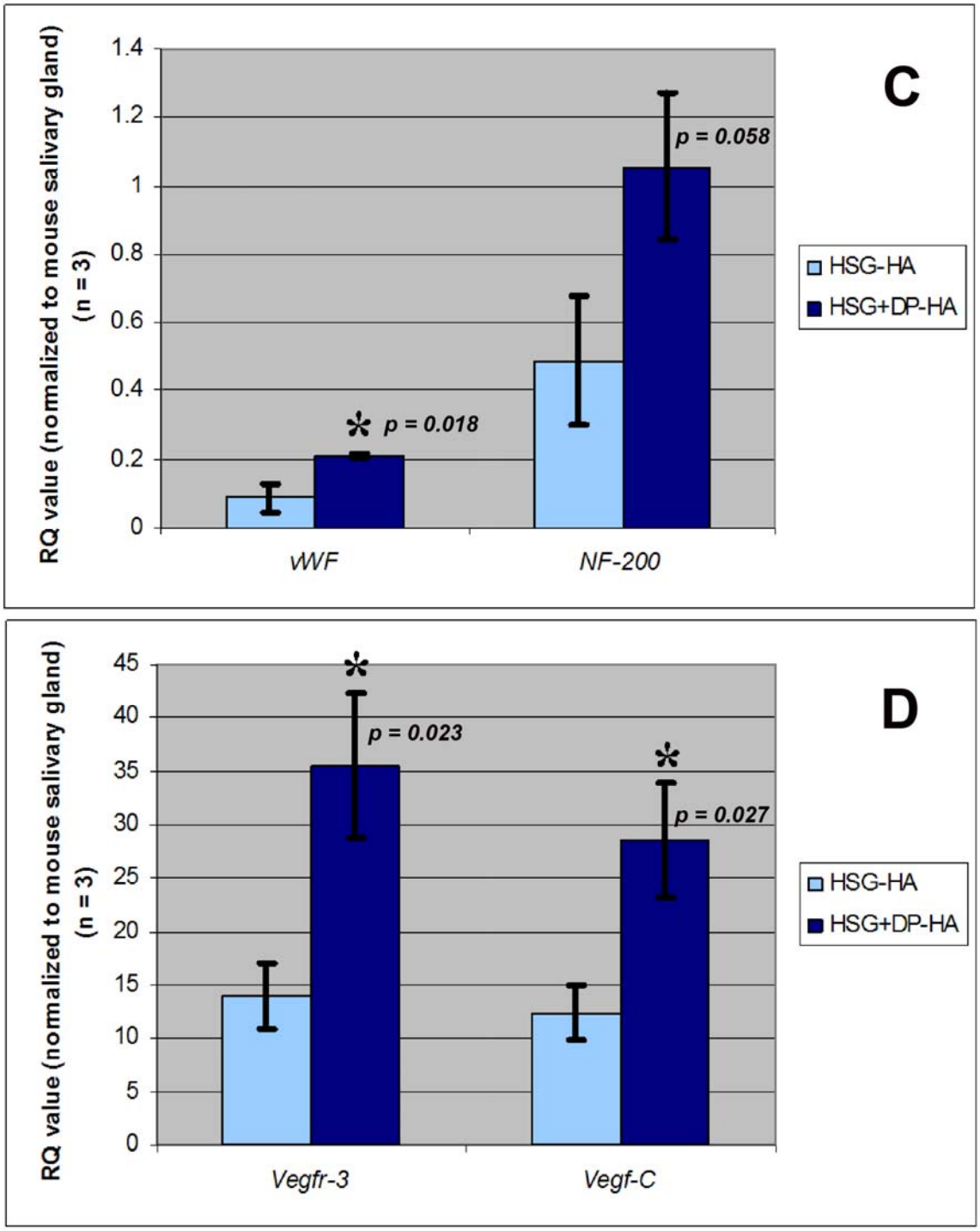

Figure 5.3 Co-transplantation of HSG and DPSCs demonstrated high expression of murine neural crest-derived mesenchymal and human salivary gland genes. (A-D) Q-RT-PCR showed RQ (Relative Quantification or Relative Expression) values demonstrating differential gene expression in HSG alone (HSG-HA) and HSG co-transplanted with DPSCs (HSG+DP-HA). The transplanted HSG and DPSCs in HA hydrogel scaffolds expressed higher levels of murine *Eda*, *Fgf-7*, and *Fgf-10*, human *EDAR*, *MUC-5B*, *MUC-7*, *AMY-1*, and *AQP-5*, as well as

murine *vWF*, *NF-200*, *Vegfr-3*, and *Vegf-C*. (A) HSG+DPSC particularly expressed significantly higher *Fgf-7* expression (> 10 folds compared to HSG transplants alone). (B) The HSG alone and HSG co-transplanted with DPSCs expressed higher level of *EDAR*, *MUC-5B*, *MUC-7*, *AMY-1*, *AQP-5* (approximately >10-150 folds compared to undifferentiated human submandibular salivary gland cells). AMY-1 was expressed significantly higher in the co-transplanted tissues. (C and D) HSG+DPSC expressed higher level of mouse *vWF*, *NF-200, Vegfr-3* and *Vegf-C* compared to HSG transplants alone. RQ values (n = 3) were normalized to the expression of mouse salivary gland or human salivary gland cells. Mouse *Gapdh* or human *GAPDH* was used for the internal control. Student's t-test calculated * $p \leq 0.05$. Error bars represent ± Standard Error of the Mean (SEM).

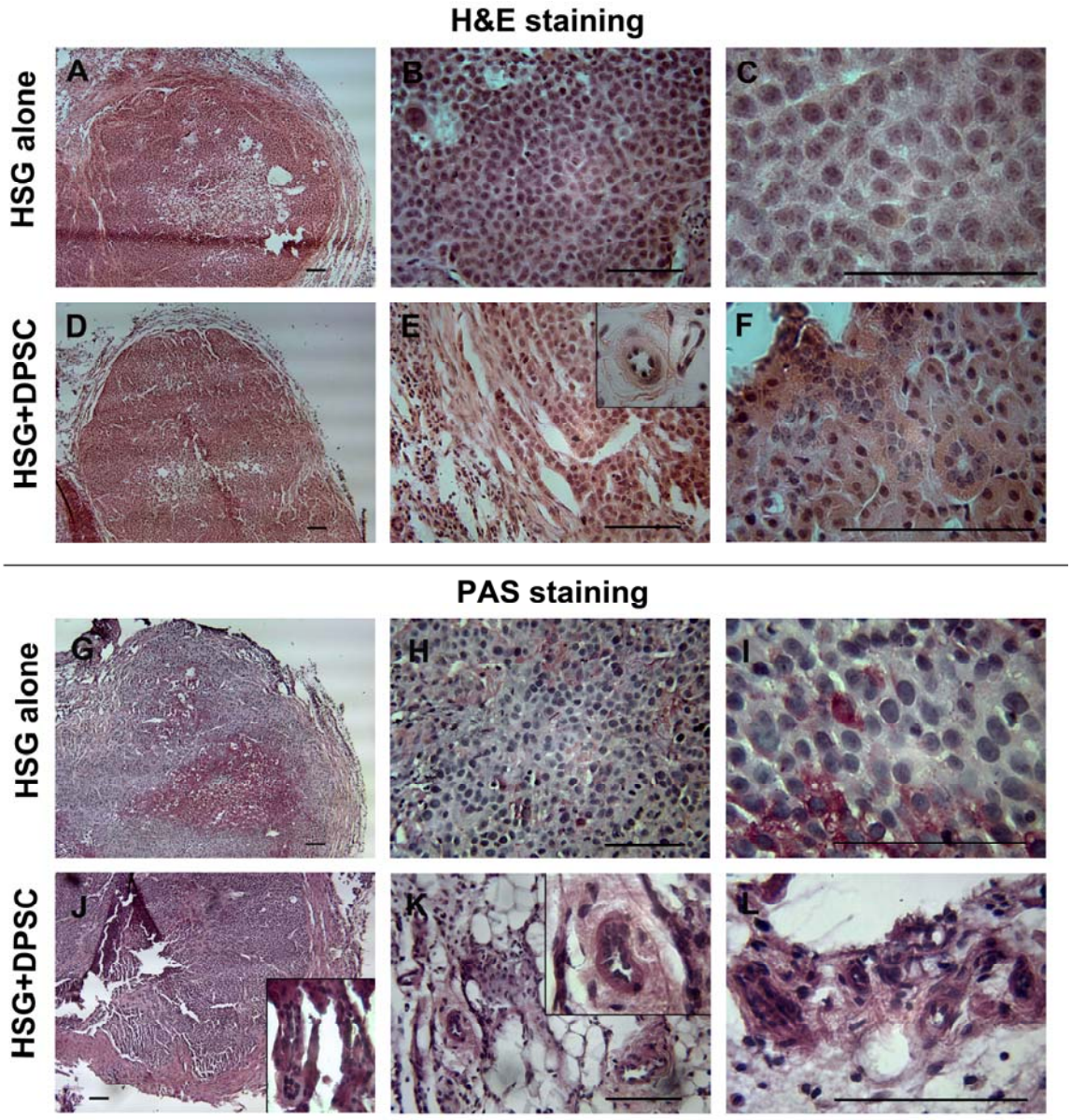

Figure 5.4 HSG co-transplanted DPSCs demonstrated glandular structures with acinar- and duct-like structures. HSG only (1 million cells) or HSG and DPSCs (1 million each) were injected in HA hydrogels subcutaneously ventrally to the submandibular salivary gland in *Rag1* -/- mice (n =3 mice per group). (A-C) H&E staining demonstrated immature cancer-like cells with large nuclei in HSG hydrogel plugs. (D-F) H&E staining showed the duct- and acinar-like structures represented by their polarized nuclei in the hydrogel plugs containing HSG and DPSCs. (G-I) PAS staining indicated some randomly positive cells (in pink) were found in the HSG transplants alone. (J-L) Clusters of PAS-positive acinar-like with some PAS-negative duct-like structures were present in the HSG+DPSC transplants. (E and K, insets, and L) Blood vessels were found at the interface of HSG and DPSCs where the glandular structures were observed. Scale bars indicate 100 μm.

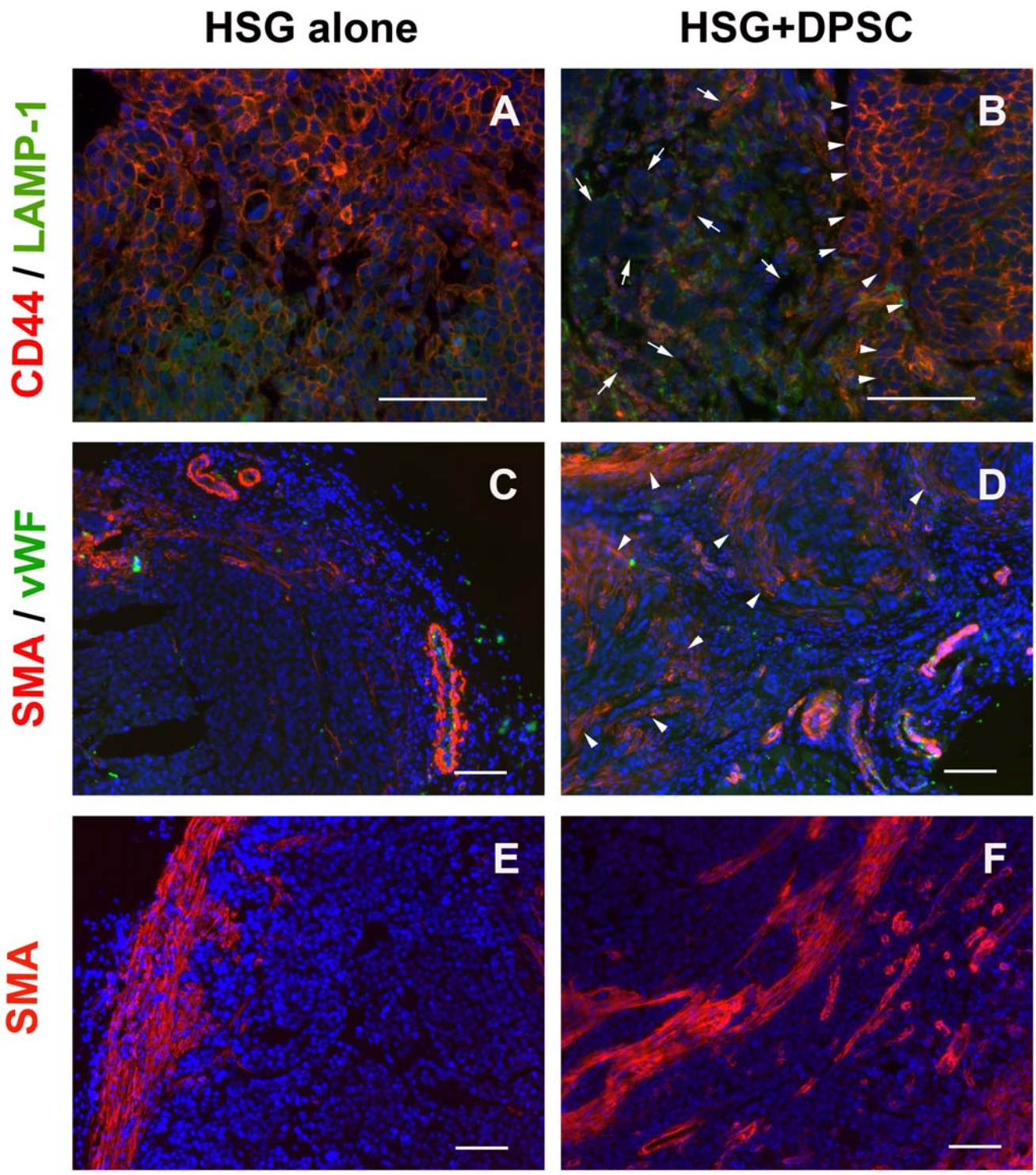
HSG alone
HSG+DPSC
CD44 / LAMP-1
SMA / vWF
SMA
A
B
C
D
E
F

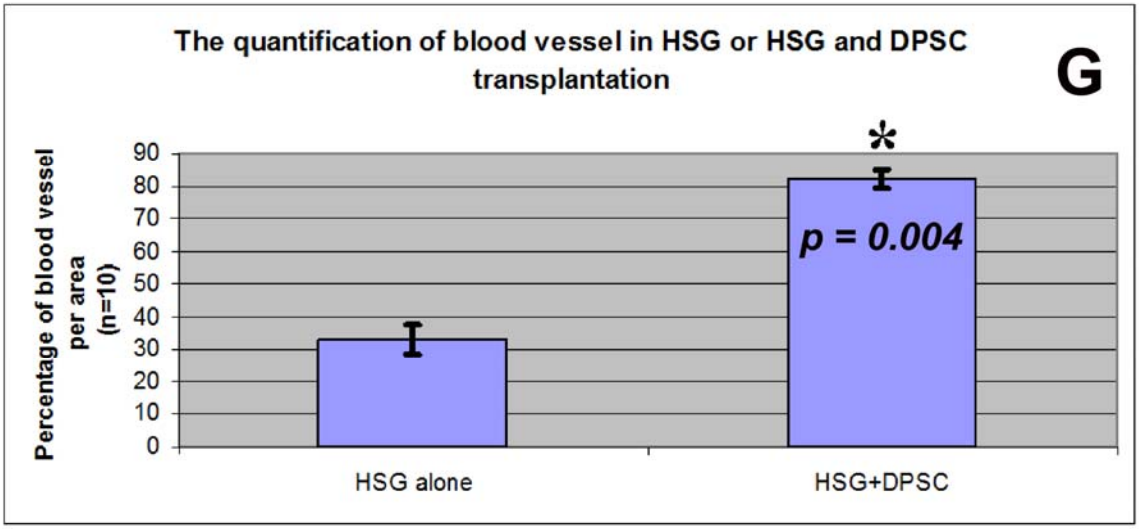

Figure 5.5 Immunohistological characterization of HSG and DPSCs in HA hydrogels. (A and B) Mature glandular structures which were double-positive for CD44 and LAMP-1 (arrows) were seen in the HSG+DPSC co-transplantation group, but not in the HSG alone. (A) The cells in HSG transplants stained positive for CD44, but negative for LAMP-1, suggesting their immature state. (B, arrowheads) Differentiated HSG cells were observed at the interface with DPSCs which encapsulated the HSG tumor. (C-F) Encapsulating DPSCs which were positively stained for SMA (arrowheads) attempted to invade into the transplanted tissue and also recruited blood vessels. The blood vessels were recognized by SMA and vWF staining. (G) The bar graph shows the quantification of blood vessels as percentage per area in both HSG and HSG+DPSC transplants. The number of blood vessels in HSG+DPSC (82% ± 1.37) was significantly higher compared to that in HSG alone (33% ± 0.91). The number of blood vessels in both transplants were measures from 10 areas of three samples per transplant (n = 10). Student's t-test calculated * $p \leq 0.05$. Error bars represent ± Standard Error of the Mean (SEM). Scale bars indicate 100 μm.

CHAPTER 6

Angiogenic capacity of pericyte-like murine dental pulp stem cells

(Janebodin et al. 2013)

6.1 Introduction

Human and mouse dental pulp stem cells (DPSCs) have been isolated, characterized both *in vitro* and *in vivo*, and proposed for regenerating dental tissue for clinical application (Gronthos et al., 2000, Huang et al., 2006, Janebodin et al., 2011). Anatomically, DPSCs are shown to be located in a perivascular niche (Shi and Gronthos, 2003, Lovschall et al., 2007). Craniofacial pericytes and DPSCs originate from cephalic neural crest (Etchevers et al., 2001, Janebodin et al., 2011). In turn, the anatomical position and developmental origin of DPSCs suggest a role as pericytes. However, the capacity of DPSCs to function as pericytes is yet to be elucidated.

Pericytes are specialized mural cells located at the interface between capillaries and surrounding tissues where they play an active role in vascular maintenance and angiogenesis (Allt and Lawrenson, 2001). Angiogenesis, the formation of new vessels from existing vessels, is orchestrated by the interaction of pericytes and endothelial cells. Pericytes enhance angiogenesis by responding to physiological or angiogenic stimuli and guiding endothelial cells to form new vessels. Pericytes induce angiogenesis via cell-cell interaction or by secreting angiogenic factors (Gerhardt and Betsholtz, 2003). Certain diseases such as cancer, diabetic microangiopathy, and tissue fibrosis manifest pericyte dysfunction, consequently resulting in pathological angiogenesis (Robison et al., 1991, Xian et al., 2006, Lin et al., 2008).

Angiogenesis is important for successful tissue regeneration, repair, and healing. Without adequate blood supply, tissue regeneration cannot be accomplished and subsequently necrotic or scar tissues are formed (Madeddu, 2005). Therefore, stem/progenitor cells that can function as pericyte-like cells that promote angiogenesis are an attractive stem cell source for tissue regeneration.

Although DPSCs have been shown to locate adjacent to blood vessels, no study has yet directly shown that DPSCs function as pericytes (Shi and Gronthos, 2003, Feng et al., 2011). Recently, I have demonstrated significant microvessel formation in subcutaneously transplanted hydroxyapatite/tricalciumphosphate plugs containing murine DPSCs that closely associated with blood vessels, mimicking the endogenous pericyte location (Janebodin *et al.*, 2011). Moreover, the co-transplantation of human submandibular salivary gland cell line (HSG) with murine DPSCs demonstrated the enhancement of salivary gland differentiation with the increased number of vessels, compared to that of HSG alone, suggesting angiogenic inducing capacity of DPSCs (Janebodin and Reyes, 2012). This result urged me to examine the pericyte-like properties of DPSCs by determining angiogenic gene expression, *in vitro* and *in vivo* capacity to induce vessel formation. Furthermore, I demonstrate that the capacity of DPSCs to function as pericytes is VEGF-dependent.

6.2 Materials and Methods

6.2.1 Cell cultures

Wnt1-Cre/R26R-LacZ derived DPSCs, *LacZ*-labeled bone marrow stromal cells (BMSCs), and GFP-cardiac endothelial cells were derived from previous studies and cultured based on the protocols previously reported (Reyes et al., 2005, Ieronimakis et al., 2008,

Janebodin et al., 2011). The frozen cells were thawed and expanded in stem cell media at 37ºC under 5% O_2 and 5% CO_2. Human umbilical vein endothelial cell (HUVEC) line was cultured in endothelial cell media at 37ºC under 5% CO_2. DPSCs and BMSCs were cultured in stem cell media and treated with soluble Flt (sFlt) (Abcam); 2.5, 5, and 10 ng/ml for 4 days before cell proliferation and gene expression analysis.

6.2.2 Dental pulp explant isolation

All mouse experiments were performed in accordance with approved Institutional Animal Care and Use Committee (IACUC) guidelines, University of Washington. Pulp tissue were isolated from first lower molar teeth of 4 to 10-day-old neonatal *Tie2*-GFP (Jackson Laboratory, Bar Harbor, ME) (n = 10 teeth), and cultured as explants separately in stem cell media to observe migrating cells and determine the presence of endothelial cells by GFP expression as previously described (Janebodin *et al.*, 2011)**.**

6.2.3 *In vitro* vascular tube formation

HUVECs and DPSCs or BMSCs (5:1 ratio) were mixed with collagen (3mg/ml) and seeded on 48-well plates pre-treated with 1% polyethyleneimine and 0.1% glutaradehyde. Co-cultures of endothelial cells with DPSCs or BMSCs (1:1 ratio) were seeded at on 48-well plates pre-treated with pure growth factor-reduced matrigel.

Vascular tubes on collagen

Type I collagen was extracted from rat tails and prepared at the concentration of 8mg/ml in 0.1% acetic acid, which was further diluted and neutralized with buffer solution (1X Medium 199, 10X M199, and 1N NaOH) on ice. Endothelial cells and DPSCs or BMSCs were trypsinized from the culture flask, centrifuged and resuspended at 10^7cells/ml. Appropriate volume of concentrated cell suspension at above concentration was mixed into the neutralized

collagen solution to achieve the concentration of collagen at 3mg/ml, the density of HUVECs at 10^6 cells/ml, and that of DPSCs or BMSCs at $2x10^5$cells/ml, resulting the ratio of HUVECs to DPSCs or BMSCs at 5:1 ratio. To set up the tube formation assay, 48- well plates were first treated with 1% poly(ethyleneimine) (PEI) solution for 10 minutes followed by 0.1% glutaradehyde (GA) for 30 min to allow the boundary adherent to collagen and prevent cells from collapsing the gel. Following that, neutralized collagen solution mixed with cells was then placed into coated wells and allowed to polymerize at 37ºC at 5% CO_2 for 20 minutes. The polymerized gel with co-cultured cells were then cultured in a tube formation media, composed of endothelial growth media supplemented with 50ng/ml TPA, 40ng/ml VEGF, 40ng/ml bFGF, and 50μg/ml ascorbic acid, for 3 days before fixing and staining. Culture cells were re-fed with the above media every two days.

Vascular tubes on matrigel

The vascular tube formation was performed by co-culturing DPSCs or BMSCs with endothelial cells on matrigel. DPSCs and BMSCs were labeled with PKH26 red fluorescent membrane dye (Sigma, St. Louis, MO) according to manufacturer's protocol. 150 μl of pure growth factor reduced matrigel (BD Biosciences, Franklin Lakes, NJ) was coated on a 48-well plate and incubated 3 hours before usage. DPSCs, BMSCs, and endothelial cells were seeded at $2.6x10^4$cells/cm^2 and incubated at 37ºC, 5% CO_2 and 5% O_2. In the co-culture group, cells were mixed well by pipetting before seeding in endothelial cell media (Ieronimakis *et al.*, 2008). PKH26-labeled DPSCs or BMSCs or GFP-endothelial cells alone were also studied in parallel. Cells were fixed following 15 hours in culture and analyzed for vascular tube formation.

6.2.4 *In vivo* matrigel plugs

The modified matrigel (MG) plug assay from the previous study (Ieronimakis *et al.*, 2008) was performed to examine *in vivo* angiogenic potential of DPSCs and BMSCs by subcutaneous injection over tibialis anterior muscles. Transplants were conducted in three groups: 1) MG plugs alone with/without sFlt, 2) MG plugs with/without sFlt and DPSCs, 3) MG plugs with/without sFlt and BMSCs (n=3 in each group). 10^6 cells were resuspended in 35 µl 75% MG with 25% PBS were injected for groups 2 and 3. 50 ng/ml of sFlt was used. Prior to resuspension in MG, donor cells were labeled with PKH26. All mice were sacrificed at 14 days post injection. The MG plugs were gently removed for tissue processing and analysis.

6.2.5 RT-PCR and Q-RT-PCR analyses

DPSCs and BMSCs were extracted for total RNA by using the RNeasy Mini Kit (Qiagen) according to the manufacturer's protocol. Quantity and purity of RNA was determined by 260/280 nm absorbance. First-strand cDNA was synthesized from 1µg of RNA using the High Capacity cDNA synthesis kit using a randomized primer (Applied Biosystems) following the manufacturer's protocol. The primer sequences were shown in Table 6.1.

cDNA (20 ng) was diluted in a final volume of 20µl per reaction using the Immomix PCR Mastermix from Bioline. PCR was performed using the following thermal cycling conditions; 95°C 7 min for initial activation followed by 95°C/30s; 57°C/30s; 72°C/45s, for 35 cycles, with a final 5-min extension at 72°C. Mouse-specific primers are listed in Table 5.1. Glyceraldehyde-3-phosphate dehydrogenase (*GAPDH*) was utilized as control reference gene. RNA extracted from mouse skeletal muscle used as positive controls while negative controls lacked cDNA.

cDNA (20 ng) for Q-RT-PCR were prepared using the Maxima SYBR Green/Rox qPCR master mix from Fermentas Life Sciences. Reactions were processed by the ABI 7900HT PCR

system with the following parameters: 50°C/2 min and 95°C/10 min, followed by 40 cycles of 95°C/15 s and 60°C/1 min. Results were analyzed using SDS 2.2 software (Applied Biosystems). The threshold cycle (Ct) value for each gene was normalized to the Ct value of *GAPDH*. The relative mRNA expression presented as Relative Quantification; RQ value) was calculated by using the comparative C_t method by the formula; $2^{-\Delta\Delta Ct}$, where $\Delta Ct = Ct_{target} - Ct_{GAPDH}$ and $\Delta\Delta Ct = \Delta Ct_{target} - \Delta Ct_{calibrator}$. Each sample was run in triplicate reactions for each gene. Error bars represent the standard error of mean calculated from three independent experiments. cDNA of mouse endothelial cells were used to calibrate samples.

6.2.6 Histology and Immunofluorescence

Matrigel plugs were fixed with 4% formaldehyde in phosphate buffer saline (PBS) (HyClone, Logan, UT) at RT for 2 hours before washing 3 times with PBS. Fixed matrigel plugs then were sunk in a series of sucrose gradients in PBS beginning with 10% for 20 min, 20% for 20 min, and then left in 30% overnight at 4°C. Next day, processed tissues were embedded in optimal cutting temperature compound (Tissue-Tek® O.C.T., Sakura Finetek, Torrance, CA), frozen with liquid nitrogen cooled isopentane, and sectioned to 10 µm thickness. Cultured cells were fixed with 4% formaldehyde in PBS at RT for 10 min and then washed before staining.

Slides or fixed cells were washed and permeabilized with 0.1% Triton X-100/PBS. FITC-conjugated BS1-lectin (1:500, Sigma) was stained for 1 h at RT and washed three times. For immunostaining, slides or cells were blocked non-specific binding with 10% normal goat or horse serum for 1 h at RT. Slides or fixed cells were then incubated with primary antibodies (shown in Table 5.2) overnight at 4°C following three times of washing. Stained sections were subsequently incubated with goat-derived anti-rabbit, goat, mouse, or rat Alexa 488, 594, or 647-conjugated antibodies (1:800, Invitrogen) for 1 h at RT, following three times of washing.

Tissues and cells were also stained with 4´,6-Diamidino-2-phenylindole dihydrochloride (DAPI) to visualize the nuclei and examined by a Zeiss Axiovert 200 fluorescence microscope. (Thornwood, NY) Images were taken with an onboard monochrome AxioCam camera. Background was reduced using brightness and contrast adjustments, and color balance was performed to enhance colors. Control images were treated the same as experimental images. All modifications were applied to the whole image using Adobe Photoshop CS2 (San Jose, CA). Quantitation of fluorescence intensity was performed using ImageJ software (NIH, Bethesda, MD)

6.2.7 Western blotting

Proteins were collected from DPSCs exposed to VEGF alone or combined with sFlt at various concentration (1:2, 1;5 and 1:10; ng/ml VEGF: ng/ml sFlt). 10 minutes after VEGF and sFlt exposure, the cells were fixed and proteins were collected from separate wells for immunofluorescence and western blotting analysis, respectively. Proteins were collected in RIPA buffer containing protease/phosphatase inhibitors and EDTA (Thermoscientific). Proteins were quantified using the BCA Protein Assay Kit (Thermoscientific). Proteins (20 μg) were loaded per sample in precast 4-20% mini Tris-Glycine gels (nUView). Gels were semi-wet transferred to PVDF membranes. To confirm appropriate transfer membranes were stained with Ponceau Red and gels with Coomassie blue. Membranes were blocked with 5% BSA for 1 h, washed 3X with TBS-T and incubated with primary antibodies for 1 h or overnight. Then stained membranes were washed 3X with TBS-T and then incubated with 2^{nd} antibody conjugated with HRP (1:3000) for 1 h and washed 5X with TBS-T. Then exposed to SuperSignal West Pico Chemiluminescent Substrate for 5 min and developed in the dark room. To quantify the expression of phosphorylated VEGFR2 (pVEGFR2) and phosphorylated ERK1/2 (pERK1/2)

the pVEGFR2 and pERK1/2 antibodies were used. The phospho-specific VEGFR2 antibody detects the level of phosphorylation of VEGFR2 (Tyr-801) and the phospho-specific Erk1/2 detects the endogenous level of p44/42 MAP kinase (ERK1/2) (Thr202/Tyr204). The signal was normalized to smooth muscle actin (SMA) expression. The quantitation of band density was performed by ImageJ software and represented as relative density to untreated cells.

6.2.8 Statistical Analysis

Statistical analysis of the results from three independent experiments was performed using the Student's t-test or one-way ANOVA. Data is presented as mean ± SEM. *P* values ≤ 0.05 or ≤ 0.0001 were considered to be statistically significant.

6.3 Results

6.3.1 *Tie2*-GFP indicated that DPSC are not derived from endothelial origin

Ten days in culture, migrating mesenchymal-like cells were observed in *Tie2*-GFP pulp explants (Figs. 6.1A-C). GFP+ cells were visible in the explant core (Figs 6.1D, G), but migrating and passaged cells were GFP negative, suggesting an absence of endothelial cells in our culture (Figs. 6.1E, F, H, I). The cultured cells also expressed angiogenic-related genes, *Flt1* and *Flk1*, but not endothelial markers *CD31* and *Ve-cadherin* (*Ve-cad*) in late passage (Fig. 6.1J). Using the *Tie2*-GFP mice I confirmed the absence of endothelial cells in my DPSC cultures.

6.3.2 Clonal DPSC culture showed homogenous cell population

I have previously shown that DPSC clones derived from the *Wnt1-Cre/R26R-LacZ* mouse are 100% β-galactosidase+ (*Wnt1*-labeled) and can differentiate into mesenchymal and non-mesenchymal neural crest lineages (Janebodin *et al.*, 2011). These *Wnt1*-labeled DPSC clones

are homogenously positive for mesenchymal markers such as CD44 and pericyte markers such as smooth muscle actin (SMA) (Fig. 6.2).

6.3.3 DPSCs enhanced *in vitro* vascular tube formation in both endothelial cell line and primary endothelial cells

To examine if DPSCs can function as pericytes, *Wnt1*-labeled DPSCs were co-cultured with human umbilical vein endothelial cells (HUVEC) or primary endothelial cells isolated from hearts of mice that ubiquitously express GFP under the chicken β-actin promoter. Cells were mixed and seeded on collagen or MG to assay the DPSC capacity to enhance endothelial cells forming vascular tubes *in vitro*. BMSCs were used as a comparison. DPSCs and BMSCs labeled with β-galactosidase were positive for X-gal (Figs. 6.3.1A arrow, B). HUVEC formed better tube-like structures that stained positive for human CD31 in the co-culture with DPSCs, as compared to BMSCs (Figs. 6.3.1C, D). DPSCs stained positive for SMA and were located adjacent to the HUVEC (Fig. 6.3.1C).

I then co-culture murine DPSCs with murine GFP-cardiac endothelial cells. Prior to co-culture we labeled DPSCs with the red fluorescence dye, PKH26 (Horan and Slezak, 1989). The co-culture of PKH26+ DPSCs (Fig. 6.3.2E) with GFP-cardiac endothelial cells (Fig. 6.3.2F) also showed endothelial cells formed tube-like structures (Figs. 6.3.2G, H). Interestingly, DPSCs were located adjacent to endothelial cells suggesting they supported vascular tube stabilization and function as pericytes *in vitro* (Figs. 6.3.2G, H, insets and arrowheads).

6.3.4 Angiogenic gene expression in DPSCs and BMSCs before and after sFlt treatment

DPSCs and BMSCs expressed *Vegf* ligands and their receptors (Figs. 6.4.1A-H). DPSCs expressed significantly higher *Vegfd*, *EphrinB2*, and *Vegfr3* levels as compared to BMSCs. To

gain insights into VEGF signaling cues, I exposed DPSCs and BMSCs to VEGF inhibitor, sFlt (2.5, 5, and 10 ng/ml). sFlt-treated DPSCs showed a dose-dependent decrease in the expression of *Vegfa*, and its receptors (*Vegfr1* and *Vegfr2*), *EphrinB2,* and *Vegfr3*, but not in *Vegfc* and *Vegfd*, as compared to untreated cells (*$p < 0.05$) (Figs. 6.4.2I-K, M-P). Only the highest dose of sFlt (10 ng/ml) significantly decreased endogenous sFlt in treated DPSCs (Fig. 6.4.2L). Surprisingly, sFlt did not significantly affect these angiogenic genes in BMSCs. Despite a negative effect on these angiogenic genes in DPSCs, sFlt did not decrease their proliferation (Fig. 6.5).

6.3.5 DPSCs enhanced *in vivo* blood vessel formation better than BMSCs.I then studied the angiogenic potential of DPSCs and their function as pericytes *in vivo*.

I utilized the MG plug assay, by subcutaneous injections of DPSCs mixed with MG over tibialis anterior muscles. As before, BMSCs were compared in parallel. Following two-week MG plugs revealed the presence of both DPSCs and BMSCs labeled with PKH26 (Figs. 6.6A, G). Staining for BS1-lectin was used to highlight the vasculature of each plug. BS1-lectin is a tetrameric agglutinin isolated from *Bandeiraea simplicifolia*, which specifically binds to lectin receptors distributed on vascular endothelial cells (Alroy *et al.*, 1987). The number of BS1+ vessels with DPSCs was significantly greater than with BMSCs (Fig. 6.7). In contrast, MG plugs without cells, generated as a control contained few blood vessels. Further staining for more specific endothelial markers, CD31 and vWF, confirmed the increase of vessels in DPSC plugs as compared to BMSC plugs (Figs. 6.6C, E, I, K, O). Staining for LYVE1, a specific marker of lymphatic vessels, was negative in both BMSC and DPSC plugs, whereas host dermal tissue adjacent to the plugs contained positive LYVE1 vessels (data not shown) (Jackson *et al.*, 2001).

6.3.6 VEGF inhibition affected the angiogenic capacity of DPSCs *in vivo*

I then surveyed the effects of VEGF inhibition when incorporating sFlt in the DPSC and BMSC plugs. Without transplanted cells, MG plugs injected with sFlt showed decreased number of blood vessels positive for BS1 vs. MG plugs alone (Figs. 6.7E, F). Plugs containing sFlt and DPSC also showed a decrease in the number of vessels stained by BS1, CD31 and vWF compared to plugs of DPSC without sFlt (Figs. 6.6C-F, O, 5.7A, B, G). In contrast, no significant difference was observed in BMSC with and without sFlt (Figs. 6.6I-L, O, 6.7C, D, G). The decrease in vessels following sFlt treatment indicates DPSC-induced angiogenesis is VEGF-dependent.

6.3.7 sFlt inhibits VEGF-A binding to VEGFR2 and downstream ERK signaling

To study the mechanisms of sFlt inhibition in DPSCs, I exposed DPSCs to VEGF alone or combined with sFlt at various concentrations (1:2, 1;5 and 1:10; ng/ml VEGF: ng/ml sFlt). VEGFR1 has higher binding affinity to VEGF-A, but undergoes minimal autophosphorylation. The primary role of VEGFR1 is not signaling but functioning as a "decoy" receptor (Waltenberger et al., 1994). Thus, I focused on VEGFR2 signaling. By immunofluorescence staining of phosphorylated VEGFR2 we determined that DPSCs exposed to VEGF displayed phosphorylated VEGFR2 and its phosphorylation was inhibited in a dose dependent manner by sFlt (Fig. 6.8.1G). Using western blotting we confirmed that VEGFR2 phosphorylation induced downstream ERK phosphorylation in DPSCs. Accordingly, ERK phosphorylation was also inhibited by sFlt (Fig. 6.8.2J). Thus, sFlt inhibits VEGF-A binding to VEGFR2, resulting in decreased VEGFR2 signaling and decreased downstream ERK signaling in DPSCs.

6.3.8 sFlt decreased blood vessel formation by inhibiting EphrinB2 signaling.

EphrinB2 is secreted by pericytes, migratory neural crest, and DPSCs, and reported to control VEGF receptor (VEGFR2 and VEGFR3) internalization necessary for VEGF signaling (Kullander and Klein, 2002, Stokowski et al., 2007, Sawamiphak et al., 2010, Wang et al., 2010). In my studies sFlt treatment decreased EphrinB2 expression (Fig. 6.4.2M). In turn, decreased EphrinB2 levels may also decrease VEGF signaling in DPSCs which seems necessary for DPSC-induced angiogenesis. Thus, EphrinB2 staining was compared between DPSC and BMSC plugs with and without sFlt. As expected, EphrinB2 staining was significantly higher in DPSC-MG as compared to DPSC-MG+sFlt and BMSC-MG. However, I did not observe a significant difference in numbers of EphrinB2+ cells between BMSC plugs with and without sFlt (Fig. 6.9). Presence of PKH26+ cells between MG plugs suggests that my results are not influence by a significant difference in the number of DPSCs or BMSCs present in each plug (Figs. 6.6A, B, G, H, 6.10). Taken together, VEGF inhibition by sFlt reduces the potential of DPSCs to promote angiogenesis. My *in vitro* data suggests this occurs via inhibition of VEGFR2 signaling and resulting down-regulation of *Vegfa*, *Vegf receptors* and *EphrinB2* expression (Fig. 6.11).

6.4 Discussion

Previous studies have shown that DPSCs are anatomically localized at the pericyte position (Shi and Gronthos, 2003, Lovschall et al., 2005). *In vivo* transplantation of DPSCs demonstrated the induction of blood vessel formation (Janebodin et al., 2011, Janebodin and Reyes, 2012). However, the function of DPSCs as pericytes has not been previously resolved. Since pericytes have been reported to enhance angiogenesis, I examined the angiogenic potential of DPSCs.

Dental pulp tissue is highly vascularized; therefore I isolated DPSCs from the *Tie2*-GFP to exclude any direct contribution of endothelial cells (Motoike *et al.*, 2000) in DPSC cultures. Endothelial cells were not found in DPSC cultures. I showed that the human endothelial cell line, HUVEC, and primary murine endothelial cells generated vascular tubes when co-cultured with DPSCs. This result is consistent with former studies reporting that human DPSC and SMA-GFP+ murine DPSC enhanced vascularization and stability of tube-like structures generated by HUVEC (Dissanayaka et al., 2012, Zhao et al., 2012). Interestingly, I found that DPSC were located adjacent to tube-like structures, adopting the natural pericyte location. My findings show that mouse DPSC promoted endothelial cells to form a more mature vascular structures than mouse BMSCs.

The pericyte function of DPSCs was confirmed by *in vivo* MG plugs showing DPSC ability to induce vessel formation more efficiently than BMSCs. DPSCs express angiogenic factors such as *EphrinB2, Vegf ligands*, and *Vegf receptors* necessary for VEGF-induced angiogenesis. Although both DPSCs and BMSCs express *Vegf* ligands and receptors, DPSCs express higher levels of *Vegfd*, *EphrinB2*, and *Vegfr3* whereas BMSCs express higher level of endogenous *sFlt*, an inhibitor of angiogenesis. This gene profile may explain differences in the angiogenic potential between the two cell populations (Fig. 6.4.2M). VEGF-D, VEGFR3, and EphrinB2 are reported to be important for lymphangiogenesis (Ferrara et al., 2003, Wang et al., 2010). However, absence of vessels positive for LYVE1, a specific marker expressed in lymphatic vessels (Jackson *et al.*, 2001) in MG plugs indicates that DPSCs and BMSCs induce angiogenesis but not lymphangiogenesis in our model.

To gain insight into the mechanism of DPSC-induced angiogenesis I treated DPSCs with exogenous sFlt, an angiogenic inhibitor, which regulates VEGF function by competitive binding

with VEGF-A (Ahmad *et al.*, 2011). *In vitro* I observed significant declines in the expression of angiogenic factors in DPSCs but not BMSCs, treated with sFlt. Accordingly, I found a dramatic decrease in the number of blood vessels in DPSC plugs containing sFlt compared to DPSC plugs without sFlt. This correlation was not found in BMSC plugs. A previous study showed that sFlt controlled endothelial cell functions and angiogenesis (Ahmad *et al.*, 2011). However, my MG plugs did not only show sFlt affect endothelial cells but also pericyte-like DPSC function, resulting in less angiogenesis in both MG plugs with and without DPSCs combined with sFlt. In addition, EphrinB2+ cells were also reduced in DPSC plugs containing sFlt as compared to DPSC plugs without sFlt. I demonstrate that sFlt inhibits VEGF-A signaling via VEGFR2 and downstream ERK pathway (Wong and Jin, 2005). Therefore, my *in vitro* and *in vivo* studies indicate that the angiogenic capacity and pericyte-like functions of DPSCs are VEGF-A dependent. This may be due to low expression of sFlt by DPSCs which differs from BMSCs, resulting in increased sensitivity of DPSCs to sFlt (Fig. 6.11N). Interestingly, sFlt does not diminish DPSC number or survival *in vitro* and *in vivo*. Thus, the decrease in angiogenic factors' expression by DPSCs is a consequence of direct VEGF inhibition by sFlt.

6.5 Conclusion

I report that DPSC function as pericyte-like cells to induce angiogenesis is VEGF-dependent. This sheds light into the mechanisms of DPSC function as pericytes and angiogenic inducing cells which is an important aspect for the use of DPSCs in clinical applications. DPSCs are an accessible stem cell source with promising angiogenic potential for tissue regeneration. This cell can also be used as a model for studying neovascularization and angiogenesis in tissue regeneration.

Table 6.1. The mouse-specific primer sequences

RT-PCR primers			
Gene	**Forward primer (5'→3')**	**Reverse primer (5'→3')**	**GenBank Accession number**
GAPDH	CTCGTCCCGTAGACAAAATGG	CGCTCCTGGAAGATGGTG	NM_008084
CD31	GGACTCACGCTGGTGCTCTAT	TTGGATACGCCATGCACCTT	NM_008816
Vegfr1 (Flt1)	GGTGAAGATTTGCGACTTTGG	CCGCATGCCTTCCTTCAG	NM_010228
Vegfr2 (Flk1)	AAAGACAACGAGACCCTGGTAGAA	CAATGACAAGAAGGAGCCAGAA	NM_010612
Tie1	TGTTCGTGGCCTCAATGCTA	TCGGATACACACCAAGGCTAA A	NM_011587
Ve-cad	CCAGCCCTACGAACCTAAAGTG	CACCCCGTTGTCTGAGATGA	NM_009868

Q-RT-PCR primers			
Gene	**Forward primer (5'→3')**	**Reverse primer (5'→3')**	**GenBank Accession number**
GAPDH	GGGAAGCCCATCACCATCT	GCCTCACCCCATTTGATGTT	NM_008084
EphrinB2	GGAGGACACGGTAGGCTATGG	CCTGGTGCGCAACCTTCT	NM_010111
sFlt	CAGTTGTCTCTTATCATCTCAGTT TATTGTT	TTTGGGAGGAGCGTTTCCT	NM_010228
Vegfa	GAGCAGAAGTCCCATGAAGTGAT	CAATCGGACGGCAGTAGCTT	NM_001025250
Vegfc	GATTCTCTGCCCCGCTTTG	GGAGGATGCTGTGTTGCTACAA	NM_009506
Vegfd	TGCGGCAACTTTCTATGACACT	ACTGGCGACTTCTACGCATGT	NM_010216
Vegfr1 (Flt1)	CGGAGCCATTCCCACAAC	TTGTCTCGGCTCTCCACATTG	NM_010228
Vegfr2 (Flk1)	ACTGCAGTGATTGCCATGTTCT	CCTTCATTGGCCCGCTTAA	NM_010612
Vegfr3	ATCGGCAACCATCTCAACGT	GCTTTGGCGCCTTCTACCA	NM_008029

Table 6.2. Lists of antibodies

Marker	Antibody	Species	Application / Dilution	Company
BS1-lectin-FITC			IHC, 1:500, 1h, RT	Sigma
CD31	Monoclonal	Rat	ICC, 1:100, overnight, 4ºC IHC, 1:100, overnight, 4ºC	eBioscience
vWF	Polyclonal	Rabbit	IHC, 1:100, overnight, 4ºC	Dako
EphrinB2	Polyclonal	Goat	IHC, 1:200, overnight, 4ºC	Abcam
CD44-PE	Monoclonal	Rat	ICC, 1:100, overnight, 4ºC	eBioscience
SMA	Monoclonal	Mouse	ICC, 1:400, overnight, 4ºC WB, 1:1000, overnight, 4ºC	Sigma
pVEGFR2	Polyclonal	Rabbit	ICC, 1:100, overnight, 4ºC WB, 1:1000, overnight, 4ºC	ECM Bioscience
pERK1/2	Polyclonal	Rabbit	WB, 1:2500, 1h, RT	Cell Signaling

IHC = Immunohistochemistry, ICC = Immunocytochemistry, WB = Western blotting

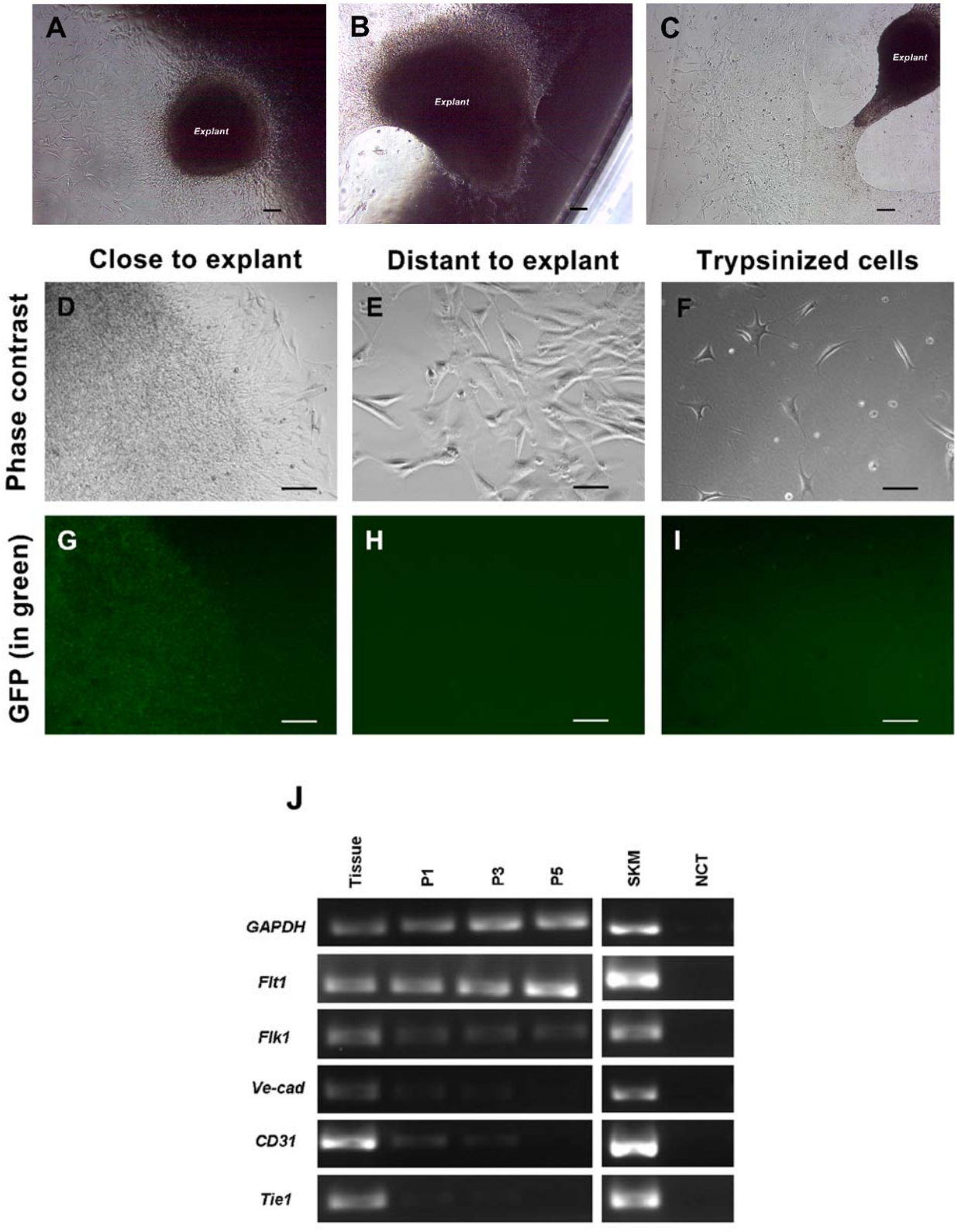
A
Explant
B
Explant
C
Explant
Close to explant
Distant to explant
Trypsinized cells
Phase contrast
D
E
F
GFP (in green)
G
H
I
J
Tissue
P1
P3
P5
SKM
NCT
GAPDH
Flt1
Flk1
Ve-cad
CD31
Tie1

Figure 6.1 *Tie2*-GFP indicated that DPSC are not derived from endothelial origin. A-C, Three representative dental pulp explants were cultured in stem cell media. The explant-derived cells gradually migrated and many were spindle-like, indicating a mesenchymal phenotype. D-I, The GFP expression was monitored in cells close and distant to explants, as well as passaged cells to determine the presence of endothelial cells in our culture. (D, G) GFP-expressing cells were found in the dental explant core. (E, F, H, I) Migrating and passaged cells were negative for GFP, indicating the absence of endothelial cells in our culture condition. (J) RT-PCR showed expression of angiogenic-related genes, *Flt1* and *Flk1*, but not endothelial-specific genes, *CD31* and *Ve-cad*, in late passage cultured cells. Tissue=dental pulp explant tissue, P1, P3, P5 = cultured dental pulp stem cells in passage 1, 3, and 5, respectively, SKM = skeletal muscle used as positive control, NCT = negative control (no template). Scale bars = 100 μm.

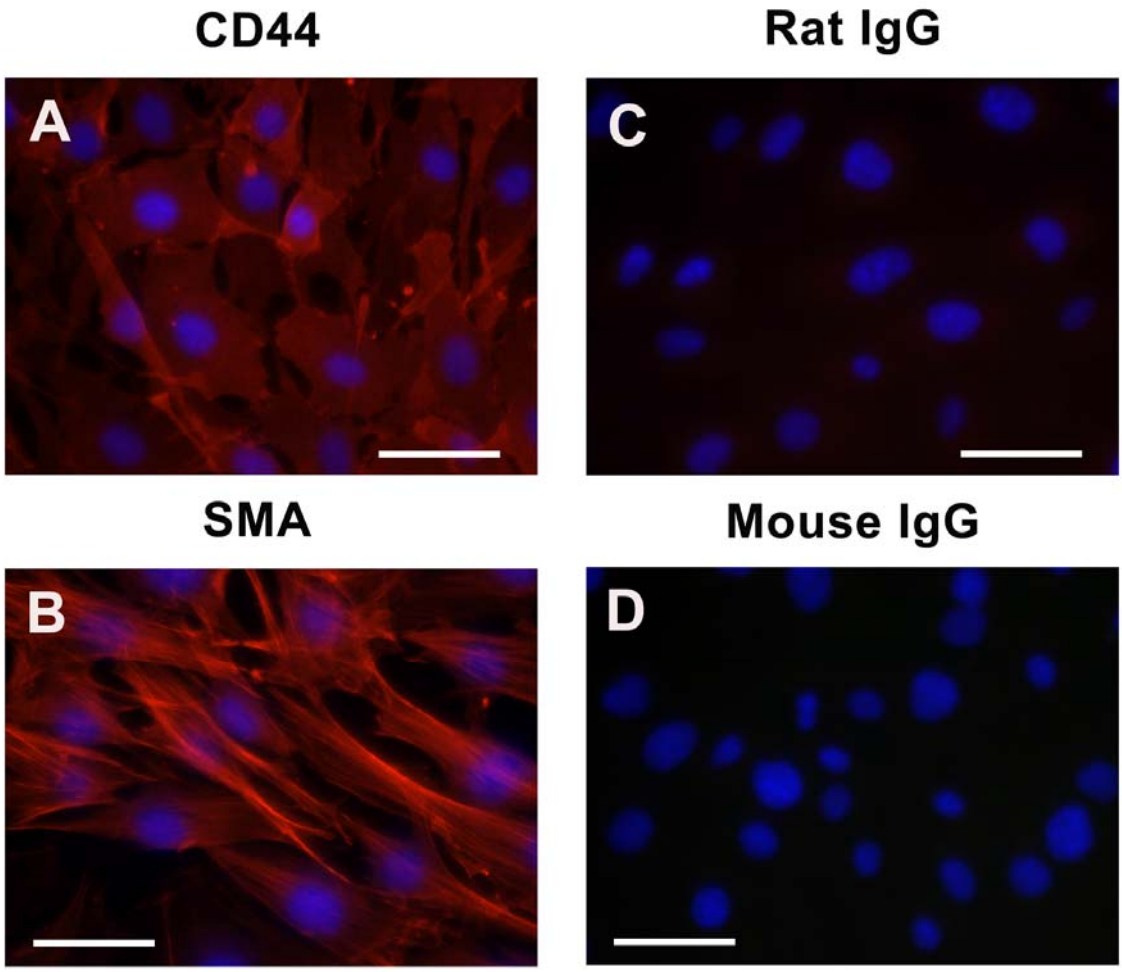

Figure 6.2 Clonal DPSC cultures. DPSC clones in our culture condition are homogenously positive for the mesenchymal marker CD44 (n = 3, n; number of clones) (A) and the pericyte marker smooth muscle actin (SMA) (n = 3, n; number of clones) (B). (C and D) IgG Isotypes were used as negative controls to demonstrate the specificity of primary antibodies. Scale bars = 50 μm.

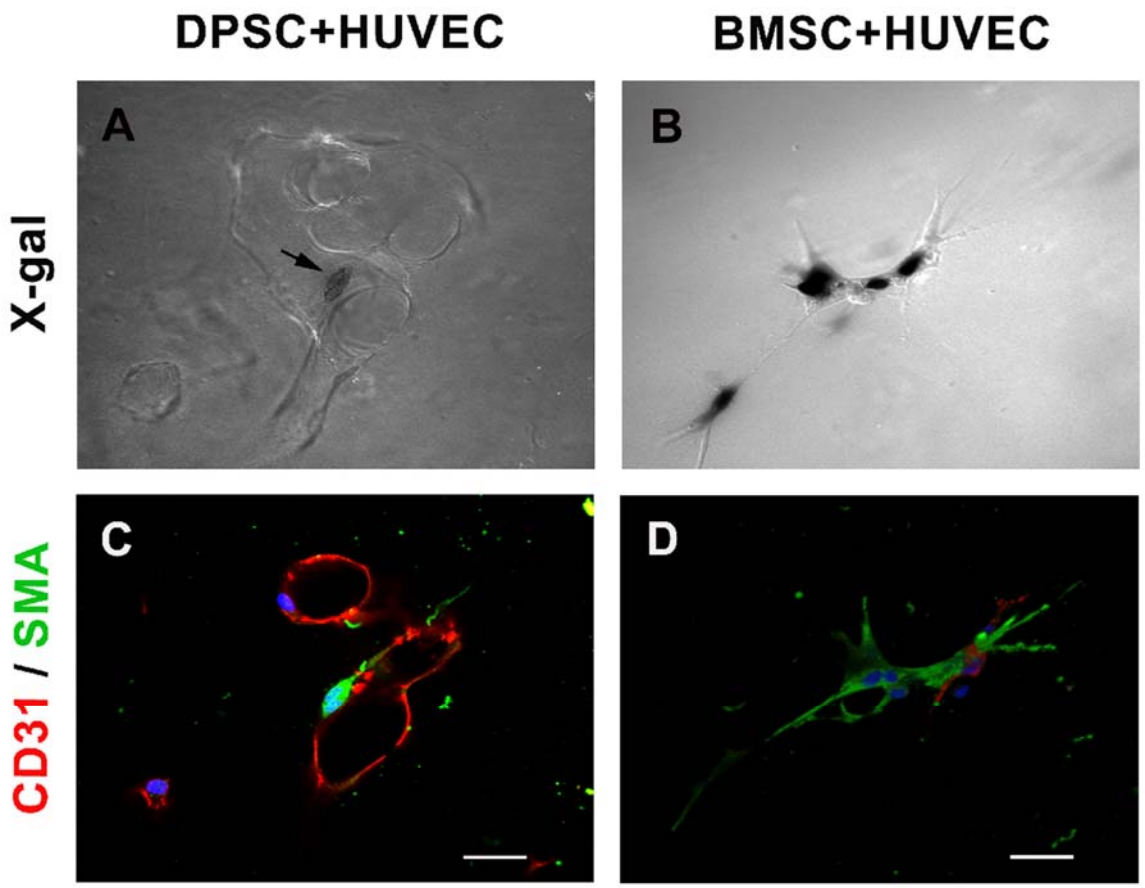

Figure 6.3.1 DPSCs enhanced HUVEC-derived vascular tube formation and were adjacent to endothelial cells, adopting a pericyte position. A-D, *LacZ*-labeled DPSCs and BMSCs were co-cultured with HUVEC on collagen to observe the capacity of endothelial cells forming tube-like structures. (A,B) DPSCs (arrow) and BMSCs were labeled with β-galactosidase shown by positive X-gal staining. (C, D) HUVEC formed tube-like structures stained positive for CD31 in red. (C) DPSCs stained SMA+ in green and were located adjacent to the endothelial cell line, indicating the pericyte location. (D) Fewer mature HUVEC vessels were seen adjacent to SMA+ BMSCs. Scale bars = 100 μm.

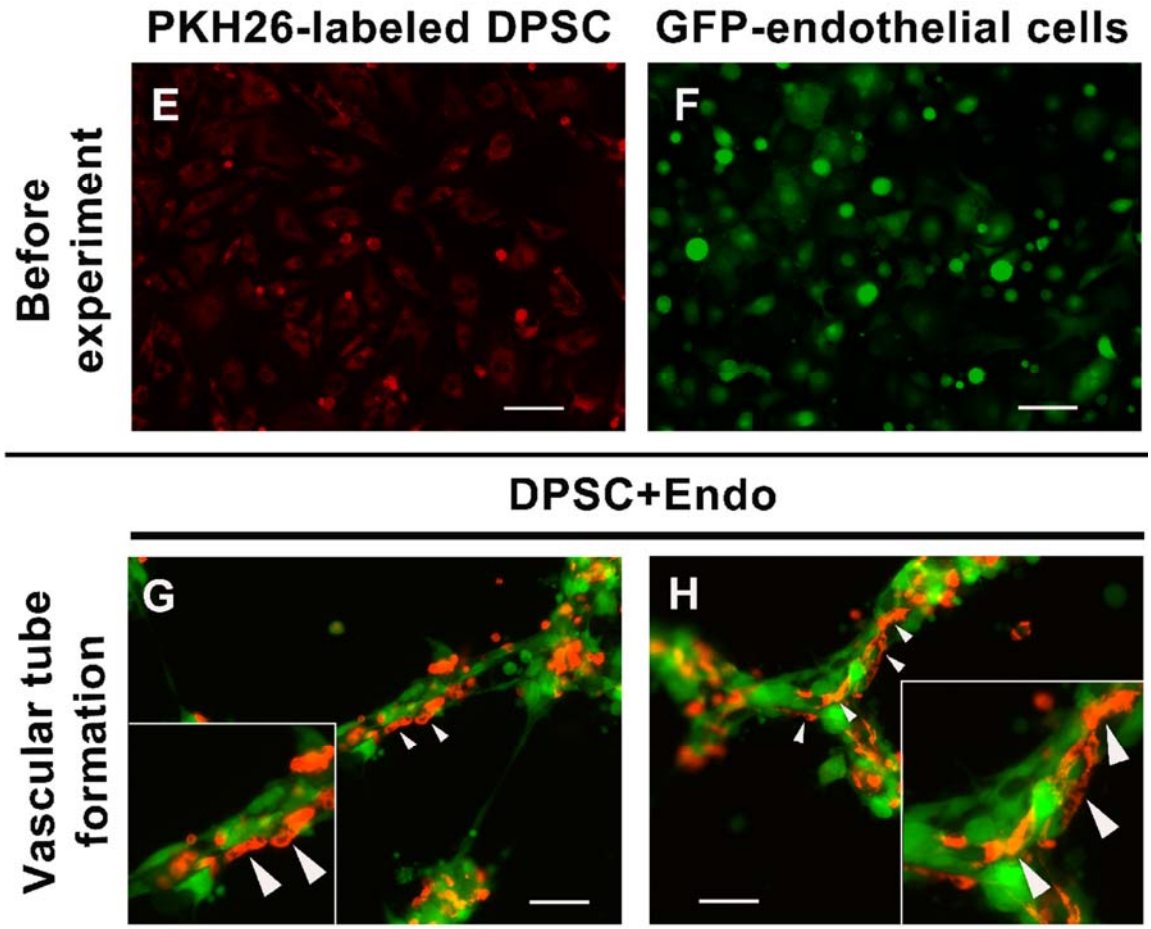

Figure 6.3.2 DPSCs enhanced vascular tube formation and were adjacent to GFP cardiac endothelial cells, mimicking a pericyte position. E-H, PKH26-labeled DPSCs were co-cultured with GFP-cardiac endothelial cells on matrigel. (E) DPSCs were labeled with PKH26 in red before co-culturing. (F) Primary cardiac endothelial cells expressed GFP in green. (G, H) Vascular tube-like structures were observed in the co-culture of DPSCs and endothelial cells after 15 hours. (G, H) DPSCs were located adjacent to endothelial cells and stabilized tube-like structures (insets and arrowheads). Scale bars = 100 μm.

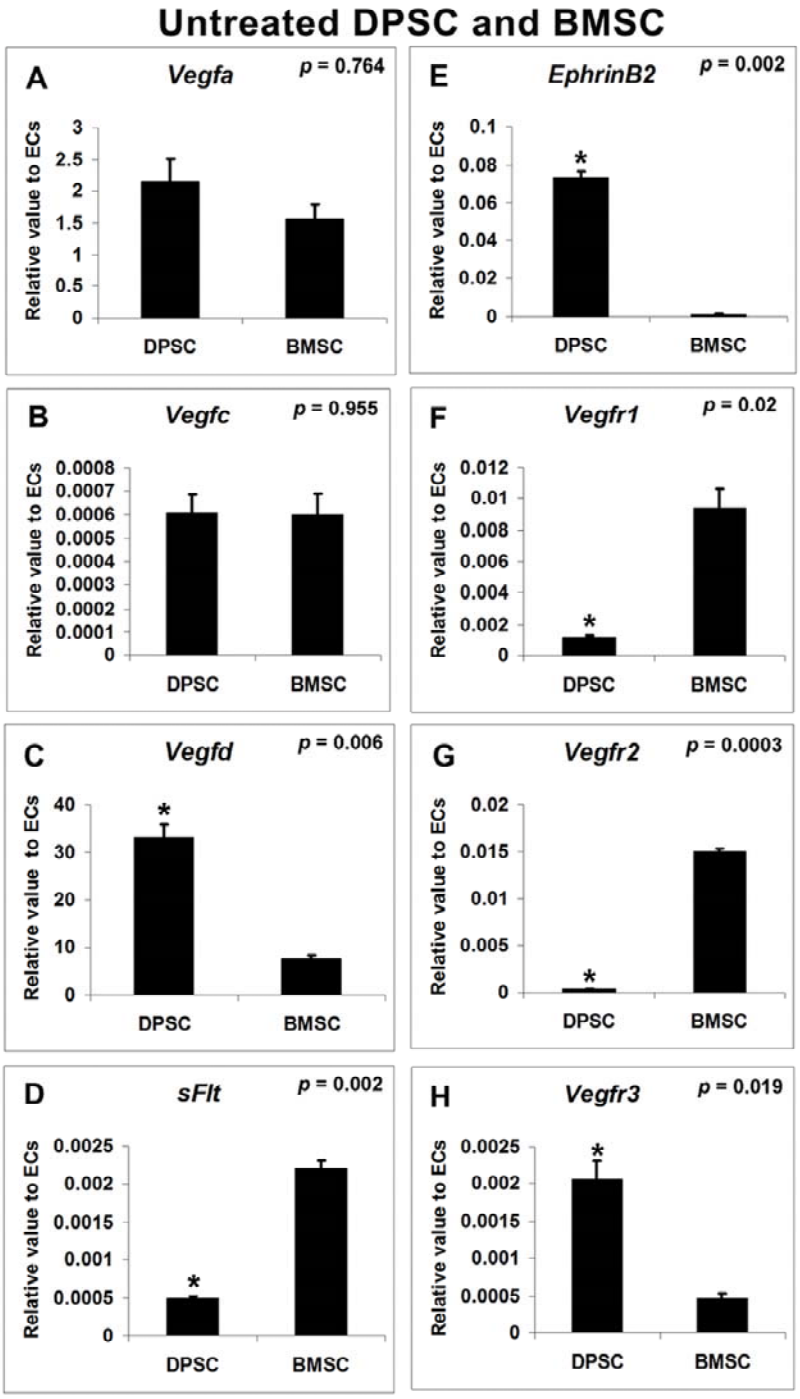

Figure 6.4.1 Angiogenic gene expression in DPSCs and BMSCs before sFlt treatment. A-H, Angiogenic genes were expressed by untreated DPSCs and BMSCs. Relative expression was relative to the expression of mouse endothelial cells (ECs) from skeletal muscles. *GAPDH* was used as the reference gene. Values were represented as mean ± Standard Error of the Mean (SEM) from three independent experiments (n = 3). (A-H) Student's t-test was analyzed to compare between untreated DPSCs and BMSCs, $*p \leq 0.05$ by Student's t-test.

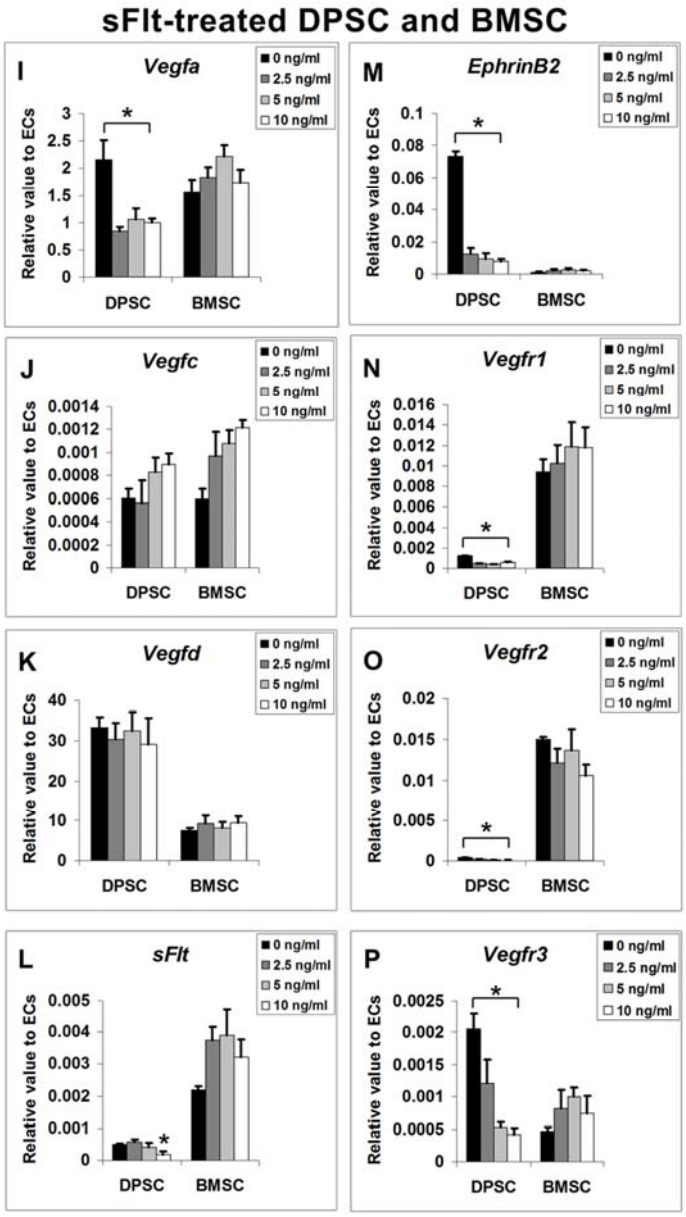

Figure 6.4.2 Angiogenic gene expression in DPSCs and BMSCs after sFlt treatment. I-P, *Vegfa, EphrinB2,* and *Vegf receptors* were down-regulated in DPSCs treated with sFlt at various concentrations (2.5, 5, and 10 ng/ml), but not in treated BMSCs. Relative expression was relative to the expression of mouse endothelial cells (ECs) from skeletal muscles. *GAPDH* was used as the reference gene. Values were represented as mean ± Standard Error of the Mean (SEM) from three independent experiments (n = 3). (I-P) One-way ANOVA was analyzed to compare differences between DPSCs and BMSCs treated with various concentrations of sFlt, $*p \leq 0.05$. *sFlt* was down-regulated only in DPSCs treated with 10ng/ml of sFlt, $*p \leq 0.05$ by Student's t-test.

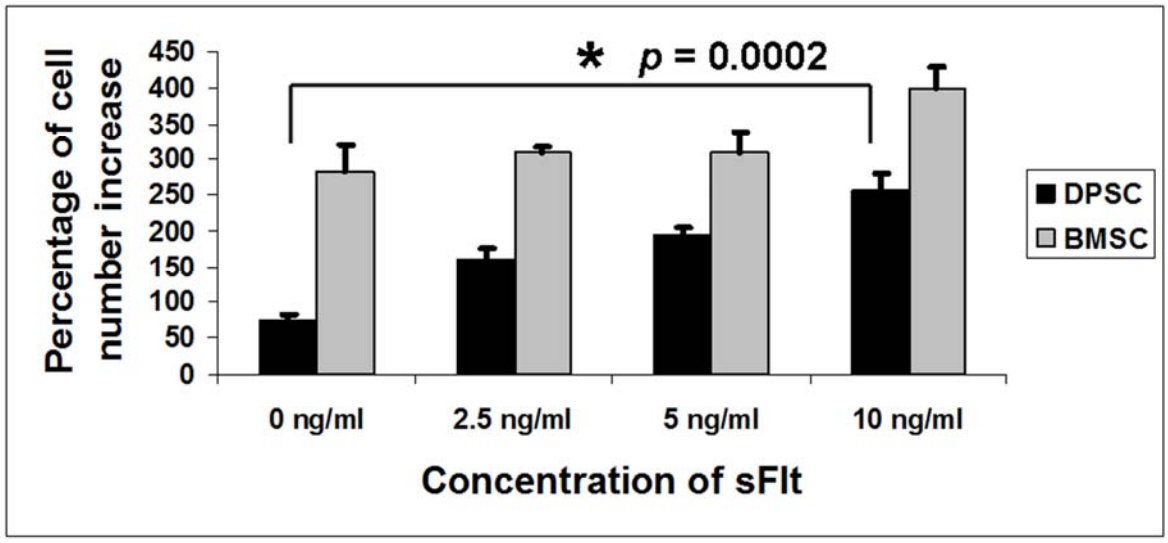

Figure 6.5 sFlt did not affect cell proliferation of DPSCs and BMSCs. The cell number of both DPSCs (black bars; n = 3) and BMSCs (gray bars; n = 3) was compared before and after sFlt treatment for 4 days at different concentrations (2.5, 5, and 10ng/ml). The cell number was calculated by the following formula; percentage of cell number increase = (Cell increased $_{d4}$ / Cell initial $_{d0}$) x 100. After 4 days, sFlt-treated DPSCs significantly increased cell number in dose-dependent manner (*$p \leq 0.001$) whereas sFlt-treated BMSC showed no significant increase in cell number. Values were represented as mean±SEM from three independent experiments. One-way ANOVA was analyzed to compare differences among treated-DPSC and treated-BMSC with various concentrations of sFlt.

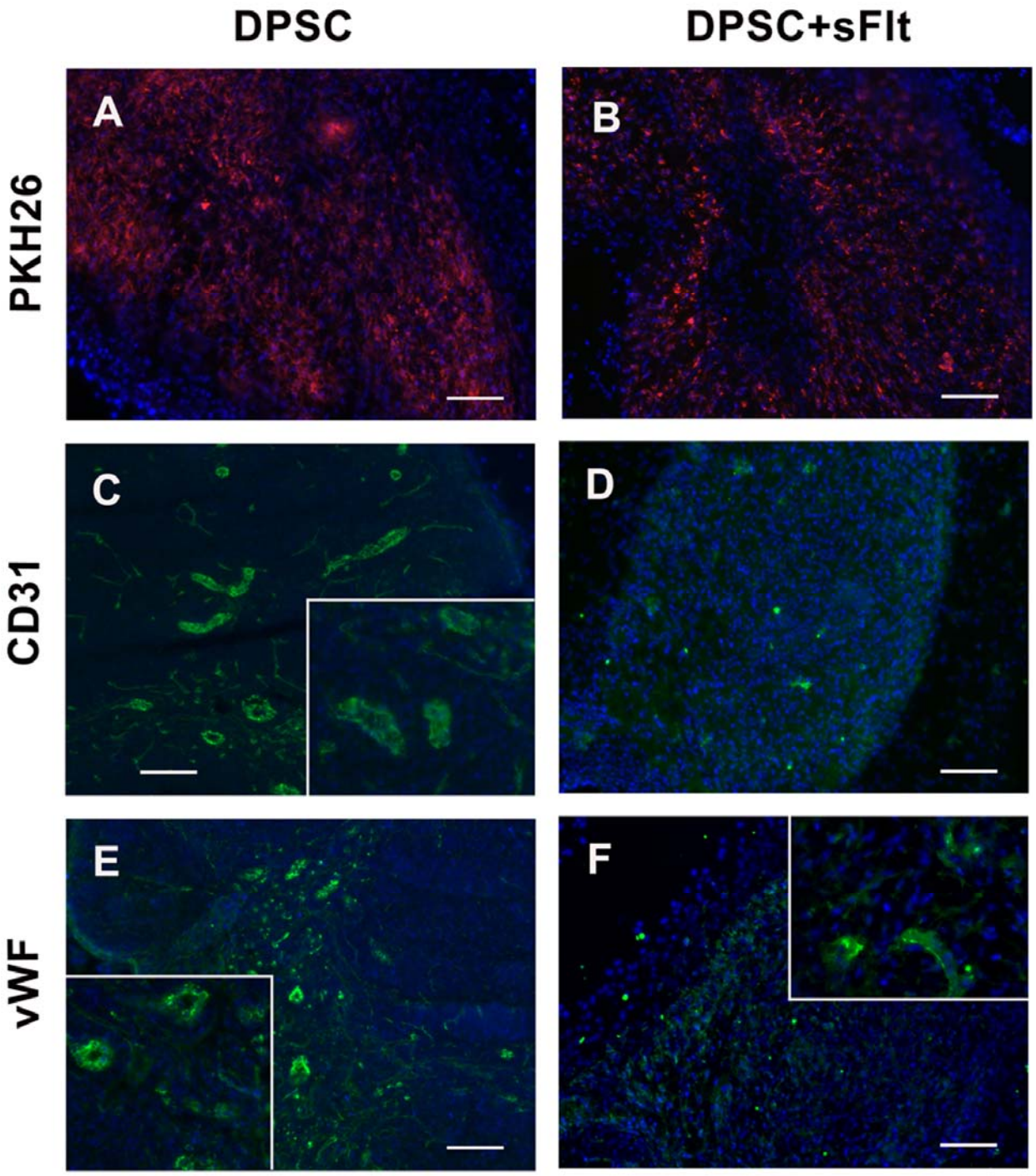
DPSC
DPSC+sFlt
PKH26
CD31
vWF
A
B
C
D
E
F

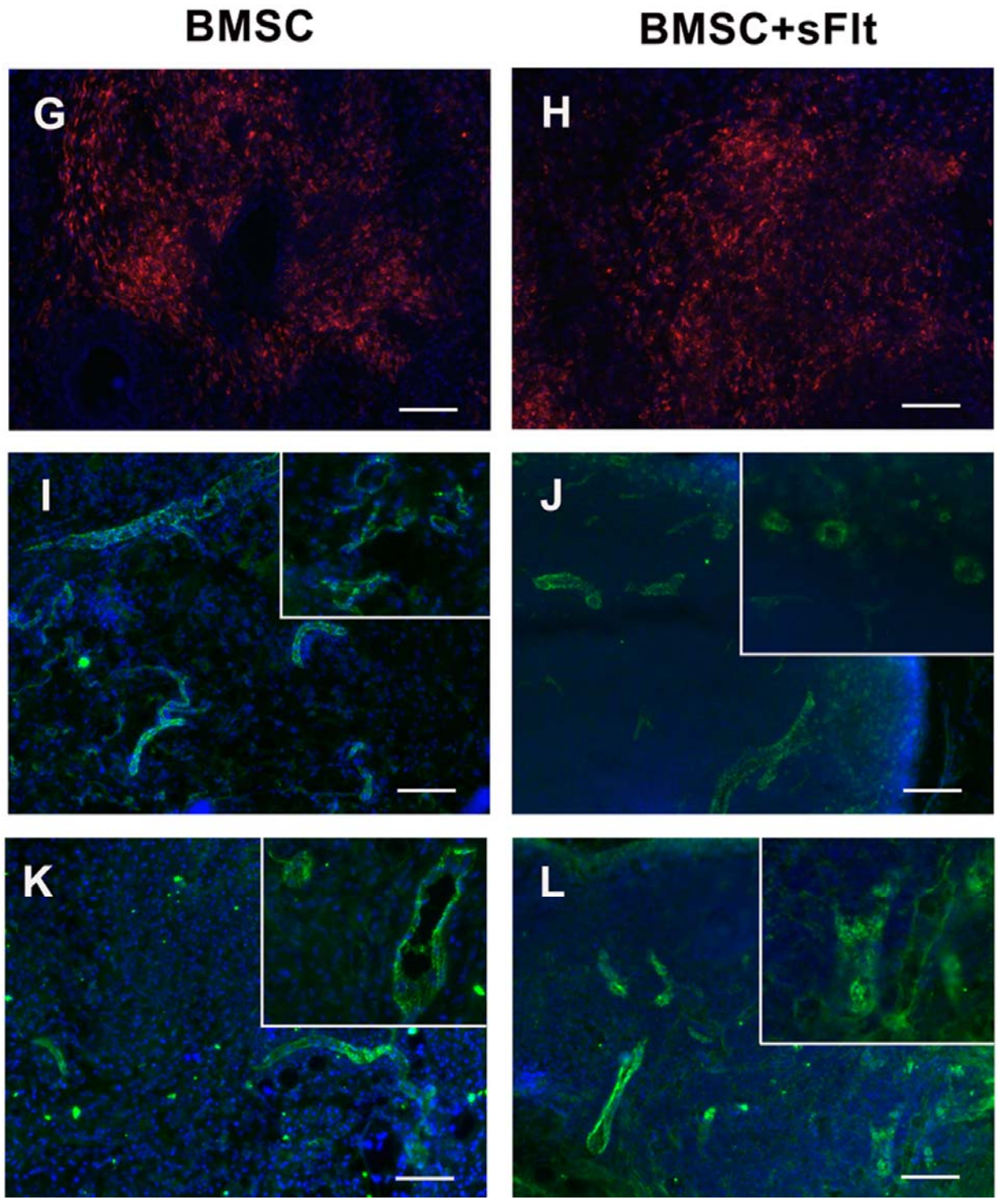
BMSC
BMSC+sFlt
G
H
I
J
K
L

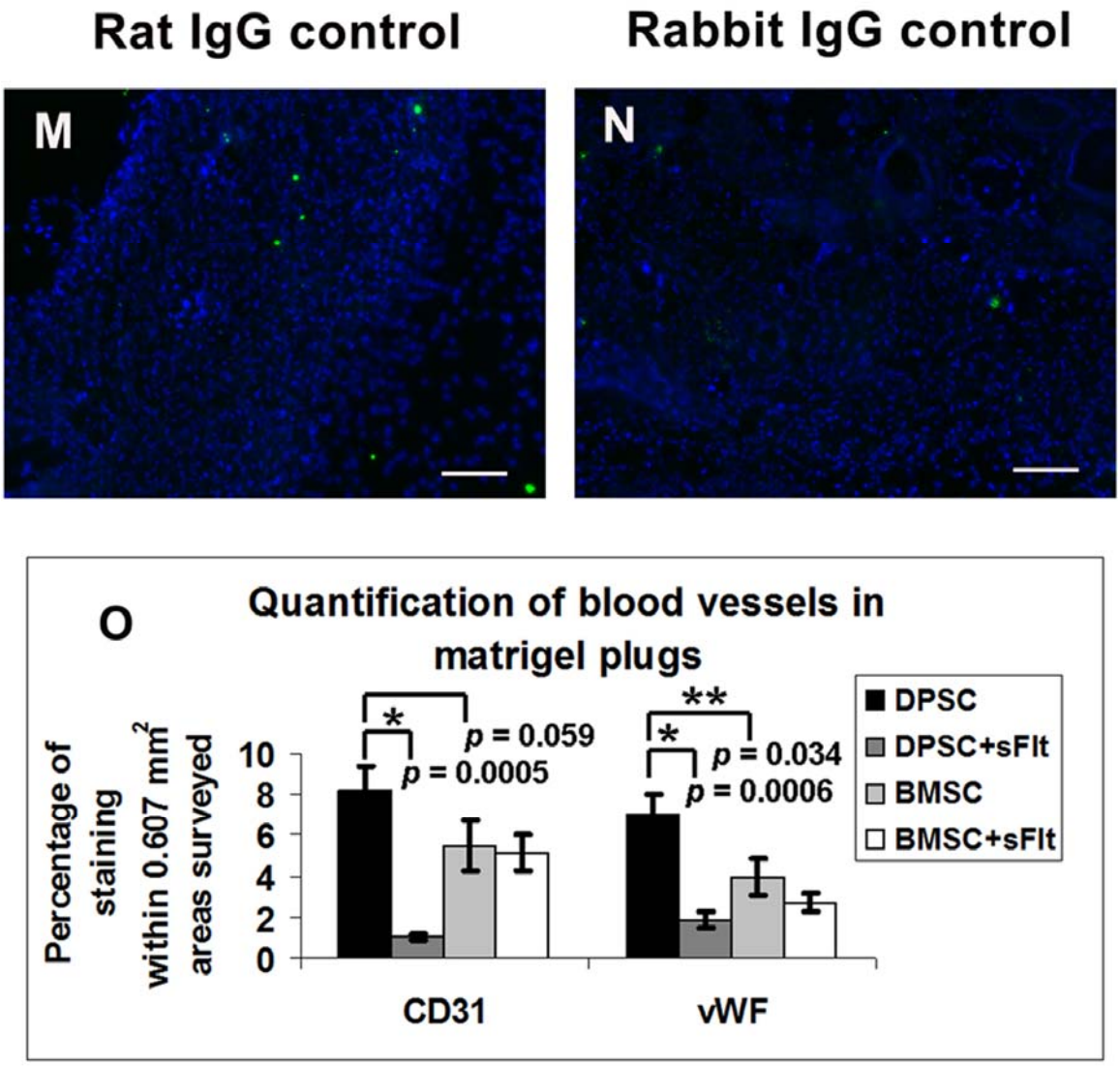

Figure 6.6 DPSCs enhanced blood vessel formation better than BMSCs *in vivo.* A-F, DPSC matrigel plugs without and with sFlt (50 ng/ml) were observed. (A, B) Strong PKH26 in red indicated that transplanted DPSCs survived and were located in the matrigel plugs even in the plugs treated with sFlt. (C-F) CD31 and vWF (in pseudo colored green) stained blood vessels which were more numerous in DPSC plugs without sFlt, compared to plugs with sFlt. G-L, BMSC matrigel plugs without and with sFlt (50ng/ml) were compared to DPSC matrigel plugs. (G, H) PKH26 labeled transplanted cells in BMSC plugs alone or with sFlt. (I-L) No difference in the induction of blood vessels stained positive for CD31 and vWF (in pseudo colored green) was found in between BMSC plugs without and with sFlt. The insets exhibited higher magnification of blood vessels in the plugs. M and N, IgG isotype staining was used as a negative control. O, The positive area of CD31 and vWF staining blood vessels in all matrigel plugs were quantified by ImageJ software and represented as percentage of staining within 0.607 mm^2 areas surveyed. DPSC matrigels (n = 14, n; numbers of measured area) showed the highest positive area of CD31 and vWF, representing the highest amount of blood vessels among all

plugs. DPSC matrigel plugs containing sFlt, DPSC+sFlt (n = 7), displayed a dramatic decrease in the number of vessels. The number of vessels as assessed by percent of positive staining in BMSC plugs was less than that in DPSC plugs, indicating BMSCs were less angiogenic. No significant difference was found in the number of vessels (positive area staining) between BMSCs alone (n = 11) and BMSCs with sFlt (n=9). Values were represented as mean±SEM from three independent experiments. Student's t-test calculated $*p \leq 0.05$ and $**p \leq 0.0001$. Scale bars = 100 μm.

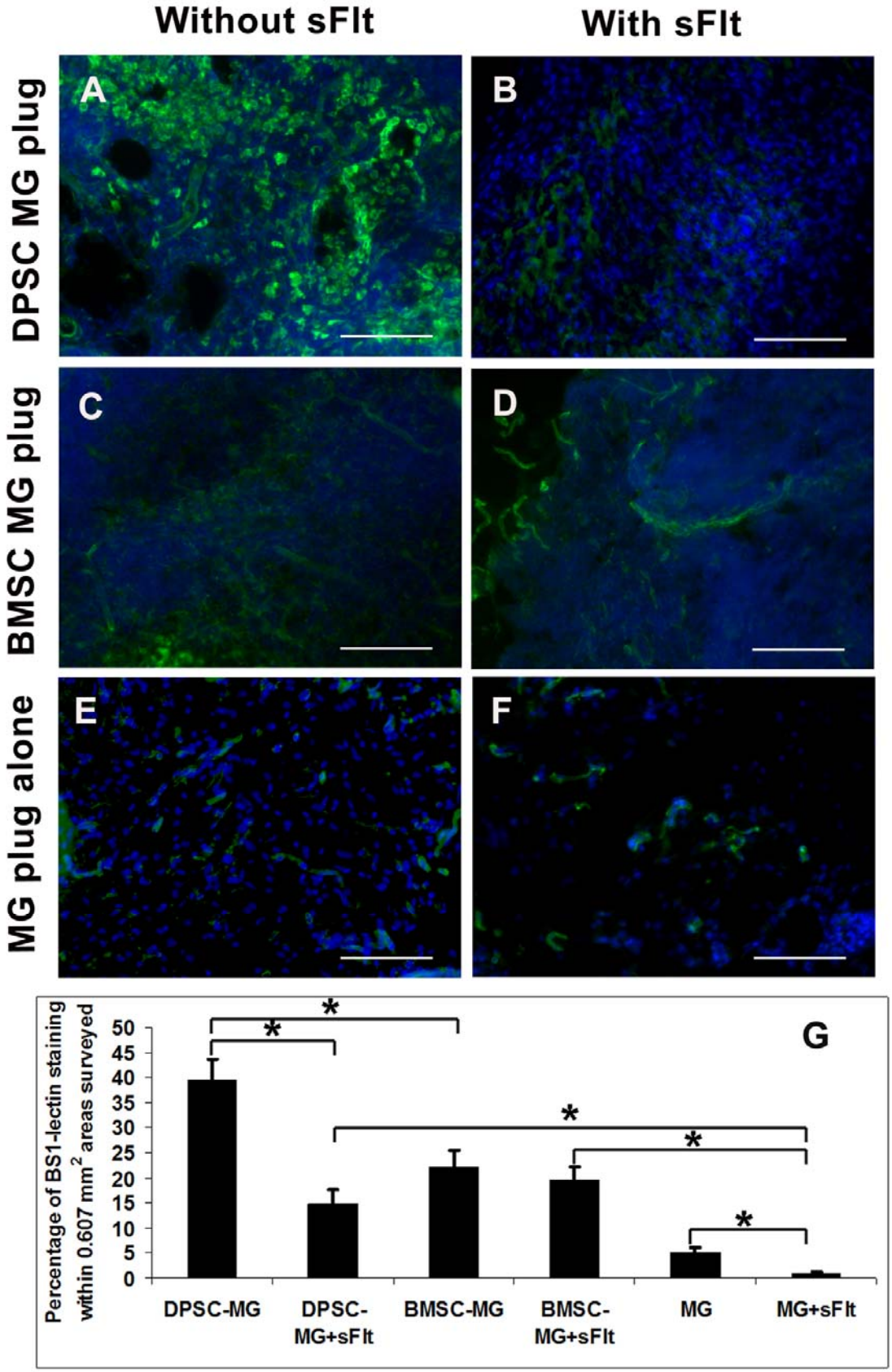
Without sFlt
With sFlt
DPSC MG plug
BMSC MG plug
MG plug alone
A
B
C
D
E
F
G
Percentage of BS1-lectin staining within 0.607 mm2 areas surveyed
50
45
40
35
30
25
20
15
10
5
0
*
*
*
*
*
DPSC-MG
DPSC-MG+sFlt
BMSC-MG
BMSC-MG+sFlt
MG
MG+sFlt

Figure 6.7 *In vivo* 2-week DPSC and BMSC matrigel (MG) plugs with and without sFlt demonstrated differences in the number of blood vessel formation. A-F, FITC-conjugated BS1-lectin (in green) located blood vessel formation in MG plugs. (A, B) DPSC plugs alone induced formation of abundant blood vessels whereas DPSC plugs combined with sFlt (50ng/ml) significantly decreased blood vessel induction. (C) BMSCs were also able to induce vessel formation but less than that in DPSC plugs. (D) No difference in vessel induction in BMSC plugs after sFlt treatment. (E) The MG plugs alone without cells generated as a control showed the induction of small blood vessels. (F) Lesser blood vessel formation was found in MG plugs alone with sFlt. (G) The area of positive BS1-lectin staining in all MG plugs without and with sFlt was quantitated by ImageJ software and represented as percentage within 0.607 mm^2 areas surveyed (n=10; n; numbers of measured area). A significant decrease in blood vessel formation was found in DPSC-MG+sFlt and BMSC-MG compared to DPSC-MG, but no significant difference in blood vessel formation was found between BMSC plugs with and without sFlt. MG plugs alone induced more blood vessels compared to MG+sFlt, but significant less amount of blood vessels compared to that in DPSC-MG and BMSC-MG. Compared to MG+sFlt, significantly more blood vessels were found in both DPSC-MG+sFlt and BMSC-MG+sFlt. Values were represented as mean ± SEM from three independent experiments. Student's t-test calculated $*p \leq 0.05$. Scale bars = 100μm. DPSC-MG = DPSC alone; DPSC-MG+sFlt = DPSC treated with sFlt; BMSC-MG = BMSC alone; BMSC-MG+sFlt = BMSC treated with sFlt; MG = matrigel alone without cells; MG+sFlt = matrigel alone without cells but treated with sFlt.

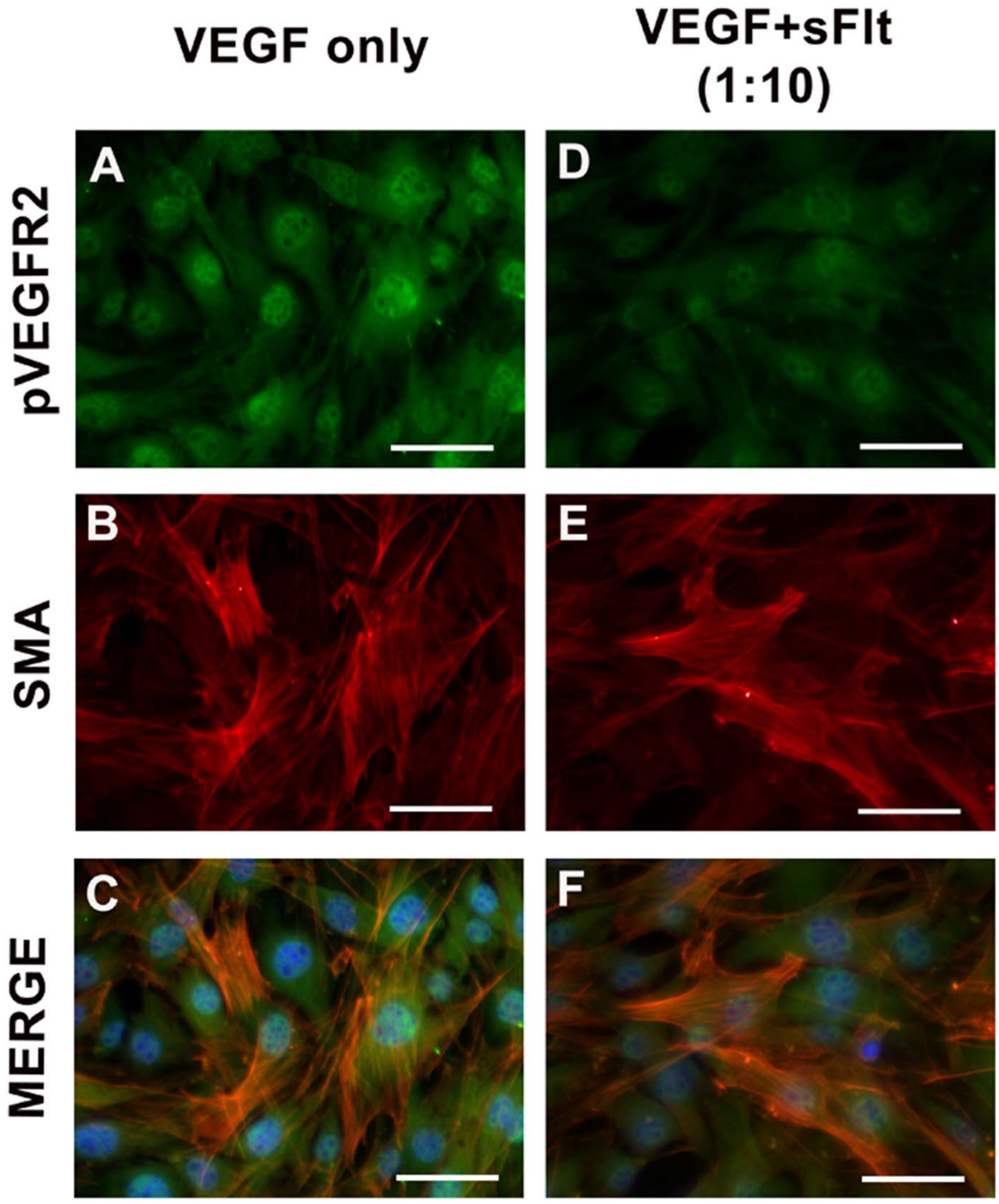
VEGF only
VEGF+sFlt
(1:10)
pVEGFR2
SMA
MERGE
A
B
C
D
E
F

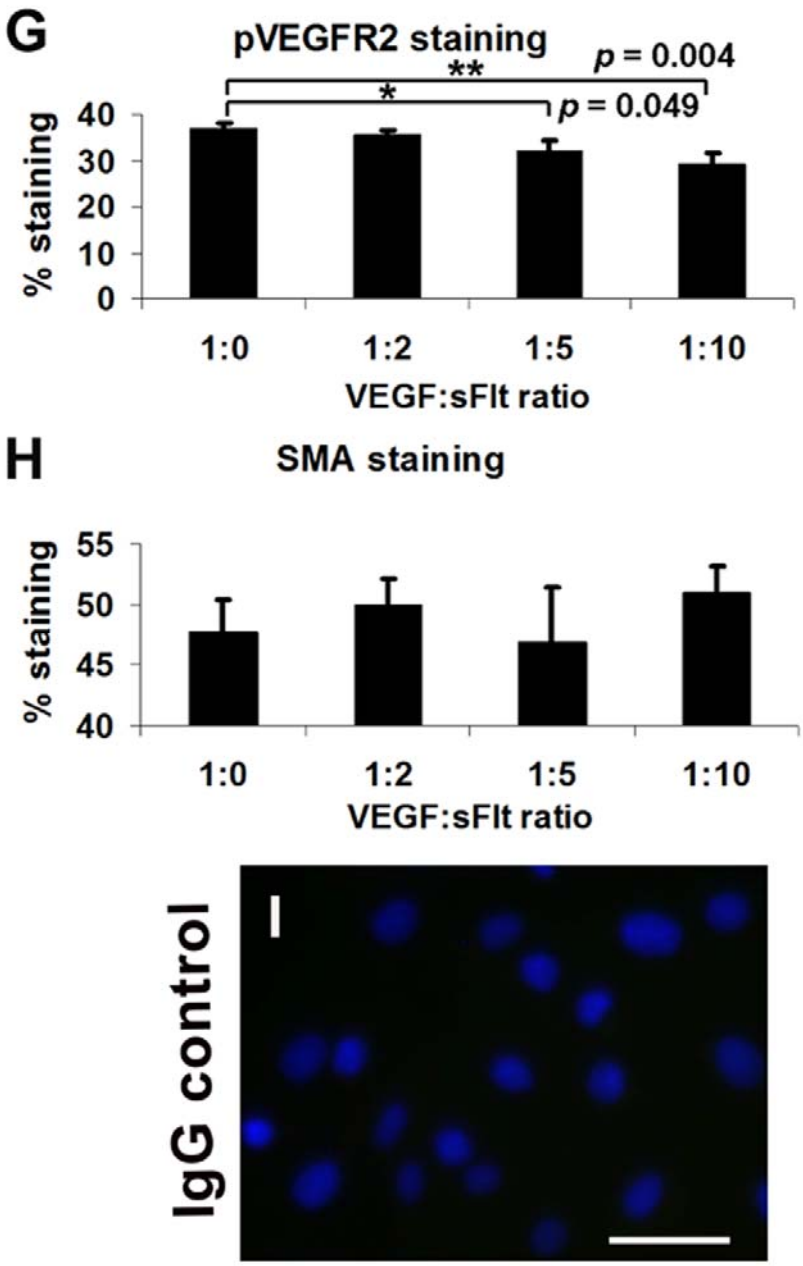

Figure 6.8.1 sFlt inhibits VEGF-A binding to VEGFR2 and decreases phosphorylated VEGFR2. DPSCs were exposed to VEGF alone or various combinations of VEGF and sFlt (1:2, 1:5 or 1:10; VEGF ng/ml to sFlt ng/ml) for 10 min and analyzed by immunofluorescence (A-I) or western blotting (J-L). Immunofluorescence staining using an antibody specific for phosphorylated VEGFR2 showed decreased phosphorylated VEGFR2 staining in DPSCs exposed to VEGF+sFlt as compared to VEGF only. J. Quantification of the percent of positive staining (within 0.035 mm^2 of area surveyed) showed significantly reduced staining of phosphorylated VEGFR2 in cells exposed to VEGF:sFlt at 1:5 or 1:10 concentrations. H, In contrast, SMA staining was consistent in all the treatments.

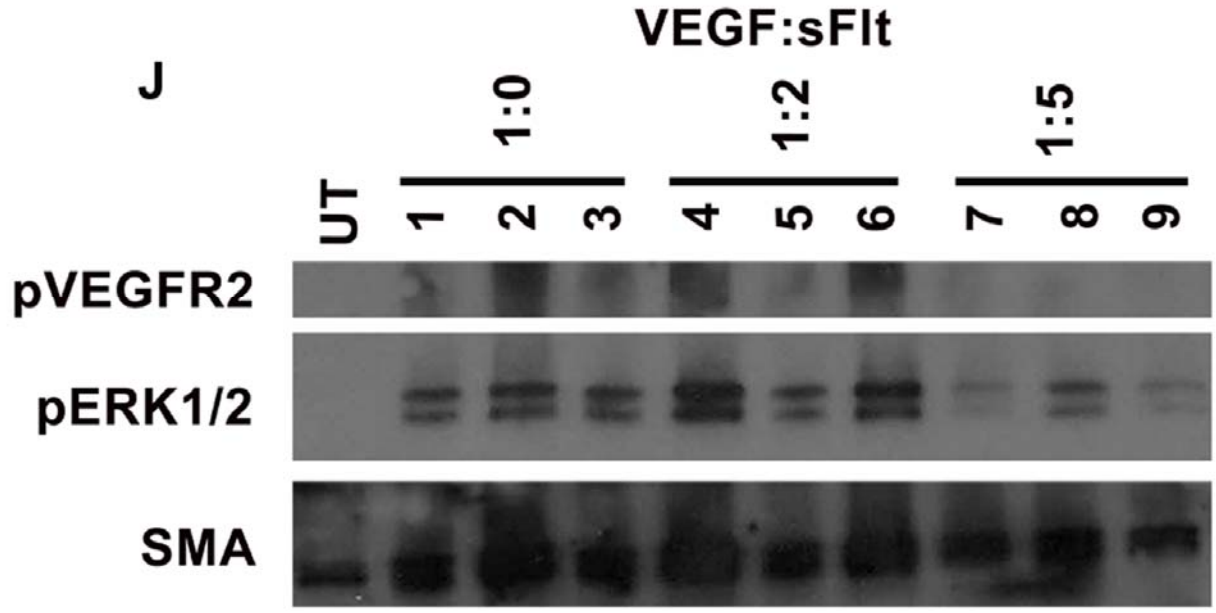
J
VEGF:sFlt
1:0
1:2
1:5
UT
1
2
3
4
5
6
7
8
9
pVEGFR2
pERK1/2
SMA

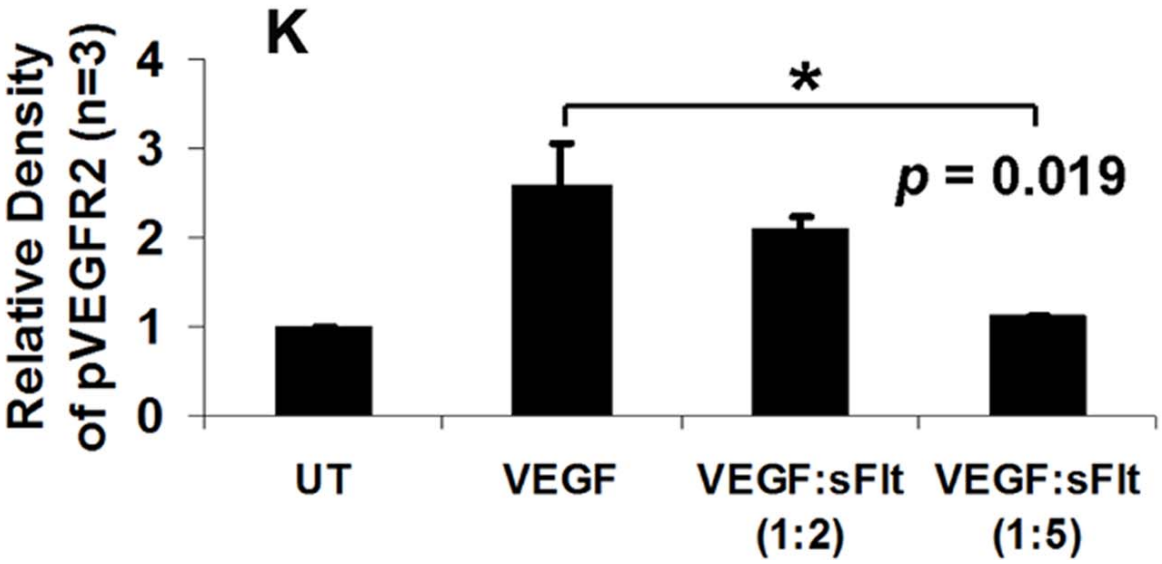
K
Relative Density of pVEGFR2 (n=3)
0
1
2
3
4
*
p = 0.019
UT
VEGF
VEGF:sFlt (1:2)
VEGF:sFlt (1:5)

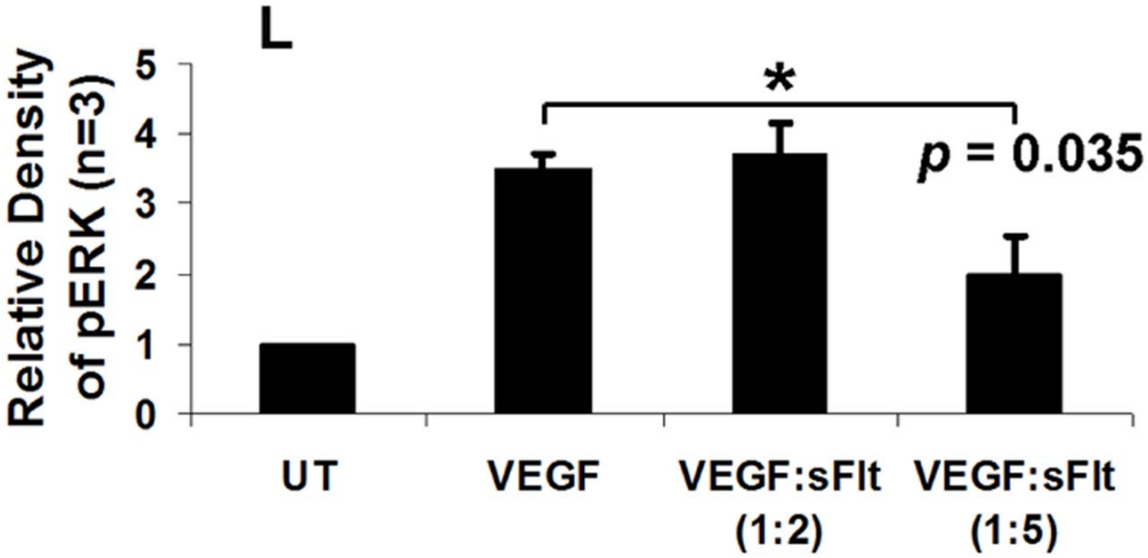

Figure 6.8.2 sFlt inhibits VEGF-A binding to VEGFR2 and downstream ERK signaling. DPSCs were exposed to VEGF alone or various combinations of VEGF and sFlt (1:2, 1:5 or 1:10; VEGF ng/ml to sFlt ng/ml) for 10 min and analyzed by western blotting (J-L). J, The immunofluorescence results were confirmed by western blotting. UT = untreated DPSCs; samples 1-3 were DPSCs exposed to VEGF only; samples 4-6 were DPSCs exposed to 50ng/ml VEGF and 100ng/ml sFlt; samples 7 to 9 were DPSCs exposed to 50ng/ml VEGF and 250ng/ml sFlt. The same membrane was stained with phosphorylated VEGFR2 (pVEGFR2) (~230 kDa) and phosphorylated ERK1/2 (pERK1/2) (42/44 kDa), sequentially. Then, the membrane was stripped and stained for SMA (42 kDa). SMA is the most abundant actin in DPSCs and thus serves as the protein loading control. Coomassie blue staining of the gel also confirmed equal protein loading in all lanes (not shown). K, Quantification of western blot band density (n = 3, three independent experiments), using ImageJ software, for pVEGFR2 relative to SMA revealed significant decrease pVEGFR2 in DPSCs exposed to 1:5 VEGF:sFlt. L, Accordingly, pERK1/2 was also significantly decreased in DPSCs exposed to 1:5 VEGF:sFlt.. Values were represented as mean ± SEM from three independent experiments. Student's t-test calculated $*p \leq 0.05$.

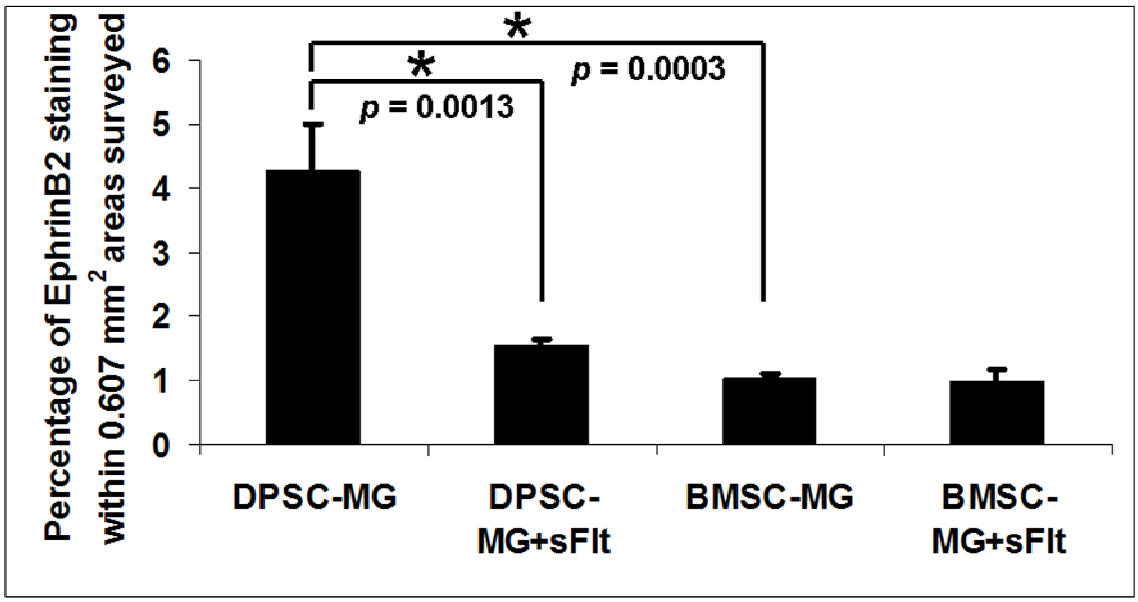

Figure 6.9 sFlt decreased blood vessel formation by inhibiting EphrinB2 signaling. EphrinB2 staining was performed and compared between matrigel (MG) plugs with and without sFlt (50ng/ml) by quantification of the positive area staining using ImageJ software and represented as percentage within 0.607 mm^2 areas surveyed (n = 9; n; numbers of measured area). The highest positive area staining of EphrinB2 was observed in DPSC-MG. The EphrinB2 staining was less in DPSC-MG+sFlt, and was very dim and scarce in both BMSC-MG with and without sFlt. The positive area staining of EphrinB2 was significantly different compared between DPSC-MG with and without sFlt, as well as DPSC and BMSC plugs, but not in BMSC with and without sFlt. Values were represented as mean ± SEM from three independent experiments. Student's t-test calculated $*p \leq 0.05$. DPSC-MG = DPSC alone; DPSC-MG+sFlt = DPSC treated with sFlt; BMSC-MG = BMSC alone; BMSC-MG+sFlt = BMSC treated with sFlt; MG = matrigel alone without cells; MG+sFlt = matrigel alone without cells but treated with sFlt.

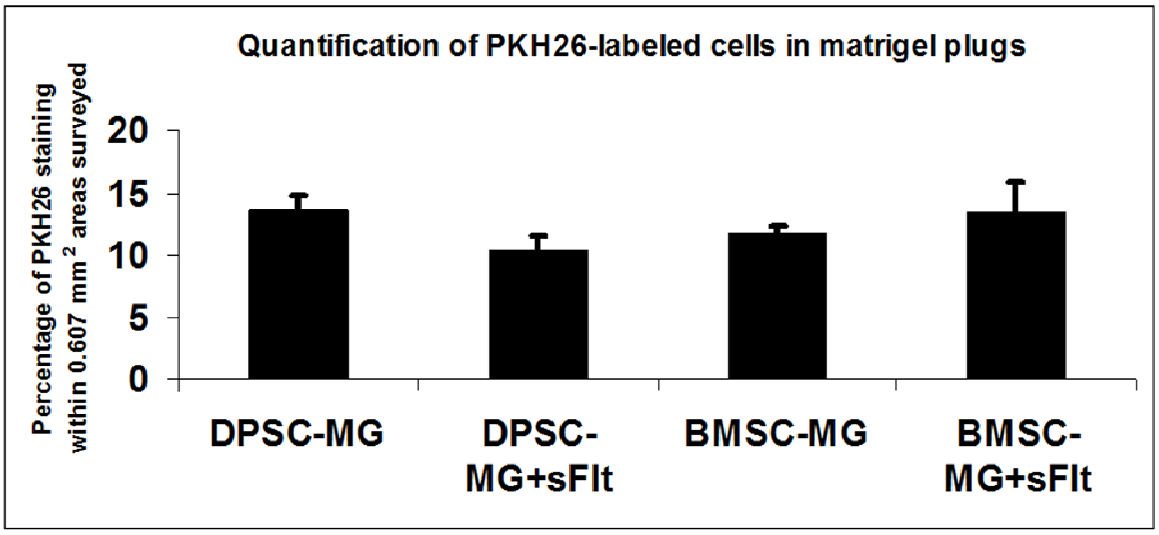

Figure 6.10 sFlt did not significantly affect the number of DPSCs and BMSCs in matrigel plugs. PKH26 staining was used to label DPSCs and BMSCs in matrigel (MG) plugs. The quantification of the positive area staining using ImageJ software and represented as percentage within 0.607 mm^2 areas surveyed (n = 5; n; numbers of measured area) demonstrated no difference in the presence of PKH26-positive cells between DPSC-MG vs. BMSC-MG plugs ($p = 0.19$), as well as MG plugs with and without sFlt ($p = 0.08$ in DPSCs, and $p = 0.51$ in BMSCs). Values were represented as mean ± SEM from three independent experiments. Student's t test ($p \leq 0.05$) was analyzed to compare differences between MG plugs. DPSC-MG = DPSC alone; DPSC-MG+sFlt = DPSC treated with sFlt; BMSC-MG = BMSC alone; BMSC-MG+sFlt = BMSC treated with sFlt; MG = matrigel alone without cells; MG+sFlt = matrigel alone without cells but treated with sFlt.

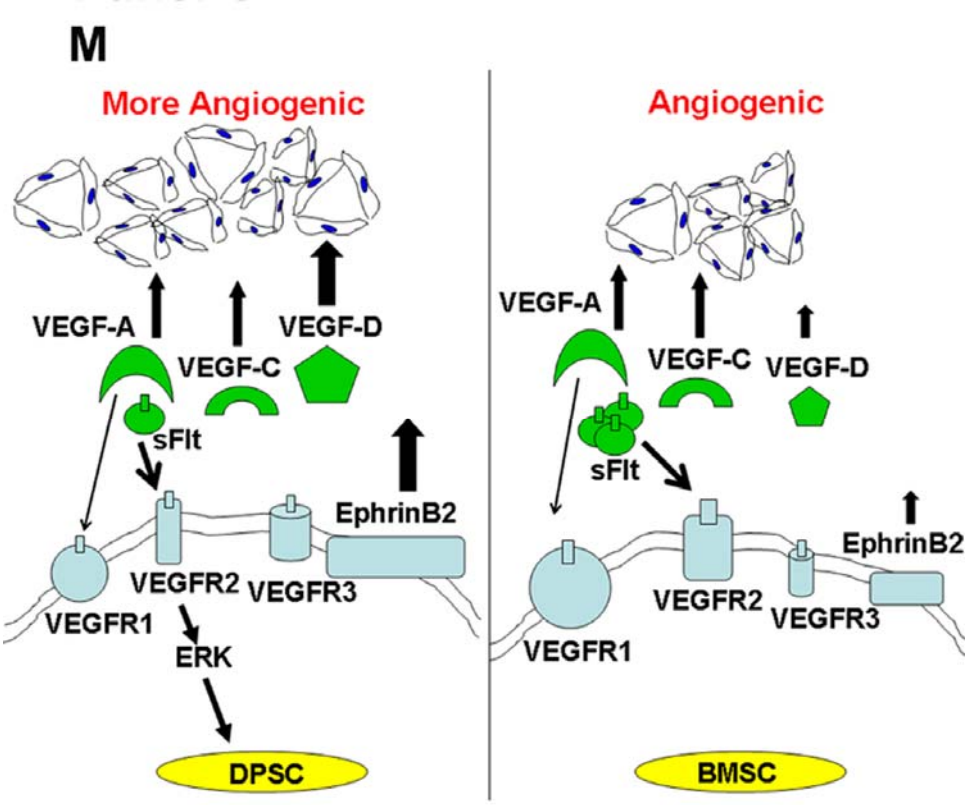
M
More Angiogenic
Angiogenic
VEGF-A
VEGF-C
VEGF-D
sFlt
EphrinB2
VEGFR2
VEGFR3
VEGFR1
ERK
DPSC
BMSC

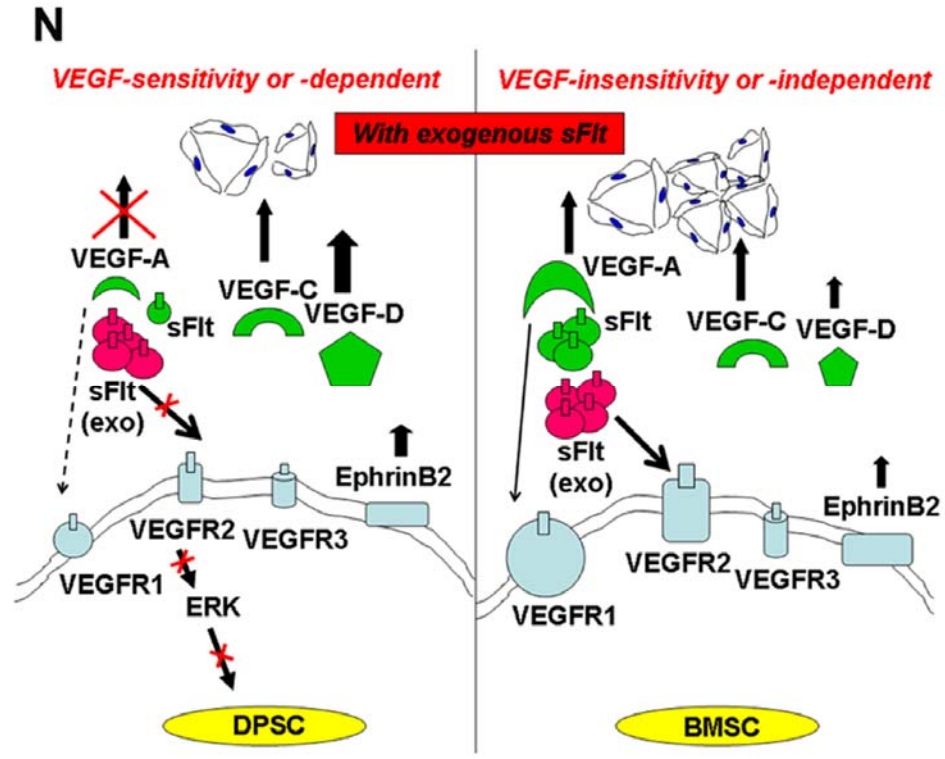
N
VEGF-sensitivity or -dependent
VEGF-insensitivity or -independent
With exogenous sFlt
VEGF-A
VEGF-C
VEGF-D
sFlt
sFlt (exo)
EphrinB2
VEGFR2
VEGFR3
VEGFR1
ERK
DPSC
BMSC

Figure 6.11 Summary of working models for potential mechanisms in angiogenesis induced by DPSCs and BMSCs. M, Both DPSCs and BMSCs exhibit angiogenic capacity with different expression levels of angiogenic growth factors and regulators, VEGF ligands (shown in green), their receptors, and EphrinB2 (shown in blue). DPSCs exhibited greater angiogenic capacity in our *in vivo* studies likely due to higher expression levels of VEGF-D, VEGFR-3, and EphrinB2, as well as lower endogenous sFlt (represented by different sizes of symbols and arrows), resulting in enhanced recruitment of endothelial cells (shown in cells with blue nuclei) and vessel formation. N, DPSCs and BMSCs demonstrate differential responses to exogenous sFlt (shown in pink). DPSCs treated with sFlt showed decreased pVEGFR2 and pERK1/2 and decreased expression of VEGF-A, all VEGF receptors, EphrinB2 (represented by decrease in sizes of symbols and arrows) whereas no difference in angiogenic gene expression was observed in BMSCs exposed to sFlt, indicating DPSCs are sensitive to sFlt. Furthermore, DPSC-induced angiogenesis is VEGF-dependent, as VEGF-A inhibition with sFlt results in decreased vessel formation. In contrast, VEGF-A inhibition by sFlt did not affect BMSC angiogenic capacity, thus, BMSC-induced angiogenesis is VEGF-independent. DPSCs do not express high level of endogenous sFlt and seem more sensitive to exogenous sFlt.

CHAPTER 7

Summation

Review of objectives, results, conclusions, possible future studies and applications

7.1 Review of objectives

The goals, results, and conclusions of this dissertation are reviewed in this chapter. The three major aims proposed in this dissertation consist of: 1) the isolation and characterization of dental pulp stem cells (DPSCs) from neonatal mice and their developmental origin, 2) the investigation of the potential role of DPSCs as ecto-mesenchyme to enhance salivary gland tissue formation, and 3) the determination of the DPSC capacity to function as pericyte-like cells in angiogenic induction.

The findings in this dissertion demonstrate the existence of highly proliferative and multipotent neural crest-derived DPSCs in murine neonatal dental pulp, and highlight two promising biological roles of DPSCs as ecto-mesenchyme and pericyte-like cells to support salivary gland differentiation and enhance angiogenesis via VEGF signaling, respectively.

DPSCs, postnatal stem cells from dental pulp tissue, were first isolated and characterized from human wisdom teeth (Gronthos et al., 2000). Although human DPSC studies showed that DPSCs are promising stem cell sources in regenerative medicine due to their multi-differentiation capacity, easy accessibility, and potential immunomodulative property, and follow-up studies attempted to characterize purer DPSC populations, the diversity of DPSC differentiation capacity and plasticity in various *in vitro* and *in vivo* studies still needs to be

addressed (Gronthos et al., 2002, Huang et al., 2006, d'Aquino et al., 2007, Stevens et al., 2008, Ryu et al., 2009, Spath et al., 2009, Egusa et al., 2012). This variability in the differentiation capacity among DPSCs suggests that dental pulp may contain several stem cell subpopulations with different proliferative capacity, differentiation capacity and developmental origins, which questions whether there are different stem cell populations in dental pulp. Alternatively, all DPSCs may derive from the same origin but their different niche and location dictate their stem cell behavioral diversity. Although neural crest embryologically contributes to a majority of cells in dental pulp and several previous studies have suggested that DPSCs are neural crest-derived, the origin of dental pulp stem cells is still unclear (Chai et al., 2000, Stokowski et al., 2007, Waddington et al., 2009).

DPSCs play an important role in dentin/pulp regeneration to maintain normal pulp function and homeostasis (Sloan and Smith, 2007). In addition to their natural stem cell function, DPSCs may be able to support the formation of both dental and non-dental tissues especially oral tissues. Salivary gland, a very important oral tissue-, can be malfunctioned by salivary gland diseases such as aging, autoimmune diseases, or radiation-induced xerostomia (Dirix et al., 2008). Even though salivary gland-derived adult stem cells have been characterized and enable to give rise into all the epithelial components of the salivary gland such as ductal and acinar cells (Lombaert et al., 2008), their application for salivary gland regeneration is hampered by the need of other supportive cells, vascularization, innervations and matrix important for functional salivary gland regeneration (Bucheler and Haisch, 2003). Like tooth formation, the epithelial-mesenchymal interaction is crucial for the salivary gland branching morphogenesis. Tooth and salivary gland development shares important characteristics involving epithelial-mesenchymal interactions and molecular cues such as secretion of fibroblast growth factors (FGF-10, FGF-7)

by the ecto-mesenchyme and expression of FGF receptors (FGFR-1, FGFR-2) by the epithelium (Hoffman et al., 2002, Jaskoll et al., 2002, Jaskoll et al., 2004, Jaskoll et al., 2005, Madan and Kramer, 2005, Patel et al., 2006, Yamamoto et al., 2008). Due to similarities in tooth and salivary gland formation, DPSCs may support and induce salivary epithelium differentiation and maintain salivary gland tissue function during injury and homeostasis.

Dental pulp is a highly vascularized tissue. After pulp injury, angiogenesis (aka neovascularization) occurs to facilitate pulp repair or regeneration. This natural process may be induced by DPSCs which are cell subpopulations in dental pulp (Sloan and Waddington, 2009). Pericytes, specialized mural cells found at the interface between capillaries and surrounding tissues, play an active role in vascular maintenance and angiogenesis (Allt and Lawrenson, 2001). Angiogenesis, the formation of new vessels from existing vessels, is orchestrated by the interaction of pericytes and endothelial cells (Gerhardt and Betsholtz, 2003). Although DPSCs have been shown to anatomically locate adjacent to blood vessels, no study has yet directly shown the potential role of DPSCs as pericytes in angigogenesis (Shi and Gronthos, 2003, Feng et al., 2011). The expression of angiogenic factors combined with the anatomical location in close relation to vessels may allow DPSCs to interact with endothelial cells and induce new blood vessel formation.

Although the field of human DPSCs has grown rapidly, many questions about this cell population still remain unanswered such as the developmental origin of DPSCs. Lineage tracing studies cannot be performed in human. These difficulties can be overcome by using murine DPSCs as a model to understand developmental and regenerative biology of DPSCs. Studying the nature and biology of DPSCs is very important to provide a better understanding for the use of this stem cell source more appropriately and effectively, as well as ultimately develop

translational models for future human clinical applications. I demonstrate that DPSCs are neural crest-derived cells with multi-differentiation capacity, angiogenic and ectomesenchyme properties as described in the previous chapters. These findings emphasize DPSCs as a promising stem cell source, and broaden the applications of DPSCs in regenerative medicine; however, further studies into the molecular mechanisms regulating their regenerative capacity remained to be explored.

The purpose of aim 1 was to evaluate the presence of DPSCs in neonatal murine dental pulp and their developmental origin. I hypothesized that dental pulp from neonatal mouse teeth contained DPSCs with mesenchymal stem cell properties which were neural crest-derived. I utilized two transgenic mouse models, *Tie2-GFP* and *Wnt1-Cre/R26R-LacZ,* to isolate and characterize DPSCs, also determine their developmental origin. The former determines the contribution of hematopoietic cells and endothelial cells in my dental pulp cultures. *Tie2-GFP* is a transgenic mouse model in which the vascular endothelial cells express green fluorescent protein (GFP) driven by the endothelial-specific receptor tyrosine kinase (*Tie2*) promoter (Motoike et al., 2000). The latter determines the genetic lineage tracing in the derivatives of neural crest cells expressing *LacZ* subsequently labeled with β-galactosidase driven by the *Wnt1* neural crest promoter (Chai et al., 2000). I initially identified stem cell locations in dental pulp by immunofluorescence of stem cell and neural crest markers. Next, I characterized neural crest-derived stem cell populations in murine neonatal dental pulp tissue by their colony-forming ability, expression of stem cell and neural crest genes, and X-gal staining. Then, *in vitro* multi-differentiation in neural crest lineage was examined by gene and protein expression of specific differentiation markers in each lineage. Finally, *in vivo* transplantation was performed in 1-month-old *Rag1-/-* null mice in two different models, dorsal subcutaneous (SC) transplantation

with HAP/TCP and intramuscular (IM) transplantation at two different time periods, 5 and 12 weeks, in comparison with bone marrow stromal cells (BMSCs).

The goal of aim 2 was to determine function of neural crest derived-DPSCs in salivary gland tissue formation. I anticipated that neural crest derived-DPSCs could function as ecto-mesenchyme and support salivary gland tissue formation. Co-culture of cells from different species between human salivary gland cell line (HSG) and murine DPSCs was conducted to determine the effect of murine DPSCs on the enhancement of HSG *in vitro* differentiation on matrigel, compared with that of HSG culture alone. The HSG differentiation capacity was determined by the ability to form acinar-like structures, size and number of acini and positive staining of specific markers expressed by salivary gland epithelium. Then, mRNA expression of murine neural crest-derived salivary gland mesenchyme and angiogenic genes was also examined in murine DPSCs to find out potential growth factors affecting salivary gland differentiation. Finally, xeno-transplantations between HSG and DPSCs were performed in subcutaneous injection with hyaluronic acid (HA) hydrogel plugs ventrally to the submandibular salivary gland without penetrating the gland in 2-month-old *Rag1-/-* null mice to demonstrate the effect of DPSCs supporting salivary gland tissue formation *in vivo*, compared to HSG transplants. The *in vivo* transplants were analyzed by quantitative RT-PCR of specific genes expressed by human salivary gland epithelium and mouse salivary gland mesenchyme, as well as histological assessment of acinar-like structures.

The objective of Aim 3 was to determine the role of DPSCs as pericyte-like cells in angiogenesis. I hypothesized that DPSCs functioned as pericyte-like cells to enhance angiogenesis via a VEGF-dependent pathway. The GFP expression of *Tie2-GFP* derived dental

pulp explants and endothelial gene expression were determined to rule out the presence of hematopoietic or endothelial cells in my culture. *In vitro* vascular tube formation was performed by co-culture of human umbilical vein endothelial cell (HUVEC) or GFP-murine primary cardiac endothelial cells with murine DPSCs on matrigel to determine the angiogenic capacity of DPSCs on endothelial cells to form vascular tube-like structures, compared to bone marrow stromal cells (BMSCs). Then, the angiogenic gene expression in DPSCs *in vitro* was investigated and compared to BMSCs to demonstrate gene profiles of the two cell populations which may affect their angiogenic capacity. The effect of DPSCs in angiogenesis, compared to that of BMSCs, was performed *in vivo* using matrigel plug transplantation. Finally, to better understand the potential molecular mechanism of DPSCs in angiogenesis, compared to that of BMSCs, I treated both DPSCs and BMSCs with sFlt-1, an angiogenic inhibitor by competitive binding with VEGF-A (Ahmad *et al.*, 2011), and then determined their *in vitro* angiogenic gene alteration, downstream signaling, and *in vivo* angiogenesis by matrigel plugs.

7.2 Results and conclusions

DPSCs isolated from neonatal *Tie2-GFP* mice were completely negative for GFP, and were negative for endothelial genes, indicating my cultures did not contain hematopoietic and/or endothelial cells. DPSCs were cultured until at least passage 14 (approximately day 90), constantly and steadily proliferated without alterations in morphology, suggesting highly proliferative characteristic of DPSCs. The expression of *Nanog, Klf4, Sox2,* and *c-Kit* which are pluripotent stem cell genes was observed, suggesting the presence of a primitive stem cell population in our cultures and indicating that these conditions support self-renewing cells. Additionally, DPSCs expressed neural crest-related genes, but not mesodermal genes, and neural

crest associated proteins. Like human DPSCs, these murine DPSCs were able to form colonies that showed variable proliferative-differentiation capacity. *In vitro* differentiation demonstrated that DPSCs were multipotent and gave rise into neural crest lineage, osteo-odontogenic, adipogenic, chondrogenic, neurogenic, and smooth muscle/pericyte-like cells by the expression of specific differentiation genes and proteins in each lineage. Moreover, DPSCs down-regulate *Nanog* and *Klf4* after differentiation, suggesting like embryonic stem cells, these pluripotent genes play a role in maintaining a stemness of DPSCs and thus are decreased during differentiation (Zhang et al., 2010).

Murine DPSCs generated dentin/pulp-like structures surrounded by elongated and polarized odontoblast-like cells in the dorsal subcutaneous DPSC transplants with HAP/TCP, and as the longer transplantation represents more mature matrices and dentin/pulp-like structure formation. In contrast, the formation of mineralized dentin-like structure is not seen in the intramuscular DPSC transplants, suggesting the skeletal muscle is not an inductive environment for formation of mature mineralized matrix despite a longer period of transplantation performed, and DPSC plasticity depends on the *in vivo* niche. In addition, abundant micro-vessel formation was observed in DPSC transplants. These *in vivo* transplants in DPSCs differ from that in bone marrow stromal cells (BMSCs) which generated bone-like structures with less micro-vessels observed.

Using the *Wnt1-Cre/R26R-LacZ* transgenic mouse model to isolate DPSCs in our culture condition, *Wnt1-Cre/R26R-LacZ* derived DPSCs were completely positive for X-gal staining, highly proliferative, enabled to form colonies, expressed stem cell and neural crest-related genes, as well as capable of differentiating into neural crest-lineage *in vitro* and *in vivo*, emphasizing the neural crest origin of DPSCs.

In addition, I provided two new insights into DPSC biological properties for future clinical application. First, I showed that neural crest-derived murine DPSCs functioned as ecto-mesenchyme supporting the differentiation of human salivary gland (HSG) cell lines. HSG co-cultured with DPSCs formed more mature and increased number of acinar-like structures *in vitro*. DPSCs shown by positive X-gal staining were clustered near HSG-derived acinar-like structure. The HSG-derived acini in both HSG alone and HSG+DPSC were positive for CD44 and LAMP-1, confirming the differentiation of HSG to acinar cells. However, strongly positive staining for LAMP-1 was observed by the acini in the HSG+DPSC group, compared to those in HSG alone, suggesting higher maturity of salivary gland acini. Undifferentiated DPSCs expressed significantly high levels of *Fgf-7* and *Fgf*-10, proteins secreted by neural crest-derived mesenchymal cells to induce branching morphogenesis during salivary gland development and formation (Morita and Nogawa, 1999, Jaskoll et al., 2005, Tucker, 2007), and greater than endogenous *Fgf-7* and *Fgf-10* expression in mouse submandibular salivary gland. The high level of *Fgf*-7 and *Fgf-10* expressed by DPSCs suggested that DPSCs may be a good source of ecto-mesenchyme supportive of salivary gland formation and regeneration. DPSCs moreover expressed high level of vascular endothelial growth factor receptor 3, *Vegfr-3*, and similar level of its ligand, *Vegf-C* but not *Vegf-A*, when compared with that of mouse salivary gland, suggesting that the angiogenic potential of DPSCs may facilitate salivary gland formation.

Xeno-transplantation of HSG and DPSCs demonstrated high expression of murine neural crest-derived mesenchymal genes, human salivary gland differentiation genes, and murine endothelial-specific, neuronal, and angiogenic genes. The gene expression exhibited in xeno-transplants indicated that DPSCs enhanced the differentiation of salivary gland cells and form salivary gland tissue by induction of blood vessel and nerve innervating formation. Histological

observation revealed glandular structures present in the HSG and DPSC co-transplantation with abundant blood vessels in HA hydrogel plugs, but not in HSG alone which exhibited only immature tumor-like structures.

Second, I demonstrated that neural crest-derived murine DPSCs played a crucial role as pericyte-like cells inducing angiogenesis by VEGF signaling. Absence of *Tie2*-GFP+ cells indicated that DPSCs are not derived from hematopoietic and/or endothelial origin and clonal DPSC culture showed homogenous cell population positive for mesenchymal markers such as CD44 and pericyte markers such as smooth muscle actin. Co-culture of DPSCs with endothelial cells revealed that DPSCs were able to enhance both endothelial cell line and primary endothelial cells forming *in vitro* vascular tube formation better than BMSCs. DPSCs were also located adjacent to endothelial cells, suggesting their supportive function as pericytes to stabilize vascular tubes *in vitro*. Even though DPSCs and BMSCs expressed *Vegf* ligands and their receptors, DPSCs expressed significantly higher *Vegfd*, *EphrinB2*, and *Vegfr3* levels, which may explain angiogenic differences between two mesenchymal stem cell populations. *In vivo* matrigel plugs demonstrated that DPSCs enhanced blood vessel formation better than BMSCs.

In order to investigate if DPSCs induced angiogenesis via VEGF signaling, we treated DPSCs and BMSCs to VEGF inhibitor, sFlt-1 in different concentrations. sFlt-1 treated DPSCs showed a dose-dependent down-regulation in the expression of *Vegfa*, and its receptors (*Vegfr1* and *Vegfr2*), *EphrinB2,* and *Vegfr3*, but not in *Vegfc* and *Vegfd*, as compared to untreated cells. sFlt-1 did not significantly affect these angiogenic genes in BMSCs. Plugs containing sFlt-1 treated DPSCs showed a decrease in the number of vessels. No significant difference was observed in BMSC with and without sFlt. The decrease in vessels following sFlt-1 treatment indicates DPSC-induced angiogenesis is VEGF-dependent. The downstream signaling mediated

by VEGFR-2 was examined by exposing DPSCs to VEGF alone or combined with sFlt-1 at various concentrations. Immunofluorescence revealed that DPSCs exposed to VEGF displayed phosphorylated VEGFR2 and its phosphorylation was inhibited in a dose dependent manner by sFlt-1. Western blotting confirmed that VEGFR-2 phosphorylation induced downstream ERK phosphorylation in DPSCs, and ERK phosphorylation was also inhibited by sFlt-1. sFlt-1 inhibits VEGF-A binding to VEGFR-2, resulting in decreased VEGFR-2 signaling and decreased downstream ERK signaling in DPSCs. In addition to inhibiting VEGF signaling, sFlt-1 decreased blood vessel formation via inhibiting EphrinB2 signaling, which was shown by EphrinB2 staining. VEGF inhibition by sFlt-1 reduces the potential of DPSCs to promote angiogenesis, which occurs via inhibition of VEGFR-2 signaling and resulting down-regulation of *Vegfa*, *Vegf receptors* and *EphrinB2* expression.

7.3 Possible future studies and applications

To gain insights into the developmental biology of DPSCs and their potential clinical applications in regenerative medicine and tissue regeneration, I characterized murine DPSCs and developed *in vitro* and *in vivo* models to study their capacity to support regeneration of several tissues.

1. Murine DPSCs isolated from *Wnt1-Cre/R26R-LacZ* are neural crest-derived, thereby β-galactosidase-labeled. Although human DPSCs have extensively been studied in the last decade, murine DPSC models offer several advantages described as follows. For instance, using the *Wnt1-Cre/R26R-LacZ* mouse model I was able to better characterize the origin of murine DPSCs. In combination with more specific stem cell markers I was able to isolate a purer DPSC population derived from neural crest. In addition, I was able to use these isolated DPSCs to study

their derivatives during the differentiation processes. These purified cells may be subjected to direct characterization at either the cellular or the molecular level, including transplantation of these cells into animal models to study tissue regeneration. The emergence of *Cre-loxP* systems allows studying genes of interest in DPSCs to gain insights into the role of these genes in DPSC function.

2. The neural crest origin of DPSCs suggests that these cells can be potentially used for regenerative medicine of not only dental tissue, but also other neural crest-derived tissues such as bone tissue, cartilage tissue, or neuronal tissue. Nonetheless, further studies are also needed to confirm the differentiation capacity or plasticity of neural crest-derived DPSCs. In order to investigate the plasticity of DPSCs, injection of DPSCs into mouse blastocysts or chick embryo to generate mouse-mouse or mouse-chick embryos, respectively, is an strategy I am exploring to study the contribution of DPSCs.

3. The *Wnt1-Cre/R26R-LacZ* mouse model demonstrates that dental pulp tissue contains a majority of neural crest-derived cells including DPSCs, and a minority of non neural crest-derived cells. Future studies comparing the differentiation capacity, contribution and cross-talk of neural crest-DPSCs and non-neural crest-derived cells from dental pulp will be very beneficial to understand tooth formation and its regeneration. The results from these studies not only can be used for tooth regeneration, but can also be applied for regeneration of other tissues which consist of both neural crest-and non-neural crest-derived cells such as salivary gland or other exocrine glands.

4. Several recent studies have shown the existence of neural crest-derived stem cells in various postnatal tissues such as dental pulp, skin, cornea, hair follicle and intestine (Kruger et al., 2002, Sieber-Blum and Hu, 2008, Stevens et al., 2008). Therefore, future studies should also

aim at understanding the interactions of neural crest-derived stem cells with their respective niches from multiple adult tissues, and a comparison of stem cell properties among neural crest-derived stem cells from different tissues should provide better understanding in the biology of neural crest-derived stem cells.

5. Understanding the molecular mechanisms that control organogenesis and adult tissue homeostasis will be instrumental for tissue engineering and tissue regeneration. Thus, studying how neural crest-derived stem cells from multiple organs such as DPSCs interact within each niche to remain either stem cells or differentiate may help elucidate the mechanisms for maintenance of tissue-specific stem cells and tissue-specific differentiation, in tissue regeneration or homeostasis.

6. Neural crest-derived DPSCs support salivary gland tissue formation. Further studies should be performed in order to better understand the molecular biology mechanisms or signaling pathways in DPSCs or neural crest-derived mesenchyme important for salivary gland differentiation. Furthermore, the study of DPSCs capacity to serve as ecto-mesenchyme using mouse models with salivary gland injury will provide very useful information that may lay the foundations for future human clinical trials to treat salivary gland diseases.

7. DPSCs function as pericyte-like cells and induce angiogenesis. Inadequate blood supply during tissue regeneration, repair, and healing results in the formation of necrotic or scar tissues. Consequently, studying the angiogenic capacity of DPSCs can also be used as an important model for neovascularization and angiogenesis in tissue regeneration, not only for dentin/pulp tissue regeneration, but also other tissue regeneration.

Current evidence has demonstrated that DPSCs are not only easily accessible from the oral cavity but can also often be obtained as a discarded biological sample. Given their easy

accessibility, extensive proliferation and differentiation capacity, DPSCs are recognized as a promising adult stem cell source of regenerative medicine. In addition, the possibility of collecting stem cells during dental treatments that can be banked for autologous therapeutic use in the future is another attractive property of DPSCs. Recently, DPSCs have been used to generate iPS cells that can be used not only for autologous cell-based regeneration of complex oral tissues but also for patient-specific modeling of oral diseases (Egusa et al., 2012). The immunomodulatory capacity of DPSCs is also an attractive property of DPSCs (Huang et al., 2009). The findings in this study reveal that neural crest-derived DPSCs can function to enhance salivary gland formation and induce angiogenesis. These results will broaden the usage of DPSCs in clinical application which includes not only their direct use for differentiation into dental or non-dental tissues, but also as trophic and angiogenic factories for tissue regeneration.

BIBLIOGRAPHY

1. Abzhanov A, Tzahor E, Lassar AB, Tabin CJ (2003). Dissimilar regulation of cell differentiation in mesencephalic (cranial) and sacral (trunk) neural crest cells in vitro. *Development* 130 (19): 4567-4579.

2. Ahmad S, Hewett PW, Al-Ani B, Sissaoui S, Fujisawa T, Cudmore MJ, Ahmed A (2011). Autocrine activity of soluble Flt-1 controls endothelial cell function and angiogenesis. *Vasc Cell* 3 (1): 15.

3. Akintoye SO, Lam T, Shi S, Brahim J, Collins MT, Robey PG (2006). Skeletal site-specific characterization of orofacial and iliac crest human bone marrow stromal cells in same individuals. *Bone* 38 (6): 758-768.

4. Akiyama K, Chen C, Gronthos S, Shi S (2012). Lineage differentiation of mesenchymal stem cells from dental pulp, apical papilla, and periodontal ligament. *Methods Mol Biol* 887 111-121.

5. Albuquerque RJ, Hayashi T, Cho WG, Kleinman ME, Dridi S, Takeda A, Baffi JZ, Yamada K, Kaneko H, Green MG, Chappell J, Wilting J, Weich HA, Yamagami S, Amano S, Mizuki N, Alexander JS, Peterson ML, Brekken RA, Hirashima M, Capoor S, Usui T, Ambati BK, Ambati J (2009). Alternatively spliced vascular endothelial growth factor receptor-2 is an essential endogenous inhibitor of lymphatic vessel growth. *Nat Med* 15 (9): 1023-1030.

6. Alliot-Licht B, Hurtrel D, Gregoire M (2001). Characterization of alpha-smooth muscle actin positive cells in mineralized human dental pulp cultures. *Arch Oral Biol* 46 (3): 221-228.

7. Allt G, Lawrenson JG (2001). Pericytes: cell biology and pathology. *Cells Tissues Organs* 169 (1): 1-11.

8. Alroy J, Goyal V, Skutelsky E (1987). Lectin histochemistry of mammalian endothelium. *Histochemistry* 86 (6): 603-607.

9. Amano O, Mizobe K, Bando Y, Sakiyama K (2012). Anatomy and histology of rodent and human major salivary glands: -overview of the Japan salivary gland society-sponsored workshop. *Acta Histochem Cytochem* 45 (5): 241-250.

10. Ambati BK, Nozaki M, Singh N, Takeda A, Jani PD, Suthar T, Albuquerque RJ, Richter E, Sakurai E, Newcomb MT, Kleinman ME, Caldwell RB, Lin Q, Ogura Y, Orecchia A, Samuelson DA, Agnew DW, St Leger J, Green WR, Mahasreshti PJ, Curiel DT, Kwan D, Marsh H, Ikeda S, Leiper LJ, Collinson JM, Bogdanovich S, Khurana TS, Shibuya M, Baldwin ME, Ferrara N, Gerber HP, De Falco S, Witta J, Baffi JZ, Raisler BJ, Ambati J (2006). Corneal avascularity is due to soluble VEGF receptor-1. *Nature* 443 (7114): 993-997.

11. Ambati BK, Patterson E, Jani P, Jenkins C, Higgins E, Singh N, Suthar T, Vira N, Smith K, Caldwell R (2007). Soluble vascular endothelial growth factor receptor-1 contributes to the corneal antiangiogenic barrier. *Br J Ophthalmol* 91 (4): 505-508.

12. Amoh Y, Li L, Katsuoka K, Penman S, Hoffman RM (2005). Multipotent nestin-positive, keratin-negative hair-follicle bulge stem cells can form neurons. *Proc Natl Acad Sci U S A* 102 (15): 5530-5534.

13. Anastasia L, Pelissero G, Venerando B, Tettamanti G (2010). Cell reprogramming: expectations and challenges for chemistry in stem cell biology and regenerative medicine. *Cell Death Differ* 17 (8): 1230-1237.

14. Armulik A, Abramsson A, Betsholtz C (2005). Endothelial/pericyte interactions. *Circ Res* 97 (6): 512-523.

15. Arnsdorf EJ, Jones LM, Carter DR, Jacobs CR (2009). The periosteum as a cellular source for functional tissue engineering. *Tissue Eng Part A* 15 (9): 2637-2642.

16. Balic A, Aguila HL, Caimano MJ, Francone VP, Mina M (2010). Characterization of stem and progenitor cells in the dental pulp of erupted and unerupted murine molars. *Bone* 46 (6): 1639-1651.

17. Banai S, Shweiki D, Pinson A, Chandra M, Lazarovici G, Keshet E (1994). Upregulation of vascular endothelial growth factor expression induced by myocardial ischaemia: implications for coronary angiogenesis. *Cardiovasc Res* 28 (8): 1176-1179.

18. Batouli S, Miura M, Brahim J, Tsutsui TW, Fisher LW, Gronthos S, Robey PG, Shi S (2003). Comparison of stem-cell-mediated osteogenesis and dentinogenesis. *J Dent Res* 82 (12): 976-981.

19. Battula VL, Evans KW, Hollier BG, Shi Y, Marini FC, Ayyanan A, Wang RY, Brisken C, Guerra R, Andreeff M, Mani SA (2010). Epithelial-mesenchymal transition-derived cells exhibit multilineage differentiation potential similar to mesenchymal stem cells. *Stem Cells* 28 (8): 1435-1445.

20. Bergers G, Song S (2005). The role of pericytes in blood-vessel formation and maintenance. *Neuro Oncol* 7 (4): 452-464.

21. Biehl JK, Russell B (2009). Introduction to stem cell therapy. *J Cardiovasc Nurs* 24 (2): 98-103; quiz 104-105.

22. Boyer LA, Lee TI, Cole MF, Johnstone SE, Levine SS, Zucker JP, Guenther MG, Kumar RM, Murray HL, Jenner RG, Gifford DK, Melton DA, Jaenisch R, Young RA (2005). Core transcriptional regulatory circuitry in human embryonic stem cells. *Cell* 122 (6): 947-956.

23. Brambrink T, Foreman R, Welstead GG, Lengner CJ, Wernig M, Suh H, Jaenisch R (2008). Sequential expression of pluripotency markers during direct reprogramming of mouse somatic cells. *Cell Stem Cell* 2 (2): 151-159.

24. Braut A, Kollar EJ, Mina M (2003). Analysis of the odontogenic and osteogenic potentials of dental pulp in vivo using a Col1a1-2.3-GFP transgene. *Int J Dev Biol* 47 (4): 281-292.

25. Breyer A, Estharabadi N, Oki M, Ulloa F, Nelson-Holte M, Lien L, Jiang Y (2006). Multipotent adult progenitor cell isolation and culture procedures. *Exp Hematol* 34 (11): 1596-1601.

26. Bronner-Fraser M (1993). Segregation of cell lineage in the neural crest. *Curr Opin Genet Dev* 3 (4): 641-647.

27. Bronner-Fraser M (1995). Origins and developmental potential of the neural crest. *Exp Cell Res* 218 (2): 405-417.

28. Bucheler M, Haisch A (2003). Tissue engineering in otorhinolaryngology. *DNA Cell Biol* 22 (9): 549-564.

29. Calvo J, BenYoucef A, Baijer J, Rouyez MC, Pflumio F (2012). Assessment of human multi-potent hematopoietic stem/progenitor cell potential using a single in vitro screening system. *PLoS One* 7 (11): e50495.

30. Carlile MJ, Sturrock MG, Chisholm DM, Ogden GR, Schor AM (2000). The presence of pericytes and transitional cells in the vasculature of the human dental pulp: an ultrastructural study. *Histochem J* 32 (4): 239-245.

31. Chai Y, Jiang X, Ito Y, Bringas P, Jr., Han J, Rowitch DH, Soriano P, McMahon AP, Sucov HM (2000). Fate of the mammalian cranial neural crest during tooth and mandibular morphogenesis. *Development* 127 (8): 1671-1679.

32. Chalothorn D, Clayton JA, Zhang H, Pomp D, Faber JE (2007). Collateral density, remodeling, and VEGF-A expression differ widely between mouse strains. *Physiol Genomics* 30 (2): 179-191.

33. Chamberlain G, Fox J, Ashton B, Middleton J (2007). Concise review: mesenchymal stem cells: their phenotype, differentiation capacity, immunological features, and potential for homing. *Stem Cells* 25 (11): 2739-2749.

34. Chen Z, Couble ML, Mouterfi N, Magloire H, Chen Z, Bleicher F (2009). Spatial and temporal expression of KLF4 and KLF5 during murine tooth development. *Arch Oral Biol* 54 (5): 403-411.

35. Cheng N, Lambert DL (2011). Mammary transplantation of stromal cells and carcinoma cells in C57BL/6J mice. *J Vis Exp* e2716 (54): doi:10.3791/2716

36. Cheung M, Chaboissier MC, Mynett A, Hirst E, Schedl A, Briscoe J (2005). The transcriptional control of trunk neural crest induction, survival, and delamination. *Dev Cell* 8 (2): 179-192.

37. Cho H, Kozasa T, Bondjers C, Betsholtz C, Kehrl JH (2003). Pericyte-specific expression of Rgs5: implications for PDGF and EDG receptor signaling during vascular maturation. *Faseb J* 17 (3): 440-442.

38. Cho SR, Yang MS, Yim SH, Park JH, Lee JE, Eom YW, Jang IK, Kim HE, Park JS, Kim HO, Lee BH, Park CI, Kim YJ (2008). Neurally induced umbilical cord blood cells modestly repair injured spinal cords. *Neuroreport* 19 (13): 1259-1263.

39. Cohn RH, Banerjee SD, Bernfield MR (1977). Basal lamina of embryonic salivary epithelia. Nature of glycosaminoglycan and organization of extracellular materials. *J Cell Biol* 73 (2): 464-478.

40. Conley BJ, Trounson AO, Mollard R (2004). Human embryonic stem cells form embryoid bodies containing visceral endoderm-like derivatives. *Fetal Diagn Ther* 19 (3): 218-223.

41. Conway SJ, Henderson DJ, Copp AJ (1997). Pax3 is required for cardiac neural crest migration in the mouse: evidence from the splotch (Sp2H) mutant. *Development* 124 (2): 505-514.

42. Cordeiro MM, Dong Z, Kaneko T, Zhang Z, Miyazawa M, Shi S, Smith AJ, Nor JE (2008). Dental pulp tissue engineering with stem cells from exfoliated deciduous teeth. *J Endod* 34 (8): 962-969.

43. Crespi R, Vinci R, Cappare P, Gherlone E, Romanos GE (2007). Calvarial versus iliac crest for autologous bone graft material for a sinus lift procedure: a histomorphometric study. *Int J Oral Maxillofac Implants* 22 (4): 527-532.

44. Crisan M, Chen CW, Corselli M, Andriolo G, Lazzari L, Peault B (2009). Perivascular multipotent progenitor cells in human organs. *Ann N Y Acad Sci* 1176 118-123.

45. Crisan M, Yap S, Casteilla L, Chen CW, Corselli M, Park TS, Andriolo G, Sun B, Zheng B, Zhang L, Norotte C, Teng PN, Traas J, Schugar R, Deasy BM, Badylak S, Buhring HJ, Giacobino JP, Lazzari L, Huard J, Peault B (2008). A perivascular origin for mesenchymal stem cells in multiple human organs. *Cell Stem Cell* 3 (3): 301-313.

46. Cumano A, Paige CJ, Iscove NN, Brady G (1992). Bipotential precursors of B cells and macrophages in murine fetal liver. *Nature* 356 (6370): 612-615.

47. Cutler LS, Christian CP, Rendell JK (1987). Glycosaminoglycan synthesis by adult rat submandibular salivary-gland secretory units. *Arch Oral Biol* 32 (6): 413-419.

48. d'Aquino R, De Rosa A, Laino G, Caruso F, Guida L, Rullo R, Checchi V, Laino L, Tirino V, Papaccio G (2009). Human dental pulp stem cells: from biology to clinical applications. *J Exp Zoolog B Mol Dev Evol* 312B (5): 408-415.

49. d'Aquino R, Graziano A, Sampaolesi M, Laino G, Pirozzi G, De Rosa A, Papaccio G (2007). Human postnatal dental pulp cells co-differentiate into osteoblasts and endotheliocytes: a pivotal synergy leading to adult bone tissue formation. *Cell Death Differ* 14 (6): 1162-1171.

50. d'Aquino R, Graziano A, Sampaolesi M, Laino G, Pirozzi G, De Rosa A, Papaccio G (2007). Human postnatal dental pulp cells co-differentiate into osteoblasts and endotheliocytes: a pivotal synergy leading to adult bone tissue formation. *Cell Death Differentiation* 14 (6): 1162-1171.

51. Dalkara T, Gursoy-Ozdemir Y, Yemisci M (2011). Brain microvascular pericytes in health and disease. *Acta Neuropathol* 122 (1): 1-9.

52. Dang H, Lin AL, Zhang B, Zhang HM, Katz MS, Yeh CK (2009). Role for Notch signaling in salivary acinar cell growth and differentiation. *Dev Dyn* 238 (3): 724-731.

53. De Bari C, Dell'Accio F, Vanlauwe J, Eyckmans J, Khan IM, Archer CW, Jones EA, McGonagle D, Mitsiadis TA, Pitzalis C, Luyten FP (2006). Mesenchymal multipotency of adult human periosteal cells demonstrated by single-cell lineage analysis. *Arthritis Rheum* 54 (4): 1209-1221.

54. Denny PC, Ball WD, Redman RS (1997). Salivary glands: a paradigm for diversity of gland development. *Crit Rev Oral Biol Med* 8 (1): 51-75.

55. Diekwisch TG (2001). The developmental biology of cementum. *Int J Dev Biol* 45 (5-6): 695-706.

56. Dirix P, Nuyts S, Vander Poorten V, Delaere P, Van den Bogaert W (2008). The influence of xerostomia after radiotherapy on quality of life: results of a questionnaire in head and neck cancer. *Support Care Cancer* 16 (2): 171-179.

57. Dissanayaka WL, Zhan X, Zhang C, Hargreaves KM, Jin L, Tong EH (2012). Coculture of dental pulp stem cells with endothelial cells enhances osteo-/odontogenic and angiogenic potential in vitro. *J Endod* 38 (4): 454-463.

58. Dominici M, Le Blanc K, Mueller I, Slaper-Cortenbach I, Marini F, Krause D, Deans R, Keating A, Prockop D, Horwitz E (2006). Minimal criteria for defining multipotent mesenchymal stromal cells. The International Society for Cellular Therapy position statement. *Cytotherapy* 8 (4): 315-317.

59. Donovan MG, Dickerson NC, Hellstein JW, Hanson LJ (1993). Autologous calvarial and iliac onlay bone grafts in miniature swine. *J Oral Maxillofac Surg* 51 (8): 898-903.

60. Dore-Duffy P, Katychev A, Wang X, Van Buren E (2006). CNS microvascular pericytes exhibit multipotential stem cell activity. *J Cereb Blood Flow Metab* 26 (5): 613-624.

61. Dougher-Vermazen M, Hulmes JD, Bohlen P, Terman BI (1994). Biological activity and phosphorylation sites of the bacterially expressed cytosolic domain of the KDR VEGF-receptor. *Biochem Biophys Res Commun* 205 (1): 728-738.

62. Duband JL, Monier F, Delannet M, Newgreen D (1995). Epithelium-mesenchyme transition during neural crest development. *Acta Anat (Basel)* 154 (1): 63-78.

63. Ducy P, Zhang R, Geoffroy V, Ridall AL, Karsenty G (1997). Osf2/Cbfa1: a transcriptional activator of osteoblast differentiation. *Cell* 89 (5): 747-754.

64. Egusa H, Sonoyama W, Nishimura M, Atsuta I, Akiyama K (2012). Stem cells in dentistry--part I: stem cell sources. *J Prosthodont Res* 56 (3): 151-165.

65. Egusa H, Sonoyama W, Nishimura M, Atsuta I, Akiyama K (2012). Stem cells in dentistry--Part II: Clinical applications. *J Prosthodont Res* 56 (4): 229-248.

66. Etchevers HC, Vincent C, Le Douarin NM, Couly GF (2001). The cephalic neural crest provides pericytes and smooth muscle cells to all blood vessels of the face and forebrain. *Development* 128 (7): 1059-1068.

67. Falk T, Zhang S, Sherman SJ (2009). Vascular endothelial growth factor B (VEGF-B) is up-regulated and exogenous VEGF-B is neuroprotective in a culture model of Parkinson's disease. *Mol Neurodegener* 4 49.

68. Feng J, Mantesso A, De Bari C, Nishiyama A, Sharpe PT (2011). Dual origin of mesenchymal stem cells contributing to organ growth and repair. *Proc Natl Acad Sci U S A* 108 (16): 6503-6508.

69. Feng J, van der Zwaag M, Stokman MA, van Os R, Coppes RP (2009). Isolation and characterization of human salivary gland cells for stem cell transplantation to reduce radiation-induced hyposalivation. *Radiother Oncol* 92 (3): 466-471.

70. Feng JQ, Huang H, Lu Y, Ye L, Xie Y, Tsutsui TW, Kunieda T, Castranio T, Scott G, Bonewald LB, Mishina Y (2003). The Dentin matrix protein 1 (Dmp1) is specifically expressed in mineralized, but not soft, tissues during development. *J Dent Res* 82 (10): 776-780.

71. Feng Z, Gao F (2012). Stem cell challenges in the treatment of neurodegenerative disease. *CNS Neurosci Ther* 18 (2): 142-148.

72. Ferrara N (2001). Role of vascular endothelial growth factor in regulation of physiological angiogenesis. *Am J Physiol Cell Physiol* 280 (6): C1358-1366.

73. Ferrara N (2005). The role of VEGF in the regulation of physiological and pathological angiogenesis. *Exs* (94): 209-231.

74. Ferrara N, Gerber HP, LeCouter J (2003). The biology of VEGF and its receptors. *Nat Med* 9 (6): 669-676.

75. Ferrara N, Henzel WJ (1989). Pituitary follicular cells secrete a novel heparin-binding growth factor specific for vascular endothelial cells. *Biochem Biophys Res Commun* 161 (2): 851-858.

76. Fong H, Foster BL, Sarikaya M, Somerman MJ (2009). Structure and mechanical properties of Ank/Ank mutant mouse dental tissues--an animal model for studying periodontal regeneration. *Arch Oral Biol* 54 (6): 570-576.

77. Fonseca I, Moura Nunes JF, Soares J (2000). Expression of CD44 isoforms in normal salivary gland tissue: an immunohistochemical and ultrastructural study. *Histochem Cell Biol* 114 (6): 483-488.

78. Friedenstein AJ, Chailakhjan RK, Lalykina KS (1970). The development of fibroblast colonies in monolayer cultures of guinea-pig bone marrow and spleen cells. *Cell Tissue Kinet* 3 (4): 393-403.

79. Friedenstein AJ, Gorskaja JF, Kulagina NN (1976). Fibroblast precursors in normal and irradiated mouse hematopoietic organs. *Exp Hematol* 4 (5): 267-274.

80. Gay IC, Chen S, MacDougall M (2007). Isolation and characterization of multipotent human periodontal ligament stem cells. *Orthod Craniofac Res* 10 (3): 149-160.

81. Gerhardt H, Betsholtz C (2003). Endothelial-pericyte interactions in angiogenesis. *Cell Tissue Res* 314 (1): 15-23.

82. Gorjup E, Danner S, Rotter N, Habermann J, Brassat U, Brummendorf TH, Wien S, Meyerhans A, Wollenberg B, Kruse C, von Briesen H (2009). Glandular tissue from human pancreas and salivary gland yields similar stem cell populations. *Eur J Cell Biol* 88 (7): 409-421.

83. Grabski AD, Shimizu T, Deou J, Mahoney WM, Jr., Reidy MA, Daum G (2009). Sphingosine-1-phosphate receptor-2 regulates expression of smooth muscle alpha-actin after arterial injury. *Arterioscler Thromb Vasc Biol* 29 (10): 1644-1650.

84. Grando Mattuella L, Westphalen Bento L, de Figueiredo JA, Nor JE, de Araujo FB, Fossati AC (2007). Vascular endothelial growth factor and its relationship with the dental pulp. *J Endod* 33 (5): 524-530.

85. Gregoire FM (2001). Adipocyte differentiation: from fibroblast to endocrine cell. *Exp Biol Med (Maywood)* 226 (11): 997-1002.

86. Gronthos S, Brahim J, Li W, Fisher LW, Cherman N, Boyde A, DenBesten P, Robey PG, Shi S (2002). Stem cell properties of human dental pulp stem cells. *Journal of Dental Research* 81 (8): 531-535.

87. Gronthos S, Brahim J, Li W, Fisher LW, Cherman N, Boyde A, DenBesten P, Robey PG, Shi S (2002). Stem cell properties of human dental pulp stem cells. *J Dent Res* 81 (8): 531-535.

88. Gronthos S, Graves SE, Ohta S, Simmons PJ (1994). The STRO-1+ fraction of adult human bone marrow contains the osteogenic precursors. *Blood* 84 (12): 4164-4173.

89. Gronthos S, Mankani M, Brahim J, Robey PG, Shi S (2000). Postnatal human dental pulp stem cells (DPSCs) in vitro and in vivo. *Proc Natl Acad Sci U S A* 97 (25): 13625-13630.

90. Grove JE, Bruscia E, Krause DS (2004). Plasticity of bone marrow-derived stem cells. *Stem Cells* 22 (4): 487-500.

91. Gudjonsson T, Magnusson MK (2005). Stem cell biology and the cellular pathways of carcinogenesis. *Apmis* 113 (11-12): 922-929.

92. Guilak F, Lott KE, Awad HA, Cao Q, Hicok KC, Fermor B, Gimble JM (2006). Clonal analysis of the differentiation potential of human adipose-derived adult stem cells. *J Cell Physiol* 206 (1): 229-237.

93. Hadj-Slimane R, Lepelletier Y, Lopez N, Garbay C, Raynaud F (2007). Short interfering RNA (siRNA), a novel therapeutic tool acting on angiogenesis. *Biochimie* 89 (10): 1234-1244.

94. Hai B, Yang Z, Millar SE, Choi YS, Taketo MM, Nagy A, Liu F (2010). Wnt/beta-catenin signaling regulates postnatal development and regeneration of the salivary gland. *Stem Cells Dev* 19 (11): 1793-1801.

95. Han J, Okada H, Takai H, Nakayama Y, Maeda T, Ogata Y (2009). Collection and culture of alveolar bone marrow multipotent mesenchymal stromal cells from older individuals. *J Cell Biochem* 107 (6): 1198-1204.

96. Hara-Kaonga B, Gao YA, Havrda M, Harrington A, Bergquist I, Liaw L (2006). Variable recombination efficiency in responder transgenes activated by Cre recombinase in the vasculature. *Transgenic Res* 15 (1): 101-106.

97. Harada H, Kettunen P, Jung HS, Mustonen T, Wang YA, Thesleff I (1999). Localization of putative stem cells in dental epithelium and their association with Notch and FGF signaling. *J Cell Biol* 147 (1): 105-120.

98. Hayashi Y, Yanagawa T, Yoshida H, Yura Y, Nitta T, Sato M (1985). Induction of other differentiation stages in neoplastic epithelial duct and myoepithelial cells from the human salivary gland grown in athymic nude mice. *Cancer* 55 (11): 2575-2583.

99. Heffernan M, Yousefi S, Dennis JW (1989). Molecular characterization of P2B/LAMP-1, a major protein target of a metastasis-associated oligosaccharide structure. *Cancer Res* 49 (21): 6077-6084.

100. Hemmat S, Lieberman DM, Most SP (2010). An introduction to stem cell biology. *Facial Plast Surg* 26 (5): 343-349.

101. Hoffman MP, Kidder BL, Steinberg ZL, Lakhani S, Ho S, Kleinman HK, Larsen M (2002). Gene expression profiles of mouse submandibular gland development: FGFR1 regulates branching morphogenesis in vitro through BMP- and FGF-dependent mechanisms. *Development* 129 (24): 5767-5778.

102. Honda MJ, Fong H, Iwatsuki S, Sumita Y, Sarikaya M (2008). Tooth-forming potential in embryonic and postnatal tooth bud cells. *Med Mol Morphol* 41 (4): 183-192.

103. Honda MJ, Imaizumi M, Tsuchiya S, Morsczeck C (2010). Dental follicle stem cells and tissue engineering. *J Oral Sci* 52 (4): 541-552.

104. Horan PK, Slezak SE (1989). Stable cell membrane labelling. *Nature* 340 (6229): 167-168.

105. Horwitz EM, Le Blanc K, Dominici M, Mueller I, Slaper-Cortenbach I, Marini FC, Deans RJ, Krause DS, Keating A (2005). Clarification of the nomenclature for MSC: The International Society for Cellular Therapy position statement. *Cytotherapy* 7 (5): 393-395.

106. Huang FJ, You WK, Bonaldo P, Seyfried TN, Pasquale EB, Stallcup WB (2010). Pericyte deficiencies lead to aberrant tumor vascularizaton in the brain of the NG2 null mouse. *Dev Biol* 344 (2): 1035-1046.

107. Huang G, Yamaza T, Shea LD, Djouad F, Kuhn NZ, Tuan R, Shi S (2009). Stem/progenitor Cell-Mediated De Novo Regeneration of Dental Pulp with Newly Deposited Continuous Layer of Dentin in an In Vivo Model. *Tissue Eng Part A*

108. Huang GT, Gronthos S, Shi S (2009). Mesenchymal stem cells derived from dental tissues vs. those from other sources: their biology and role in regenerative medicine. *J Dent Res* 88 (9): 792-806.

109. Huang GT, Shagramanova K, Chan SW (2006). Formation of odontoblast-like cells from cultured human dental pulp cells on dentin in vitro. *J Endod* 32 (11): 1066-1073.

110. Huang GT, Shagramanova K, Chan SW (2006). Formation of odontoblast-like cells from cultured human dental pulp cells on dentin in vitro. *Journal of Endodontics* 32 (11): 1066-1073.

111. Huang GT, Sonoyama W, Liu Y, Liu H, Wang S, Shi S (2008). The hidden treasure in apical papilla: the potential role in pulp/dentin regeneration and bioroot engineering. *J Endod* 34 (6): 645-651.

112. Hunt DP, Sajic M, Phillips H, Henderson D, Compston A, Smith K, Chandran S (2009). Origins of gliogenic stem cell populations within adult skin and bone marrow. *Stem Cells Dev* 19 (7): 1055-1065.

113. Huusko J, Merentie M, Dijkstra MH, Ryhanen MM, Karvinen H, Rissanen TT, Vanwildemeersch M, Hedman M, Lipponen J, Heinonen SE, Eriksson U, Shibuya M,

Yla-Herttuala S (2010). The effects of VEGF-R1 and VEGF-R2 ligands on angiogenic responses and left ventricular function in mice. *Cardiovasc Res* 86 (1): 122-130.

114. Ieronimakis N, Balasundaram G, Reyes M (2008). Direct isolation, culture and transplant of mouse skeletal muscle derived endothelial cells with angiogenic potential. *PLoS One* 3 (3): e0001753.

115. Ikeda E, Yagi K, Kojima M, Yagyuu T, Ohshima A, Sobajima S, Tadokoro M, Katsube Y, Isoda K, Kondoh M, Kawase M, Go MJ, Adachi H, Yokota Y, Kirita T, Ohgushi H (2008). Multipotent cells from the human third molar: feasibility of cell-based therapy for liver disease. *Differentiation* 76 (5): 495-505.

116. Ishii M, Koike C, Igarashi A, Yamanaka K, Pan H, Higashi Y, Kawaguchi H, Sugiyama M, Kamata N, Iwata T, Matsubara T, Nakamura K, Kurihara H, Tsuji K, Kato Y (2005). Molecular markers distinguish bone marrow mesenchymal stem cells from fibroblasts. *Biochem Biophys Res Commun* 332 (1): 297-303.

117. Izumi K, Feinberg SE, Terashi H, Marcelo CL (2003). Evaluation of transplanted tissue-engineered oral mucosa equivalents in severe combined immunodeficient mice. *Tissue Eng* 9 (1): 163-174.

118. Jackson DG, Prevo R, Clasper S, Banerji S (2001). LYVE-1, the lymphatic system and tumor lymphangiogenesis. *Trends Immunol* 22 (6): 317-321.

119. Janebodin K, Horst OV, Ieronimakis N, Balasundaram G, Reesukumal K, Pratumvinit B, Reyes M (2011). Isolation and characterization of neural crest-derived stem cells from dental pulp of neonatal mice. *PLoS One* 6 (11): e27526.

120. Janebodin K, Reyes M (2012). Neural Crest-Derived Dental Pulp Stem Cells Function as Ectomesenchyme to Support Salivary Gland Tissue Formation. *Dentistry* S13:001. doi:10.4172/2161-1122.S13-001

121. Jaskoll T, Abichaker G, Witcher D, Sala FG, Bellusci S, Hajihosseini MK, Melnick M (2005). FGF10/FGFR2b signaling plays essential roles during in vivo embryonic submandibular salivary gland morphogenesis. *BMC Dev Biol* 5 11.

122. Jaskoll T, Leo T, Witcher D, Ormestad M, Astorga J, Bringas P, Jr., Carlsson P, Melnick M (2004). Sonic hedgehog signaling plays an essential role during embryonic salivary gland epithelial branching morphogenesis. *Dev Dyn* 229 (4): 722-732.

123. Jaskoll T, Witcher D, Toreno L, Bringas P, Moon AM, Melnick M (2004). FGF8 dose-dependent regulation of embryonic submandibular salivary gland morphogenesis. *Dev Biol* 268 (2): 457-469.

124. Jaskoll T, Zhou YM, Chai Y, Makarenkova HP, Collinson JM, West JD, Hajihosseini MK, Lee J, Melnick M (2002). Embryonic submandibular gland morphogenesis: stage-specific protein localization of FGFs, BMPs, Pax6 and Pax9 in normal mice and abnormal SMG

phenotypes in FgfR2-IIIc(+/Delta), BMP7(-/-) and Pax6(-/-) mice. *Cells Tissues Organs* 170 (2-3): 83-98.

125. Ji X, Chen D, Xu C, Harris SE, Mundy GR, Yoneda T (2000). Patterns of gene expression associated with BMP-2-induced osteoblast and adipocyte differentiation of mesenchymal progenitor cell 3T3-F442A. *J Bone Miner Metab* 18 (3): 132-139.

126. Jiang Y, Henderson D, Blackstad M, Chen A, Miller RF, Verfaillie CM (2003). Neuroectodermal differentiation from mouse multipotent adult progenitor cells. *Proc Natl Acad Sci U S A* 100 Suppl 1 11854-11860.

127. Jiang Y, Jahagirdar BN, Reinhardt RL, Schwartz RE, Keene CD, Ortiz-Gonzalez XR, Reyes M, Lenvik T, Lund T, Blackstad M, Du J, Aldrich S, Lisberg A, Low WC, Largaespada DA, Verfaillie CM (2002). Pluripotency of mesenchymal stem cells derived from adult marrow. *Nature* 418 (6893): 41-49.

128. Johnstone B, Hering TM, Caplan AI, Goldberg VM, Yoo JU (1998). In vitro chondrogenesis of bone marrow-derived mesenchymal progenitor cells. *Exp Cell Res* 238 (1): 265-272.

129. Junker JP, Sommar P, Skog M, Johnson H, Kratz G (2010). Adipogenic, chondrogenic and osteogenic differentiation of clonally derived human dermal fibroblasts. *Cells Tissues Organs* 191 (2): 105-118.

130. Kadivar M, Khatami S, Mortazavi Y, Shokrgozar MA, Taghikhani M, Soleimani M (2006). In vitro cardiomyogenic potential of human umbilical vein-derived mesenchymal stem cells. *Biochem Biophys Res Commun* 340 (2): 639-647.

131. Kamnasaran D, Guha A (2005). Expression of GATA6 in the human and mouse central nervous system. *Brain Res Dev Brain Res* 160 (1): 90-95.

132. Kappas NC, Zeng G, Chappell JC, Kearney JB, Hazarika S, Kallianos KG, Patterson C, Annex BH, Bautch VL (2008). The VEGF receptor Flt-1 spatially modulates Flk-1 signaling and blood vessel branching. *J Cell Biol* 181 (5): 847-858.

133. Kerkis I, Kerkis A, Dozortsev D, Stukart-Parsons GC, Gomes Massironi SM, Pereira LV, Caplan AI, Cerruti HF (2006). Isolation and characterization of a population of immature dental pulp stem cells expressing OCT-4 and other embryonic stem cell markers. *Cells Tissues Organs* 184 (3-4): 105-116.

134. Khokhlatchev AV, Canagarajah B, Wilsbacher J, Robinson M, Atkinson M, Goldsmith E, Cobb MH (1998). Phosphorylation of the MAP kinase ERK2 promotes its homodimerization and nuclear translocation. *Cell* 93 (4): 605-615.

135. Kiel MJ, Morrison SJ (2006). Maintaining hematopoietic stem cells in the vascular niche. *Immunity* 25 (6): 862-864.

136. Kiernan J (ed) (2009) Histological and histochemical methods; theory and practice. Scion Publishing Ltd

137. Kiernan J (ed) (2009) Histological and histochemical methods; theory and practice. Scion Publishing Ltd.

138. Kilarski W, Bikfalvi A (2007). [Experimental approaches to study in vivo angiogenesis]. *Bull Cancer* 94 Spec No S166-169.

139. Kishi T, Takao T, Fujita K, Taniguchi H (2006). Clonal proliferation of multipotent stem/progenitor cells in the neonatal and adult salivary glands. *Biochem Biophys Res Commun* 340 (2): 544-552.

140. Kitamura C, Kimura K, Nakayama T, Terashita M (1999). Temporal and spatial expression of c-jun and jun-B proto-oncogenes in pulp cells involved with reparative dentinogenesis after cavity preparation of rat molars. *J Dent Res* 78 (2): 673-680.

141. Knox SM, Lombaert IM, Reed X, Vitale-Cross L, Gutkind JS, Hoffman MP (2010). Parasympathetic innervation maintains epithelial progenitor cells during salivary organogenesis. *Science* 329 (5999): 1645-1647.

142. Koch S, Tugues S, Li X, Gualandi L, Claesson-Welsh L (2012). Signal transduction by vascular endothelial growth factor receptors. *Biochem J* 437 (2): 169-183.

143. Kogler G, Sensken S, Airey JA, Trapp T, Muschen M, Feldhahn N, Liedtke S, Sorg RV, Fischer J, Rosenbaum C, Greschat S, Knipper A, Bender J, Degistirici O, Gao J, Caplan AI, Colletti EJ, Almeida-Porada G, Muller HW, Zanjani E, Wernet P (2004). A new human somatic stem cell from placental cord blood with intrinsic pluripotent differentiation potential. *J Exp Med* 200 (2): 123-135.

144. Krause DS, Theise ND, Collector MI, Henegariu O, Hwang S, Gardner R, Neutzel S, Sharkis SJ (2001). Multi-organ, multi-lineage engraftment by a single bone marrow-derived stem cell. *Cell* 105 (3): 369-377.

145. Kruger GM, Mosher JT, Bixby S, Joseph N, Iwashita T, Morrison SJ (2002). Neural crest stem cells persist in the adult gut but undergo changes in self-renewal, neuronal subtype potential, and factor responsiveness. *Neuron* 35 (4): 657-669.

146. Kullander K, Klein R (2002). Mechanisms and functions of Eph and ephrin signalling. *Nat Rev Mol Cell Biol* 3 (7): 475-486.

147. Kuratani SC, Kirby ML (1991). Initial migration and distribution of the cardiac neural crest in the avian embryo: an introduction to the concept of the circumpharyngeal crest. *Am J Anat* 191 (3): 215-227.

148. Lahteenvuo JE, Lahteenvuo MT, Kivela A, Rosenlew C, Falkevall A, Klar J, Heikura T, Rissanen TT, Vahakangas E, Korpisalo P, Enholm B, Carmeliet P, Alitalo K, Eriksson U, Yla-Herttuala S (2009). Vascular endothelial growth factor-B induces myocardium-

specific angiogenesis and arteriogenesis via vascular endothelial growth factor receptor-1- and neuropilin receptor-1-dependent mechanisms. *Circulation* 119 (6): 845-856.

149. Laino G, Carinci F, Graziano A, d'Aquino R, Lanza V, De Rosa A, Gombos F, Caruso F, Guida L, Rullo R, Menditti D, Papaccio G (2006). In vitro bone production using stem cells derived from human dental pulp. *J Craniofac Surg* 17 (3): 511-515.

150. Laino G, d'Aquino R, Graziano A, Lanza V, Carinci F, Naro F, Pirozzi G, Papaccio G (2005). A new population of human adult dental pulp stem cells: a useful source of living autologous fibrous bone tissue (LAB). *J Bone Miner Res* 20 (8): 1394-1402.

151. Laino G, Graziano A, d'Aquino R, Pirozzi G, Lanza V, Valiante S, De Rosa A, Naro F, Vivarelli E, Papaccio G (2006). An approachable human adult stem cell source for hard-tissue engineering. *J Cell Physiol* 206 (3): 693-701.

152. Lawson KA (1972). The role of mesenchyme in the morphogenesis and functional differentiation of rat salivary epithelium. *J Embryol Exp Morphol* 27 (3): 497-513.

153. Le Douarin NM, Creuzet S, Couly G, Dupin E (2004). Neural crest cell plasticity and its limits. *Development* 131 (19): 4637-4650.

154. Le Douarin NM, Teillet MA (1973). The migration of neural crest cells to the wall of the digestive tract in avian embryo. *J Embryol Exp Morphol* 30 (1): 31-48.

155. Lee DS, Park JT, Kim HM, Ko JS, Son HH, Gronostajski RM, Cho MI, Choung PH, Park JC (2009). Nuclear factor I-C is essential for odontogenic cell proliferation and odontoblast differentiation during tooth root development. *J Biol Chem* 284 (25): 17293-17303.

156. Lefebvre V, Huang W, Harley VR, Goodfellow PN, de Crombrugghe B (1997). SOX9 is a potent activator of the chondrocyte-specific enhancer of the pro alpha1(II) collagen gene. *Mol Cell Biol* 17 (4): 2336-2346.

157. Li J, Goodyer CG, Fellows F, Wang R (2006). Stem cell factor/c-Kit interactions regulate human islet-epithelial cluster proliferation and differentiation. *Int J Biochem Cell Biol* 38 (5-6): 961-972.

158. Li X, Lee C, Tang Z, Zhang F, Arjunan P, Li Y, Hou X, Kumar A, Dong L (2009). VEGF-B: a survival, or an angiogenic factor? *Cell Adh Migr* 3 (4): 322-327.

159. Lian JB, Stein GS, Javed A, van Wijnen AJ, Stein JL, Montecino M, Hassan MQ, Gaur T, Lengner CJ, Young DW (2006). Networks and hubs for the transcriptional control of osteoblastogenesis. *Rev Endocr Metab Disord* 7 (1-2): 1-16.

160. Lin SL, Kisseleva T, Brenner DA, Duffield JS (2008). Pericytes and perivascular fibroblasts are the primary source of collagen-producing cells in obstructive fibrosis of the kidney. *Am J Pathol* 173 (6): 1617-1627.

161. Lin W, Jiang L, Chen Y, She F, Han S, Zhu J, Zhou L, Tang N, Wang X, Li X (2012). Vascular endothelial growth factor-D promotes growth, lymphangiogenesis and lymphatic metastasis in gallbladder cancer. *Cancer Lett* 314 (2): 127-136.

162. Lombaert IM, Brunsting JF, Wierenga PK, Faber H, Stokman MA, Kok T, Visser WH, Kampinga HH, de Haan G, Coppes RP (2008). Rescue of salivary gland function after stem cell transplantation in irradiated glands. *PLoS One* 3 (4): e2063.

163. Lombaert IM, Brunsting JF, Wierenga PK, Kampinga HH, de Haan G, Coppes RP (2008). Cytokine treatment improves parenchymal and vascular damage of salivary glands after irradiation. *Clin Cancer Res* 14 (23): 7741-7750.

164. Lombaert IM, Brunsting JF, Wierenga PK, Kampinga HH, de Haan G, Coppes RP (2008). Keratinocyte growth factor prevents radiation damage to salivary glands by expansion of the stem/progenitor pool. *Stem Cells* 26 (10): 2595-2601.

165. Long MA, Rossi FM (2009). Silencing inhibits Cre-mediated recombination of the Z/AP and Z/EG reporters in adult cells. *PLoS One* 4 (5): e5435.

166. Lovschall H, Mitsiadis TA, Poulsen K, Jensen KH, Kjeldsen AL (2007). Coexpression of Notch3 and Rgs5 in the pericyte-vascular smooth muscle cell axis in response to pulp injury. *Int J Dev Biol* 51 (8): 715-721.

167. Lovschall H, Tummers M, Thesleff I, Fuchtbauer EM, Poulsen K (2005). Activation of the Notch signaling pathway in response to pulp capping of rat molars. *Eur J Oral Sci* 113 (4): 312-317.

168. Ma T, Grayson WL, Frohlich M, Vunjak-Novakovic G (2009). Hypoxia and stem cell-based engineering of mesenchymal tissues. *Biotechnol Prog* 25 (1): 32-42.

169. Madan AK, Kramer B (2005). Immunolocalization of fibroblast growth factor-2 (FGF-2) during embryonic development of the rat submandibular gland. *Sadj* 60 (2): 58, 60-51.

170. Madeddu P (2005). Therapeutic angiogenesis and vasculogenesis for tissue regeneration. *Exp Physiol* 90 (3): 315-326.

171. Maherali N, Sridharan R, Xie W, Utikal J, Eminli S, Arnold K, Stadtfeld M, Yachechko R, Tchieu J, Jaenisch R, Plath K, Hochedlinger K (2007). Directly reprogrammed fibroblasts show global epigenetic remodeling and widespread tissue contribution. *Cell Stem Cell* 1 (1): 55-70.

172. Mahevas M, Vaida I, Le Page L, Sid-Idris S, Royer B, Garedi R, Damaj G, Duhaut P, Claisse JF, Ducroix JP, Marolleau JP (2008). Haematopoietic stem cell transplantation in the treatment of autoimmune diseases. *Rev Med Interne* 29 (2): 115-121.

173. Makarenkova HP, Hoffman MP, Beenken A, Eliseenkova AV, Meech R, Tsau C, Patel VN, Lang RA, Mohammadi M (2009). Differential interactions of FGFs with heparan sulfate control gradient formation and branching morphogenesis. *Sci Signal* 2 (88): ra55.

174. Man YG, Ball WD, Marchetti L, Hand AR (2001). Contributions of intercalated duct cells to the normal parenchyma of submandibular glands of adult rats. *Anat Rec* 263 (2): 202-214.

175. Mao JJ (2008). Stem cells and the future of dental care. *N Y State Dent J* 74 (2): 20-24.

176. Marchionni C, Bonsi L, Alviano F, Lanzoni G, Di Tullio A, Costa R, Montanari M, Tazzari PL, Ricci F, Pasquinelli G, Orrico C, Grossi A, Prati C, Bagnara GP (2009). Angiogenic potential of human dental pulp stromal (stem) cells. *International Journal of Immunopathology and Pharmacology* 22 (3): 699-706.

177. Maria OM, Maria O, Liu Y, Komarova SV, Tran SD (2011). Matrigel improves functional properties of human submandibular salivary gland cell line. *Int J Biochem Cell Biol* 43 (4): 622-631.

178. Maria OM, Zeitouni A, Gologan O, Tran SD (2011). Matrigel improves functional properties of primary human salivary gland cells. *Tissue Eng Part A* 17 (9-10): 1229-1238.

179. Martin BL, Kimelman D (2008). Regulation of canonical Wnt signaling by Brachyury is essential for posterior mesoderm formation. *Dev Cell* 15 (1): 121-133.

180. Marynka-Kalmani K, Treves S, Yafee M, Rachima H, Gafni Y, Cohen MA, Pitaru S (2010). The lamina propria of adult human oral mucosa harbors a novel stem cell population. *Stem Cells* 28 (5): 984-995.

181. Matsushita K, Motani R, Sakuta T, Yamaguchi N, Koga T, Matsuo K, Nagaoka S, Abeyama K, Maruyama I, Torii M (2000). The role of vascular endothelial growth factor in human dental pulp cells: induction of chemotaxis, proliferation, and differentiation and activation of the AP-1-dependent signaling pathway. *J Dent Res* 79 (8): 1596-1603.

182. McCollum M, Sharpe PT (2001). Evolution and development of teeth. *J Anat* 199 (Pt 1-2): 153-159.

183. Meulemans D, Bronner-Fraser M (2005). Central role of gene cooption in neural crest evolution. *J Exp Zool B Mol Dev Evol* 304 (4): 298-303.

184. Miki T, Lehmann T, Cai H, Stolz DB, Strom SC (2005). Stem cell characteristics of amniotic epithelial cells. *Stem Cells* 23 (10): 1549-1559.

185. Mikkelsen TS, Hanna J, Zhang X, Ku M, Wernig M, Schorderet P, Bernstein BE, Jaenisch R, Lander ES, Meissner A (2008). Dissecting direct reprogramming through integrative genomic analysis. *Nature* 454 (7200): 49-55.

186. Millauer B, Shawver LK, Plate KH, Risau W, Ullrich A (1994). Glioblastoma growth inhibited in vivo by a dominant-negative Flk-1 mutant. *Nature* 367 (6463): 576-579.

187. Millauer B, Wizigmann-Voos S, Schnurch H, Martinez R, Moller NP, Risau W, Ullrich A (1993). High affinity VEGF binding and developmental expression suggest Flk-1 as a major regulator of vasculogenesis and angiogenesis. *Cell* 72 (6): 835-846.

188. Miura M, Gronthos S, Zhao M, Lu B, Fisher LW, Robey PG, Shi S (2003). SHED: stem cells from human exfoliated deciduous teeth. *Proc Natl Acad Sci U S A* 100 (10): 5807-5812.

189. Morita K, Nogawa H (1999). EGF-dependent lobule formation and FGF7-dependent stalk elongation in branching morphogenesis of mouse salivary epithelium in vitro. *Dev Dyn* 215 (2): 148-154.

190. Morrison SJ, White PM, Zock C, Anderson DJ (1999). Prospective identification, isolation by flow cytometry, and in vivo self-renewal of multipotent mammalian neural crest stem cells. *Cell* 96 (5): 737-749.

191. Morsczeck C, Gotz W, Schierholz J, Zeilhofer F, Kuhn U, Mohl C, Sippel C, Hoffmann KH (2005). Isolation of precursor cells (PCs) from human dental follicle of wisdom teeth. *Matrix Biol* 24 (2): 155-165.

192. Mothe AJ, Tator CH (2012). Advances in stem cell therapy for spinal cord injury. *J Clin Invest* 122 (11): 3824-3834.

193. Motoike T, Loughna S, Perens E, Roman BL, Liao W, Chau TC, Richardson CD, Kawate T, Kuno J, Weinstein BM, Stainier DY, Sato TN (2000). Universal GFP reporter for the study of vascular development. *Genesis* 28 (2): 75-81.

194. Mummery C, Ward-van Oostwaard D, Doevendans P, Spijker R, van den Brink S, Hassink R, van der Heyden M, Opthof T, Pera M, de la Riviere AB, Passier R, Tertoolen L (2003). Differentiation of human embryonic stem cells to cardiomyocytes: role of coculture with visceral endoderm-like cells. *Circulation* 107 (21): 2733-2740.

195. Murphy M, Bernard O, Reid K, Bartlett PF (1991). Cell lines derived from mouse neural crest are representative of cells at various stages of differentiation. *J Neurobiol* 22 (5): 522-535.

196. Nakagawa M, Koyanagi M, Tanabe K, Takahashi K, Ichisaka T, Aoi T, Okita K, Mochiduki Y, Takizawa N, Yamanaka S (2008). Generation of induced pluripotent stem cells without Myc from mouse and human fibroblasts. *Nat Biotechnol* 26 (1): 101-106.

197. Nakashima K, Zhou X, Kunkel G, Zhang Z, Deng JM, Behringer RR, de Crombrugghe B (2002). The novel zinc finger-containing transcription factor osterix is required for osteoblast differentiation and bone formation. *Cell* 108 (1): 17-29.

198. Nakashima M, Iohara K, Zheng L (2006). Gene therapy for dentin regeneration with bone morphogenetic proteins. *Curr Gene Ther* 6 (5): 551-560.

199. Nanduri LS, Maimets M, Pringle SA, van der Zwaag M, van Os RP, Coppes RP (2011). Regeneration of irradiated salivary glands with stem cell marker expressing cells. *Radiother Oncol* 99 (3): 367-372.

200. Napenas JJ, Brennan MT, Fox PC (2009). Diagnosis and treatment of xerostomia (dry mouth). *Odontology* 97 (2): 76-83.

201. Nehls V, Drenckhahn D (1993). The versatility of microvascular pericytes: from mesenchyme to smooth muscle? *Histochemistry* 99 (1): 1-12.

202. Nishiyama A, Yang Z, Butt A (2005). Astrocytes and NG2-glia: what's in a name? *J Anat* 207 (6): 687-693.

203. Norrby K (2006). In vivo models of angiogenesis. *J Cell Mol Med* 10 (3): 588-612.

204. Noth U, Rackwitz L, Heymer A, Weber M, Baumann B, Steinert A, Schutze N, Jakob F, Eulert J (2007). Chondrogenic differentiation of human mesenchymal stem cells in collagen type I hydrogels. *J Biomed Mater Res A* 83 (3): 626-635.

205. O'Connor TP, Crystal RG (2006). Genetic medicines: treatment strategies for hereditary disorders. *Nat Rev Genet* 7 (4): 261-276.

206. Oesser S, Seifert J (2003). Stimulation of type II collagen biosynthesis and secretion in bovine chondrocytes cultured with degraded collagen. *Cell Tissue Res* 311 (3): 393-399.

207. Ohno M, Nakamura T, Kunimoto Y, Nishimura K, Chung-Kang C, Kuroda Y (2003). Lymphagenesis correlates with expression of vascular endothelial growth factor-C in colorectal cancer. *Oncol Rep* 10 (4): 939-943.

208. Okumura K SM, Endo F. (2012). Capability of Tissue Stem Cells to Organize into Salivary Rudiments. *Stem Cells Int* 2012 (502136): 1-11.

209. Orpana A, Salven P (2002). Angiogenic and lymphangiogenic molecules in hematological malignancies. *Leuk Lymphoma* 43 (2): 219-224.

210. Papagerakis P, Berdal A, Mesbah M, Peuchmaur M, Malaval L, Nydegger J, Simmer J, Macdougall M (2002). Investigation of osteocalcin, osteonectin, and dentin sialophosphoprotein in developing human teeth. *Bone* 30 (2): 377-385.

211. Partanen TA, Arola J, Saaristo A, Jussila L, Ora A, Miettinen M, Stacker SA, Achen MG, Alitalo K (2000). VEGF-C and VEGF-D expression in neuroendocrine cells and their receptor, VEGFR-3, in fenestrated blood vessels in human tissues. *Faseb J* 14 (13): 2087-2096.

212. Patel VN, Rebustini IT, Hoffman MP (2006). Salivary gland branching morphogenesis. *Differentiation* 74 (7): 349-364.

213. Pavlov MI, Sautier JM, Oboeuf M, Asselin A, Berdal A (2003). Chondrogenic differentiation during midfacial development in the mouse: in vivo and in vitro studies. *Biol Cell* 95 (2): 75-86.

214. Pittenger MF, Mackay AM, Beck SC, Jaiswal RK, Douglas R, Mosca JD, Moorman MA, Simonetti DW, Craig S, Marshak DR (1999). Multilineage potential of adult human mesenchymal stem cells. *Science* 284 (5411): 143-147.

215. Ponticelli S, Marasco D, Tarallo V, Albuquerque RJ, Mitola S, Takeda A, Stassen JM, Presta M, Ambati J, Ruvo M, De Falco S (2008). Modulation of angiogenesis by a tetrameric tripeptide that antagonizes vascular endothelial growth factor receptor 1. *J Biol Chem* 283 (49): 34250-34259.

216. Pradhan S, Liu C, Zhang C, Jia X, Farach-Carson MC, Witt RL Lumen formation in three-dimensional cultures of salivary acinar cells. *Otolaryngol Head Neck Surg* 142 (2): 191-195.

217. Prescott RS, Alsanea R, Fayad MI, Johnson BR, Wenckus CS, Hao J, John AS, George A (2008). In vivo generation of dental pulp-like tissue by using dental pulp stem cells, a collagen scaffold, and dentin matrix protein 1 after subcutaneous transplantation in mice. *J Endod* 34 (4): 421-426.

218. Randall VA, Jenner TJ, Hibberts NA, De Oliveira IO, Vafaee T (2008). Stem cell factor/c-Kit signalling in normal and androgenetic alopecia hair follicles. *J Endocrinol* 197 (1): 11-23.

219. Ranly DM (1998). Early orofacial development. *J Clin Pediatr Dent* 22 (4): 267-275.

220. Rao MS, Anderson DJ (1997). Immortalization and controlled in vitro differentiation of murine multipotent neural crest stem cells. *J Neurobiol* 32 (7): 722-746.

221. Ratajczak MZ, Machalinski B, Wojakowski W, Ratajczak J, Kucia M (2007). A hypothesis for an embryonic origin of pluripotent Oct-4(+) stem cells in adult bone marrow and other tissues. *Leukemia* 21 (5): 860-867.

222. Redman RS, Sreebny LM (1971). Morphologic and biochemical observations on the development of the rat parotid gland. *Dev Biol* 25 (2): 248-279.

223. Reyes M, Li S, Foraker J, Kimura E, Chamberlain JS (2005). Donor origin of multipotent adult progenitor cells in radiation chimeras. *Blood* 106 (10): 3646-3649.

224. Riazi AM, Kwon SY, Stanford WL (2009). Stem cell sources for regenerative medicine. *Methods Mol Biol* 482 55-90.

225. Ribatti D (2005). The crucial role of vascular permeability factor/vascular endothelial growth factor in angiogenesis: a historical review. *Br J Haematol* 128 (3): 303-309.

226. Roberts-Clark DJ, Smith AJ (2000). Angiogenic growth factors in human dentine matrix. *Arch Oral Biol* 45 (11): 1013-1016.

227. Robison WG, Jr., McCaleb ML, Feld LG, Michaelis OEt, Laver N, Mercandetti M (1991). Degenerated intramural pericytes ('ghost cells') in the retinal capillaries of diabetic rats. *Curr Eye Res* 10 (4): 339-350.

228. Rolletschek A, Blyszczuk P, Wobus AM (2004). Embryonic stem cell-derived cardiac, neuronal and pancreatic cells as model systems to study toxicological effects. *Toxicol Lett* 149 (1-3): 361-369.

229. Ross JJ, Hong Z, Willenbring B, Zeng L, Isenberg B, Lee EH, Reyes M, Keirstead SA, Weir EK, Tranquillo RT, Verfaillie CM (2006). Cytokine-induced differentiation of multipotent adult progenitor cells into functional smooth muscle cells. *J Clin Invest* 116 (12): 3139-3149.

230. Rossi CA, Pozzobon M, Ditadi A, Archacka K, Gastaldello A, Sanna M, Franzin C, Malerba A, Milan G, Cananzi M, Schiaffino S, Campanella M, Vettor R, De Coppi P (2010). Clonal characterization of rat muscle satellite cells: proliferation, metabolism and differentiation define an intrinsic heterogeneity. *PLoS One* 5 (1): e8523.

231. Ryu JS, Ko K, Lee JW, Park SB, Byun SJ, Jeong EJ, Ko K, Choo YK (2009). Gangliosides are involved in neural differentiation of human dental pulp-derived stem cells. *Biochem Biophys Res Commun* 387 (2): 266-271.

232. Sacco A, Doyonnas R, LaBarge MA, Hammer MM, Kraft P, Blau HM (2005). IGF-I increases bone marrow contribution to adult skeletal muscle and enhances the fusion of myelomonocytic precursors. *J Cell Biol* 171 (3): 483-492.

233. Saga Y, Hata N, Koseki H, Taketo MM (1997). Mesp2: a novel mouse gene expressed in the presegmented mesoderm and essential for segmentation initiation. *Genes Dev* 11 (14): 1827-1839.

234. Sato M, Hayashi Y, Yanagawa T, Yoshida H, Yura Y, Azuma M, Ueno A (1985). Intermediate-sized filaments and specific markers in a human salivary gland adenocarcinoma cell line and its nude mouse tumors. *Cancer Res* 45 (8): 3878-3890.

235. Satomura K, Krebsbach P, Bianco P, Gehron Robey P (2000). Osteogenic imprinting upstream of marrow stromal cell differentiation. *J Cell Biochem* 78 (3): 391-403.

236. Sawada K, Konishi Y, Tominaga M, Watanabe Y, Hirano J, Inoue S, Kageyama R, Blum M, Tominaga A (2000). Goosecoid suppresses cell growth and enhances neuronal differentiation of PC12 cells. *J Cell Sci* 113 (Pt 15) 2705-2713.

237. Sawamiphak S, Seidel S, Essmann CL, Wilkinson GA, Pitulescu ME, Acker T, Acker-Palmer A (2010). Ephrin-B2 regulates VEGFR2 function in developmental and tumour angiogenesis. *Nature* 465 (7297): 487-491.

238. Schupbach P, Gaberthuel T, Lutz F, Guggenheim B (1993). Periodontal repair or regeneration: structures of different types of new attachment. *J Periodontal Res* 28 (4): 281-293.

239. Sedgley CM, Botero TM (2012). Dental stem cells and their sources. *Dent Clin North Am* 56 (3): 549-561.

240. Seetharam L, Gotoh N, Maru Y, Neufeld G, Yamaguchi S, Shibuya M (1995). A unique signal transduction from FLT tyrosine kinase, a receptor for vascular endothelial growth factor VEGF. *Oncogene* 10 (1): 135-147.

241. Seo BM, Miura M, Gronthos S, Bartold PM, Batouli S, Brahim J, Young M, Robey PG, Wang CY, Shi S (2004). Investigation of multipotent postnatal stem cells from human periodontal ligament. *Lancet* 364 (9429): 149-155.

242. Seo BM, Miura M, Sonoyama W, Coppe C, Stanyon R, Shi S (2005). Recovery of stem cells from cryopreserved periodontal ligament. *J Dent Res* 84 (10): 907-912.

243. Seo BM, Sonoyama W, Yamaza T, Coppe C, Kikuiri T, Akiyama K, Lee JS, Shi S (2008). SHED repair critical-size calvarial defects in mice. *Oral Dis* 14 (5): 428-434.

244. Serbedzija GN, Bronner-Fraser M, Fraser SE (1992). Vital dye analysis of cranial neural crest cell migration in the mouse embryo. *Development* 116 (2): 297-307.

245. Sharpe PT (2001). Neural crest and tooth morphogenesis. *Adv Dent Res* 15 4-7.

246. Shi S, Bartold PM, Miura M, Seo BM, Robey PG, Gronthos S (2005). The efficacy of mesenchymal stem cells to regenerate and repair dental structures. *Orthod Craniofac Res* 8 (3): 191-199.

247. Shi S, Gronthos S (2003). Perivascular niche of postnatal mesenchymal stem cells in human bone marrow and dental pulp. *J Bone Miner Res* 18 (4): 696-704.

248. Shi S, Robey PG, Gronthos S (2001). Comparison of human dental pulp and bone marrow stromal stem cells by cDNA microarray analysis. *Bone* 29 (6): 532-539.

249. Shibuya M (2001). Structure and function of VEGF/VEGF-receptor system involved in angiogenesis. *Cell Struct Funct* 26 (1): 25-35.

250. Shirasuna K, Sato M, Miyazaki T (1981). A neoplastic epithelial duct cell line established from an irradiated human salivary gland. *Cancer* 48 (3): 745-752.

251. Sieber-Blum M, Hu Y (2008). Epidermal neural crest stem cells (EPI-NCSC) and pluripotency. *Stem Cell Rev* 4 (4): 256-260.

252. Sieber-Blum M, Hu Y (2008). Epidermal neural crest stem cells (EPI-NCSC) and pluripotency. *Stem Cell Reveiws* 4 (4): 256-260.

253. Singhatanadgit W, Donos N, Olsen I (2009). Isolation and characterization of stem cell clones from adult human ligament. *Tissue Eng Part A* 15 (9): 2625-2636.

254. Siqueira da Fonseca SA, Abdelmassih S, de Mello Cintra Lavagnolli T, Serafim RC, Clemente Santos EJ, Mota Mendes C, de Souza Pereira V, Ambrosio CE, Miglino MA, Visintin JA, Abdelmassih R, Kerkis A, Kerkis I (2009). Human immature dental pulp stem cells' contribution to developing mouse embryos: production of human/mouse preterm chimaeras. *Cell Prolif* 42 (2): 132-140.

255. Slack JM (2008). Origin of stem cells in organogenesis. *Science* 322 (5907): 1498-1501.

256. Sloan AJ, Smith AJ (2007). Stem cells and the dental pulp: potential roles in dentine regeneration and repair. *Oral Dis* 13 (2): 151-157.

257. Sloan AJ, Waddington RJ (2009). Dental pulp stem cells: what, where, how? *Int J Paediatr Dent* 19 (1): 61-70.

258. Sommer B, Bickel M, Hofstetter W, Wetterwald A (1996). Expression of matrix proteins during the development of mineralized tissues. *Bone* 19 (4): 371-380.

259. Sonoyama W, Liu Y, Fang D, Yamaza T, Seo BM, Zhang C, Liu H, Gronthos S, Wang CY, Wang S, Shi S (2006). Mesenchymal stem cell-mediated functional tooth regeneration in swine. *PLoS One* 1 e79.

260. Sonoyama W, Liu Y, Yamaza T, Tuan RS, Wang S, Shi S, Huang GT (2008). Characterization of the apical papilla and its residing stem cells from human immature permanent teeth: a pilot study. *J Endod* 34 (2): 166-171.

261. Spath L, Rotilio V, Alessandrini M, Gambara G, De Angelis L, Mancini M, Mitsiadis TA, Vivarelli E, Naro F, Filippini A, Papaccio G (2009). Explant-derived human dental pulp stem cells enhance differentiation and proliferation potentials. *J Cell Mol Med* 14 (6B): 1635-1644.

262. Spath L, Rotilio V, Alessandrini M, Gambara G, De Angelis L, Mancini M, Mitsiadis TA, Vivarelli E, Naro F, Filippini A, Papaccio G (2009). Explant-Derived Human Dental Pulp Stem Cells Enhance Differentiation and Proliferation Potentials. *J Cell Mol Med*

263. Stevens A, Zuliani T, Olejnik C, LeRoy H, Obriot H, Kerr-Conte J, Formstecher P, Bailliez Y, Polakowska RR (2008). Human dental pulp stem cells differentiate into neural crest-derived melanocytes and have label-retaining and sphere-forming abilities. *Stem Cells Dev* 17 (6): 1175-1184.

264. Stokowski A, Shi S, Sun T, Bartold PM, Koblar SA, Gronthos S (2007). EphB/ephrin-B interaction mediates adult stem cell attachment, spreading, and migration: implications for dental tissue repair. *Stem Cells* 25 (1): 156-164.

265. Takahashi K, Tanabe K, Ohnuki M, Narita M, Ichisaka T, Tomoda K, Yamanaka S (2007). Induction of pluripotent stem cells from adult human fibroblasts by defined factors. *Cell* 131 (5): 861-872.

266. Takahashi K, Yamanaka S (2006). Induction of pluripotent stem cells from mouse embryonic and adult fibroblast cultures by defined factors. *Cell* 126 (4): 663-676.

267. Takakura N, Yoshida H, Ogura Y, Kataoka H, Nishikawa S, Nishikawa S (1997). PDGFR alpha expression during mouse embryogenesis: immunolocalization analyzed by whole-mount immunohistostaining using the monoclonal anti-mouse PDGFR alpha antibody APA5. *J Histochem Cytochem* 45 (6): 883-893.

268. Tapp H, Hanley EN, Jr., Patt JC, Gruber HE (2009). Adipose-derived stem cells: characterization and current application in orthopaedic tissue repair. *Exp Biol Med (Maywood)* 234 (1): 1-9.

269. Tavazoie M, Van der Veken L, Silva-Vargas V, Louissaint M, Colonna L, Zaidi B, Garcia-Verdugo JM, Doetsch F (2008). A specialized vascular niche for adult neural stem cells. *Cell Stem Cell* 3 (3): 279-288.

270. Terpe HJ, Stark H, Prehm P, Gunthert U (1994). CD44 variant isoforms are preferentially expressed in basal epithelial of non-malignant human fetal and adult tissues. *Histochemistry* 101 (2): 79-89.

271. Tessarollo L, Tsoulfas P, Martin-Zanca D, Gilbert DJ, Jenkins NA, Copeland NG, Parada LF (1993). trkC, a receptor for neurotrophin-3, is widely expressed in the developing nervous system and in non-neuronal tissues. *Development* 118 (2): 463-475.

272. Thesleff I (2003). Developmental biology and building a tooth. *Quintessence Int* 34 (8): 613-620.

273. Thesleff I (2003). Epithelial-mesenchymal signalling regulating tooth morphogenesis. *J Cell Sci* 116 (Pt 9): 1647-1648.

274. Thesleff I (2003). Epithelial-mesenchymal signalling regulating tooth morphogenesis. *Journal of Cell Science* 116 (9): 1647-1648.

275. Thesleff I, Tummers M (2003). Stem cells and tissue engineering: prospects for regenerating tissues in dental practice. *Med Princ Pract* 12 Suppl 1 43-50.

276. Thompson TJ, Owens PD, Wilson DJ (1989). Intramembranous osteogenesis and angiogenesis in the chick embryo. *J Anat* 166 55-65.

277. Thomson JA, Itskovitz-Eldor J, Shapiro SS, Waknitz MA, Swiergiel JJ, Marshall VS, Jones JM (1998). Embryonic stem cell lines derived from human blastocysts. *Science* 282 (5391): 1145-1147.

278. Tibbitts D, Rao RR, Shin S, West FD, Stice SL (2006). Uniform adherent neural progenitor populations from rhesus embryonic stem cells. *Stem Cells Dev* 15 (2): 200-208.

279. Tomar GB, Srivastava RK, Gupta N, Barhanpurkar AP, Pote ST, Jhaveri HM, Mishra GC, Wani MR (2010). Human gingiva-derived mesenchymal stem cells are superior to bone marrow-derived mesenchymal stem cells for cell therapy in regenerative medicine. *Biochem Biophys Res Commun* 393 (3): 377-383.

280. Tomita Y, Matsumura K, Wakamatsu Y, Matsuzaki Y, Shibuya I, Kawaguchi H, Ieda M, Kanakubo S, Shimazaki T, Ogawa S, Osumi N, Okano H, Fukuda K (2005). Cardiac neural crest cells contribute to the dormant multipotent stem cell in the mammalian heart. *J Cell Biol* 170 (7): 1135-1146.

281. Torreggiani E, Lisignoli G, Manferdini C, Lambertini E, Penolazzi L, Vecchiatini R, Gabusi E, Chieco P, Facchini A, Gambari R, Piva R (2011). Role of Slug transcription factor in human mesenchymal stem cells. *J Cell Mol Med*

282. Trainor PA (2005). Specification and patterning of neural crest cells during craniofacial development. *Brain Behav Evol* 66 (4): 266-280.

283. Tran-Hung L, Mathieu S, About I (2006). Role of human pulp fibroblasts in angiogenesis. *J Dent Res* 85 (9): 819-823.

284. Trounson A (2006). The production and directed differentiation of human embryonic stem cells. *Endocr Rev* 27 (2): 208-219.

285. Trowbridge HO (2003). Pulp biology: progress during the past 25 years. *Aust Endod J* 29 (1): 5-12.

286. Tscheudschilsuren G, Bosserhoff AK, Schlegel J, Vollmer D, Anton A, Alt V, Schnettler R, Brandt J, Proetzel G (2006). Regulation of mesenchymal stem cell and chondrocyte differentiation by MIA. *Exp Cell Res* 312 (1): 63-72.

287. Tucker A, Sharpe P (2004). The cutting-edge of mammalian development; how the embryo makes teeth. *Nat Rev Genet* 5 (7): 499-508.

288. Tucker AS (2007). Salivary gland development. *Semin Cell Dev Biol* 18 (2): 237-244.

289. Vag J, Byrne EM, Hughes DH, Hoffman M, Ambudkar I, Maguire P, O'Connell BC (2007). Morphological and functional differentiation of HSG cells: role of extracellular matrix and trpc 1. *J Cell Physiol* 212 (2): 416-423.

290. Waddington RJ, Youde SJ, Lee CP, Sloan AJ (2009). Isolation of distinct progenitor stem cell populations from dental pulp. *Cells Tissues Organs* 189 (1-4): 268-274.

291. Wafai R, Tudor EM, Angus JA, Wright CE (2009). Vascular effects of FGF-2 and VEGF-B in rabbits with bilateral hind limb ischemia. *J Vasc Res* 46 (1): 45-54.

292. Waltenberger J, Claesson-Welsh L, Siegbahn A, Shibuya M, Heldin CH (1994). Different signal transduction properties of KDR and Flt1, two receptors for vascular endothelial growth factor. *J Biol Chem* 269 (43): 26988-26995.

293. Wang J, Wang X, Sun Z, Wang X, Yang H, Shi S, Wang S (2010). Stem cells from human-exfoliated deciduous teeth can differentiate into dopaminergic neuron-like cells. *Stem Cells Dev* 19 (9): 1375-1383.

294. Wang L, Shen H, Zheng W, Tang L, Yang Z, Gao Y, Yang Q, Wang C, Duan Y, Jin Y (2011). Characterization of stem cells from alveolar periodontal ligament. *Tissue Eng Part A* 17 (7-8): 1015-1026.

295. Wang Q, Huang C, Zeng F, Xue M, Zhang X (2010). Activation of the Hh pathway in periosteum-derived mesenchymal stem cells induces bone formation in vivo: implication for postnatal bone repair. *Am J Pathol* 177 (6): 3100-3111.

296. Wang WG, Lou SQ, Ju XD, Xia K, Xia JH (2003). In vitro chondrogenesis of human bone marrow-derived mesenchymal progenitor cells in monolayer culture: activation by transfection with TGF-beta2. *Tissue Cell* 35 (1): 69-77.

297. Wang Y, Nakayama M, Pitulescu ME, Schmidt TS, Bochenek ML, Sakakibara A, Adams S, Davy A, Deutsch U, Luthi U, Barberis A, Benjamin LE, Makinen T, Nobes CD, Adams RH (2010). Ephrin-B2 controls VEGF-induced angiogenesis and lymphangiogenesis. *Nature* 465 (7297): 483-486.

298. Wang Z, Wang DZ, Pipes GC, Olson EN (2003). Myocardin is a master regulator of smooth muscle gene expression. *Proc Natl Acad Sci U S A* 100 (12): 7129-7134.

299. Watanabe D, Suzuma K, Suzuma I, Ohashi H, Ojima T, Kurimoto M, Murakami T, Kimura T, Takagi H (2005). Vitreous levels of angiopoietin 2 and vascular endothelial growth factor in patients with proliferative diabetic retinopathy. *Am J Ophthalmol* 139 (3): 476-481.

300. Wernig M, Meissner A, Foreman R, Brambrink T, Ku M, Hochedlinger K, Bernstein BE, Jaenisch R (2007). In vitro reprogramming of fibroblasts into a pluripotent ES-cell-like state. *Nature* 448 (7151): 318-324.

301. Winkler EA, Bell RD, Zlokovic BV (2010). Pericyte-specific expression of PDGF beta receptor in mouse models with normal and deficient PDGF beta receptor signaling. *Mol Neurodegener* 5 32.

302. Wislet-Gendebien S, Laudet E, Neirinckx V, Rogister B (2012). Adult Bone Marrow: Which Stem Cells for Cellular Therapy Protocols in Neurodegenerative Disorders? *J. Biomed. Biotechnol.* 2012 (601560): 1-10.

303. Wobus AM, Boheler KR (2005). Embryonic stem cells: prospects for developmental biology and cell therapy. *Physiol Rev* 85 (2): 635-678.

304. Wong C, Jin ZG (2005). Protein kinase C-dependent protein kinase D activation modulates ERK signal pathway and endothelial cell proliferation by vascular endothelial growth factor. *J Biol Chem* 280 (39): 33262-33269.

305. Xian X, Hakansson J, Stahlberg A, Lindblom P, Betsholtz C, Gerhardt H, Semb H (2006). Pericytes limit tumor cell metastasis. *J Clin Invest* 116 (3): 642-651.

306. Xing R, Regezi JA, Stern M, Shuster S, Stern R (1998). Hyaluronan and CD44 expression in minor salivary gland tumors. *Oral Dis* 4 (4): 241-247.

307. Yamamoto S, Fukumoto E, Yoshizaki K, Iwamoto T, Yamada A, Tanaka K, Suzuki H, Aizawa S, Arakaki M, Yuasa K, Oka K, Chai Y, Nonaka K, Fukumoto S (2008). Platelet-derived growth factor receptor regulates salivary gland morphogenesis via fibroblast growth factor expression. *J Biol Chem* 283 (34): 23139-23149.

308. Yamauchi Y, Abe K, Mantani A, Hitoshi Y, Suzuki M, Osuzu F, Kuratani S, Yamamura K (1999). A novel transgenic technique that allows specific marking of the neural crest cell lineage in mice. *Dev Biol* 212 (1): 191-203.

309. Yang X, Walboomers XF, van den Beucken JJ, Bian Z, Fan M, Jansen JA (2009). Hard Tissue Formation of STRO-1-Selected Rat Dental Pulp Stem Cells In Vivo. *Tissue Eng Part A* 15 (2): 367-375.

310. Yoshida S, Ohshima H (1996). Distribution and organization of peripheral capillaries in dental pulp and their relationship to odontoblasts. *Anat Rec* 245 (2): 313-326.

311. Yu J, Vodyanik MA, Smuga-Otto K, Antosiewicz-Bourget J, Frane JL, Tian S, Nie J, Jonsdottir GA, Ruotti V, Stewart R, Slukvin, II, Thomson JA (2007). Induced pluripotent stem cell lines derived from human somatic cells. *Science* 318 (5858): 1917-1920.

312. Yu J, Wang Y, Deng Z, Tang L, Li Y, Shi J, Jin Y (2007). Odontogenic capability: bone marrow stromal stem cells versus dental pulp stem cells. *Biol Cell* 99 (8): 465-474.

313. Zachary I (2001). Signaling mechanisms mediating vascular protective actions of vascular endothelial growth factor. *Am J Physiol Cell Physiol* 280 (6): C1375-1386.

314. Zhang F, Tang Z, Hou X, Lennartsson J, Li Y, Koch AW, Scotney P, Lee C, Arjunan P, Dong L, Kumar A, Rissanen TT, Wang B, Nagai N, Fons P, Fariss R, Zhang Y, Wawrousek E, Tansey G, Raber J, Fong GH, Ding H, Greenberg DA, Becker KG, Herbert JM, Nash A, Yla-Herttuala S, Cao Y, Watts RJ, Li X (2009). VEGF-B is dispensable for blood vessel growth but critical for their survival, and VEGF-B targeting inhibits pathological angiogenesis. *Proc Natl Acad Sci U S A* 106 (15): 6152-6157.

315. Zhang J, Duan X, Zhang H, Deng Z, Zhou Z, Wen N, Smith AJ, Zhao W, Jin Y (2006). Isolation of neural crest-derived stem cells from rat embryonic mandibular processes. *Biol Cell* 98 (10): 567-575.

316. Zhang P, Andrianakos R, Yang Y, Liu C, Lu W (2010). Kruppel-like factor 4 (Klf4) prevents embryonic stem (ES) cell differentiation by regulating Nanog gene expression. *J Biol Chem* 285 (12): 9180-9189.

317. Zhang W, Walboomers XF, Shi S, Fan M, Jansen JA (2006). Multilineage differentiation potential of stem cells derived from human dental pulp after cryopreservation. *Tissue Eng* 12 (10): 2813-2823.

318. Zhang W, Walboomers XF, van Osch GJ, van den Dolder J, Jansen JA (2008). Hard tissue formation in a porous HA/TCP ceramic scaffold loaded with stromal cells derived from dental pulp and bone marrow. *Tissue Eng Part A* 14 (2): 285-294.

319. Zhang W, Walboomers XF, Wolke JG, Bian Z, Fan MW, Jansen JA (2005). Differentiation ability of rat postnatal dental pulp cells in vitro. *Tissue Eng* 11 (3-4): 357-368.

320. Zhao X, Gong P, Lin Y, Wang J, Yang X, Cai X (2012). Characterization of alpha-smooth muscle actin positive cells during multilineage differentiation of dental pulp stem cells. *Cell Prolif.* 45 259-265.

321. Zheng C, Cotrim AP, Rowzee A, Swaim W, Sowers A, Mitchell JB, Baum BJ (2011). Prevention of radiation-induced salivary hypofunction following hKGF gene delivery to murine submandibular glands. *Clin Cancer Res* 17 (9): 2842-2851.

Curriculum Vitae

NAME

Kajohnkiart Janebodin

EDUCATION

INSTITUTION AND LOCATION	DEGREE	YEAR	FIELD OF STUDY
Mahidol University, Bangkok, Thailand	DDS	2003	Dentistry
University of Washington, Seattle, WA	PhD	2013	Oral Biology

A. Position and Honors:

Positions and Employments

2003-2007 General Practice Dental Service, Mahidol University Dental Hospital
2003-Present Instructor, Department of Anatomy, Faculty of Dentistry, Mahidol University

Other Experiences and Professional Memberships

2002-2003 President, Dental Student Society, Faculty of Dentistry, Mahidol University
2002-2003 Board, Thai Dental Student Association, Thailand
2003-2007 Student Advisory Board, Faculty of Dentistry, Mahidol University
2003-2007 Committee, Department of Anatomy, Faculty of Dentistry, Mahidol University
2003-Present Member, Dental Council of Thailand
2003-Present Member, Society of Anatomy of Thailand
2012-Present Member, International Association for Dental Research (IADR)

Honors and Awards

1997-2003 First Class Honor Student, School of Dentistry, Mahidol University
2002 Moral and Ethical Student Achievement Award from the Buddhist Association of Thailand
2003 1) Dental Student Academic Outstanding Award in Biochemistry and Physiology
2) Dental Student Achievement Award, Faculty of Dentistry, Mahidol University
2004 1) The 2nd Honor Best Research Award for "Lethal Effects of *Morinda citrifolia* Extract on Oral Squamous Carcinoma Cells", the 7th Dental Association of Thailand/DENTSPLY Student Clinician Program Competition
2) Best Research and Poster Presentation Award for "*Morinda citrifolia* Extract Induces Matrix Mineralization by Human Periodontal Ligament

	Cells", The 27th Annual Scientific Anatomy Meeting of The Society of Anatomy, Thailand
2005	Best Research and Poster Presentation Award for "Development of *Morinda citrifolia* Gel on Human Bone Cells as an Osteoinductive Agent", The 28th Annual Scientific Anatomy Meeting of The Society of Anatomy, Thailand
2006	King Anandamahidol Scholarship of Thailand, The Best Student in Dental Education (Under the royal patronage of HRH King Bhumipol of Thailand)
2007	1) Top Scholar Award, Graduate School, University of Washington 2) Outstanding Staff Award, Faculty of Dentistry, Mahidol University, Bangkok, Thailand
2010	The 3rd Prize Research Poster Presentation for "Isolation and Characterization of Neural Crest-Derived Stem Cells from Dental Pulp of Neonatal Mice", The 5th Annual SLUG Poster Show 2010, University of Washington
2011	1) UW Magnuson Scholar Award, School of Dentistry, University of Washington 2) New Investigator Honorable Mention for a poster presentation entitled "Isolation and Characterization of Neural Crest-Derived Neonatal Murine Dental Pulp Stem Cells", The 1st International Conference on Dental and Craniofacial Stem Cells 2011, New York City, New York 3) Travel Award for Trainees, International Conference on Dental and Craniofacial Stem Cells

B. Abstracts and Presentations:

Oral Presentation

1. Isolation and Characterization of Neural Crest-Derived Neonatal Murine Dental Pulp Stem Cells; Their Developmental Origin and Plasticity. Annual SLUG Research Symposium, University of Washington, 2011.

2. Dental Pulp Stem Cells. ISCRM Research Update Meeting, SLU Medicine Research Center, University of Washington, 2011.

3. Dental Pulp Stem Cells; Developmental Biology and Plasticity. Oral Biology Seminar, University of Washington, 2010.

4. Dental Pulp Multipotent Progenitor Cells (DPMPCs); Differentiation Capacity and Origin. ISCRM Research Update Meeting, SLU Medicine Research Center, University of Washington, 2010.

5. Effect of *Boesenbergia pandurata* on oral squamous carcinoma cell line and human gingival fibroblast. The 8th Meeting of Academic and Research Presentation Thai Dental Faculties Board. The 10th Anniversary Faculty of Dentistry Naresuan University, 2007

Poster Presentation

1. **Janebodin K**, Ieronimakis N, Reyes M. Angiogenic Capacity of Pericyte-like Dental Pulp Stem Cells. Proceeding in the Research Day 2011, University of Washington, School of Dentistry, Seattle, Washington, USA

2. **Janebodin K**, Horst OV, Ieronimakis N, Balasundaram G, Reesukumal K, Pratumvinit B, Reyes M. Isolation and Characterization of Neural Crest-Derived Neonatal Murine Dental Pulp Stem Cells. Proceeding in the 1st International Conference on Dental and Craniofacial Stem Cells 2011, New York City, New York, USA

3. **Janebodin K**, Horst OV, Ieronimakis N, Balasundaram G, Reesukumal K, Pratumvinit B, Reyes M. Plasticity of Neural Crest-derived Murine Dental Pulp Stem Cells. Proceeding in the ISCRM's annual Stem Cell Symposium 2010, University of Washington, Seattle, Washington, USA

4. **Janebodin K**, Horst OV, Ieronimakis N, Balasundaram G, Reesukumal K, Pratumvinit B, Reyes M. Plasticity of Dental Pulp Stem Cells Depends on The *In Vivo* Niche. Proceeding in the Research Day 2010, University of Washington, School of Dentistry, Seattle, Washington, USA

5. **Janebodin K**, Horst OV, Ieronimakis N, Balasundaram G, Reesukumal K, Pratumvinit B, Reyes M. Isolation and Characterization of Neural Crest-Derived Stem Cells from Dental Pulp of Neonatal Mice. Proceeding in the 5th Annual SLUG Poster Show 2010, University of Washington, Seattle, Washington, USA

6. Preusch MR, Srirangam K, Ieronimakis N, **Janebodin K**, Callegari A, Reyes M, Rosenfeld ME. Perivascular cells are a potential source of chondrocyte-like cells in atherosclerotic lesions of apolipoprotein E deficient mice. Proceeding in the American Heart Association (AHA) Meeting 2009, Orlando, Florida, USA

7. Nasingkan J, **Janebodin K**, Boonanantanasarn K, Arayapisit T, Suppakpatana P. *Tinospora crispa* induces matrix mineralization by human bone cells. Proceeding in the 3rd International Dental Congress of the Mekong River Region (IDCMR) 2006, Kunming, China

8. Termvidchakorn O, Boonanantanasarn K, **Janebodin K**, Arayapisit T, Sertkhamsorn P, Chatchiganan M, Niracharopas L. *Morinda citrifolia* Leaf Extract Induces Matrix Mineralization by MC3T3-E1 cell line. Proceedings in the 29th Annual Meeting of Anatomy Society 2006; Chonburi, Thailand

9. **Janebodin K**, Boonanantanasarn K, Srisatjaluk R, Muadcheingka T, Sripairojthikoon W, Arayapisit T, Suppakpattana P, Termwidchakorn O, Ochareon P, Rodsutthi J, Chunhabundit P. Effects of *Boesenbergia pandurata* Extract on *Lactobacillus spp.* and *Candida albicans*. Proceedings in the 2nd International Dental Congress of the Mekong River Region 2005; Ho Chi Minh City, Vietnam

10. Ochareon P, Boonanantanasarn K, **Janebodin K**, Arayapisit T, Suppakpattana P, Termwidchakorn O, Ochareon P, Rodsutthi J, Chunhabundit P. Chitin membrane: A Promising Biocompatible Periodontal Membrane. Proceedings in the 2nd International Dental Congress of the Mekong River Region 2005; Ho Chi Minh City, Vietnam

11. Suppakpattana P, Boonanantanasarn K, **Janebodin K**, Nasingkan J, Chunhabundit P, Arayapisit T, Sripairojthikoon W, Termwidchakorn O, Ochareon P, Rodsutthi J. Noni-Gel-Coated Squid Pen: Another Option for Osteoconductive Materials. Proceedings in the 2nd International Dental Congress of the Mekong River Region 2005; Ho Chi Minh City, Vietnam

12. Termwidchakorn O, Boonanantanasarn K, **Janebodin K**, Arayapisit T, Suppakpattana P, Nasingkan C, Sripairojthikoon W, Ochareon P, Rodsutthi J, Chunhabundit P. *Curcuma longa* Extract Induces Human Bone Cell Mineralization *In Vitro.* Proceedings in the 2nd International Dental Congress of the Mekong River Region 2005; Ho Chi Minh City, Vietnam

13. rayapisit T, Boonanantanasarn K, Srisatjaluk R, Muadcheingka T, **Janebodin K**, Suppakpattana P, Sripairojthikoon W, Termwidchakorn O, Ochareon P, Rodsutthi J, Chunhabundit P. Antimicrobial Activity of Four Thai Herbs on *Streptococcus mutans*. Proceedings in the 2nd International Dental Congress of the Mekong River Region 2005; Ho Chi Minh City, Vietnam

14. Boonanantanasarn K, Lohalertket C, Kurupinsiri P, Utchariyaprasit N, Yodboriboon, **Janebodin K**, Chunhabundit P. Lethal effect of *Morinda citrifolia* Extract on Oral Squamous Carcinoma Cells. Proceedings in the 2nd International Dental Congress of the Mekong River Region 2005; Ho Chi Minh City, Vietnam

15. Boonanantanasarn K, **Janebodin K**, Arayapisit T, Suppakpattana P, Sripairojthikoon W, Termwidchakorn O, Ochareon P, Rodsutthi J, Nasingkan C, Chunhabundit P. Development of *Morinda citrifolia* Gel as an Osteoinductive Agent on Human Bone Cells. Proceedings in the 28th Annual Meeting of Anatomy Society 2005; Ubonrachathanee, Thailand

16. Suppakpattana P, Boonanantanasarn K, **Janebodin K**, Arayapisit T, Sripairojthikoon W, Termwidchakorn O, Ochareon P, Rodsutthi J, Nasingkan C, Sabai J, Chunhabundit P. The Biocompatible Role of Fish Scales on Human Periodontal Ligament Progenitor Cells as a Scaffold Membrane. Proceedings in the 28th Annual Meeting of Anatomy Society 2005; Ubonrachathanee, Thailand

17. Chunhabundit P, Boonanantanasarn K, **Janebodin K**, Sripairojthikoon W, Suppakpattana P. Nacre Induces Mineralized Nodule Formation by Human Periodontal Ligament Cells. Proceedings in the 6th International Congress on Maxillofacial Rehabilitation 2004, Maastricht, Netherlands.

18. Chunhabundit P, Sripairojthikoon W, Suppukpatana P, Boonanantanasan K, **Janebodin K**. Nacre Induces Mineralized Nodule Formation by Human Dental Pulp Cells. Proceeding in

the 82nd General Session & Exhibition of the International Association Dental Research (IADR); March 10-13, 2004; Honolulu, Hawaii, USA.

19. **Janebodin K**, Boonanantanasarn K, Suppakpattana P, Arayapisit T, Sripairojthikoon W, Chunhabundit P. Cytotoxicity of Intracanal Medication on Mouse Osteoblast *In Vitro*. Proceedings in the 19th IADR/SEA Meeting 2004; Koh Samui, Thailand

20. Boonanantanasarn K, **Janebodin K**, Suppakpattana P, Arayapisit T, Sripairojthikoon W, Chuhabundit P. *Morinda citrifolia* Promotes Alkaline Phosphatase Activity by hPDL Cells. Proceedings in the 19th IADR/SEA Meeting 2004; Koh Samui, Thailand

21. Suppakpattana P, Boonanantanasarn K, **Janebodin K**, Arayapisit T, Sripairojthikoon W, Chunhabundit P. Osteoconductive Role of Squid Pen from *Loligo opalescens*. Proceedings in the 19th IADR/SEA Meeting 2004; Koh Samui, Thailand

22. Arayapisit T, Boonanantanasarn K, Suppakpattana P, **Janebodin K**, , Sripairojthikoon W, Chunhabundit P. Effect of Thai Herbs on Oral Squamous Cell Carcinoma. Proceedings in the 19th IADR/SEA Meeting 2004; Koh Samui, Thailand

23. **Janebodin K**, Boonanantanasarn K, Suppakpattana P, Wannapanit K, Worawetmongkol D, Laungrungrong N, Vatanarom P, Sripairojthikoon W and Chunhabundit P. Effects of *Morinda citrifolia* Extracts on Cell Proliferation and Alkaline Phosphatase Activity in Rat Dental Pulp Cells and Mouse Osteoblasts. Proceedings in the 27th Annual Meeting of Anatomy Society 2004; Petchaburi, Thailand

24. Boonanantanasarn K**, Janebodin K**, Suppakpattana P, Sripairojthikoon W, Chunhabundit P. *Morinda citrifolia* Extract Induces Matrix Mineralization by Human Periodontal Ligament Cells. Proceedings in the 27th Annual Meeting of Anatomy Society 2004; Petchaburi, Thailand

25. Boonanantanasarn K, **Janebodin K**, Suppakpattana P, Sripairojthikoon W, Chunhabundit P. Effect of *Citrus maxima* Seed Extract on Alkaline Phosphatase Activity in Human Dental Pulp, Gingival Fibroblast and Periodontal Ligament Cells. Proceedings in the 27th Annual Meeting of Anatomy Society 2004; Petchaburi, Thailand

26. Suppakpattana P, Boonanantanasarn K, **Janebodin K**, Sripairojthikoon W, Chunhabundit P. *Cassia fistula* Leaf Extract Increases Alkaline Phosphatase Activity in Cultured Human Dental Pulp, Gingival Fibroblast and Periodental Ligament Cells. Proceedings in the 27th Annual Meeting of Anatomy Society 2004; Petchaburi, Thailand

C. Publications:

1. **Janebodin K**, Zeng Y, Buranaphatthana W, Ieronimakis N, Reyes M. Angiogenic capacity of pericyte-like murine dental pulp stem cells. Journal of Dental Research 2013. Accepted.

2. **Janebodin K**, Buranaphatthana W, Ieronimakis N, Hays AL, Reyes M. An *in vitro* culture system for long-term expansion of epithelial and mesenchymal salivary gland cells: Role of TGF-β1 in salivary gland epithelial and mesenchymal differentiation. BioMed Research International 2013. Submitted.

3. Ieronimakis N, Hays AL, **Janebodin K**, Mahoney W, Majesky MW, Duffield J, Reyes M. Coronary adventitial cells are responsible for perivascular cardiac fibrosis in the *mdx* mouse model of Duchenne Muscular Dystrophy. Journal of Molecular and Cellular Cardiology 2013. Submitted.

4. Nemeth C, **Janebodin K**, Yuan A, Reyes M, Kim DH. Nanopatterned hyaluronan hydrogels enhance *in vitro* spheroid formation and chondrogenesis in dental pulp stem cells. In preparation.

5. Pratumvinit B, Reesukumal K, **Janebodin K,** Ieronimakis N, Reyes M. Isolation, Characterization, and Transplantation of Cardiac Endothelial Cells. In preparation.

6. Boonanantanasarn K, **Janebodin K**, Suppakpatana P, Arayapisit T, Rodsutthi JA, Chunhabundit P, Boonanuntanasarn S, Sripairojthikoon W. *Morinda citrifolia* leaves enhance osteogenic differentiation and mineralization of human periodontal ligament cells. Dent Mater J. 2012;31(5):863-71.

7. Janebodin K and Reyes M. Neural crest-derived dental pulp stem cells function as ectomesenchyme to support salivary gland tissue formation. Dentistry 2012; 2(2): S13.

8. Reesukumal K, Pratumvinit B, Rudakova M, **Janebodin K**, Reyes M. Purification, Expansion and Characterization of Putative Murine Cardiac Progenitor Cells. Stem Cell Research & Therapy 2011; S1:002. doi:10.4172/2157-7633.

9. **Janebodin K**, Horst OV, Ieronimakis N, Balasundaram G, Reesukumal K, Pratumvinit B, Reyes M. Isolation and Characterization of Neural Crest-derived Stem Cells from Dental Pulp of Neonatal Mice. *PLoS ONE* 2011; 6(11): e27526. Epub 2011 Nov 8

10. **Janebodin K,** Arayapisit T, Thongsagulwong C, Munkong R, Jirawattanakul Y, Sripairojthikoon W. Apoptotic Induction of *Boesenbergia pandurata* Extract on Oral Squamous Carcinoma Cells. *Mahidol Dent J* 2011; 31: 89-100.

11. **Janenodin K**, Horst OV, Osathanon T. Dental Pulp Response to Pulp Capping Materials and Bioactive Molecules. *CU Dent J* 2010; 33: 229-48.

12. **Janebodin K**, Sripairojthikoon W, Arayapisit T, Arom C, Wongsopa N, Klabwihok R. Effect of *Boesenbergia pandurata* on oral squamous carcinoma cell line and human gingival fibroblast. *Mahidol Dent J* 2008; 28: 141-8.

13. Boonanantantasarn K, Termvidchakorn O, **Janebodin K**, Arayapisit T, Chatchaiganan M, Niracharopas L, Sertkhamsorn P. *Morinda citrifolia L*. leaf extract induces matrix mineralization by MC3T3-E1 cell line. *Mahidol Dent J* 2008; 28: 53-60.

14. Boonanantantasarn K, Chunhabundit P, **Janebodin K**, Kurupinsiri P, Utchariyaprasit N, Lohalertkit C, Yodboriboon A. Lethal effect of *Morinda citrifolia L*. extracts on oral squamous carcinoma cell**.** *J Dent Assoc Thai* 2006; 56: 87-96.